9th South African Conference on Photonic Materials 2023

SACPM 2023

8 – 12 May 2023
Nombolo Mdhluli Conference Centre
Skukuza Rest Camp
Kruger National Park
South Africa

Hosted by the Division for Physics of Condensed Matter and the Applied Physics Division of the South African Institute of Physics

http://events.saip.org.za/event/sacpm2023

Morning Programme

Time	Monday	Tuesday	Wednesday	Thursday	Friday
	8 May	9 May	10 May	11 May	12 May
07:00- 08:00		Breakfast	Breakfast	Breakfast	Breakfast
08:00 - 8:10		Session 1 Opening **Ernest van Dyk**	Session 4 (Announcements) **Richard Harris**	Session 7 (Announcements) **Walter Meyer**	
08:10 - 8:20 08:20 - 8:30 08:30 - 8:40 08:40 - 8:50		Plenary 1 **James Blakesley**	Plenary 2 **Bryce Richards**	Plenary 3 **Anne Hemeryck**	
08:50 - 09:00 09:00 - 09:10		Presentation 1 **Roelof Roodt**	Presentation 11 **Jorma Hölsä**	Plenary 4 **Layla Martin-Samos**	
09:10 - 09:20 09:20 - 09:30		Presentation 2 **Roelof Roodt**	Presentation 12 **Govind Nair**		
09:30 - 09:40 09:40 - 09:50		Presentation 3 **Eduard Madirov**	Presentation 13 **Ivan Ivanov**	Presentation 21 **Rositsa Yakimova**	Checkout before 10:00
09:50 - 10:00		Discussion	Discussion	Discussion	
10:00 - 10:10 10:10 - 10:20		Tea & Coffee break	Tea & Coffee break	Tea & Coffee break	
		Session 2 **Hendrik Swart**	Session 5 **Koos Terblans**	Session 8 **Johan Janse van Rensburg**	
10:20 - 10:30 10:30 - 10:40 10:40 - 10:50		Invited 1 **Andrey Turshatov**	Edinburgh Instruments Invited 4 **Weimin Chen**	Invited 5 **Jai Prakash**	
10:50 - 11:00 11:00 -11:10		Presentation 4 **Patrick Mokoena**		Presentation 22 **Delicacy Ntshalintshali**	
11:10 - 11:20 11:20 - 11:30		Presentation 5 **Abongile Bele**	Presentation 14 **Irina Buyanova**	Presentation 23 **Lucas Erasmus**	
11:30 - 11:40 11:40 - 11:50		Presentation 6 **N J Shivaramu**	Presentation 15 **Emad Hasabeldaim**	Presentation 24 **Leonato Nchinda**	
11:50 - 12:00 12:00 - 12:10		Presentation 7 **Simon Ogugua**	Presentation 16 **Assane Talla**	Presentation 25 **Fokotsa Victor Molefe**	
12:10 - 12:20		Discussion	Discussion	Discussion	
12:20 - 12:30 12:30 - 12:40 12:40 - 12:50 12:50 - 13:00 13:00 - 13:10 13:10 - 13:20		Lunch	Lunch	Lunch	

Afternoon Programme

Time	Monday	Tuesday	Wednesday	Thursday	Friday
	8 May	9 May	10 May	11 May	12 May
		Session 3 **Ted Kroon**	Session 6 **Reinhardt Botha**	Session 9 **Andre Venter**	
13:20 - 13:30 13:30 - 13:40		Invited 2 **Andrej Kuznetsov**	Presentation 17 **Irfan Ayoub**	Presentation 26 **Walter Meyer**	
13:40 - 13:50			Presentation 18 **Zelalem Urgessa**	Presentation 27 **JAA Engelbrecht**	
13:50 - 14:00		Presentation 8 **Valentine Muramba**	Presentation 19 **Michael Lee**	Presentation 28 **Mmantsae Diale**	
14:00 - 14:10 14:10 - 14:20	Arrival & Registration	Presentation 9 **Boitumelo Tladi**	Presentation 20 **Rebecca Letsoalo**	Discussion	
14:20 - 14:30		Presentation 10 **Edward Lee**	Discussion	Tea & Coffee break	
14:30 - 14:40		Discussion		Prize giving Closure	
14:40 - 14:50				Conference Photo	
14:50 - 15:00 15:00 - 15:10 15:10 - 15:20 15:20 - 15:30 15:30 - 15:40 15:40 - 15:50 15:50 - 16:00 16:00 - 16:10 16:10 - 16:20 16:30 - 16:40 16:40 - 16:50 16:50 - 17:00					
17:00 - 17:10 17:10 - 17:20 17:20 -17:30 17:30 - 17:40				Game Drive to Bush Braai	
17:40 - 17:50 17:50 - 18:00 18:00 - 18:10 18:10 - 18:20 18:20 - 18:30 18:30 - 18:40 18:40 - 18:50 18:50 - 19:00		Poster Session with Cocktail Function	Poster Session		
19:00 - 19:10 19:10 - 19:20 19:20 - 19:30	Conference function & Dinner			Conference Function (Bush Braai)	
19:30 - 19:40 19:40 - 19:50 19:50 - 20:00 20:00 - 20:10 20:10 - 20:20 20:20 - 20:30 20:30 - 20:40 20:40 - 20:50 20:50 - 21:00			Dinner		

Table of Contents

University of Pretoria
Department of Physics





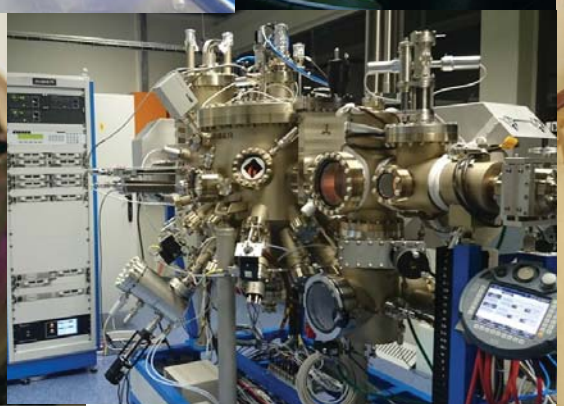

We offer postgraduate opportunities in the following research focus areas

Materials
- Nuclear applications
- Semiconductors
- Solar cells
- Opto-electronics
- Carbon-based
- Nano-magnetism

Theoretical Physics
- Mathematical physics
- High energy theory
- Quantum information theory
- Computational solid state physics

Astronomy

Biophysics
- Light-harvesting mechanisms
- Single-molecule spectroscopy
- Femtosecond laser spectroscopy
- Theoretical modelling

Enquiries about postgraduate studies
Prof Chris Theron
Head: Department of Physics

Email: Chris.Theron@up.ac.za
Tel: +27 12 420 2455
Web: **http://www.up.ac.za/physics**

UNIVERSITEIT VAN PRETORIA
UNIVERSITY OF PRETORIA
YUNIBESITHI YA PRETORIA
Faculty of Natural and Agricultural Sciences

Organizing Committee

Prof Reinhardt Botha	NMU	Proceedings co-editor
Mrs Thereza Botha	Technoscene	Conference secretary
Dr Richard Harris	UFS	NRF KIC application
Mr Johan Janse van Rensburg	UP	Conference programme
Prof Ted Kroon	UFS	Conference website & proceedings co-editor
Prof Walter Meyer	UP	Finances & vice chairperson
Prof Jackie Nel	UP	Conference chairperson
Prof Martin Ntwaeaborwa	WITS	Proceedings editor
Prof Hendrik Swart	UFS	Prize awards
Prof Koos Terblans	UFS	Additional member
Prof Ernest van Dyk	NMU	Finances
Prof Andre Venter	NMU	Additional member
Dr Freddie Vorster	NMU	Abstract review

NMU: Nelson Mandela Univesity, **UFS**: University of the Free State, **UP**: University of Pretoria

The committee was assisted by the Office of the South African Institute of Physics, particularly Mr Brian Masara (logistics and finances) as well as Mrs Tebogo Mokhine (Website and registration support).

List of Sponsors

Blue Stallion Technologies CC	www.bluestallion.co.za	Prize sponsor
National Research Foundation: Knowledge, Interchange and Collaboration – KIC (Local Events support grant KIC22081049647, UID 150403)	www.nrf.ac.za	Conference grant
Busch Vacuum Solutions South Africa	www.buschvacuum.com/za/en/	Exhibitor
Cengage SA	www.cengage.uk/south-africa/	Prize sponsor
Hamamatsu Photonics UK	www.hamamatsu.com	Gold sponsor
Edinburgh Instruments	www.edinst.com	Super Exhibitor
Hitech Lasers	www.hitechlasers.co.za	Exhibitor
University of the Free State: Faculty of Natural and Agricultural Sciences	www.ufs.ac.za/natagri/	Gold sponsor
CB Van Wyk Family Trust (University of the Free State - Physics Department)	https://www.ufs.ac.za/natagri/departments-and-divisions/physics-home	Platinum sponsor
Wirsam Scientific & Precision Equipment (Pty) Ltd	https://wirsam.com	Exhibitor
Hiden Analytical Ltd	www.hidenanalytical.com	Gold sponsor
Wiley and Sons	www.wiley.com	Prize sponsor

Sponsors

UNIVERSITEIT VAN PRETORIA
UNIVERSITY OF PRETORIA
YUNIBESITHI YA PRETORIA

UNIVERSITY OF THE
FREE STATE
UNIVERSITEIT VAN DIE
VRYSTAAT
YUNIVESITHI YA
FREISTATA

UFS·UV
NATURAL AND
AGRICULTURAL SCIENCES
NATUUR- EN
LANDBOUWETENSKAPPE

NELSON MANDELA
UNIVERSITY

CB van Wyk Family Trust

CB van Wyk Family Trust

A Visionary Whose Legacy Lives On

During 1953 two Professors from the University of the Free State had a dream of organizing a Physics Conference in South Africa. Prof CB van Wyk (Applied Mathematics) and Prof JHN Loubser (Physics) wrote to 27 scientists to determine the interest and feasibility of such an event. The response was overwhelmingly positive and resulted in a letter to Dr Ernest Marais, head of the National Physical Laboratory.

A meeting took place on 17 August 1953, and it was decided by the provisional committee of the “South African Institute of Physics”, that a conference would take place during July 1954 in Pretoria. Prof Van Wyk and Prof Loubser continued to invite all Physicists to the conference where the establishment of the Institute for Physics was discussed.

The vision of Prof van Wyk contributed to the foundation of the South African Institute of Physics. This year the Institute turn 69 years and is going from strength to strength. Prof van Wyk’s honourable legacy is still present through the CB van Wyk Gesinstrust, sponsoring plenary speakers at this conference.

Don't stop dreaming.

Department of Physics

T: +27(0)51-401 2531 | natagri@ufs.ac.za | www.ufs.ac.za/natagri

UFSUV | UFSweb | UFSweb

Inspiring excellence.
Transforming lives.

UNIVERSITY OF THE
FREE STATE
UNIVERSITEIT VAN DIE
VRYSTAAT
YUNIVESITHI YA
FREISTATA

UFS·UV
NATURAL AND
AGRICULTURAL SCIENCES
NATUUR- EN
LANDBOUWETENSKAPPE

Message from the SAIP President

Dear colleagues,

I am delighted to welcome you to the 9th South African Conference on Photonic Materials (SACPM 2023) hosted by the Physics Department at the University of Pretoria, together with the Physics Departments of the University of the Free State, Nelson Mandela University and the University of Witwatersrand, with involvement of the Division for Condensed Matter Physics and Materials, and the Division of Applied Physics, of the South African Institute of Physics. This conference comes at the back of an enforced two-year hiatus and is a welcome return to an established tradition within the photonics materials research community.

Since its inception, the SACPM series has developed a well-earned reputation for high quality presentations on topical issues within condensed matter and related areas of physics. Having attended a number of previous conferences, I remember that the style and pace of these meetings not only allows for formal engagements within plenaries but also leaves ample time for informal discussions outside the set schedule times. In Skukuza Camp, the organisers could not have chosen a better venue because Kruger National Park within whose confines the camp lies is a true prime example of the successes of nature conservation in Africa. The park has an unrivalled diversity of game and its hosts reflect the exuberance that is unique to only Africa. That alone justifies the choice to combine the business of physics with the pleasure of game viewing.

I convey a special welcome to the international invited speakers who have travelled from around the world to present highlights of their work in the field of Photonic Materials. I hope that you will have time to meet with students and emerging researchers to impart your expertise and knowhow and will be open to fostering mutually beneficial collaborations with research groups within the country.

On behalf of the South African Institute of Physics, I am delighted to welcome you to the 9th South African Conference on Photonic Materials. I wish you all a very successful conference.

Makaiko Chithambo
SAIP President

HiCube™

The modular pumping stations for all applications in high and ultra-high vacuum

BUSCH VACUUM SOLUTIONS

Official distributor of PFEIFFER VACUUM

Busch Vacuum Solutions | sales@busch.co.za | +27 11 8560650 | www.busch.co.za

Plenary Speakers

James Blakesley

National Physical Laboratory
United Kingdom

Seeing into devices: New optical techniques for device characterisation

James is a Principal Research Scientist and Science Area Leader for Electronic and Magnetic Materials at the National Physical Laboratory, United Kingdom. He specialises in the development of measurement techniques for new and emerging devices, materials and applications, particularly in photovoltaic technologies. The aim is to apply measurement science to improve performance, quality and yield of devices and to accelerate the translation of emerging technologies from basic research to application. He is also an IEC technical committee expert and contributes to the development of performance standards for photovoltaics and emerging electronic materials. James obtained a PhD from the University of Cambridge for work on novel single-photon detectors for quantum cryptography. He worked at University College London, the University of Cambridge and Potsdam University on projects including novel x-ray detectors, charge transport in organic semiconductors and new photovoltaic materials. Since then, he joined NPL, the UK's national metrology institute, where he has worked for 10 years.

Prof Dr Bryce S Richards

Institute for Microstructure Technology (IMT)
Nanophotonics for Energy, Faculty of Electrical Engineering and Information Technology, Karlsruhe Institute of Technology (KIT), Eggenstein-Leopoldshafen
Germany

A load of rubbish or a big opportunity for luminescent materials?

Bryce Richards studied physics at the Victoria University of Wellington (New Zealand) before completing a Masters and PhD in electrical engineering at Univ. of New South Wales (Australia), in 1998 and 2002, respectively. He worked at both UNSW and the Australian National University. In 2006, he joined Heriot-Watt University (Edinburgh, U.K.) as a lecturer, being promoted to full professor in 2008. Since 2014 he is co-director of the Institute for Microstructure Technology (IMT) and Light Technology Institute (LTI) within the Karlsruhe Institute of Technology (Germany). His primary research areas lie in third generation photovoltaics (including perovskite solar cells), spectral conversion (up- and down-conversion), luminescent materials, light management, and solar-powered water treatment systems.

Dr Anne Hémeryck
LAAS-CNRS
Toulouse
France

Formation of defects in semiconductors: what contribution from atomistic modeling?

Anne Hémeryck has been a full-time researcher at the Laboratory for Analysis and Architecture of Systems at the French National Centre for Scientific Research (CNRS) since 2011. In April 2016, she created the M3 Team at LAAS-CNRS for Multilevels Modeling of Materials. She is nowadays the Head of the M3 Research Team. Since nearly 16 years, Anne Hémeryck performs intensive calculations to address materials science issues. During all her past professional experience, she always focused her research activities on modeling and simulation approaches dedicated to a variety of microelectronics topics, such as silicon oxidation (PhD in CEA-DAM, Arpajon, France), catalysis activity at the surface a gas sensor (postdoctoral fellow in LAAS-CNRS, Toulouse, France), nanoindentation simulations and hydrogen production enhanced by Al supernanoparticle (Postdoc fellow in University of Southern California in Priya Vashishta's Team, Los Angeles, USA), preparation and coating of surface through molecular passivation and functionalization (6 months contractual work at the IRCP, Paris, France), assembly of nanoparticles thanks to DNA (in 2012 in LAAS-CNRS). Her research focuses on the nanoengineering of materials encountered in microelectronics by considering them in an atomic point of view and focus on the critical issue of the surface and interface phenomena and properties. She aims at focusing on the development and application of multi-levels computational methods, dedicated to physical and chemical problems in material science, notably on the predictive simulation concerning properties of materials directly integrated.

Prof Dr Layla Martin-Samos Colomer
CNR-IOM Democritos
Trieste
Italy

Defect signatures in semi-conductors and insulators: understanding and modelling

Prof. Dr. Layla Martin-Samos is a researcher from the Italian National Research Council (CNR-IOM) leading a group of three postdocs and one PhD student. She is also external associated professor at the University of Nova Gorica. After a PhD in Computational Material Science in Paris (2004) devoted to the modelling of defects in amorphous SiO2 from first-principles, she moved to the INFM-S3 center in Modena (Italy) where she developed SaX (Self-energies And eXitations), a software package based on Many-Body Perturbation Theory. SaX was the first Open Source freely available software released (GPL) for the modelling of electronic excitations, including optical excitations, within the GW approximation and the Bethe-Salpeter Equation. In 2009, she moved to Trieste (Italy) where she worked as development scientist for

Quantum ESPRESSO. In 2012 she became assistant Professor at the University of Nova Gorica (Slovenia) in the Materials Research Laboratory. Her research interests include software development, refactoring and optimization (enabling High Performance Computing and High Through Put) and connection between theory and experiments, including multi-scaling and methodological developments. She is actively involved in a longstanding multi-partner collaboration (CEA-DIF, CNRSLAAS and SISSA), devoted to understanding and modeling defects and irradiation effects in semiconductors and insulators. She also participates in the activities of the Electronic Structure Library initiative and she is member of the psi-k (Ab-initio calculation of complex processes in materials) working group 'Software engineering'. She is author/co-author of more than 50 papers published in peer reviewed international journals. She is PI of WP4 'Multi-Scale Modeling' of H2020 FETOPEN MAGNELIQ and project manager of several industrial research contracts.

Invited Speakers

Prof Weimin M. Chen
Linköping University
Sweden
Founding director of the Swedish Interdisciplinary Magnetic Resonance Center (SIMARC)

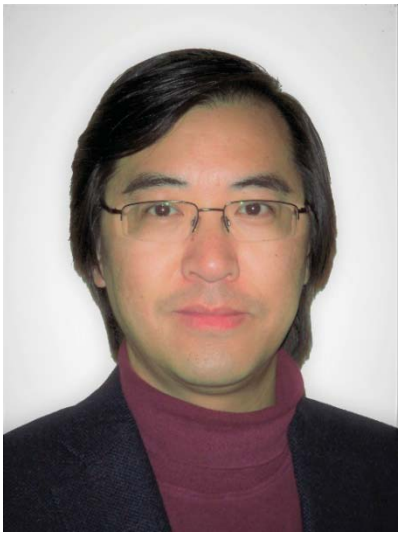

Towards fully spin- and optically-polarized light-emitting semiconductor nanostructures for room-temperature opto-spintronics

Weimin M. Chen is a full professor in physics in the Department of Physics, Chemistry and Biology at Linköping University (Sweden) since 1999, and the founding director of the Swedish Interdisciplinary Magnetic Resonance Center (SIMARC) since 1998. He received his Ph.D. degree in materials physics from Linköping University in 1989 and completed his postdoctoral research during 1991-1993 at University of California at Berkeley (USA) before returning back to the faculty at Linköping University. His main research interests are electronic, optical, defect and spin-related properties of semiconductor materials and nanostructures, covering a wide range of materials systems including inorganic III-V and II-VI compound semiconductors, organic semiconductors and halide perovskites. His most recent research activities focus on development, understanding and exploration of novel opto-spintronic semiconductor nanostructures for future spintronic and opto-spintronic applications. He is the author of more than 700 scientific articles, 38 review articles and book chapters, and 3 books.

Dr Andrey Turshatov
Institute of Microstructure Technology (IMT),
Karlsruhe Institute of technology (KIT)
Eggenstein-Leopoldshafen
Germany

Fundamentals and applications of upconversion in lanthanide-doped alkaline-earth fluorides

Andrey Turshatov is the Group Leader for the Materials for Spectral Conversion Group. His research interests include synthesis and photophysical characterization of luminescent materials, e.g. organic dyes, quantum dots, lanthanide-doped inorganic materials; time-resolved optical spectroscopy; photon up-conversion; light–matter interaction; super-resolution optical microscopy; functional optical materials for solar light conversion.

Prof Andrej Kuznetsov
University of Oslo
Norway

Gallium oxide polymorph heterostructures: physics, fabrication, and potential applications

Andrej Kuznetsov was awarded with his PhD degree in physics from the Russian Academy of Sciences in 1992 and accomplished his habilitation in solid state electronics in 2000 at the Royal Institute of Technology in Sweden. In 2001 he joined the Department of Physics at the University of Oslo in Norway as an associate professor and was subsequently promoted to the full professor rank in 2003. From 2018 he has acted as the Chair of the Centre of Excellence: Light and Electricity from Novel Semiconductors (LENS) - as a part of the Centre for Materials Science and Nanotechnology at the University of Oslo. His focus is to understand novel semiconductors, searching for new fundamental phenomena and enabling new device functionalities. His work resulted in more than 200 peer-review publications, scoring more than 6000 citations, h = 41 by August 2022. He taught at different levels, at present gives an introductory condensed matter physics course at the BSc level, as well as supervised numerous students at the MSc and PhD levels. He managed research funds in Sweden, Norway, as well as EU grants.

Dr Jai Prakash
National Institute of Technology, Hamirpur
India

Plasmonic photocatalysts: Tailoring of optical properties and advanced multifunctional applications

Dr. Jai Prakash is working as Assistant Professor in the Department of Chemistry, NIT Hamirpur. Previously, he worked as 'INSPIRE Faculty' in the Department of Chemical Engineering at Indian Institute of Technology (IIT) Kanpur, India (2016-2018). His PhD (2007-2012), carried out at and sponsored by IUAC (formerly, Nuclear Science Center), New Delhi, was awarded by CCS University, Meerut (India). He worked as a postdoctoral researcher at INRS-EMT, Quebec (Canada), Aix-Marseille University (France), Universite Libre de Bruselles (Belgium) and University of the Free State (South Africa). He has received several national and international scientific awards including DAAD Academic Award (2018), Merit Scholarship Award (ranked# 1) (2017) from Quebec Govt. (Canada), Promising Young Researcher Award (2016) from NRF (South Africa), Prestigious INSPIRE faculty award (2015-2016) and Young Scientist Fast Track (2012) award from DST (India), Guest scientist (2014) from NIMS (Japan), and Senior Research Fellow (2011) from CSIR (India). He has published more than 80 research articles including book/chapters in international scientific peer reviewed journals. Recently, he has been listed among World's Top 2% Scientists List created by Stanford University (2021). His major research fields are functional nanomaterials, surface science, ion beam modifications of nanomaterials and chemistry of materials. His highly interdisciplinary research includes synthesis/ characterizations of plasmonic, polymers, metal-oxides semiconductors nanomaterials, their nanocomposites for sensing, solar cell, optical, photocatalysis, SERS related environmental and energy applications.

www.hidenanalytical.com
info@hiden.co.uk

HIDEN ANALYTICAL

Instruments for Surface Analysis

Depth Profiling and Surface Imaging at the Nanoscale

Mass spectrometers for vacuum, gas, plasma and surface science

ToF-qSIMS

Investigate a full spectrum of materials, from alloys to pharmaceuticals, down to sub-ppm levels with the ToF-qSIMS.

Compact SIMS

Easily and quickly characterise nanoscale layer structures with 2D and 3D imaging plus mass spectral data using the Compact SIMS.

Hi5 SIMS

Simultaneously acquire positive and negative ions for complimentary data in a single shot using the Hi5 SIMS.

FIB-SIMS

Meet the analytical requirements of various depth profiling and nanoscale surface imaging applications using FIB-SIMS.

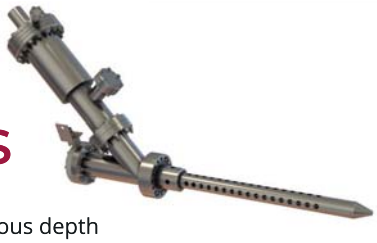

W www.HidenAnalytical.com E info@hiden.co.uk

Scientific Program & Abstracts
Tuesday 9 May

Time	Activity
07:00 – 08:00	Breakfast
	PRESENTATION SESSION 1: Chairperson – **Ernest van Dyk**
08:00 – 08:10	Opening – **Jackie Nel**
08:10 – 08:50	Plenary Talk 1: **James Blakesley** Seeing into devices: New optical techniques for device characterisation
08:50 – 09:10	Presentation 1: **Roelof Roodt** Optimisation of luminescence imaging of solar cells
09:10 – 09:30	Presentation 2: **Roelof Roodt** Individual layer luminescence image characterisation of multijunction solar cell degradation
09:30 – 09:50	Presentation 3: **Eduard Madirov** Spectral conversion in doped BaF_2 crystals for photovoltaic applications
09:50 – 10:00	Discussion
10:00 – 10:20	Tea & Coffee break
	PRESENTATION SESSION 2: Chairperson – **Hendrik Swart**
10:20 – 10:50	Invited Talk 1: **Andrey Turshatov** Fundamentals and applications of upconversion in lanthanide-doped alkaline-earth fluorides
10:50 – 11:10	Presentation 4: **Patrick Mokoena** Red Emission Stimulated by Electric-Dipole Transition of Eu3+-codoped MgAl2O4:Sm3+ Nanophosphors Synthesized via Citrate Sol-Gel Method
11:10 – 11:30	Presentation 5: **Abongile Bele** Investigating the effects of varying Gd^{3+} concentration on the structure, morphology and photoluminescence properties of $MgAl_2O_4$/MgO/$BaAl_2O_4$/$GaAlO_3$: x% Gd^{3+} ($0 \leq x \leq 1.1$) mixed phases via sol-gel method
11:30 – 11:50	Presentation 6: **N J Shivaramu** Influence of annealing temperature on the crystal structural, morphology and photoluminescence of $BaAl_2O_4$:Eu
11:50 – 12:10	Presentation 7: **Simon Ogugua** Synthesis and the thermometry properties of $Sr_{2.9}Al_2O_5Cl_2$:0.1Eu^{2+} phosphor
12:10 – 12:20	Discussion
12:20 – 13:20	Lunch
	PRESENTATION SESSION 3: Chairperson – **Ted Kroon**
13:20 – 13:50	Invited Talk 2: **Andrej Kuznetsov** Gallium oxide polymorph heterostructures: physics, fabrication, and potential applications
13:50 – 14:10	Presentation 8: **Valentine Muramba** Synthesis and electrical characterization of β-Gallium Oxide
14:10 – 14:30	Presentation 9: **Boitumelo Tladi** Effect of graphene oxide coatings on the optical properties of pulsed laser deposited ZnO:Zn thin films
14:30 – 14:50	Presentation 10: **Edward Lee** Strontium vanadate a possible addition to transparent conductive thin films
14:50 – 15:00	Discussion
17:40 – 21:00	Poster Session with cocktail function

Seeing into devices: New optical techniques for device characterisation

James C Blakesley[1], George Koutsourakis[1], Sebastian Wood[1], Yameng Cao[1], Daniel Parsons[1], Aidas Baltušis[1,2], Fernando Castro[1,2]

[1]National Physical Laboratory, Hampton Road, Teddington TW11 0LW, United Kingdom
[2]Advanced Technology Institute, University of Surrey, Guildford, Surrey, GU2 7XH, United Kingdom
Corresponding author e-mail address: james.blakesley@npl.co.uk

1. Introduction

There is a continuous pipeline of new and emerging electronic materials and devices at various stages of maturity. These include perovskites for photovoltaics, organic and dye-sensitized absorbers for indoor photovoltaics, heterostructure devices, wide bandgap semiconductors for power electronics, thin-film semiconductors, 2D materials and flexible and printed electronic materials. Many of these have theoretical potential to outperform the incumbent technology, but are hindered by issues with stability, consistency or quality, particularly when scaled up for volume manufacture. To understand and resolve these issues requires fast, flexible characterisation tools capable of quantitative measurement functional properties of materials and devices and linking these to structure, processing and material quality. The National Physical Laboratory (NPL) is the UK's National Measurement Institute. It supports industry, science, and quality of life by the application of measurement science. As part of this, we research and develop innovative measurement methods to support emerging needs of science and industry. In this talk we will present examples of recent NPL work developing new characterisation techniques for semiconductor devices supporting science and scale up of emerging electronic materials:

2D and 3D functional imaging with spatial light modulation: Spatial light modulation can be used to encode spatial information in light patterns, enabling new modes of measurement. This has been demonstrated previously in single pixel imagers, where a 2D image is created from a single pixel detector, and snapshot imaging, where a multidimensional measurement is captured on a 2D focal plane array in a single frame. We use this approach in different modes, including photocurrent/ quantum efficiency mapping, hyperspectral imaging and time-resolved photoluminescence imaging. The benefits compared to traditional methods, based on raster scanning, are due to optimised encoding of information resulting in increased signal and common noise rejection. These effects can be explained by Information Theory or Deign of Experiments. They enable faster image acquisition, but also completely new measurement modes that were previously impossible to realise.

Quantitative photoluminescence imaging of perovskite photovoltaics: Perovskites are a promising material class for efficient photovoltaics, but many issues remain unresolved in scale up and stability. We use in-situ and operando voltage and irradiance-dependent photoluminescence imaging of perovskite PV devices to quantify degradation and to show how hysteresis can be spatially localised to defects and edges. This is a powerful tool for understanding how processing impacts device performance and stability.

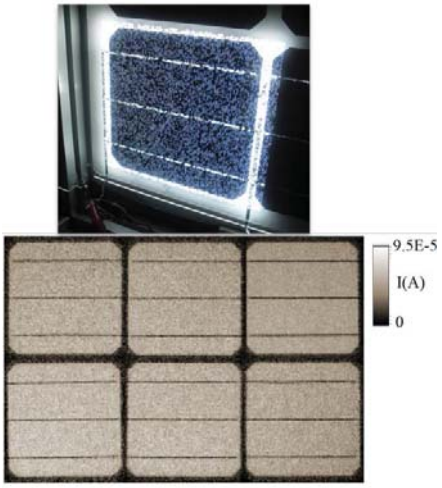

Fig. 2: Compressive photocurrent mapping of individual cells in a PV module. Compared to traditional EL or PL imaging, the image is not distorted by cell mismatch.

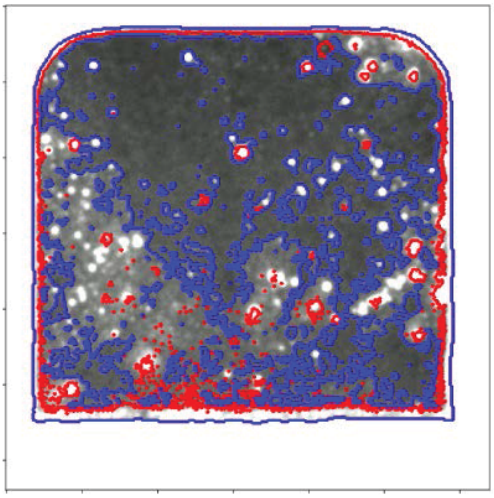

Fig. 1: In situ PL imaging of perovskite PV cell under exposure to UV + O_2. Red boundary: initial defective area. Blue boundary: defective area after exposure.

2. References

[1] Koutsourakis, G., Thompson, A. and Blakesley, J.C. (2022), Toward Megapixel Resolution Compressed Sensing Current Mapping of Photovoltaic Devices Using Digital Light Processing. Sol. RRL, 6: 2100467. https://doi.org/10.1002/solr.202100467

Optimisation of luminescence imaging of solar cells

Roelof P Roodt[1], **Ross M Dix-Peek**[1], **E Ernest van Dyk**[1], **Jacqui L Crozier McCleland**[1]

[1]*Nelson Mandela University, University Way, Summerstrand, Port Elizabeth*
Corresponding author e-mail address: s217357709@mandela.ac.za

1. Introduction

Electroluminescence (EL) and Photoluminescence (PL) imaging of Photovoltaic (PV) devices are well known qualitative and quantitative, non-destructive characterisation techniques. The quality of an image is important in luminescence image quantification. Aside from basic optical optimisation (such as focus, relative position, lens distortion and contrast), a camera's sensor's properties can affect an image's quality. Some of the factors that decrease the quality of the image are diffraction of the incident light, chromatic aberration, photon scattering within the sensor, light trapping and other image convoluting mechanisms. In literature, a process has been developed to correct for these factors when capturing EL and PL images of silicon PV devices[1]. However, this procedure has not been investigated to test its functionality with other PV materials, such as perovskite, multi-junction III-V concentrator cells, etc. Therefore, it is necessary to further develop this process and investigate it for other PV devices, as it would be different for each material's luminescence spectrum[2]. This study illustrates how the process is investigated and used in correcting images acquired for Silicon, multi-junction III-V concentrator cells, and perovskite solar cells.

2. Results

Fig. 1 shows an electroluminescence image of the top layer of a multi-junction III-V solar cell before processing and Fig. 2 shows the corrected image for the same area of the solar cell after the optimisation procedure has been implemented. The improvement in image quality allows for better qualitative analysis of the imaging results.

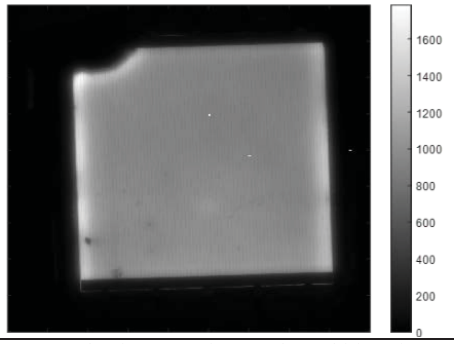

Fig. 1: Raw luminescence image of a multi-junction III-V concentrator cell

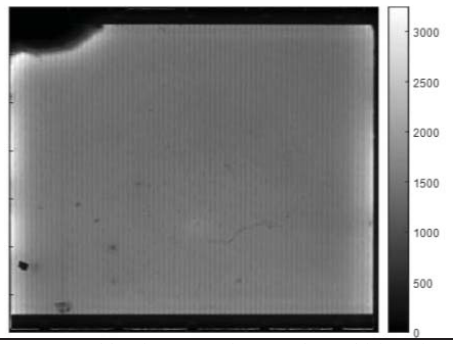

Fig. 2: Corrected luminescence image of a multi-junction III-V concentrator

3. References

[1] K.G. Bedrich, M. Bliss, T.R. Betts, R. Gottschalg, Electroluminescence imaging of PV devices: Camera calibration and image correction, in: Conference Record of the IEEE Photovoltaic Specialists Conference, Institute of Electrical and Electronics Engineers Inc., 2016: pp. 1532–1537. https://doi.org/10.1109/PVSC.2016.7749875.

[2] D. Walter, A. Fell, E. Franklin, D. MacDonald, B. Mitchell, T. Trupke, The impact of silicon CCD photon spread on quantitative analyses of luminescence images, IEEE J Photovolt. 4 (2014) 368–373. https://doi.org/10.1109/JPHOTOV.2013.2287912.

Individual layer luminescence image characterisation of multijunction solar cell degradation

Ross M Dix-Peek[1], Roelof P Roodt[1], E Ernest van Dyk

[1] Nelson Mandela University, University Way, Summerstrand, Gqeberha
Corresponding author e-mail address: Ross.Dix-Peek@mandela.ac.za

1. Introduction

Multijunction solar cells (MJSCs) are photovoltaic (PV) devices typically manufactured from multiple sub-cells layered on each other. These devices are usually manufactured from group III/V materials and the cost per unit area would make them economically infeasible. However, considering that they currently have the highest conversion efficiency [1], light concentrating optics have been used to decrease the active area of the semiconductive material required. While this does increase the economic feasibility of the devices, high light concentration and heat has the potential to degrade the material. As the sub-cells are connected in series, photocurrent mismatch is a major concern [2, 3]. It is plausible that the different sub-cells of a MJSC will have differing degradation rates which has potential to exacerbate this concern. In this study, two similar experimental setups were developed to identify performance degrading defects in two layers of a three junction PV cell and three layers of the five junction PV cell. The first system can perform photoluminescence and electroluminescence imaging of the complete device. While the second system can perform micro-luminescence imaging of specific regions of the device. These systems were used to identify the extent of the material damage caused by high intensity laser probing of a MJSC.

2. Results

Fig.1 is a micro electroluminescence (EL) image of the laser probe damage in the top layer (InGaP) of a MJSC and Fig. 2 is the corresponding micro EL image of the damage in the InGaAs layer. In both figures the path of the laser probe is visible. The laser probe damage occurred during high intensity laser beam induced current measurements (LBIC). The positions where the laser probe was incident on during an electrical measurement are shown by increased damage (dark lines and spots). This is due to the increased time the probe was incident at the positions during electrical measurements.

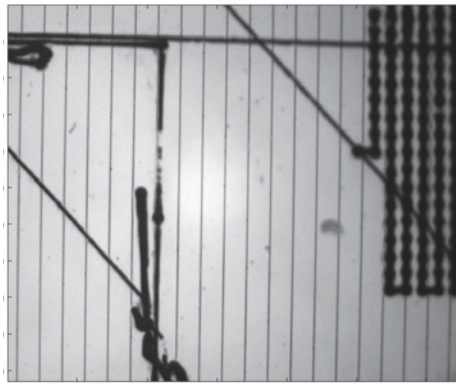

Fig. 1: micro-EL intensity image of laser damage of InGaP layer of MJSC

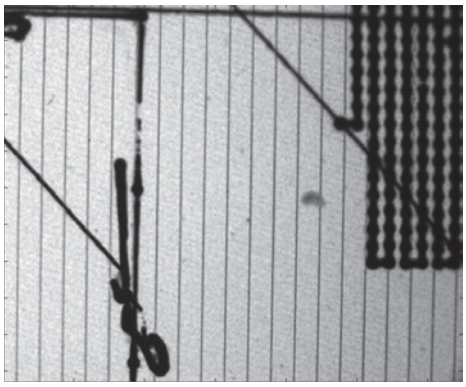

Fig. 2: micro-EL intensity image of laser damage of InGaAs layer of MJSC

3. References

[1] Green, M.A. et al. (2022) "Solar Cell Efficiency Tables (version 60)," Progress in Photovoltaics: Research and Applications, 30(7), pp. 687–701. Available at: https://doi.org/10.1002/pip.3595.
[2] H. Cotal, C. Fetzer, J. Boisvert, G. Kinsey, R. King, P. Hebert, H. Yoon, and N. Karam." III-V multijunction solar cells for concentrating photovoltaics". Energy & Environmental Science, 2:174–192, 2008. A. Bauknecht, S. Siebentritt, J. Albert and M. C. Lux-Steiner. *J. Appl. Phys.* **89** (2001) 4391.
[3] Schultz, R.D. (2015) On the characterisation of diffused light and optical elements in high concentrator photovoltaic modules. thesis.

Spectral conversion in doped BaF_2 crystals for photovoltaic applications

Eduard Madirov[1], **Bryce S. Richards**[1,2], **Andrey Turshatov**[1]

[1] *Institute of Microstructure Technology, Karlsruhe Institute of Technology, Hermann-von-Helmholtz-Platz 1, 76344 Eggenstein-Leopoldshafen, Germany*
[2]*Light Technology Institute, Karlsruhe Institute of Technology, Engesserstrasse 13, 76131 Karlsruhe, Germany*
Corresponding author e-mail address: eduard.madirov@kit.edu

1. Introduction

Finding new ways to improve the performance of existing solar cells is a hot topic. There are several approaches to overcome this challenge. The combination of solar cells with a material capable of spectral conversion is one of the methods attracting considerable attention [1].

Fluorides possess key properties such as low phonon energy and good chemical stability, which make them promising inorganic hosts for spectral conversion materials. Er^{3+}/Yb^{3+} is a pair of doping ions that can be used to obtain a wide range of absorption and emission bands, enabling multiphoton processes such as upconversion (UC) or down-shifting (DS). It has been reported that high values of luminescence quantum yield (ϕ) can be obtained when doped into a crystalline host with MF_2 (M=Ca, Sr) structure [2]. The next ion in this series is Ba^{2+}. According to previous research, larger size of the cation leads to higher efficiency of the energy conversion process. In order to study these materials, two series of BaF_2 single crystals co-doped with Yb^{3+}(2-15 mol. %)/Er^{3+}(2 mol. %) and Yb^{3+}(3 mol. %)/Er^{3+}(2-15 mol. %) as well as a series of single crystals doped with Er^{3+}(2-25 mol. %) were prepared.

2. Results

Co-doped samples were used to obtain UC emission under NIR excitation. The ϕ_{UC} values were obtained under 976 nm excitation in a wide intensity range from 0.1 to 490 W/cm^2.The highest ϕ_{UC} value of 10.0 % is found in the BaF_2: Yb^{3+}(3 mol. %)/Er^{3+}(2 mol. %) sample under 490 W/cm^2 of 976 nm excitation (Fig.1) [3]. This is comparable to the highest reported ϕ_{UC} value of 10.5 % found in β-$NaYF_4$: 21.4 mol.% Yb^{3+}, 2.2 mol.% Er^{3+} particles[4].

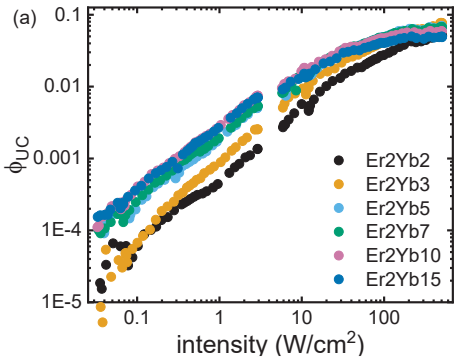

Fig. 1: ϕ_{UC} of the BaF2:Er/Yb samples under 976 nm excitation.

Single-doped samples are used to study the DS emission upon excitation in the visible region. In a certain concentration range of Er^{3+} ions (3-12 mol. %) ϕ_{DS} values exceed 100 % under 405 nm excitation, indicating the presence of quantum cutting process.

BaF_2:Yb^{3+}(15 mol.%)/Er^{3+}(2 mol.%) was tested as a spectral conversion material that can enhance the response of perovskite solar cells. The crystal was designed to convert sub-bandgap near infrared photons into the visible region, where perovskite solar cells have maximum response. When tested under a combination of simulated terrestrial sunlight (above the perovskite's bandgap) and sub-bandgap illumination at 980 nm, the upconverted photons contributed to a 0.38 mA/cm^2 increase in short circuit current density (J_{sc}) at an intensity of ~100 suns[5].

BaF_2: Er^{3+}(3-12 mol. %) crystals are combined with a Ge-photodiode in order to test the possibility of enhancing the spectral response of photovoltaic elements with maximum sensitivity in the NIR spectral region. Under simulated terrestrial sunlight in the range of 350 – 850 nm, an enhancement of 0.5 mA/cm^2 in J_{sc} was observed.

3. References

[1] B. S. Richards, et al., *Chem. Rev.*, **121**, (2021), 9165-9195.
[2] D. Saleta Reig, et al., *J. of Mater. Chem. C*, **8**, (2020), 4093-4101.
[3] E. I. Madirov, et al., *J. of Mater. Chem. C*, **9**, (2021), 3493-3503.
[4] M. Kaiser, et al., *Nanoscale*, **9**, (2017), 10051-10058.
[5] R. Singh, et al., *ACS Appl. Mater. Interfaces*, **13**, (2021), 54874-54883.

Fundamentals and applications of upconversion in lanthanide-doped alkaline-earth fluorides

Andrey Turshatov, Eduard Madirov, Dmitry Busko, Ian A. Howard, Bryce S. Richards

[1] *Institute of Microstructure Technology, Karlsruhe Institute of Technology, Hermann-von-Helmholtz-Platz 1, 76344, Eggenstein-Leopoldshafen, Germany*
Corresponding author e-mail address: andrey.turshatov@kit.edu

1. Introduction

The synthesis of materials with efficient upconversion (UC) luminescence is a hot topic in the field of materials science due to their use in a variety of applications. These include photovoltaics, security markers, luminescent thermometry, tracers for advanced plastic sorting and many others. In case of materials doped with lanthanides the UC is usually realised *via* excited state absorption, photon avalanche or energy transfer up-conversion (ETU). ETU is the mechanism that provides highest photoluminescence quantum yield (ϕ_{UC}) under the intensity that can considered low in other cases (< 40 W/cm^2). Recently there has been increasing attention to ETU UC in crystalline materials with MF_2 (M = Ca, Sr, Ba, Pb) hosts doped with Er^{3+} and Yb^{3+}[1,2]. These hosts generally have cubic unit cell that is considered unfavourable for radiative transitions and efficient energy transfer between doping ions, which is crucial for ETU process. However, when doped with trivalent lanthanide ions the symmetry of the local surrounding reduces increasing the probability of the transitions. This happens because trivalent ions substitute divalent cations and require charge compensation via negative fluoride ions (F^-). As well as this, MF_2 hosts tend to have phonon energy that is lower than other fluoride hosts (CaF_2 – 320 cm^{-1}, SrF_2 – 284 cm^{-1}, BaF_2 – 240 cm^{-1}, PbF_2 – 257 cm^{-1} *vs* β-$NaYF_4$ – 360 cm^{-1} and LaF_3 – 350 cm^{-1}), which may be advantageous for high ϕ_{UC} values.

2. Results

Our work presents a comprehensive spectroscopic study of CaF_2, SrF_2, BaF_2, PbF_2 crystals doped with Er^{3+} and Yb^{3+}, as well as analysis of single crystals and powder samples by the Judd-Ofelt method. In order to describe the UC properties of the studied materials power density – dependent ϕ_{UC} and decay times under 976 nm excitation as well as down-shifting ϕ_{UC} and decay times under 522 and 652 nm excitation were obtained. Among a number of investigated crystals, an exceptionally high value of ϕ_{UC} = 10% was discovered for the BaF_2:Yb^{3+},Er^{3+} crystal [2]. The BaF_2:Yb^{3+}, Er^{3+} crystal was tested as a spectral conversion material that can enhance the spectral response of perovskite solar cells [3]. The crystal was designed to convert sub-bandgap near infrared photons into visible range, where perovskite solar cells have maximum responsivity (Fig.1). Another interesting application of MF_2 UC crystal is illustrated in Fig.2, where SrF_2:Yb^{3+}, Er^{3+} crystal is utilized as a reference material for determination of ϕ_{UC} of UC nanocrystals (NC) [4]. The intensity dependence of ϕ_{UC} for the NCs determined using the reference crystal exhibits very good agreement with the results obtained with an integrating sphere.

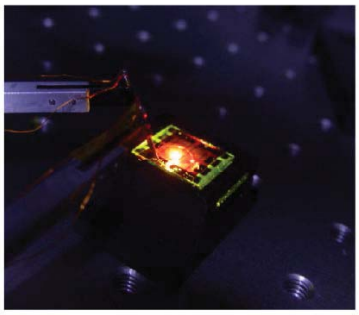

Fig. 1: Image of bifacial solar cell and UC crystal under 980 nm illumination at the intensity of 4.5W/cm^2.

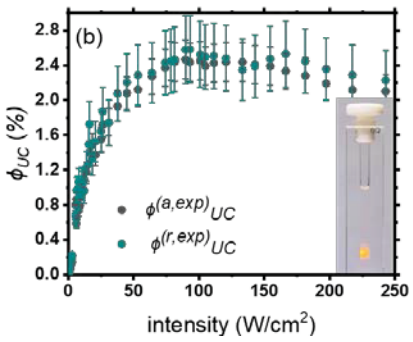

Fig. 2: Intensity dependence of ϕ_{UC} of α-$NaYF_4$: Yb^{3+}, Er^{3+}@CaF_2 NCs estimated using absolute and relative methods. The insert shows the reference crystal in a quartz cuvette under 976 nm excitation.

3. References

[1] D. Reig, B. Grauel, V. Konyushkin, A. Nakladov, P. Fedorov, D. Busko, I. Howard, B. Richards, U. Resch-Genger, S. Kuznetsov, A. Turshatov, and C. Würth *Journal of Materials Chemistry C* **8** (2020) 4093.
[2] E. Madirov, V. Konyushkin, A. Nakladov, P. Fedorov, T. Bergfeldt, D. Busko, I. Howard, B. Richards, S. Kuznetsov, and A. Turshatov *Journal of Materials Chemistry C* **9** (2021) 3493.
[3] R. Singh, E. Madirov, D. Busko, I. Hossain, V. Konyushkin, A. Nakladov, S. Kuznetsov, A. Farooq, S. Gharibzadeh, U. Paetzold, B. Richards, and A. Turshatov *ACS Applied Materials & Interfaces* **13** (2021) 54874.
[4] E. Madirov, D. Busko, F. Cardona, D. Hudry, S. Kuznetsov, V. Konyushkin, A. Nakladov, A. Alexandrov, I. Howard, B. Richards, and A. Turshatov *Advanced Photonics Research* (2022) 2200187.

Red Emission Stimulated by Electric-Dipole Transition of Eu^{3+}-codoped $MgAl_2O_4:Sm^{3+}$ Nanophosphors Synthesized via Citrate Sol-Gel Method: Luminescence Studies

S. Siboza[1], M.R. Mhlongo[1], T.P. Mokoena[1]

[1]Department of Physics, Sefako Makgatho Health Sciences University, P.O. Box 94, Medunsa, 0204, South Africa
Corresponding author e-mail address:teboho.mokoena@smu.ac.za

1. Introduction

Luminescent rare earths activated phosphor materials have shown their worth in different fields of solid state lighting applications, light emitting diodes, illumination, displays, the electronics sector, sensing technologies, biomedical applications, and detection. Samarium (Sm^{3+}) and europium (Eu^{3+}) ions are widely used as activators for red-emitting phosphors because they produce narrowband orange-red luminescence in the spectrum varying from 550 to 650 nm, which is assigned to their $^4G_{5/2}\rightarrow{}^6H_{J/2}$ and $^5D_0\rightarrow{}^7F_J$ transitions, respectively [1]. Magnesium aluminate nanophosphor doped with samarium ions ($MgAl_2O_4$: 1 mol% Sm^{3+}) and co-doped with various concentrations of europium ions ($MgAl_2O_4$): x% Eu^{3+} were prepared by citrate sol-gel method. The crystallography features were confirmed by x-ray diffraction (XRD). The particle morphology and elemental composition were analysed by scanning electron microscopy (SEM), transmission electron microscopy (TEM), and energy dispersive x-ray spectroscopy (EDS), respectively. The luminescence characteristics of nanophosphors were analysed by photoluminescence (PL).

2. Results

Fig.1 presents the PL excitation and emission spectra of nanophosphors monitored at the emission wavelength of 613 nm and excitation wavelength of 240 nm, respectively. The broad peak around 240 nm confirmed the charge transfer band from O^{2-} to Eu^{3+}, and several sharp excitation peaks from 394 to 466 nm were assigned to Eu^{3+} transitions. PL emission spectra confirmed a sharp intense red emission induced by the electric-dipole transition of Eu^{3+} [2]. In Fig.2 the red emission increased with the increase in Eu^{3+} concentrations.

.

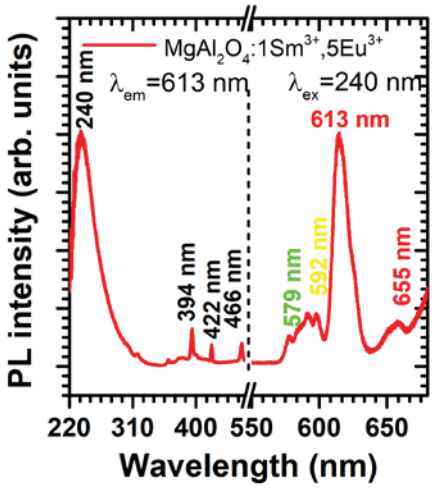

Fig. 1: PL excitation and emission spectra of $MgAl_2O_4:Sm^{3+}$, Eu^{3+} nanophosphors.

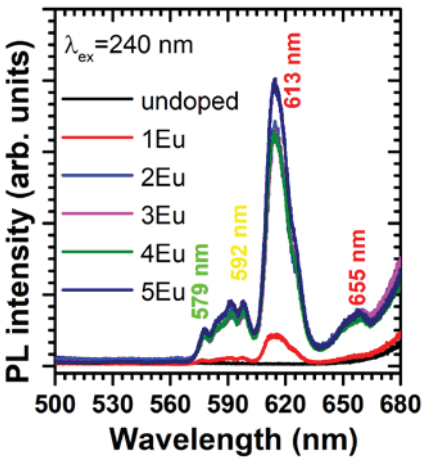

Fig. 2: PL emission spectra of $MgAl_2O_4:Sm^{3+}$, Eu^{3+} nanophosphors under the excitation wavelength of 240 nm.

3. References

[1] Z. Zhang, L. Mei, N. Liu, Q. Guo, L. Liao, *J. Lumin.*, **240** (2021) 118414.
[2] A. Balakrishna, L. Reddy, O.M. Ntwaeaborwa, H.C. Swart, *J. Mol. Struct.*, **1203** (2020) 127375.

Investigating the effects of varying Gd^{3+} concentration on the structure, morphology and photoluminescence properties of $MgAl_2O_4/MgO/BaAl_2O_4/GaAlO_3$: x% Gd^{3+} ($0 \leq x \leq 1.1$) mixed phases via sol-gel method

A. Bele[1*], M.R. Mhlongo[1], L.F. Koao[2], T.E. Motaung[3,4], R. E. Kroon[5], T.T. Hlatshwayo[6], S.V. Motloung[1,7]**

[1]Department of Physics, Sefako Makgatho Health Science University, P. O. Box 94, Medunsa, 0204, South Africa
[2]Department of Physics, University of the Free State (Qwaqwa Campus), Private Bag X 13, Phuthaditjhaba, 9866, South Africa
[3]Department of Chemistry, Sefako Makgatho Health Science University, P. O. Box 65, Medunsa, 0204, South Africa
[4]Department of Chemistry, University of South Africa, P.O. Box 392, UNISA 0003, South Africa
[5]Department of Physics, University of the Free State, P.O. Box 339, Bloemfontein, 9300, South Africa
[6]Department of Physics, University of Pretoria, Pretoria, 0002, South Africa
[7]Department of Chemical and Physical Sciences, Walter Sisulu University, Mthatha, 3886, South Africa

Corresponding authors: abongile.bele@gmail.com and cchataa@gmail.com

1. Introduction

Rare earth ions (RE^{3+}) doped nanophosphors have emerged as materials with great potential in light emitting diode (LED) manufacturing [1]. Although investigations have been done on single phase host materials, a little has been explored on the mixed phases [2-5]. Mixed phases might possibly result on the new and advanced phosphors materials with the combined properties of their bulk counterparts. For an example, Yuan et al. [3] showed that the mixed oxide $ZnO/ZnAl_2O_4$ has excellent stability and much higher photocatalytic activity than their bulk oxide counterparts. This study investigates the effect of varying Gd^{3+} concentration on the structure, morphology and optical properties of $MgAl_2O_4/MgO/BaAl_2O_4/GaAlO_3$:x% Gd^{3+} ($0 \leq x \leq 1.1$) (hereafter called MMBG:x% Gd^{3+}) mixed phases nanophosphor.

2. Results

MMBG:x% Gd^{3+} mixed phases nanophosphors were successfully synthesized via citrate sol-gel method. The effect of varying Gd^{3+} concentration on the structure, morphology and photoluminescence properties of the prepared nanophosphors were investigated. X-ray diffraction (XRD) suggested that the prepared nanophosphor consists of cubic ($MgAl_2O_4$ and MgO), hexagonal ($BaAl_2O_4$) and orthorhombic ($GaAlO_3$) structures. Scanning electron microscopy (SEM) revealed that the morphology of the prepared nanophosphors depends on Gd^{3+} concentration. Energy dispersive spectroscopy (EDS) confirmed the expected elements being Mg, Ba, Al, O and Gd. Transmission electron microscopy (TEM) confirmed that the prepared phosphor particles are in the nanoscale range. Photoluminescence (PL) results in Fig. 1 shows the emission spectra of MMBG:x% Gd^{3+}. The results showed emission peak at 312 which is ascribed to $^6P_{7/2} \rightarrow {}^6S_{7/2}$ Gd^{3+} transition. Other emission peaks at (336 and 616 nm) and (652 and 730 nm) originate from the intrinsic defects within the $BaAl_2O_4$ and $MgAl_2O_4$, respectively. Commission Internationale de l'éclairage (CIE) shows that the Gd^{3+} doped samples emitted violet colour.

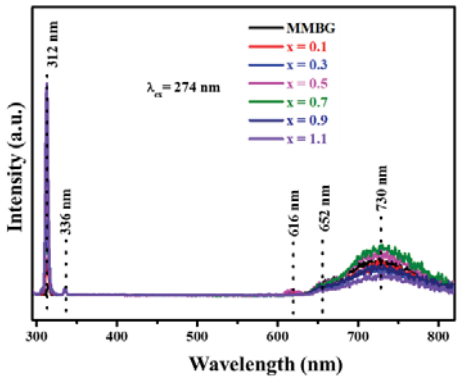

Fig. 1: the emission spectra of MMBG:x% Gd^{3+}

3. References

[1] E.N. Alvar, M. Rezaei, H.N. Alvar. *Powder Tech*. **198** (2010) 275.
[2] Y. H. Li, X.L. Zhang, C.X. Fan, M. Liu, B. Zhai, H. Lin. *Adv. Mat. Res.* **399-401** (2012) 904
[3] X. Yuan, X. Cherng, Q. Jing, J. Niu, D. Peng, Z. Feng, X. Wu. *Mat*. **11** (2018) 1624.
[4] Y. Takebuchi, H. Fukushima, T. Kato, D. Nakauchi, N. Kawaguchi, T. Yanagida. *Jap. J. of App. Phys.* **59** (2020) 052007.
[5] W. Nantharak, W. Wattanathana, W. Klysubun, T. Rimpongpisarn, C. Veranitisagul, N. Koonsaeng, A. Laobuthee,. *J. of All and Comps*. **701** (2017) 1019.

Influence of annealing temperature on the crystal structural, morphology and photoluminescence of $BaAl_2O_4$:Eu

N.J. Shivaramu, E. Coetsee, H.C. Swart

[1]*Department of Physics, University of the Free State, Bloemfontein, ZA-9300, South Africa*
Corresponding author e-mail address: CoetseeE@ufs.ac.za (E. Coetsee)

1. Introduction

Barium aluminate ($BaAl_2O_4$) is one of the best aluminate materials for fabricating light-emitting diodes and long persistent luminescence [1]. Alkaline earth aluminates are chemically and thermally stable at room temperature and atmospheric pressure [1]. Oxygen interstitials or vacancies are created in the barium aluminate matrix after the substitution of trivalent or divalent lanthanide ions at alkaline metal ion sites [1]. Oxygen interstitials and vacancies act as hole and electron traps located above the valence band and below the conduction band of the host. These traps store absorbed energy, which enhances the emission intensities and persistent luminescence. In this study, a $BaAl_2O_4$:Eu (1 mol%) powder was prepared using a solution combustion method and annealed at different temperatures ranging from 900-1300 °C for 2 h in air. X-ray powder diffraction (XRPD), field emission scanning electron microscopy, energy dispersive X-ray spectroscopy and UV-vis diffuse reflectance spectra (DRS) were used to study the influence of annealing on the crystal structure, grain size, morphology, elemental distributions, and optical band gap of the material. The oxidation state of the Eu ion and the luminescence properties were studied using photoluminescence (PL) spectroscopy.

2. Results

The XRPD patterns of the $BaAl_2O_4$: 1 mol% Eu nanophosphors annealed at 1000-1300 °C were in good agreement with the single phase XRPD pattern of $BaAl_2O_4$ (COD # 2002225) [2]. The crystallite size increased from 50 to 70 nm whereas the lattice strain decreased from 0.07 to 0.05 % with an increase in the annealing temperature. The annealed materials exhibited hexagonal shapes with an average grain size of 200 - 530 nm. The Eu-doped $BaAl_2O_4$ showed the characteristic orange emission of Eu^{3+} at 251 nm (see Fig.1(a)) and 464 nm excitations, while excitations at 340, 362 and 380 nm (see Fig. 1(b)) showed white emission. The PL results reveal the presence of Eu^{2+} and Eu^{3+} ions. Energy is transferred from the charge transfer band (251 nm) to the different energy levels of the Eu^{2+} and Eu^{3+} ions (see Fig. 1(a)). Strong emission was observed in the material annealed at 900 °C due to small crystallite and grain sizes of the $BaAl_2O_4$:1 mol% Eu nanophosphor. Oxygen interstitial and vacancies occurred in the Eu-doped $BaAl_2O_4$ nanophosphor due to charge imbalance. The existence of Cr ion impurities in the aluminates was confirmed by UV-vis absorbance and PL spectroscopy. The present results suggest that two positive defects, $2[Eu^{3+}]^{\bullet}_{Ba}$, were created by each substitution of every two Eu^{3+} ions in the compound. The resultants introduced two electron traps and one hole trap in the host that acted as luminescent centers for white emission from $BaAl_2O_4$:Eu^{3+}.

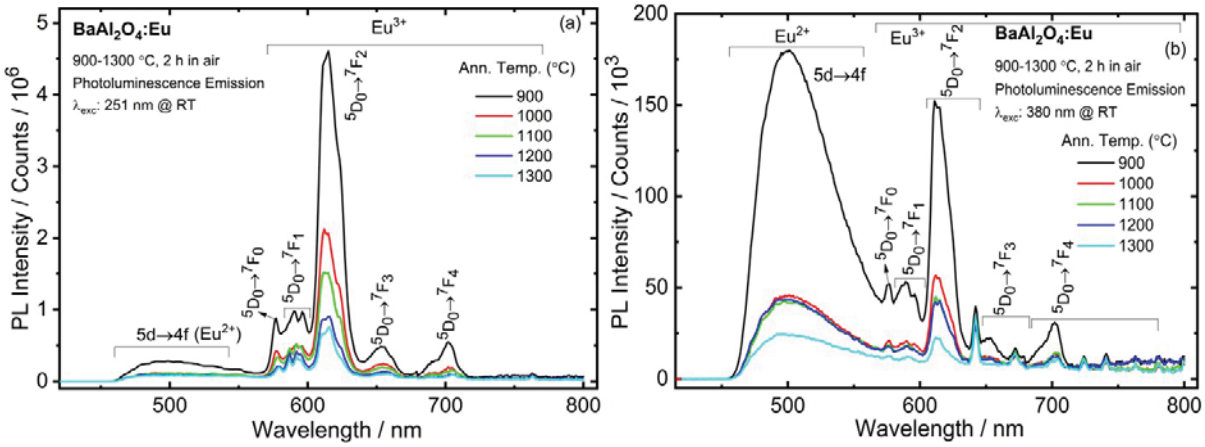

Fig. 1: PL emission spectra for the Eu-doped $BaAl_2O_4$ upon excitation at 251 nm (a) and 380 nm (b).

3. References

[1] M. V. do.S. Rezende, P.J.R Montes, M.E.G. Valerio and R.A. Jackson, *Opt. Mater (Amst).* **83** (2018) 328.
[2] W. Horkner and H. k. Muller-Buschbaum, *Zeitschrift fur anorganische und allgemeine Chemie*, **451** (1979) 40.

Synthesis and the thermometry properties of $Sr_{2.9}Al_2O_5Cl_2:0.1Eu^{2+}$ phosphor

Simon N. Ogugua, Hendrik C. Swart

Department of Physics, University of the Free State, Bloemfontein, ZA9300, South Africa
Corresponding author e-mail address: oguason@yahoo.com

1. Introduction

As a fundamental parameter, temperature governs the basic principles of numerous natural phenomena and industrial processes; for instant, temperature plays a critical role in phenomena such as thermal convection and biological system networking [1,2]. In medicine, enormous heat production is involved in the pathogenesis of diseases such as cancer [3]. In addition, the brain's local temperature and thermal dynamics can help understand its physiology and be used as a diagnostic tool [4]. Temperature sensors are also used in aerosol systems, military applications, home appliances, metrology, agriculture, and turbines. Thermographic phosphors can provide robust solutions for remote temperature measurements. To improve our understanding of the underlying physical, chemical, and biological processes, advanced optical measurement techniques sensitive to the temperature ranges at which these processes operate are essential. Compared to other medical imaging techniques, such as magnetic resonance imaging, positron emission tomography, and computerized tomography by X-rays, luminescence-based temperature imaging produces high-resolution images at a high acquisition rate. It can eliminate the need for ionization radiation or radiative agents. It also requires a relatively simple setup which makes it cost-effective. In addition, it is the only technique that can measure temperature at the intercellular level [2]. Phosphor thermometry is a luminescence-based thermometry technique that utilizes temperature-sensitive powders, usually consisting of host materials doped with small amounts of activator ions such as rare-earth and/or transition metal ions. Thermographic phosphors exhibit a change in the luminescence emission intensity, a change in the emission spectrum, or a decrease in the lifetime with temperature, from which the temperature can be obtained after calibration.

2. Results

Herein, we report the synthesis and luminescence thermometry properties of $Sr_{2.9}Al_2O_5Cl_2:0.1Eu^{2+}$ phosphor derived from the temperature dependent of the luminescence intensity ratio (LIR), and the lifetime, in the temperature range of 23 ˚C to 164 ˚C. The luminescence emission spectrum, excited using the second harmonic (355 nm) of the Nd: YAG laser, covers the entire visible spectrum with two bands at 450 and 600 nm assigned to the 5d→4f transition of Eu^{2+} [5]. The temperature dependent luminescence of the phosphor, Fig. 1(a), showed a strong thermal quenching, and the corresponding relative temperature sensitivity, Fig. 1(b), obtained using the LIR method showed relatively high values around room temperature and a maximum value of ∼1.9 %/K at 48 ˚C. Temperature resolution of 0.34 ˚C at 23 ˚C and 0.29 ˚C at 48 ˚C were obtained from the LIR method. Additionally, the temperature dependent decay curves, Fig. 2(a), showed a strong thermal quenching, with relatively high temperature sensitivity (temperature read out from 600 nm) around room temperature, as shown in Fig. 2(b). Temperature resolutions of 0.09 and 0.05 ˚C were obtained at 23 ˚C and 130 ˚C, respectively, from the lifetime method. These properties suggest that this material has the potential for thermometric applications.

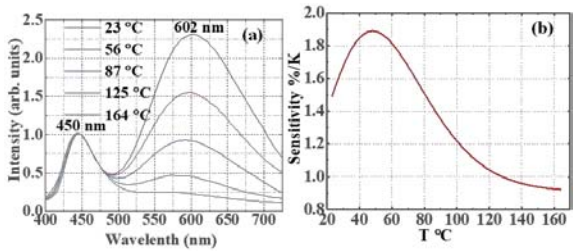

Fig. 1: (a) The temperature dependent luminescence and (b) the relative temperature sensitivity of $Sr_{2.9}Al_2O_5Cl_2:0.1Eu^{2+}$.

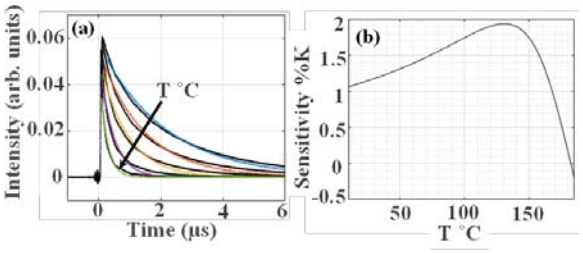

Fig. 2: (a) The temperature dependent lifetime and (b) the relative temperature sensitivity of $Sr_{2.9}Al_2O_5Cl_2:0.1Eu^{2+}$.

3. References

[1] G.M. Laskowski, S.P. Kearney, G. Evans and R. Greif. *Int. J. Heat Fluid Fl.* **28** (2007) 454.
[2] K. Okabe, N. Inada, C. Gota, Y. Harada, TFunatsu and S. Uchiyama. *Nat. Commun.* **3** (2012) 705.
[3] M. Monti, L. Brandt, J. Ikomi-Kumm, H. Olsson. *Scand. J. Haematol.* **36** (1986) 353.
[4] B. del Rosal, D. Ruiz, I. Chaves-Coira, B.H. Juárez, L. Monge, G. Hong, N. Fernández and D. Jaque, *Adv. Funct. Mater.* **28** (2018) 1806088.
[5] Z. Wang, Q. Zhang, M. Rong, H. Tan, Q. Wang, Q. Zhou and G. Chen, *Chem. Phys. Lett.* **658** (2016) 324.

Gallium oxide polymorph heterostructures: physics, fabrication, and potential applications

Andrej Kuznetsov

Department of Physics, University of Oslo, 24 Sem Sælandsvei, N-0371, Oslo, Norway
Corresponding author e-mail address: andrej.kuznetsov@fys.uio.no

1. Introduction

There are no perfectly regular organized systems in nature. In crystals, there are always defects occurring in lattices, e.g. in form of vacancies, helping to decrease the Gibbs energy due to increasing entropy. Nevertheless, on many occasions, structural defects bare a negative connotation, provoking efforts to reduce their contents. On the other hand, many unique material properties may become possible only with defects in materials. In this talk, I will review a recent observation of the disorder-induced ordering in gallium oxide controlled by the accumulation of intrinsic defects.

2. Results

Indeed, polymorphs are common in nature and can be stabilized by applying external pressure in materials. The pressure/strain can also be induced by the gradually accumulated radiation disorder. However, in semiconductors, the radiation disorder accumulation typically results in the amorphization instead of engaging polymorphism. By studying these phenomena in gallium oxide, we found that the amorphization may be prominently suppressed by the formation of a new polymorph. Utilizing this discovery, we fabricated polymorph heterostructures having unprecedently sharp interfaces, potentially applicable in devices. Exploring this system, we detected a novel mode of a lateral polymorphic regrowth not previously observed in solids [1].

3. References

[1] A. Azarov, C. Bazioti, V. Venkatachalapathy, P. Vajeeston, E. Monakhov and A.Yu.Kuznetsov, “Disorder-induced ordering in gallium oxide polymorphs”, Phys. Rev. Lett., 128, 15704 (2022).

Synthesis and electrical characterization of β-Gallium Oxide

Valentine W. Muramba[1,2], Jacqueline M. Nel[1]
[1]*Department of Physics, University of Pretoria, Private bag X20, Hatfield, Republic of South Africa.*
[2]*Department of Mathematics & Physics, Technical University of Mombasa, P.o. Box, 90420-80100 Mombasa, Kenya*

Corresponding author e-mail address: valentinewabwire@gmail.com

1. Introduction

The energy crisis and environment pollution are some of the main global challenges that hampers economic development. Renewable energy including solar, geothermal and wind energy are promising sources of energy that can be converted to electricity to address this global concern. Consequently, research calls on materials effective in enhancement of renewable energy production and also in high powered optical and electronic application is a step in the right direction [1]. Wide band gap semiconductors are appropriately applicable in wind and geothermal energy conversion to electricity and high-power optoelectronics since they commonly have high breakdown voltage, high thermal stability, low ON state resistance, low leakage current and good thermal conductivity [2]. Metal oxides [3], particularly gallium trioxide turns out to be very ideal [4]. They can also be applied in dielectric coatings of solar cells and their passivation to minimize reflection and corrosion to increase their stability and hence lifespan [5]. This project seeks investigation of beta-gallium trioxide (β-Ga_2O_3) for diodes and transistors in electronic application with attention to semiconductor-metal contact as limiting factor to its application. In spray pyrolysis, tetrahydroxogallate (III) ammonium was deposited on 1cm^2-n-type silicon substrate at 200°C and 2.4kPa. Same precursor was applied in spin coating, but its viscosity was improved by the addition of Monoethanolamine. Electrical characterization was done by determining electrical conductivity of the oxide whereas I-V and C-V characterization of metal electrodes were done by Electron Beam Evaporator (EBE).

2. Results

Sprayed sample of 12.5at%, 10at% and 7.5at% demonstrated higher conductivities of 52.6 $\Omega^{-1}cm^{-1}$, 45.9 $\Omega^{-1}cm^{-1}$ and 47.0 $\Omega^{-1}cm^{-1}$ respectively compared to spin coated with 48.6 Ω^{-1} cm^{-1}, 37.5 $\Omega^{-1}cm^{-1}$ and 38.6 $\Omega^{-1}cm^{-1}$. Metal electrodes contacts on 10at% sprayed sample demonstrated ideality factor of 2.05 and best lowest I-V Schottky barrier height (SBH) of 0.37eV compared to spin coated sample of same concentration with ideality factor of 2.34 and SBH of 0.39eV. Built in voltage (V_{hi}) of 0.77 eV and 0.86 eV were also reported for 10at% sprayed and spin coated samples respectively with saturation current (I_S) of 7.03 x 10^{-6} A and 6,98 x 10^{-6} A respectively. These characterization properties placed 10at%β-Ga_2O_3 as optimal concentration of this study with metal stakes of Ti/Al/Ni/Au for ohmic contacts and Pd/Au for schottky contacts for diode electrodes compared to earlier stakes so far reported.

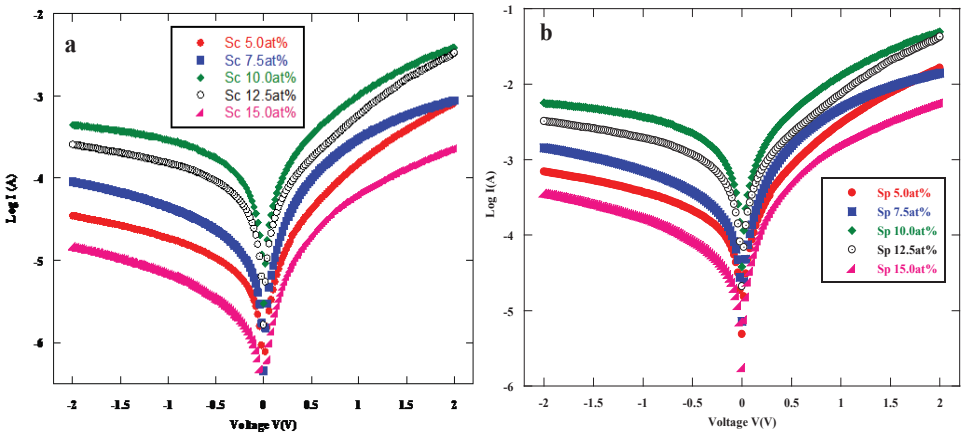

Fig. 1: Comparison of logarithmic I-V characterization of (a) spin coated and (b) pyrolytically sprayed samples of β-Ga_2O_3 at varied concentrations.

3. References

[1]. M.H. Wong, Y. Nakata, A. Kuramata, S. Yamakoshi, M. Higashiwaki (2017), *"Enhancement-mode Ga_2O_3 MOSFETs with Si-ionimplanted source and drain"*, Applied Physics Express 10, 041101; DOI. https://doi.org/10.7567/APEX.10.041101

[2]. Y. Jae-Hyuck, R. Subrina, A. Lange, Z. Hongping, E. Selim (2018); *"Lifetime laser damage performance of β-Ga_2O_3 for high power applications"*, Applied Physics Letters Materials. 6, 036105; https://doi.org/10.1063/1.5021603

[3]. M. Kim, J. Seo, U. Singisetti, Z. Ma (2017), *"Recent advances in freestanding single crystalline wide band-gap semiconductors and their applications: GaN, SiC, ZnO, β-Ga_2O_3, and Diamond"*, Journal of Material Chemistry Vol. 5, 8338–8354; DOI:10.1039/d0nr05860b

[4]. S.J. Pearton . Y. Jiancheng, C.H. Patrick, R. Fangfang, K Jihyun, M.J. Tadjer, M. A. Mastro (2018), *"A review of Ga_2O_3 materials, processing, and devices"*, Applied Physics Reviews Vol 5, Issue No. 011301; https://doi.org/10.1063/1.5006941

[5]. D. Huiyang, K. J. Leedle, Y. Miao, B.S. Dylan, K. E. Urbanek, J. McNeur, M. Kozák, A. Ceballos, P. Hommelhoff, O. Solgaard, R. L. Byer, J. S. Harris (2020); *"Gallium Oxide for High-Power Optical Applications"*,Advanced Optical Materials 8, 1901522 PP. 1-6; https://doi.org/10.1002/adom.201901522

Effect of graphene oxide coatings on the optical properties of pulsed laser deposited ZnO:Zn thin films

B.C. Tladi, H.C. Swart, D.E. Motaung, R.E. Kroon

Department of Physics, University of the Free State, Bloemfontein 9300, South Africa
Corresponding author email address: KroonRE@ufs.ac.za

1. Introduction

Surface coatings have been widely used to improve phosphor characteristics, to increase luminescence intensity and to protect against degradation. Zinc oxide (ZnO) is a wide-gap semiconductor, with a direct energy band gap (3.37 eV) and a large exciton binding energy (60 meV) at room temperature, making it suitable for a wide range of optoelectronic applications [1]. ZnO:Zn phosphor thin films prepared by physical methods may have the characteristics of being smooth and having excellent adhesion to the substrate. However, the key problem is that the luminescent intensity is not sufficient strong compared to that of powder phosphors [2]. By controlling the grain size, morphology, and microstructure by changing the preparation and annealing conditions, both the photoluminescence (PL) wavelength and relative intensity of ZnO can be modulated efficiently [3]. Another means to enhance the PL properties involves the hybridization of the material with carbon-based nanomaterials such as carbon nanotubes, carbon quantum dots, or graphene among carbon allotropes [4]. Considering the excellent properties of graphene oxide (GO), reduced graphene oxide (rGO) and ZnO, the combination of GO/rGO and ZnO particles may provide enhanced performances. ZnO thin films were successfully coated with GO using a nebuliser spray coating and the structural, morphological and optical properties of the films were studied. The samples were also annealed under different conditions to compare the optical properties of the ZnO-GO and ZnO-rGO films.

2. Results

Highly *c*-axis orientated ZnO thin films with a thickness of approximately 183 nm were successfully prepared by pulsed laser deposition. The coated GO sheets showed non-uniform and defective textures on the surface of the ZnO films, while heavily crumbled sheets were observed for rGO annealed in Ar, and wrinkled sheets were observed for rGO annealed in Ar/H_2. PL measurements (Fig. 1) exhibited an ultraviolet band at ~390 nm for the uncoated ZnO film, attributed to the recombination of excitons, and a broad band in the visible range of 400-600 nm centred at ~450 nm attributed to zinc interstitials. The blue emission at ~450 nm of ZnO was enhanced by coating with GO and/or rGO, which was attributed to the coupling of the light emitting centres with localized surface plasmon resonances from the GO/rGO sheets. These results showed a possibility of producing rGO/ZnO:Zn films for different optoelectronic applications such as ultraviolet or blue coloured light emitting diodes.

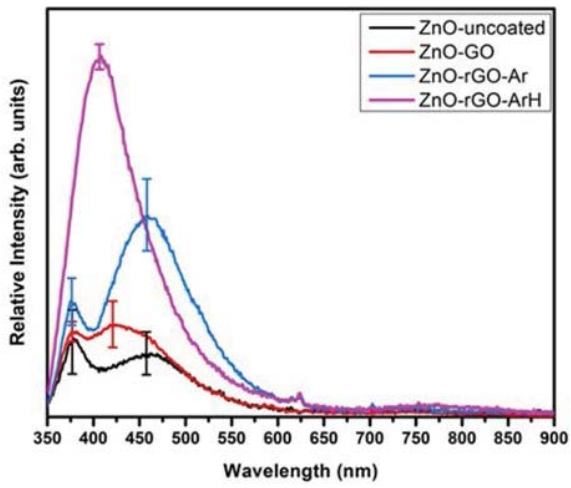

Fig. 1: Emission spectra of ZnO:Zn thin films coated with GO and rGO excited at 325 nm.

3. References

[1] E. Hasabeldaim, O.M. Ntwaeaborwa, R.E. Kroon, V. Craciun, E. Coetsee, H.C. Swart. *Appl. Surf. Sci.* **424** (2017) 412–420.
[2] Z. Wang, C. Lin, X. Liu, G. Li, Y. Luo, Z. Quan, H. Xiang, J. Lin. *J. Phys. Chem. B* **110** (2006) 9469–9476.
[3] Y.T. Li, J.M. Xu, Z.J. Tang, T.T. Xu, X.J. Li. *J. Alloys Compd.* **715** (2017) 122–128.
[4] P. Rauwel, M. Salumaa, A. Aasna, A. Galeckas, E. Rauwel. *J. Nanomater.* **2016** (2016) 5320625.

Strontium vanadate a possible addition to transparent conductive thin films

Edward Lee[1], **Richard A. Harris**[1], **Jacobus J. Terblans**[1], **Hendrik C. Swart**[1]

[1] *Department of Physics, University of the Free State, Bloemfontein, South Africa.*
Corresponding author e-mail address: LeeE@ufs.ac.za

1. Introduction

Transparent conductive oxide (TCO) thin films have received significant interest in recent years because they are transparent in the visible light region while still being electrically conductive. Currently, indium tin oxide (ITO) films are the most widely used TCO, making up close to 90 % of the commercial applications such as: displays, electronic, and energy devices. Tin doped indium oxide (ITO) has seen some adoption in electronic applications due to its wide transparency in the visible region (> 85 %), high electrical conductivity, and carrier concentration on the order of 10^{-4} Ω cm and 10^{21} cm^{-3} respectively[1]. However, indium resources are of great concern due to their increasing scarcity, resulting in a limited supply and higher cost[2]. Therefore, it is desirable to develop a cost-effective ITO alternative. Strontium vanadate ($SrVO_3$) was first synthesised in the 1950's and was later shown to exhibit metal-like electronic properties[3]. Early reports showed that $SrVO_3$ thin films with a thickness of 12 nm displayed a resistivity of 4.15 x 10^{-5} Ωm with a transparency of 80 % in the visible region[4]. More importantly, the cost of the raw materials was significantly lower than that of ITO.

2. Results

The XRD pattern of the as prepared powder product and the effect of annealing time in a reducing atmosphere on the final phase of the product is shown in Fig 1. All reflections of the as prepared product indicated the formation of $Sr_2V_2O_7$ with a triclinic crystal structure in space group $P\bar{1}$. A phase transformation from a triclinic to a trigonal crystal structure was observed and found to be $Sr_3(VO_4)_2$ in space group $R\bar{3}m$ after annealing for 8 h with some triclinic structure still present. After 24 h of annealing only trigonal $Sr_3(VO_4)_2$ structures were observed. Finally, after 48 h of annealing, a cubic crystal structure corresponding to that of $SrVO_3$ in the space group $Pm\bar{3}m$ was achieved with some $Sr_3(VO_4)_2$ still present. To study the resistivity of $SrVO_3$ thin films, pulsed laser deposition (PLD) was used to produce the thin films. During deposition, parameters such as the laser energy (40 mJ), argon pressure (40 mTorr) and number of pulses (20 000 pulses) were kept constant, while the substrate temperature was changed (22 ºC, 150 ºC and 300 ºC) to study their effects on the final thin films. Fig 2 shows the current density vs voltage curve of $SrVO_3$ thin films prepared at the above-mentioned substrate temperatures and shows that heating the substrate to 150 ºC during deposition yielded the lowest resistance and in turn the lowest resistivity.

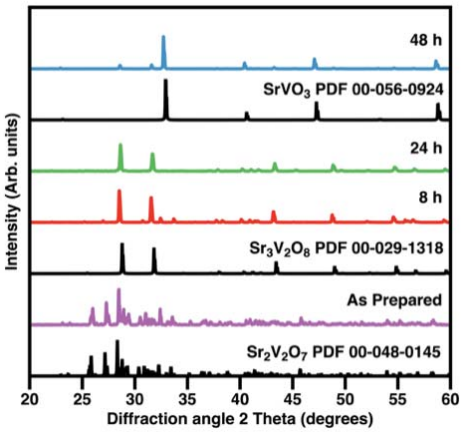

Fig. 1: X-ray powder diffraction patterns of the as prepared $Sr_2V_2O_7$ and after various annealing times.

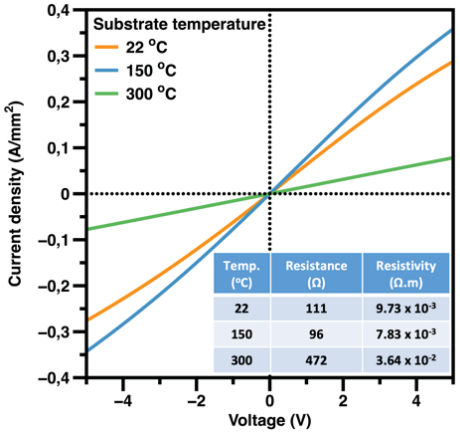

Fig. 2: Current density as a function of voltage curve of $SrVO_3$ thin films prepared with varying substate temperatures.

3. References

[1] Jayathilake D.S.Y., Nirmal Peiris T.A. SF J Material Chem Eng. **1(1)** (2018) 1004.
[2] Lokanc, M., Eggert, R. and Redlinger, M. The Availability of Indium: The Present, Medium Term, and Long Term, Colorado, NREL (2015).
[3] Kestigian, M.J., Dickinson, J.G. and Ward, J. (1957) J. Am. Chem. Soc. **79** (1957) 5589.
[4] Frank G., Köstlin H. *Appl. Phys. A* **27** (1982) 197–206.

Wednesday 10 May

Time	Activity
07:00 – 08:00	Breakfast
	PRESENTATION SESSION 4: Chairperson – **Richard Harris**
08:00 – 08:10	Announcements
08:10 – 08:50	Plenary Talk 2: **Bryce Richards** A load of rubbish or a big opportunity for luminescent materials?
08:50 – 09:10	Presentation 11: **Jorma Hölsä** Persistent Luminescence of $Sr_3SiO_5:Eu^{2+},R^{3+}$ (R: Y, La-Nd, Sm-Lu)
09:10 – 09:30	Presentation 12: **Govind Nair** Rod-shaped LaOF:Yb^{3+},Er^{3+} upconversion nanoparticles for nanothermometry
09:30 – 09:50	Presentation 13: **Ivan Ivanov** Vanadium in 3C-SiC: Efficient emitter in the optical telecom band
09:50 – 10:00	Discussion
10:00 – 10:20	Tea & Coffee break
	PRESENTATION SESSION 5: Chairperson – **Koos Terblans**
10:20 – 10:40	Edinburgh Instruments Presentation
10:40 – 11:10	Invited Talk 4: **Weimin Chen** Towards fully spin- and optically-polarized light-emitting semiconductor nanostructures for room-temperature opto-spintronics
11:10 – 11:30	Presentation 14: **Irina Buyanova** Design Rules for an Efficient Photon Upconversion in Semiconductor Nanostructuctures
11:30 – 11:50	Presentation 15: **Emad Hasabeldaim** Stability of Y_2O_3:Tm,Yb phosphor thin films during upconversion and cathodoluminescence
11:50 – 12:10	Presentation 16: **Assane Talla** Temperature-dependent photoluminescence characteristics of bulk anatase TiO_2 crystal
12:10 – 12:20	Discussion
12:20 – 13:20	Lunch
	PRESENTATION SESSION 6: Chairperson – **Reinhardt Botha**
13:20 – 13:40	Presentation 17: **Irfan Ayoub** Structural and Optical Characteristics of Green Emitting Tb^{3+} Doped $BaGd_2ZnO_5$ Nanophosphor for LED Applications
13:40 – 14:00	Presentation 18: **Zelalem Urgessa** Structural characteristics of anodic TiO_2 on titanium foil after annealing in oxygen-rich atmosphere
14:00 – 14:20	Presentation 19: **Michael Lee** SHI radiation induced tetragonal transformation in bulk monoclinic zirconia
14:20 – 14:40	Presentation 20: **Rebecca Letsoalo** Fabrication, characterization, and gas detection performance of Co_3O_4 hierarchical structures
14:40 – 14:50	Discussion
17:40 – 19:30	Poster Session
19:30 – 21:00	Dinner

A load of rubbish or a big opportunity for luminescent materials?

Bryce S. Richards [a,b*], Dmitry Busko [a], Damien Hudry [a], Ian A. Howard [a,b], Andrey Turshatov [a]

Karlsruhe Institute of Technology (KIT), Hermann-von-Helmholtz-Platz 1, 76344 Eggenstein-Leopoldshafen, Germany:
[a] Institute of Microstructure Technology (IMT)
[b] Light Technology Institute (LTI)
** Corresponding author e-mail address: bryce.richards@kit.edu*

The production of high-quality plastic recyclate to replace virgin polymer resins is viewed as being a cornerstone for achieving a circular economy. Several polymers are known to be difficult to recycle (e.g. polypropylene), while others should be retained separately to maintain their position in the value chain. Three examples of the latter case are: i) food and non-food grade plastics; ii) bio-derived polymers; and iii) certain large producers who want to mark their own packaging for internal reprocessing.

Introducing luminescent taggants into plastics can allow rapid automated sorting into such streams and allow these to be differentiated beyond the chemical classification of near infrared (NIR)-based sorting. In this presentation, photonic markers based on upconversion materials are investigated as another promising option. Phosphors - typically excited at 980nm - exhibit unique upconversion emission spectra ranging from the blue to 800nm. These can be introduced directly into plastic (allowing sorting post shredding) or into package labelling. The number of fluorescent taggants required to tag a wide range of polymers relies on the number of realisable UC material systems, along with the resolution at which the luminescence signal can be readout (differentiated). This presentation will discuss the potential for such luminescent taggants for achieving a circular economy, alongside the most important material considerations.

Persistent Luminescence of $Sr_3SiO_5:Eu^{2+},R^{3+}$ (R: Y, La-Nd, Sm-Lu)

Aleksei Kotlov[1], Taneli Laamanen[2], Mika Lastusaari[2], Marja Malkamäki[2], Edmund Welter[1], Dariusz Hreniak[3], Hendrik C. Swart[4], Jorma Hölsä[2,3,4]

[1]Deutsches Elektronen-Synchrotron, a Research Centre of the Helmholtz Association, Hamburg, Germany
[2]University of Turku, Department of Chemistry, Turku, Finland
[3]Institute of Low Temperature and Structure Research, PAN, Wroclaw, Poland
[4]University of the Free State, Department of Physics, Bloemfontein, South Africa
Corresponding author e-mail address: jholsa@utu.fi

1. Introduction

The composition of persistent luminescence materials must be carefully thought over: at the same time a *stable but flexible host* must accommodate an *efficient dopant (absorber/emitter)* with *suitable excitation/emission* properties and, most of all, a *co-dopant able to form traps* for energy store. Triple (or quadruple if the host is counted in) combinations stand out from the crowd: silicate (eg Sr_3SiO_5) or aluminate (eg $Sr_2MgSi_2O_7$) hosts with Sr^{2+} site(s) to accommodate the efficient (band - not line - emitter with *small Stokes shift*) optically active centre (eg Eu^{2+}) and the R^{3+} co-dopant(s) as trap forming unit(s). A Sr^{2+} host is required to eliminate charge compensation (CC) problems between the dopant and host cations (Sr^{2+} vs Eu^{2+}: the *same size* [1] and *charge*). Less clear in this, if one can say, Holy Trinity is why the Dy^{3+} is the co-dopant. The role of Dy^{3+} as an electron trap due to excess positive charge in the $R_{Sr}^{\bullet}$ substitutional site is clear but why not any other R^{3+} (or other M^{3+}) co-dopant? In this contribution solutions to the remaining issues of persistent luminescence are sought for. The reader can judge if the authors have succeeded in this task where so many others have done less well during the last 26 years… [2].

2. Results

The R^{3+} doping increased both the intensity and duration of persistent luminescence of Eu^{2+} doped Sr_3SiO_5 without changing the Eu^{2+} band position or shape. That said, Fano resonance [3] where interference with the band produces an asymmetric line-shape, was observed with Nd^{3+} co-doping. The duration of persistent emission was enhanced the most by Nd^{3+}, not by Dy^{3+}. This may be due to the structural details favouring Nd^{3+} instead of Dy^{3+}.

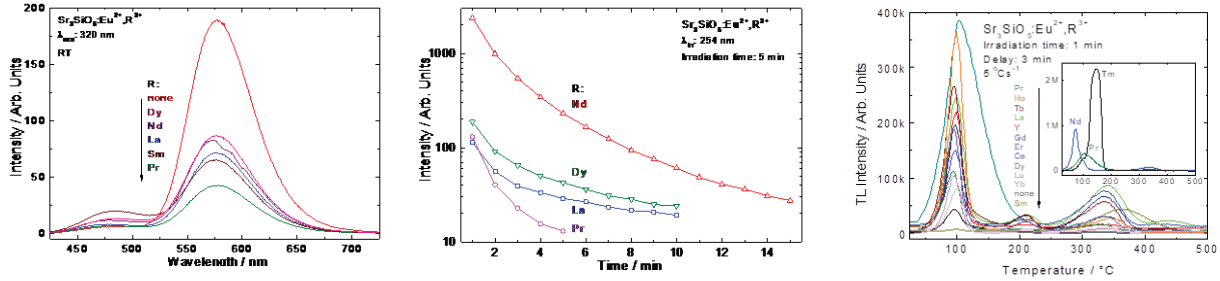

Fig. 1: UV excited (left), duration of persistent luminescence (middle) and thermoluminescence (TL) glow curves (right) of $Sr_3SiO_5:Eu^{2+},R^{3+}$.

The dominant TL band is at ca 100 ºC which is a bit too high a temperature (too deep trap) for efficient RT persistent luminescence. The weaker TL bands are at too high temperatures. Rate of trap's bleaching depends exponentially on the trap depth and thus even very small differences in the trap depths count.

The phosphor compound should be neutral. Excess positive charge due to R^{3+} doping should be neutralized. The actual CC scheme should consume as little energy as possible and thus the introduction of omnipresent oxygen as O^{2-} should be preferred. This requires some space in the crystal structure which is usually readily available in silicates/aluminates as voids or channels. Indeed, there is just enough space in the Sr2 layer to replace non-bonding Sr2-Sr2 with a R^{3+}-O^{2-}- R^{3+} chain (Fig. 2). This arrangement enhances the energy transfer between R^{3+} (co)dopants as observed for the easy quenching of the $^5D_3$ emission in Tb^{3+} doped $Ba_2Al_2O_4$ even on trace Tb^{3+} levels [5].

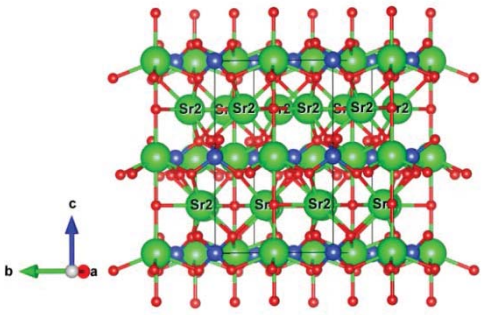

Fig. 2: Crystal structure of $Sr_3SiO_5:Eu^{2+},R^{3+}$.

3. References

[1] RD Shannon, *Acta Cryst A.* **32** (1976) 751.
[2] Adries Meijerink posed a question to JH at 4PPP (Beijing, 2018): Jorma, do you know why the Sr + Eu + Dy combination gives (always) the best persistent luminescence? Reply: Not completely but I'll find it out. Then came the Covid 19… but that's another story.
[3] AK Kunti, HC Swart, J Hölsä, unpublished (2019).
[4] U Fano, *Phys. Rev.* **124** (1961) 1866.
[5] NJ Shivaramu, E Coetsee, J Hölsä, HC Swart, submitted (2023).

Rod-shaped LaOF:Yb^{3+},Er^{3+} upconversion nanoparticles for nanothermometry

Govind B. Nair[1], **Sumedha Tamboli, S. J. Dhoble**[2], **H. C. Swart**[1]

[1] *Department of Physics, University of the Free State, P. O. Box 339, Bloemfontein, 9300, South Africa*
[2] *Department of Physics, R.T.M. Nagpur University, Nagpur, 440033, India*
Corresponding author e-mail address: Nair.GB@ufs.ac.za

1. Introduction

Luminescence thermometers operating in the biological windows (BW) are significant due to their ability to use the wavelengths that are least absorbed by the biological tissues [1]. Lanthanide (Ln^{3+})-doped nanophosphors, that are excited by near infra-red (NIR) light and produce emissions in the spectral regions covered under the BWs, would assist in the precise diagnosis and treatment of diseases in the biological tissues. The BWs are divided into four regions: I, II, II and IV. Among these, the first biological window is the most explored region for nanothermometry [2]. However, interest in other regions is also increasing as they grant the advantage of better contrast and higher penetration depth within the tissue. Phosphors doped with Er^{3+} and Yb^{3+} are the most explored materials for luminescence nanothermometry of the BWs. The strong NIR absorption of Yb^{3+} and the emissions of Er^{3+} in the BW I and II provide a superior strategy for temperature-sensing. In this work, rod-shaped LaOF:Yb^{3},Er^{3+} upconversion nanophosphors (UCNPs) were prepared using a microwave-assisted hydrothermal method. Their photoluminescence (PL) emissions in the NIR region and the UC emissions in the visible region were studied for nanothermometry applications.

2. Results

The LaOF:Yb^{3},Er^{3+} UCNPs exhibited a trigonal phase (space group $R\bar{3}m$) and rod-shaped morphology. The optical band gap of the UCNPs decreased with Er^{3+}-doping. The optimal Er concentration was determined to be 0.02. The UCNPs showed intense UC emissions in the green and red regions under 980 nm excitation. The UC emissions in the red region were interesting because they fell under the first BW. The UCNPs showed NIR emissions in the third BW when excited by a 980 nm laser. The UC and NIR emissions were recorded by varying the temperature from 303 to 573 K and the relative intensities of the thermally coupled and non-thermally coupled levels were studied as shown in Fig. 1 and 2.

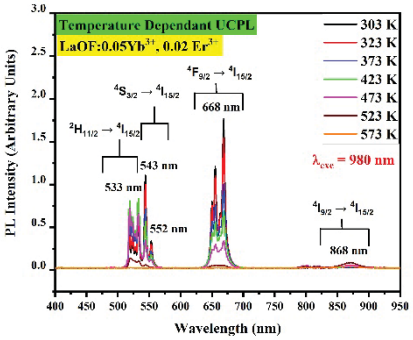

Fig. 1: Temperature dependent UCPL spectra of LaOF:Yb^{3+},Er^{3+} UCNPs.

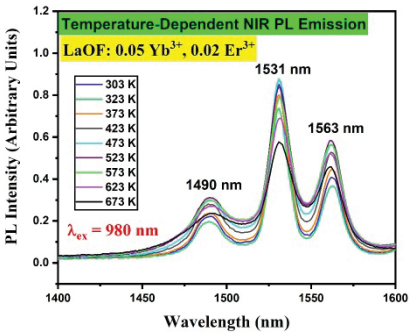

Fig. 2: Temperature dependent NIR PL spectra of LaOF:Yb^{3+},Er^{3+} UCNPs.

3. References

[1] A. Bednarkiewicz, L. Marciniak, L. D. Carlos, and D. Jaque. *Nanoscale*. **27** (2020) 14405-14421.
[2] A. Nexha, J. D. Carvajal, M. C. Pujol, F. Diaz and M. Aguilo. *Nanoscale*. **17** (2021) 7913-7987.

Vanadium in 3C-SiC: Efficient emitter in the optical telecom band

Ivan G. Ivanov[1], **Danial Shafizadeh**[1], **V. Jokubavicius**[1], **Rositsa Yakimova**[1], **Adam Gali**[2,3], **Nguyen T. Son**[1]

[1]*Department of Physics, Chemistry and Biology, Linköping University, IFM/Fysikhuset, 581 83 Linköping, Sweden*
[2]*Department of Atomic Physics, Budapest University of Technology and Economics, Budafoki út 8., Budapest H-1111, Hungary*
[3]*Wigner Research Centre for Physics, P.O. Box 49, Budapest H-1525, Hungary*
Corresponding author e-mail address: ivan.gueorguiev.ivanov@liu.se

1. Introduction

The photoluminescence (PL) spectrum of vanadium (V) in the hexagonal 4H- and 6H-SiC polytypes has been known for three decades [1]. The PL emission from V in the cubic 3C-SiC was deemed impossible because the corresponding excited state of the neutral V^{4+} donor was estimated to be resonant with the conduction band [2]. Nevertheless, in subsequent work the same authors clearly observe an absorption peak from V^{4+} in magnetic circular dichroism of absorption (MCDA) [3]. The peak is unambiguously related to V^{4+} because the MCD-EPR (EPR - electron paramagnetic resonance) spectrum measured with optical detection on this peak exhibits the characteristic eightfold splitting associated with the nuclear spin (7/2) of ^{51}V. In addition, later work reported on PL in the range of 1495 nm, presumably associated with vanadium [4]. This spectral position is advantageous for quantum communications because it falls in the S-band near the minimum of the fiber transmission losses in the telecom optical wavelength bands (see Fig. 1). This makes V in 3C-SiC beneficial for use, e.g., as a single photon emitter in quantum communications, thereby stimulating further studies of this defect.

2. Results and discussion

Our experiments with PL investigation of newly grown 3C-SiC samples intentionally doped with V show unambiguously that the doublet observed around 1495 nm is related to vanadium in 3C-SiC, thus contradicting the previous notion that luminescence from V in 3C-SiC cannot be observed. The PL spectrum of V in 3C-SiC is compared to the known V spectra in 4H- and 6H-SiC in Fig. 2. We notice that the observed spectral doublet in 3C-SiC, 1494 and 1496 nm (0.8298 and 0.8286 eV, respectively) is essentially at the same position as the absorption peak observed in MCDA in [3], 0.828 eV [3]. Failure to observe the PL of V in 3C-SiC in the early work is most likely attributed to inferior sample quality.

We discuss further the electronic structure of the V defect in 3C-SiC and we show that the V emission in 3C-SiC can be viewed as due to recombination of an exciton bound to V. This is in contrast to the model developed for 6H-SiC (applicable also for 4H-SiC) which considers intracentre transitions described in early work in the frame of a crystal-field model. By examining the temperature dependence of the PL spectrum, we show that the observed doublet is due to splitting of the ground state of the defect, most likely caused by Jahn – Teller effect. No further excited states appear in the temperature dependence of the spectrum, and we discuss the apparent difference from the hexagonal polytypes, for which the excited state also exhibits a few-millielectronvolt split-off counterpart seen at slightly elevated temperature (cf. the inset in Fig. 2). We present also detailed data on the excitation properties of V in 3C-SiC (photoluminescence excitation spectroscopy).

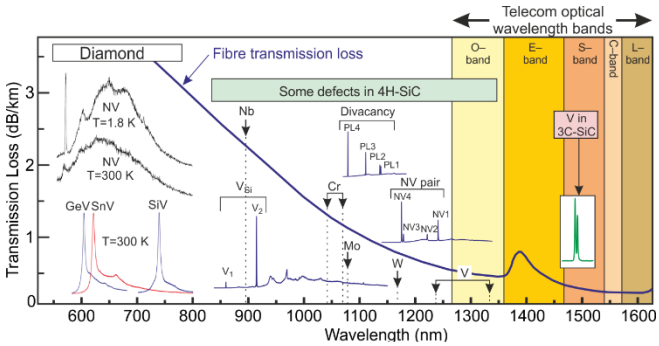

Fig. 1: Spectral positions of the PL emission of several defects in diamond and 4H-SiC compared to the PL spectrum of V in 3C-SiC. The corresponding defects in 6H-SiC are in the same range as in 4H-SiC. The approximate fiber transmission loss and the telecom bands are indicated.

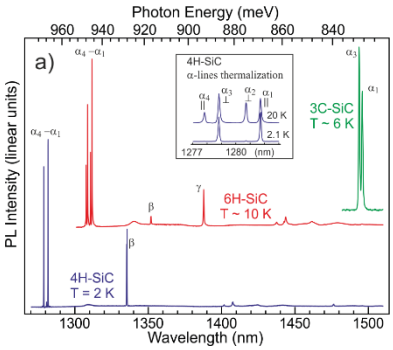

Fig. 2: Comparison between the low-temperature PL spectra of V in 3C-, 4H- and 6H-SiC. The inset shows the thermalization of the α -lines in 4H-SiC, observed also in 6H-SiC, but not in 3C-SiC.

3. References

[1] J. Schneider, H.D. Müller, et al., Appl. Phys. Lett. 56, 1184 (1990).
[2] K.F. Dombrowski, U. Kaufmann, et al., Appl. Phys. Lett. 65, 1811 (1994).
[3] K.F. Dombrowski, U. Kaufmann, et al., Phys. Rev. B 50, 18034 (1994).
[4] R. Yakimova, I.G. Ivanov, et al., ECS J. Solid State Sci. Technol. 6, P741 (2017).
[5] B. Kaufmann, A. Dörnen, F.S. Ham, Phys. Rev. B 55, 13009 (1997).

Towards fully spin- and optically-polarized light-emitting semiconductor nanostructures for room-temperature opto-spintronics

Y.Q. Huang[1], V. Polojärvi[2], S. Hiura[3], P. Höjer[1], A. Aho [2], R. Isoaho[2], T. Hakkarainen[2], M. Guina[2], S. Sato[3], J. Takayama[3], Akihiro Murayama[3], I.A. Buyanova[1], W.M. Chen[1]

[1] Department of Physics, Chemistry and Biology, Linköping University, Sweden
[2] Optoelectronics Research Centre, Physics Unit, Tampere University, Finland
[3] Faculty of Information Science and Technology, Hokkaido University, Japan
Corresponding author e-mail address: weimin.chen@liu.se

1. Introduction

Spintronics represents a new paradigm for future electronics, photonics and information technology, which explores the spin degree of freedom of the electron for information storage, processing and transfer. Since 1990s, we have witnessed great success of metal-based spintronics that has revolutionized the mass data storage industry. There has also been an enormous push for semiconductor spintronics during the past three decades, with the aim to capitalize the past and current success of charge-based semiconductor technology and to make its spin counterpart the backbone of future spintronics just like semiconductors have done in today's electronics/photonics.

An exclusive advantage of semiconductor spintronics is its potential for opto-spintronics that will allow integration of spin-based information processing and storage with photon-based information transfer and communications on the same chip based on a single material/technology platform. Unfortunately, progresses of semiconductor spintronics and opto-spintronics have so far been severely hampered by the failure to generate nearly fully spin-polarized charge carriers and associated fully polarized light emissions in semiconductors at and above room temperature (RT) at which today's devices operate. To date, the highest conduction electron spin polarization achievable at RT remains ≤60% (see Fig.1).

2. Results

In this work, we succeed to achieve conduction electron spin polarization and the resulting circular polarization of light emission exceeding 90% at RT in a semiconductor nanostructure, which remains steadily high even up to 110°C [1]. This represents the highest value ever reported in any semiconductor by any approach! This breakthrough is accomplished by a conceptually new approach of defect-engineered remote spin filtering and amplification of InAs quantum-dot (QD) electrons via an adjacent tunnelling-coupled GaNAs quantum well acting as a spin filter. The extraordinary spin filtering effect in GaNAs is enabled by spin-dependent recombination via spin-polarized defects, i.e. grown-in Ga self-interstitials, which selectively deplete conduction electrons with an opposite spin orientation to that of the defect electron. In sharp contrast to the general trend of deteriorating spin polarization with increasing temperature seen in all other approaches of spin generation as seen in Fig.1, our approach is gifted with an opposite temperature dependence up to RT thanks to a thermally accelerated remote spin-filtering effect as a result of thermally activated recombination via the defects. We further show that the QD electron spin can be remotely manipulated by spin control in the adjacent spin filter, paving the way for remote spin encoding and writing of quantum memory as well as for remote spin control of spin-photon interfaces. The fact that the demonstrated spin functionality is implemented in a commonly used semiconductor optoelectronic nanostructure system (i.e. InAs/GaAs QDs) based on the mature GaAs technology can greatly facilitate the integration of spin functionalities with the existing electronic and photonic devices. It could also pave the way for a range of potential spintronic and opto-spintronic applications exploiting the state-of-the-art GaAs technology platform, such as spin-LEDs, spin lasers, spin-polarized single-photon sources, quantum spin-photon interfaces, spin qubits, etc. This work demonstrates the feasibility to implement opto-spintronic functionality under practical device operation conditions in a semiconductor nanostructure system based on the mature III-V semiconductor technology commonly used for today's optoelectronics and photonics.

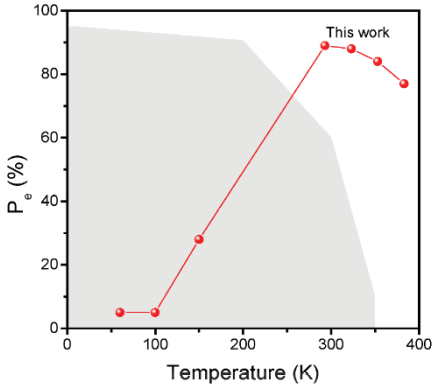

Fig. 1: State-of-art spin generation in semiconductor materials. The steady-state conduction electron spin polarization P_e achieved in this work. The grey shaded area indicates the range of the measured P_e and measurement temperature where earlier studies have been restricted to.

3. References

[1] Y.Q. Huang, V. Polojärvi, S. Hiura, P. Höjer, A. Aho, R. Isoaho, T. Hakkarainen, M. Guina, S. Sato, J. Takayama, A. Murayama, I.A. Buyanova and W.M. Chen, *Nature Photonics* **15**, (2021) 475.

Design Rules for an Efficient Photon Upconversion in Semiconductor Nanostructuctures

Mattias Jansson[1], Fumitaro Ishikawa[2], Weimin M Chen[1] and Irina A. Buyanova[1]

[1] Department of Physics, Chemistry and Biology, Linköping University, SE-58183 Linköping, Sweden
[2] Research Center for Integrated Quantum Electronics, Hokkaido University, Sapporo 060-8628, Japan
Corresponding author e-mail address: irina.bouianova@liu.se

1. Introduction

Photon energy upconversion, i.e. a process in which several low-energy photons are converted into a high-energy photon, is of significant importance in a wide variety of research fields ranging from biological labelling and images, to drag delivery, infrared light visualization, lasing and efficient energy harvesting. Semiconductor nanostructures, such as nanowires (NWs) from III-V compounds and related alloys, represent an important class of upconverting materials that are particularly desirable for applications in nano- optoelectronics and photonics. However, to date, the reported upconversion efficiency in III-V nanostructures, as well as other semiconductor nanostructures remains relatively low, typically less than 0.1%, especially at low excitation powers [1, 2].

In this work we push the limit of low-power upconversion efficiency in semiconductor nanostructures, through a novel approach of radial heterostructure engineering of NWs by exploring radial core/shell NWs with a N-free III-V core and a dilute-nitride shell of a lower bandgap with a favourable band alignment between the core and shell.

Specifically, we show [3] that efficiency of energy upconversion due to two-photon absorption (TPA) can be boosted in NW heterostructures engineered so that (i) an intermediate TPA step involves band states of the narrow bandgap region; (ii) at least one of the carriers created after the first photon absorption can freely diffuse to the wider bandgap region; and (iii) carriers generated after the intermediate step have a long lifetime. These conditions are shown to be satisfied in radial GaNAs(P)/GaAs(P) NW heterostructures leading to up to 500 times increase in the upconversion efficiency relative to that of the constituent materials. The upconversion efficiency is found to be independent of the excitation power and can be further enhanced (up to 15%) in hybrid NW-on-gold structures, engineered to maximize light absorption within the shell region under the upconversion conditions. This work, therefore, demonstrates the great potential of dilute nitride NWs as energy upconverters and provides general guidelines for designing efficient nanoscale photon upconverters based on NW heterostructures.

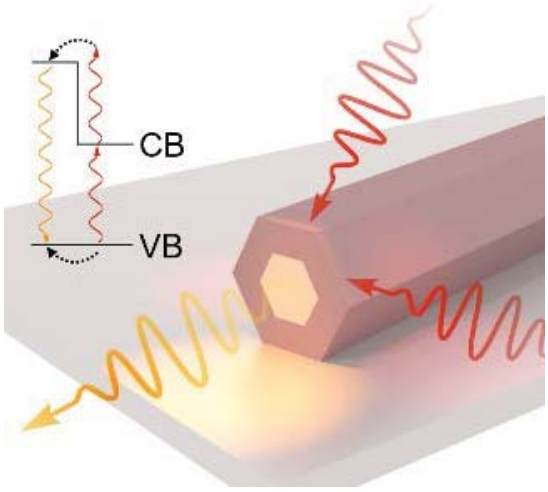

Fig. 1: Schematic illustrating the core/shell design of the studied NWs and the mechanism of the TPA process leading to photon upconversion.

2. References

[1] P. P Paskov et al, *Jpn. J. Appl. Phys.* **40** (2001) 2080.
[2] R. Cheriton et al. *Commun. Mater*. **1** (2020) 63.
[3] M. Jansson , F. Fumitaro, W. M. Chen and I. A. Buyanova. *ACS Nano* **16**, (2022) 12666.

Stability of Y_2O_3:Tm,Yb phosphor thin films during upconversion and cathodoluminescence

Emad Hasabeldaim, H.C. Swart, R.E. Kroon

Department of Physics, University of the Free State, Bloemfontein, 9300, South Africa
Corresponding author e-mail address: kroonre@ufs.ac.za

1. Introduction

Due to the matching oxidation states and similar ionic radii of yttrium (Y^{3+}) and rare earth (RE^{3+}) ions, Y_2O_3:RE^{3+} phosphors are considered among the most important materials for photonic applications [1]. Their stability under different conditions is critical to extend their use. In this study a Y_2O_3:Tm(0.1%),Yb(2%) thin film was produced by spin coating a sol-gel stock solution on a Si substrate followed by annealing at 900 °C. X-ray diffraction measurement confirmed the formation of Y_2O_3 having cubic phase. The stability of the emission from the film was assessed during upconversion photoluminescence (UCPL) for irradiation with a high power (1.5 W) infrared laser (980 nm) in air, as well as during cathodoluminescence (CL) using a 10 µA, 2000 V electron beam under vacuum of 3.5 x 10^{-8} Torr.

2. Results

Figure 1 shows the UCPL profile and degradation behaviour of the film. The sample exhibited two emission bands at 488 and 655 nm due to the $^1G_4$-$^3H_6$ and $^1G_4$-$^3F_4$ transitions of Tm^{3+} ions, respectively [2], which were excited by energy transfer upconversion from the Yb^{3+} ions absorbing the incident 980 nm radiation. The infrared wavelength band was blocked to the detector by a filter during the measurements. The dominant blue emission at 488 nm remained stable during irradiation for 28 h. This shows that the phosphor is very stable under continuous high power infrared laser irradiation for an extended period, hence it is useful for upconversion applications. Despite the high power of the excitation laser, the individual 980 nm infrared photons have relatively low energy and therefore degradation is inhibited. Figure 2 shows the CL spectra and degradation of the same film. Although the 488 nm emission observed for UCPL is also present for CL, it is weak and forms only a shoulder to the dominant emission at 459 nm, which is ascribed to the $^1D_2$-$^3F_4$ transitions of Tm^{3+} ions. Excitation of the $^1D_2$ energy level lying above the $^1G_4$ energy level is difficult during upconversion, but occurred easily when the high energy electrons excited the material during CL. No filter was applied to the detector, and infrared emissions of the Tm^{3+} ions at 811 nm due to $^3H_4$-$^3H_6$ transitions and of Yb^{3+} ions at 975 nm due to $^2F_{5/2}$-$^2F_{7/2}$ transitions could also be observed. The CL emission lost approximately two thirds of its intensity (68% at 459 nm for Tm^{3+} ions and 67% at 975 nm for Yb^{3+} ions) after an irradiation dose of 100 C/cm^2 and then stabilized. To investigate the reason for this degradation, Auger electron spectroscopy was used to monitor the chemical state of the phosphor surface concurrently with the CL intensity using the same electron beam. Auger peaks associated with carbon, yttrium, and oxygen were detected and their Auger peak-to-peak heights were used to monitor their surface concentrations. This revealed that carbon was removed from the surface during the initial stage (up to 15 C/cm^2) of degradation, yttrium was almost unchanged, whereas oxygen was increased initially during removal of the carbon from the surface and then start decreasing at a very low rate. This suggests the desorption of oxygen atoms from the surface via the Knotek-Feibelman mechanism and the subsequent creation of oxygen vacancy defects which may have been responsible for the CL degradation [3].

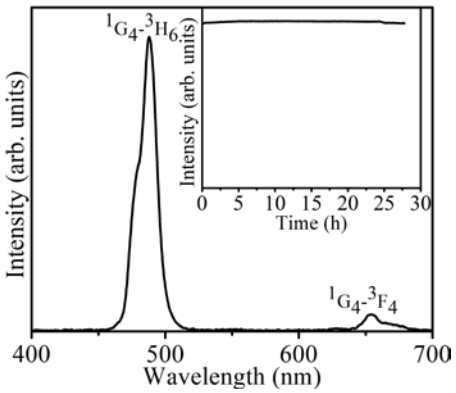

Fig. 1: UCPL profile, inset is 488 nm PL intensity as a function of time.

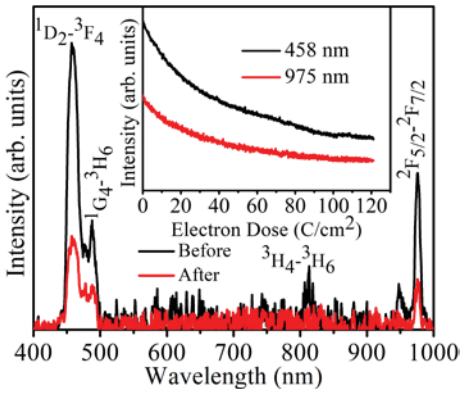

Fig. 2: CL spectra before and after degradation, inset is the 459 and 975 nm CL intensities as a function of electron dose.

3. References

[1] A. Gupta, N. Brahme and D. P. Bisen. *J. Lumin.* **155** (2014) 112-118.
[2] H. Zhang, T. Jia, X. Shang, S. Zhang, Z. Sun and J. Qiu, *Phys. Chem. Chem. Phys.* **18** (2016) 25905-25914.
[3] E. H. H. Hasabeldaim, O. M. Ntwaeaborwa, R. E. Kroon, E. Coetsee and H. C. Swart. *Appl. Surf. Sci.* **484** (2019) 105-111.

Temperature-dependent photoluminescence characteristics of bulk anatase TiO_2 crystal

Assane Talla[1], **Zelalem Urgessa**[1], **and Johannes Reinhardt Botha**[1]

[1] *Department of Physics, Nelson Mandela University, P.O. Box 77000, Gqeberha 6031, South Africa*
Corresponding author e-mail address: s217063969@mandela.ac.za

1. Introduction

Efficient applications of Titania rely on its optical properties for better performance in energy-related applications and optoelectronics [1,2]. Hydrogen is a common impurity in titanium oxide (TiO_2) and strongly impacts its optical properties [2]. It should be noted that in TiO_2, it is very difficult to observe near band edge photoluminescence (PL) emissions due to strong photon-phonon coupling and the indirect band gap nature of the material. To the best of our knowledge, the origin of shallow donor PL recombination with noticeable temperature dependence in TiO_2 is not known in literature. This work presents 5.5 K photoluminescence (PL) and temperature-dependent PL characteristics of virgin anatase (non-annealed).

2. Results

The 5.5 K PL spectrum in Fig. 1 a) shows that the PL consists of two emissions regions: A broad band deep-level emission and near band edge (NBE) emission. The broad band emission is attributed to the recombination of self-trapped exciton (STE). The NBE contains several emission lines: including possibly indirect free exciton (FX_{ind}), shallow donor-bound exciton (D^oX), free to-bound transitions (e,A) and donor-acceptor pair (DAP) transitions with their respective phonon replicas. Fig. 1 b) presents temperature dependent (5.5 to 80 K) PL characteristics of the NBE emission line. The origins and temperature behaviours of each emission line will be investigated and presented in detail.

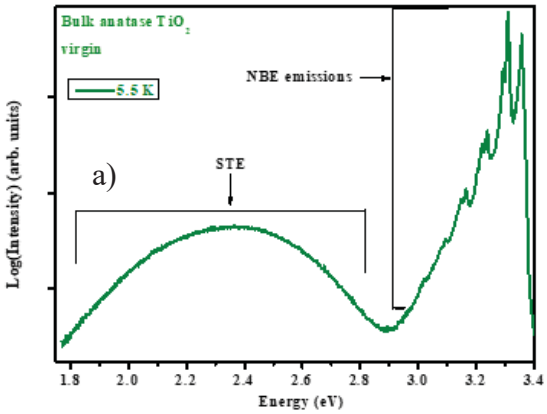

Fig. 1: 5.5 K PL spectra of bulk anatase TiO_2 crystals.

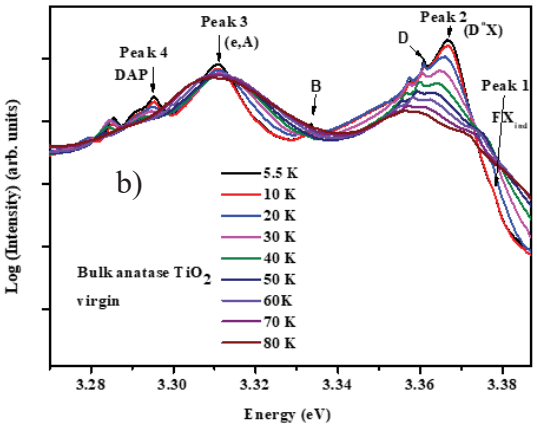

Fig. 2: Temperature dependent PL of bulk anatase crystal.

3. References

[1] A. Fujishima and K. Honda, Nature **238**, (1972) 37
[2] E. Lavrov, I. chaplygin, F. Herklotz and Y. Kutin J. Appl. Phys. **131**, (2022) 030902

Structural and Optical Characteristics of Green Emitting Tb^{3+} Doped $BaGd_2ZnO_5$ Nanophosphor for LED Applications

Irfan Ayoub[1], Vijay Kumar[1,2], Hendrik C Swart[2]

[1]Department of Physics, National Institute of Technology Srinagar, Jammu and Kashmir - 190006, India
[2]Department of Physics, University of the Free State, P.O. Box 339, Bloemfontein ZA9300, South Africa
Corresponding authors e-mail address: irfan.ayoub498@gmail.com (I. Ayoub)

1. Introduction

In the current state of the technological world, solid-state lighting based on white-LEDs has modified the conventional sources of energy being utilized all over the globe, thereby reshaping the globalized economy [1]. Due to the well-known characteristics of LEDs, such as their environmental friendliness, luminance efficiency, low power consumption, and quick reaction time, they have attracted significantly attention from researchers and industrialists [2]. However, for the fabrication of an efficient LED, which will be beneficial for opto-electronic, photonic, and lasing applications, the selection of a suitable matrix and activator is a challenge. In this regard, lanthanide ions (Ln^{3+}) and trivalent terbium (Tb^{3+}) ions, serve as excellent activators for inorganic host matrix. The emission spectra of the Tb^{3+} ions exhibit two prominent peaks for the transitions $^5D_3$-^7F_J and $^5D_4$-$^7F_5$ which correspond to blue and green colors, respectively. The non-radiative, cross-relaxation process between the $^5D_3$ and $^5D_4$ excited states causes the luminescence emission to shift from blue to green at higher concentrations of the Tb^{3+} ion [3]. To date, numerous studies have been carried out wherein the impact of Tb^{3+} ions on different properties has been observed. However, the effect of Tb^{3+} doping on the characteristics of $BaGd_2ZnO_5$ has not yet been studied. Therefore, considering the excellent PL characteristics of Tb^{3+} ions, in the current study efforts were made to investigate the crystal structure and the optical properties of $BaGd_{2-x}ZnO^5$:xTb^{3+}.

2. Result

An orthorhombic symmetry-based $BaGd_{2-x}ZnO_5$:xTb^{3+} (x = 0-6 mol %) nanophosphor was synthesized via urea-assisted solution combustion synthesis. The phase and crystallinity of the synthesized nanophosphors were confirmed through X-ray diffraction analysis (Figure 1). Field emission scanning electron microscopy analysis revealed the agglomeration of particles possessing a non-uniform shape with crystal and grain size of approximately 12 nm and 25–30 nm, respectively. The Kubelka-Munk function was employed to analyze the impact of doping on the optical bandgap of the synthesized nanophosphors. Under an excitation wavelength of 275 nm, the emission spectrum displayed a dominate peak around 550 nm, which corresponds to the transitions from the $^5D_4 \rightarrow {}^7F_5$. Colour tuning was obtained from blue to green. The observed results show that the synthesized nanophosphors can effectively be used for the green-emitting UV-convertible phosphors as well as for the UV-excited wLEDs.

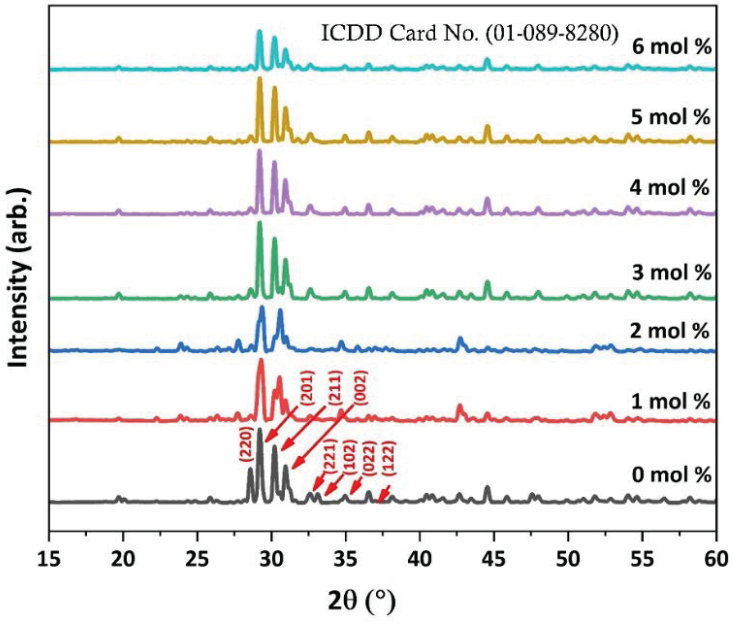

Figure 1: X-ray diffraction pattern of $BaGd_{2-x}ZnO_5$:xTb^{3+} (x= 0-6 mol %) nanophosphor synthesized through the combustion route.

3. References

[1] V. Singh, G. Lakshminarayana, A. Wagh, *J. Electron. Mater.* **2020**, *49*, 510.
[2] P. Sehrawat, R. K. Malik, R. Punia, S. Maken, N. Kumari, *Chem. Phys. Lett.* **2022**, *792*, 139399.
[3] Z. Zhang, B. Devakumar, S. Wang, L. Sun, N. Ma, W. Li, X. Huang, *Mater. Today Chem.* **2021**, *20*, 100471.

Structural characteristics of anodic TiO_2 on titanium foil after annealing in oxygen-rich atmosphere

Assane Talla[1], Andi Pujirana[1], Ngcali Tile[1] Sinoyolo Ngongo[2], William Goosen[2], Ettienne Minnaar[1], Zelalem Urgessa[1] Setumo Victor Motloung[3,4] and Johannes Reinhardt Botha[1]

[1]Department of Physics, Nelson Mandela University, P.O. Box 77000, Gqeberha 6031, South Africa
[2]Centre for High Resolution Transmission Electron Microscopy, Nelson Mandela University, P.O. Box 77000, Gqeberha, 6031, South Africa
[3]Department of Chemical and Physical Sciences, Walter Sisulu University, Private Bag X1, Mthatha, South Africa
[4]Department of Physics, Sefako Makgatho Health Science University, P. O. Box 94, Medunsa, 0204, South Africa
Corresponding author e-mail address: s217063969@mandela.ac.za

1. Introduction

Because of their structural properties like high surface area, nanostructured titanium dioxide (TiO_2) nanotubes (TNTs) have attracted the scientific community due to their potential use in solar cells and photocatalytic applications [1]. TiO_2 has several phases, among which anatase and rutile are the most useful for applications [1].The predominance of these phases has been shown to depend strongly on the annealing atmosphere [2]. This study presents the structural characteristics of the TNTs obtained by anodizing titanium foil, followed by annealing in an oxygen-rich atmosphere. The evolution of phase transformation from anatase to rutile for the sample annealed in an oxygen-rich environment is investigated in detail. Transmission electron microscopy shows that the oxidation of the titanium foil favours the nucleation of the rutile phase from the bottom. The activation energies of anatase to rutile transition and anatase crystal growth are estimated.

2. Results

Fig.1 presents cross-sectional SEM micrographs of TNTs annealed at 600 °C in oxygen. As can be seen from the micrograph, the cross-sectional image shows three distinct regions. The bottom layer is the top part of the Ti foil, while the two upper layers form part of the TNT film. The image illustrates that the middle layer (blue arrow) is compact, whereas the top layer (red arrow) comprises tubular structures. Fig. 2 presents a TEM image of the two upper layers described in Fig.1 with selective area diffraction (SAED) patterns. From the SAED, it is confirmed that the bottom compact layer is a rutile phase whereas the upper tubular layer is made of anatase. Complementary structural investigations with Raman analysis confirm the TEM results. XRD shows that both TNTs films and Ti foil peak diffractions shift to the lower angles as the annealing temperature increases. The results are compared with samples annealed in air, nitrogen and vacuum. The results provide suitable annealing conditions to control the phase content and morphology of anodic TiO_2. A detailed mechanism of phase transformation will be investigated and presented in detail.

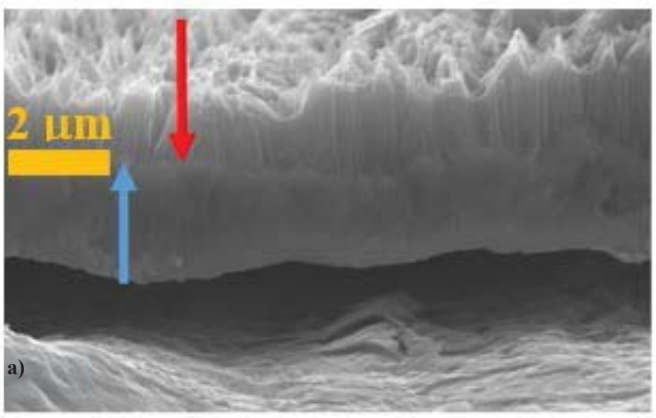

Fig. 1: Cross-sectional SEM micrographs of TNTs annealed at 600 °C in oxygen.

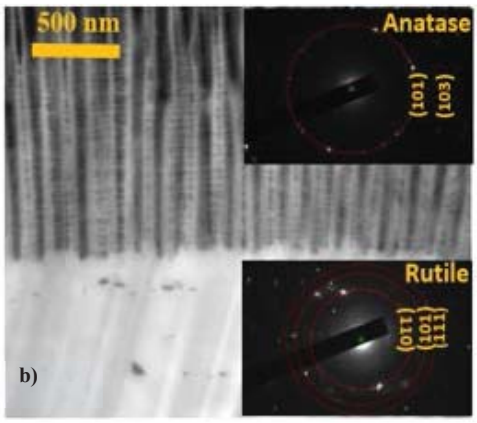

Fig. 2: Bright field TEM micrograph with SAD patterns, showing anatase and rutile phases.

3. References

[1] S.M. Gupta and M. Tripathi. Chin. Sci. Bull. **56** (2011) 1639.
[2] A. Talla, N.J. Suliali, W.E. Goosen b, Z.N. Urgessa, S.V. Motloung and J.R. Botha. Physica B **640** (2022) 414026.

SHI radiation induced tetragonal transformation in bulk monoclinic zirconia

M E Lee[1], **J.H O'Connell**[1], **V.A Skuratov**[2]

[1] *Centre for HRTEM, Nelson Mandela University, Gqeberha, South Africa*
[2] *Flerov Laboratory for Nuclear Research, JINR, Dubna, Russia*
Corresponding author e-mail address: michael.lee@mandela..ac.za

1. Introduction

Zirconia ceramics have found broad applications in a variety of energy and biomedical applications because of their unusual combination of structural, mechanical and optical properties [1]. These properties include, superior hardness, good chemical and photochemical stability, high resistance to corrosion, low thermal conductivity high thermomechanical resistance, a high refractive index and a high optical transparency in the 0.3–8.0 mm range with two direct band-to band transitions at 5.2 and 5.8 eV [2]. For many applications, the material performance in extreme environments such as thermo-mechanical stresses, severe radiation environments or chemical reactive conditions, is very important.

Pure bulk zirconia (ZrO_2) is a polymorphic oxide that exists in three different low pressure crystal structures below its melting point namely, the high temperature phases cubic and tetragonal as well as the low temperature monoclinic phase [3]. However, tetragonal zirconia has been reported to be stabilized at RT as crystallites/grains having dimensions of the order 3-100 nm during the formation of polycrystalline bulk material, thin layers or precipitated powders [4]. Alternatively, tetragonal zirconia has been shown to stabilize at RT by doping mainly with calcium, magnesium, yttrium, and cerium oxides [5].

In this work, we analyse the effects of radiation damage in zirconia and therefore provide direct evidence for the formation of individual ion tracks produced in bulk monoclinic zirconia by the irradiation with swift heavy ions (SHI) namely 167 MeV Xe, at fluences of 2 x 10^{10} cm^{-2}. These ion tracks have been observed and characterized by transmission electron microscopy (TEM) at room temperature as well as under in situ annealing.

2. Results

Individual ion tracks were found to be composed of the high temperature stable tetragonal phase. Discontinuities in the tetragonal phase (segments) together with a slight misalignment relative to the ion path was ascribed to the difference in a-c angle between the tetragonal and monoclinic phase as shown in figure 1.

Although stressed, the tetragonal inclusions were found to be stable at room temperature although thermal excitation as well as excitation by high energy electrons was able to transform the tetragonal phase back into the monoclinic phase leaving behind a train of defect clusters (Figure 2) as is typical of ion tracks in non-amorphizable material.

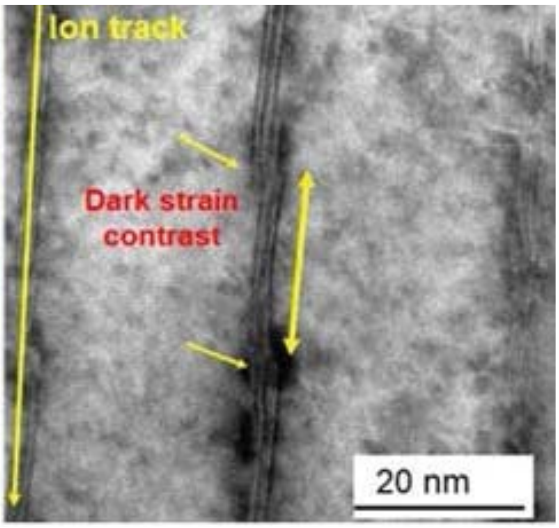

Fig. 1: TEM BF cross sectional image of tetragonal ion tracks in monoclinic zirconia showing strain contrast at the junctions.

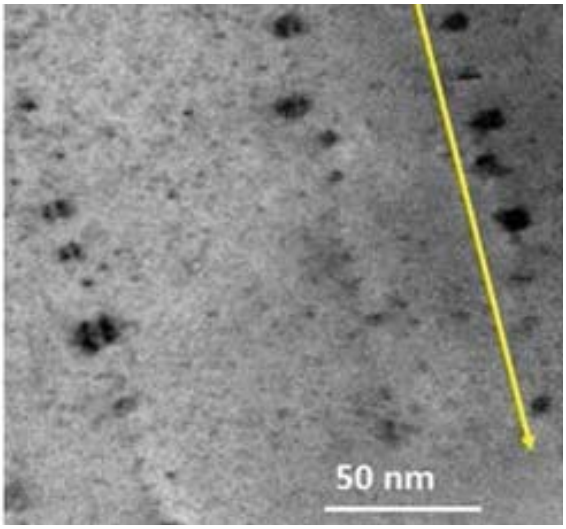

Fig. 2: TEM BF cross section image of defect clusters formed along ion tracks after in situ heating.

3. References

[1] J.F. Castillo, J. Isasi, M. Perez, I. Aldama, P. Arevalo, C. Dıaz-Guerra, J. Lumin. **131** (2011) 2128
[2] M. Fernandez-Garcıa, A. Martınez-Arias, J.C. Hanson, J.A. Rodrıguez, Chem. Rev. **104** (2004) 4063
[3] J.E. Bailey, *Proc. R. Soc. A. Math. Phys. Sci.*, **279** (1964) 395
[4] R.C. Garvie, J. Phys. Chem., **82**, 1978, 218
[5]R.H.J. Hannink, P.M. Kelly, B.C. Muddle, *J. Am. Ceram. Soc.*, **83** (2000) 461

Fabrication, characterization, and gas detection performance of Co_3O_4 hierarchical structures

Modjadji Rebecca Letsoalo[1, 2], **Eric Maluta**[2], **Katekani Shingange**[1]

[1] *DSI/CSIR National Centre for Nanostructured Materials, Council for Scientific and Industrial Research, Pretoria 0001, South Africa*
[2] *Department of Physics,University of Venda, P/ Bag X 5050, Thohoyandou, 0950*
Corresponding author email address: kshingange@csir.co.za

1. Introduction

There is an increasing need for improved gas-sensors with high sensitivity and selectivity, and the use of a suitable materials with the essential surface and bulk functionalities is crucial [1]. Nanostructured semiconductor metal oxide (SMO) based gas sensors are generating interest due to their low-cost, easy fabrication and modifications. In contrast to n-type SMOs, p-type SMOs have been extensively reported to be efficient catalysts for improving selectivity to volatile organic compounds [2]. In general, intrinsic acceptor states occur in p-type SMO, which are initiated by surplus oxygen at interstitial sites and/or metal vacancies in the crystal lattice. Extra chemically adsorbed oxygen species may increase on their surfaces [3]. As a result, they still have enormous potential for developing high-performance chemi-resistors. As a typical p-type SMO, spinel cobalt oxide (Co_3O_4) has been used for gas detection, and it has been discovered that the gas detection properties are heavily dependent on the dimension, morphology, and porosity of the Co_3O_4 material [4].

In this work, three structures of Co_3O_4 were synthesized using the hydrothermal method through variation of the oven duration time ranging from 6 to 24 hours. The structural, morphological, and porosity characteristics were analysed using XRD, SEM and BET, respectively. Whereas, the optical characteristics were examined using UV-vis and PL. Gas sensing tests toward ammonia, carbon monoxide, methane, methanol, ethylene, and benzene were conducted at operating temperatures in the range from room temperature to 200 ° C. The gas-sensing mechanism was further explained through DFT calculations.

2. Results

Morphology characteristics of the three CO_3O_4 samples were examined and are shown in Fig. 1. All three samples revealed hierarchical structures made from sheets assembly, respectively. The photoluminescence (PL) of the samples was performed at room temperature at an excitation wavelength of 325 nm and the results are shown in Fig.2. The PL intensity centered at 432 nm decreased with increasing duration time, suggesting a decrease in the quantity of defects of the samples.

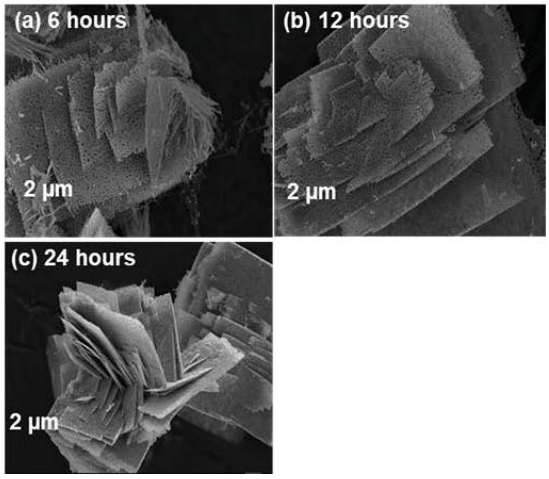

Fig. 1: SEM images of the Co_3O_4 hierarchical structures

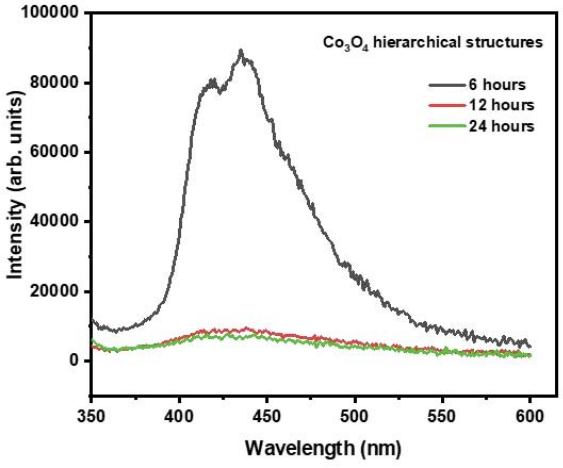

Fig. 2: PL of the Co_3O_4 hierarchical structures

3. References

[1]. G. Eranna, B.C. Joshi, D.P. Runthala, R.P. Gupta, *Crit. Rev. Solid State Mater. Sci.* **29** (2004) 111–183.
[2] S.-Y. Cho, H.-W. Yoo, J.Y. Kim, W.-B. Jung, M.L. Jin, J.-S. Kim, H.-J. Jeon, H.-T. Jung. *Nano Lett.* 16 (2016) 4508–4515.
[3] J.M. Xu, J.P. Cheng. *J. Alloys Compd.* 686 (2016) 753–768.
[4] M.J. Wang, Z.R. Shen, X.D. Zhao, F.P. Duanmu, H.J. Yu, H.M. Ji. *J. Hazard. Mater*. 371 (2019) 352–361.

Pursuing the possibilities of light

Pioneering the field of photonics materials through research, development and commercialization of light-related devices for the future.

research
material science
environmental
high energy physics
medical
life sciences
consumer devices
analytical
industrial
security
automotive

HAMAMATSU
PHOTON IS OUR BUSINESS

A Gold Sponsor of SACPM 2023

Thursday 11 May

Time	Activity
07:00 – 08:00	Breakfast
	PRESENTATION SESSION 7: Chairperson – **Walter Meyer**
08:00 – 08:10	Announcements
08:10 – 08:50	Plenary Talk 3: **Anne Hemeryck** Formation of defects in semiconductors: what contribution from atomistic modeling?
08:50 – 09:30	Plenary Talk 4: **Layla Martin-Samos** Defect signatures in semi-conductors and insulators: understanding and modeling
09:30 – 09:50	Presentation 21: **Rositsa Yakimova** Evolution of metal nanostructures on dangling bond free substrates
9:50 – 10:00	Discussion
10:00 – 10:20	Tea & Coffee break
	PRESENTATION SESSION 8: Chairperson – **Johan Janse van Rensburg**
10:20 – 10:50	Invited Talk 5: **Jai Prakash** Plasmonic photocatalysts: Tailoring of optical properties and advanced multifunctional applications
10:50 – 11:10	Presentation 22: **Delicacy Ntshalintshali** Effect of Annealing Time on CdSe Thin Films Prepared by Photo-Assisted Chemical Bath Deposition
11:10 – 11:30	Presentation 23: **Lucas Erasmus** Integrating a phosphor material into an optical waveguide
11:30 – 11:50	Presentation 24: **Leonato Nchinda** Thermal stability of diketopyrrolopyrrole-based terpolymers with tunable broad band absorption for polymer solar cells
11:50 – 12:10	Presentation 25: **Fokotsa Victor Molefe** Simple approach to growth and characterization of GO/ZnO/P3HT layered nanostructures for solar cell devices
12:10 – 12:20	Discussion
12:20 – 13:20	Lunch
	PRESENTATION SESSION 9: Chairperson – **Andre Venter**
13:20 – 13:40	Presentation 27: **Walter Meyer** Deep-level transient spectroscopy study of the effect of Pd deposition on radiation induced defects in Si
13:40 – 14:00	Presentation 28: **JAA Engelbrecht** Comments on the refractive index of $Al_xGa_{1-x}As$
14:00 – 14:20	Presentation 29: **Mmantsae Diale** Development of 2D/3D stable tin-based halide perovskite solar cell
14:20 – 14:30	Discussion
14:30 – 14:50	Tea & Coffee break
14:50 – 15:20	Prize giving and closure: **Jackie Nel**
15:20 – 15:30	Conference Photograph
17:00 – 19:00	Game drive to bush braai
19:00 – 21:00	Bush braai

Formation of defects in semiconductors: what contribution from atomistic modeling?

Anne Hemeryck[1], **Layla Martin Samos**[2], **Antoine Jay**[1], **Nicolas Salles**[2]
Pierre-Louis Julliard[1], **Fuccio Cristiano**[1], **Thomas Jarrin**[3] , **Nicolas Richard**[3]

[1] *Laboratoire d'analyse et d'architecture des systèmes, CNRS, 31031 Toulouse cédex 4, France*
[2] *CNR-IOM/Democritos National Simulation Center, Istituto Officina dei Materiali, c/o SISSA, via Bonomea 265, IT-34136 Trieste, Italy*
[3] *CEA, DAM, DIF, F-91297 Arpajon, France*

Corresponding author e-mail address: anne.hemeryck@laas.fr

One of the main drawbacks of the continuous miniaturization of MOS transistors is the increased variability of the device characteristics, in particular the threshold voltage drift. This drift is associated with charge capture and emission phenomena, arising from the presence of defects in the atomic structure of the device that induce electronic states in the band gap of the semiconductor, which can then act as bridges for electrons to thermally cross the band gap, or they become traps for free carriers. These problems stimulate a growing activity around defects in semiconductor materials. In this context, multiscale simulation should allow to anticipate the problems of industrial materials by offering the possibility to review different technological possibilities at lower cost, to help to understand, to optimize and to design new improved materials adapted to specific applications.

In this study, using modeling tools with atomistic granularity, we focus on the atomic mechanisms that cause the presence of these defects in devices, i.e. the mechanisms of defect formation. These defects can be formed either during the manufacturing process, such as ion implantation, or during the use of the components as in radiative environments. In both cases, the ions arriving at high speed destroy the crystal structure of the semiconductor material as they pass through it, leaving behind them defects at the atomic scale. Several approaches ranging from ab initio to industrial technology computer aided design (TCAD) codes will be described and how they can contribute to the understanding of defect formation.

As an example, it will be described how ab initio calculations can help to improve TCAD tools in an industrial context for dopant implantation problems. Another example will be the use of molecular dynamics to simulate defects formed under irradiation from the first instants of the cascade. The complexity of modeling the growth of material as for example in the case of the growth of silicon oxide will be highlighted.

Defect signatures in semi-conductors and insulators: understanding and modeling

Layla Martin-Samos[1], Anne Hemeryck[2], Gabriela Herrero-Saboya[1], Matic Poberznik[1], Nicolas Richard[3], Antoine Jay[2], Nicolas Salles[1]

[1] CNR-IOM, via Bonomea 265 c/o SISSA, 34134 Trieste, Italy
2 Laboratoire d'analyse et d'architecture des syst`emes, CNRS, 31031 Toulouse cedex 4, France
3 CEA, DAM, DIF, F-91297 Arpajon, France
Corresponding author e-mail address: marsamos@iom.cnr.it

Defects are at the very basis of our nowadays technology. Whether on purpose, accidentally (manufacturing) or because of the operando conditions, defects affects and control the opto-electronic properties of semi-conductors and insulators. For instance, defects might promote the generation of free-carriers, might act as recombination centers and/or as charge traps. They might also absorb and/or emit light (color centers). After more than 70 years from the first silicon-based transistor, and even more for the first silica-based optical fiber, one would expect all details of those materials to be fully understood. Furthermore, with the boom of High Performance Computing and the promise of turn-key solutions in first-principle modelling, why should we still discuss about defects in semi-conductors and insulators?

Through some examples we will show how one should keep busy with semiconductors, whose intrinsic properties are dominated by dirt effects, constituting the complex and rich field of defects in semiconductors.

Evolution of metal nanostructures on dangling bond free substrates

Rositsa Yakimova[1], Ivan Shtepliuk[1], Milena Beshkova[2], Kostas Sarakinos[3,4], Filippo Giannazzo[5], Ivan G. Ivanov[1]

[1] *Department of Physics, Chemistry and Biology-IFM, Linköping University, S-58183 Linköping, Sweden*

[2] *Institute of Electronics, Bulgarian Academy of Sciences, 72 Tzarigradsko Chaussee Blvd, 1784 Sofia, Bulgaria*

[3] *Department of Physics, University of Helsinki, P.O. Box 43, FI-00014 Helsinki, Finland*

[4] *KTH Royal Institute of Technology, Department of Physics, Roslagstullsbacken 21, 114 21 Stockholm, Sweden*

[5] *CNR-IMM, Strada VIII, 5, 95121 Catania, Italy*

rositsa.yakimova@liu.se

1. Introduction

Integration of material structures with different dimensionality is a winning strategy for achieving new functionalities of traditional materials towards novel devices with superior performance. Epitaxial graphene, formed through thermal decomposition of SiC substrates, is an exciting example of native 2D/3D integration, which can be used as a basic platform for other material growth [1,2]. Graphene on SiC is a dangling bond free surface that can provide favourable conditions for high-quality epitaxial growth of diverse nanostructures, remote epitaxy, van-der-Waals epitaxy, etc. Moreover, the interface between graphene and SiC (known as buffer layer) is a C-rich reconstruction which mediates the kinetic properties of materials deposited on graphene and may experience intercalation which decouples it from SiC to form graphene. These unique surfaces create a platform of diverse nano materials growth which will be partly considered in this report.

2. Results

Here we present key results on the growth features and physical properties of ultrathin metal layers, silver (Ag) and gold (Au), grown on epitaxial graphene/4H-SiC. A comparison is made with the case of buffer layer. As an illustration of the versatility of the proposed substrate concept, results on growth of metal nitride (AlN) and metal oxide (Al_2O_3) are also discussed in view of their application related significance. Magnetron-sputtered Ag and Au, chosen as model metals, are comprehensively investigated to reveal the representative growth mechanism of mono-elemental materials on dangling-bond-free surface of epitaxial graphene. We demonstrate the vital role of metal-graphene interaction in determining the preferred growth mode. Particularly, the weaker interaction between gold and epitaxial graphene compared to that between silver and epi-graphene leads to the formation of fractal-like gold nanostructures by surface diffusion-limited aggregation mechanism. While Volmer-Weber mechanism mainly governs island-like growth of silver nano-layers on epitaxial graphene on 4H-SiC. We further link the annealing-induced de-wetting of the metal layers to changes in the interlayer interaction and hence charge transfer at the metal-graphene-SiC heterointerfaces. The analysis of the kinetic parameters is performed via first principle calculations and evidenced experimentally.

Atomic layer deposition (ALD) is employed to epitaxially grow bi-elemental materials like AlN and Al_2O_3 on graphene/4H-SiC. AlN nanoscale islands with roughness of 3.854 nm are formed on epitaxial graphene on 4H-SiC during 40 ALD cycles at 450 °C, which contrasts with growth of the high-quality continuous AlN layers (with as small roughness as 0.255 nm) formed at graphene-free 4H-SiC surface under the same conditions. We ascribe this difference to the difference in surface energies between graphene and 4H-SiC. Finally, we demonstrate the principal possibility of seed-layer-free ALD growth (at 250°C) of highly uniform Al_2O_3 layers on epitaxial graphene/4H-SiC using trimethyl aluminium (TMA) as the Al precursor. We highlight the critical role of water molecules as the co-reactant to provide many nuclei for Al_2O_3 formation. The excellent insulating properties of AlN and Al_2O_3 compounds grown on epitaxial graphene on SiC create good prerequisites of boosting the development of novel 2D/3D-heterojunction-based electronic components with high breakdown voltage.
The properties of the grown nanostructures in this study are assessed by means of advanced structure – sensitive and optical techniques along with theoretical modelling.

3. References

[1] I. Shtepliuk, F. Giannazzo, R. Yakimova. *Appl. Sci.* ***11*** (2021) 5784.
[2] Shtepliuk, I.G. Ivanov, M. Vagin, Z. Khan, T. Iakimov, N. Pliatsikas, K. Sarakinos, F. Giannazzo,
[3] R. Yakimova. Materials Today: Proceedings ***20*** (2020) 37.

Plasmonic photocatalysts: Tailoring of optical properties and advanced multifunctional applications

Jai Prakash

Department of Chemistry, National Institute of Technology, Hamirpur, Hamirpur –177005 (H.P.), India
jaip@nith.ac.in and jai.gupta1983@gmail.com

Photocatalysis is one of the unique processes occurs in the presence of solar radiation and is potentially utilized for various field including energy production, controlling the environmental pollution and improving the health of the society etc. Plasmonic photocatalyst nanomaterials composed of photocatalyst semiconductors and plasmonic nanostructures are promising multifunctional nanomaterials which have gained considerable attention in the field of interdisciplinary research. These nanomaterials show multifunctional applications in the field of health, energy and environment due to the synergetic contribution from the photocatalytic and plasmonic properties of the constituents. This talk will address the fundamentals of these nanostructured materials, tailoring of their optical properties and their applications in various fields including photocatalysis, sensing, solar cells and antimicrobial activities along with their potential applications in controlling/inactivation of corona virus.

Keywords: Photocatalysis, Semiconductors, Plasmonic, Multifunctional applications.

Effect of Annealing Time on CdSe Thin Films Prepared by Photo-Assisted Chemical Bath Deposition

Delicacy Ntshalintshali[1,2], **Lehlohonolo F. Koao**[1], **Hendrik C. Swart**[2]

[1] *Department of Physics, University of the Free State (Qwaqwa campus), Private Bag X13, Phuthaditjhaba, 9866, South Africa*
[2]*Department of Physics, University of the Free State, P.O. Box 339, Bloemfontein 9300, South Africa*
Corresponding author e-mail address: delicacy74@gmail.com

1. Introduction

The class of II-VI semiconductor compounds has recently attracted much attention due to their optoelectronic properties and applications. Cadmium Selenide (CdSe), a notable member of the II-VI group, is a compound semiconductor. Transparent conducting films based on CdSe are widely used in photovoltaic and optoelectronic applications due to their low electrical resistance and high optical transparency. The emission properties of semiconductor nanocrystals can be characterized by four fundamental parameters: brightness, emission colour, colour purity, and emission stability. Due to quantum size effects, the band gap of CdSe nanocrystals increases as their size decreases, and thus the emission colour of the band-edge PL of the nanocrystals shifts continuously from red (centered at 650 nm) to blue (centered at 450 nm) as the size of the nanocrystals decreases [1]. It has a suitable direct intrinsic band gap of 1.74 eV. It often possesses n-type conductivity in bulk and thin film form, making them interesting for photoelectrochemical applications [2]. It is well known that doping is a useful way to improve the photoelectric properties of materials, including absorptivity, conductivity, and mobility. Doping with Mn^{2+} significantly influences the optical properties and improves the electrical conductivity of the host matrix. Photo-assisted chemical bath deposition (PCBD) is used to produce Mn-doped CdSe thin films. PCBD was used because of the competent conversion of the reactants to the required product and the higher detection rate. CdSe has enormous potential for application in light-emitting diodes and other optoelectronic devices.

2. Results

The X-ray diffraction results showed that All the CdSe:x%Mn^{2+} ($0 \leq x \leq 0.7$) thin films annealed at 250°C possess a typical cubic structure. It was observed that the XRD diffraction intensities decrease with the increase in Mn^{2+} concentration. Scanning electron microscopy observations showed the spherical nanoparticles with some boundaries between them and spread throughout the thin films. These grains comprised small spherical particles agglomerated together to form one colossal particle. There was no change in the nanoparticle size with an increase in the amount of Mn^{2+}. The UV-Vis spectra showed that the absorption edges red shift slightly with an increase in the molar concentration of Mn^{2+}. Fig. 1(a) shows the PL emission spectra of CdSe:x%Mn2+ ($0 \leq x \leq 0.7$) thin film samples excited at 325 nm (3.8 eV) by a He-Cd laser source. All samples show four luminescence peaks: three prominent ones and one shoulder band are located at 391 nm, 541 nm, 659 nm, and 709 nm, respectively. These major emissions are thought to be the consequence of electron recombination in the conduction band (CB) and hole recombination in the valence band (VB), inferred as excitonic emission from the band edge of CdSe. The photoluminescence results showed that the maximum intensity was obtained for CdSe:0.7% Mn^{2+} film. The CIE colour coordinate is shown in fig. 1(b), and a white light colour emission is displayed with only one outlier for CdSe:0.7% Mn^{2+} film.

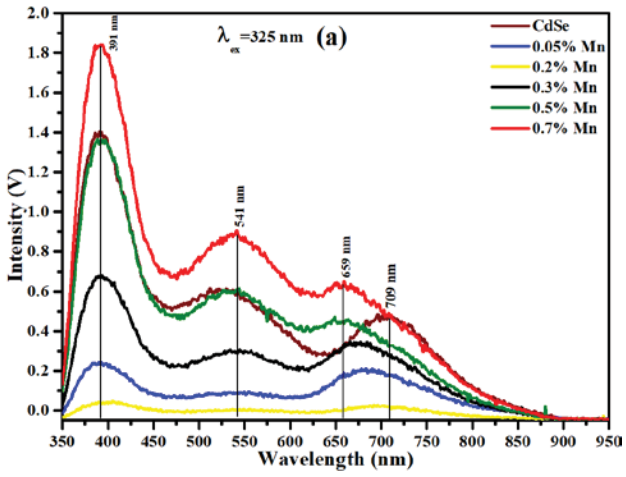

Fig. 1: Emission spectra for CdSe:x%Mn^{2+} ($0 \leq x \leq 0.7$) thin films annealed at 250°C.

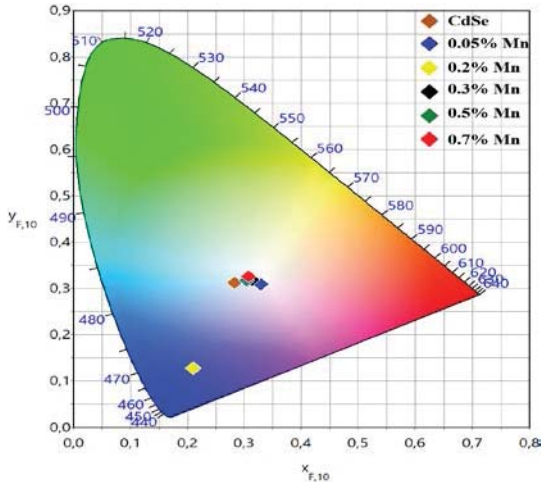

Fig. 2: CIE Chromaticity diagram for CdSe:x%Mn^{2+} ($0 \leq x \leq 0.7$) thin films annealed at 250°C.

3. References

[1] L. Qu, X. Peng. *J Am Chem Soc*. 124 (2002) 2049–2055.
[2] A.A. Yadav, M.A. Barote, E.U. Masumdar. *Mater Chem Phys.* 121 (2010) 53–57.

Integrating a phosphor material into an optical waveguide

Lucas J B Erasmus[1,2], Philippe F Smet[2], Dirk Poelman[2], Jacobus J Terblans[1] and Hendrik C Swart[1]

[1] Department of Physics, University of the Free State, Bloemfontein, South Africa
[2] Department of Solid State Sciences, Ghent University, Ghent, Belgium
Corresponding author e-mail address: erasmuslb@ufs.ac.za

1. Introduction

This study investigated the use of phosphor materials in luminescent solar concentrators (LSC). Figure 1 shows that an LSC typically consists of a transparent waveguide with an embedded luminescent material [1]. In our case, the luminescent material was in the form of a phosphor. The large area of the waveguide collects solar radiation while the luminescent material absorbs the energy and downshifts it to longer wavelengths. To allow the propagation of the emitted light over a relatively long distance in the waveguide, there must be little to no spectral overlap between the absorption and emission of the luminescent material. In addition, the refractive indices of the luminescent material and the waveguide should be closely matched to reduce scattering [2]. Internal reflection aids in directing the emitted light towards smaller areas on the sides. The strategically placed solar cells on the waveguide edges were then used to convert the concentrated light into electricity. Hence, a large collection area was coupled with a limited solar cell area.

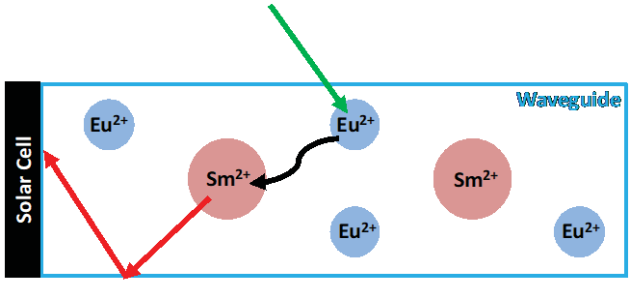

Fig. 1: Edge-on schematic explaining the basic principle of a luminescent solar concentrator. The phosphor absorbs solar radiation. This energy is transferred, downshifted, and emitted in the near-infrared region. This radiation is guided towards the edges of the waveguide, where a solar cell is used for energy conversion.

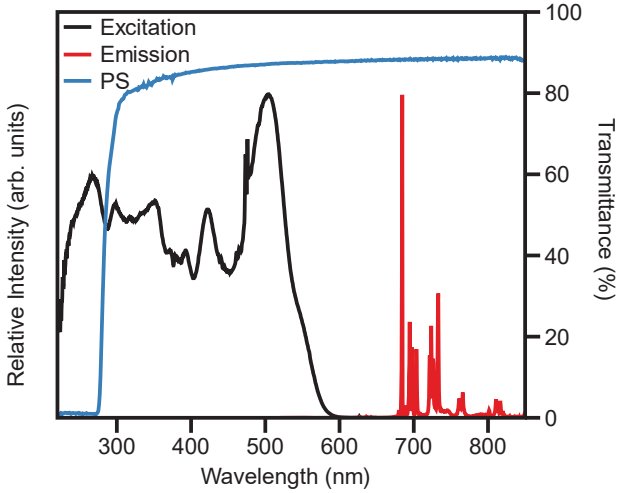

Fig. 2: Excitation (λ_{em} = 684.5 nm) and emission (λ_{ex} = 508.5 nm) spectra of the optimised phosphor material, together with the transmission spectrum of the polystyrene (PS) waveguide.

2. Results

Strontium hexaborate doped with europium and samarium (SrB_6O_{10}:Eu, Sm) was considered a suitable phosphor for this application. These ions were successfully incorporated into the SrB_6O_{10} host material using a conventional solid-state reaction method. Using empirical methods, the phosphor materials have been optimised for application in solar technology. Figure 2 shows that the optimised material has a broad excitation range from 220 to 600 nm, containing contributions from the Eu^{2+} and Sm^{2+} ions. The material exhibited strong and narrow emissions from 650 to 850 nm following radiative transitions within the Sm^{2+} ions. The internal luminescence quantum efficiency of the optimised material was 79% (λ_{ex} = 508.5 nm). There is little to no spectral overlap between the excitation and emission, which reduces the probability of reabsorption. These characteristics make this phosphor material a promising candidate for LSC applications. The optimised phosphor was encapsulated in a polystyrene waveguide. Polystyrene was chosen because of its wide optical transparency range of 300 to 1350 nm and refractive index, which closely matches that of the SrB_6O_{10} host material [3]. The refractive index of the host material was determined to be 1.61, while the polystyrene waveguide has a measured refractive index of 1.58. The successful incorporation of the phosphor material into the optical waveguide resulted in a prototype system that may be appropriate for use as an LSC.

3. References

[1] C. Yang, R.R. Lunt, Advanced Optical Materials **5,** 1600851 (2017) 1–10
[2] D.K.G. de Boer, D.J. Broer, M.G. Debije, W. Keur, A. Meijerink C.R. Ronda, et al. Optical Society of America **021111** (OCIS, 2011) 1197–9
[3] X. Zhang, J. Qiu, X. Li, J. Zhao, L. Liu, Applied Optics **59,** 8 (2020) 2337–44

Thermal stability of diketopyrrolopyrrole-based terpolymers with tunable broad band absorption for polymer solar cells

Leonato T. Nchinda[1], Newayemedhin A. Tegegne[1,2], and Tjaart P.J. Krüger[1]

[1]University of Pretoria, Department of Physics, South Africa.
[2]Addis Ababa University, Department of Physics, Ethiopia.
Corresponding author e-mail address: nchindaleonato@gmail.com

With the advent of novel polymers, organic solar cell (OSC) research has evolved significantly over the past decade. The molecular engineering of terpolymers has allowed for simple morphological control in binary devices over ternary blends, with the highest power conversion efficiencies (PCEs) exceeding 18%. Unlike photovoltaics based on inorganic semiconductors such as silicon, OSCs deteriorate during illumination and in the dark. In this regard, we examined the thermal stability of a series of terpolymers comprising one electron donor (BDTT) and two types of electron acceptors (FTAZ and TTDPP), blended with $PC_{71}BM$. The terpolymers exhibited very broad absorption spanning from 300 to 900 nm, illustrating the success of the terpolymer approach. Thin films of the terpolymers blended with $PC_{71}BM$ were degraded at 85 °C and characterized as potential active layers for OSCs. The fresh films had a PCE of 5.7% with a short-circuit current density of 15.2 mA/cm^2, demonstrating strong complementarity in the absorption of the donor and acceptor materials. After thermal annealing at 85 °C, the fullwidth at half-maximum of the symmetric C=C stretching mode, the C=C/C-C intensity ratio, and the Raman shift of the C=C mode of pristine terpolymers revealed that incorporation of the TTDPP acceptor improves the thermal stability of the terpolymer:$PC_{71}BM$ active layers. However, prolonged thermal annealing times (>3 hours) resulted in the development of $PC_{71}BM$ aggregates. We revealed the thermally-induced morphological changes by means of atomic force microscopy, transmission electron microscopy, and optical spectroscopy. Our findings indicate that by gradually annealing the blend films using an appropriate annealing time, the diffusion of $PC_{71}BM$ molecules to form aggregates can be carefully regulated, resulting in a nanostructure critical to the efficiency of organic solar cells. Provisional transient-absorption spectroscopy results shed further light on the energy transfer pathways and timescales within the terpolymers.
.

Simple approach to growth and characterization of GO/ZnO/P3HT layered nanostructures for solar cell devices

Fokotsa Victor Molefe[1,2], **Mokhotjwa Simon Dhlamini**[1], **Bakang Moses Mothudi**[1]

[1] *Department of Physics, University of South Africa, Private Bag X 6, Florida, 1710, South Africa*
[2] *Department of Physics, Tshwane University of Technology, Private Bag X 680, Pretoria, 0001, South Africa*
Corresponding author e-mail address: volksfmv@gmail.com

1. Introduction

While graphene remains a "super star" nanomaterial for various applications including aerospace, medicine, energy storage and electronic devices, its association with semiconductor nanomaterials is at the core of significant research investigations for almost two decades [1]. In the field of photovoltaic (PV) energy devices, the use of carbon-based nanomaterials such as carbon nanotubes, fullerenes and graphene were proved to be successful strategy to enhance solar cell performance. That was achieved by exploiting the specific electronic properties of graphene nanomaterial linked with its high charge carrier mobility, that can be further tuned by functionalization using various inorganic semiconductors and introducing rare earth ions by method of doping. Multiple routes have been taken to achieve efficient charge transfer between P3HT and graphene, but to the best of our knowledge a lot has not been done on the use of graphene oxide (GO) tailored with semiconductor materials for PV applications.

In this work, we illustrate the relevance of GO/ZnO layered nanostructure as charge extraction layer in organic solar cells. We discuss the properties of sol-gel derived ZnO [2] and graphene oxide prepared by chemical oxidation of graphite [3]. The obtained solutions we utilized to grow layered nanostructures using the spin coating technique. The properties of GO/ZnO layered nanostructures were investigated using X-ray diffraction, scanning electron microscopy, Fourier transform infrared spectroscopy, UV-Vis, Photoluminescence and J-V techniques.

The electron transfer is investigated by calculating the quenching efficiency parameter η using equation (1) [4]

$$\eta = 1 - (I / I_0) \qquad (1)$$

where I_0 and I represents the integrated PL intensities of the donor (P3HT) prior and after growth of the accepter of electrons.

2. Results

The beneficial effect of GO is revealed through PL quenching indicative of charge transfer from the active layer as presented in Fig. 1. A high quality intimate electronic contact was achieved at the interface of GO/ZnO layered nanostructures. This effect is exploited for organic PV applications as shown in Fig. 2.

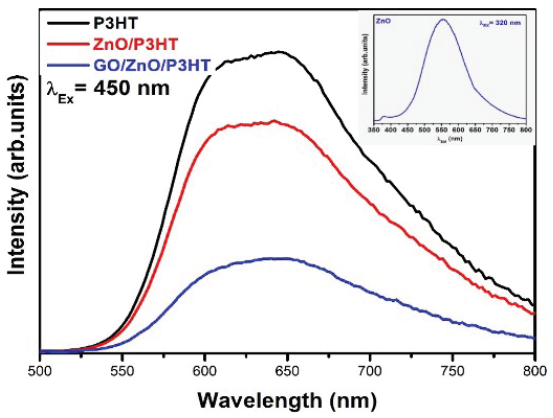

Fig. 1: PL emission spectra of P3HT, ZnO/P3HT and GO/ZnO/P3HT layered nanostructures.

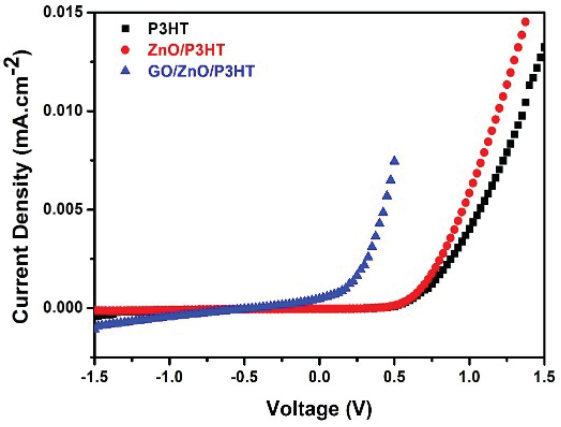

Fig. 2: I-V characteristics of P3HT, ZnO/P3HT and GO/ZnO/P3HT devices under illumination.

3. References

[1] H. Lin, Q. Jiang, X. Bai, D. Li, Z. Huang, W. Huang and S. Feng. *Appl. Therm. Eng.* **218** (2023) 119176.
[2] G.L. kabongo, P.S. Mbule, G.H. Mhlongo, B.M. Mothudi, K.T. Hillie and M.S. Dhlamini. *Nanoscale Res. Lett.* **11** (2016) 418.
[3] F.V. Molefe, M. Khenfouch, M.S. Dhlamini and B.M. Mothudi. *Adv. Mater. Lett.* **8** (2017) 246.
[4] R. Bkakri, O.E. Kusmartseva, F.V. Kusmartsev, M. Song and A. Bouazizi. *J. Lumin.* **161** (2015) 264.

Deep-level transient spectroscopy study of the effect of Pd deposition on radiation induced defects in Si

Willem Barnard, Danie Auret, Walter Meyer

[1] *Department of Physics, University of Pretoria, Pretoria, South Africa*

Corresponding author e-mail address: walter.meyer@up.ac.za

1. Introduction

The properties of Si as semiconductor have been studied for many decades, however there are still new and unexpected results obtained. In this study we found that, contrary to expectation, the set of deep levels observed in an electron-irradiated Schottky diode depended on the order in which the sample was irradiated and the Schottky contact was deposited. We carefully investigated this phenomenon using deep-level transient spectroscopy.

2. Experimental

In order to determine the origin of the effect, Schottky diodes on Si samples were produced using the standard HF cleaning techniques followed by resistive physical vapour deposition of Pd. Some samples (which we will refer to as "pre-irradiated") were irradiated before cleaning and deposition of the Pd, while others (which we will refer to as "post-irradiated") were irradiated after deposition of the Pd contacts. This procedure as repeated with various metals as well as a combination where various thicknesses of Au was deposited before the Pd was deposited.

In the post-irradiated samples, the well-known radiation-induced defects were observed [1]: C_iO_i, C_i, VO_i, C_iC_s, $VV^{=}$, VV^{-} and the VP_s were observed with activation energies of E_C − 0.07, 0.110, 0.170, 0.170, 0.230 ,0.360 and 0.460 eV were observed. However, in the pre-irradiated samples, a completely different set of defects with activation energies of E_C − 0.053, 0.092, 0.140, 0.182, 0.220, 0.261, 0.360, 0.423, 0.443, 0.469, 0.486, and 0.607 eV were observed. This effect was only observed with Pd, while other metals such as Au and Ni had no observable effect on irradiation-induced complexes in Si. When an intermediate Au layer was deposited, the Au layer partially inhibited the effect, so that with a layer thickness of 4 nm, both sets of peaks were visible, as shown in Figure 1.

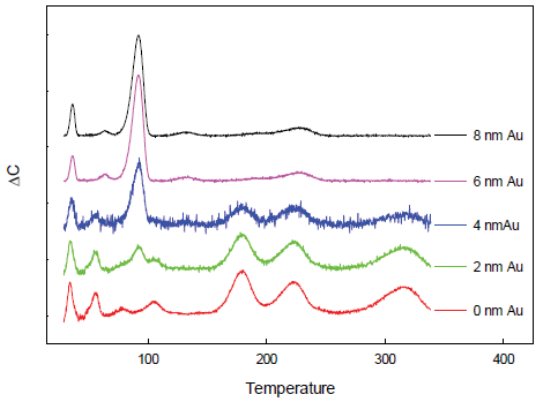

Fig. 1: DLTS spectra of pre-irradiated diodes in which an intermediate Au layer of varying thickness was deposited after irradiation.

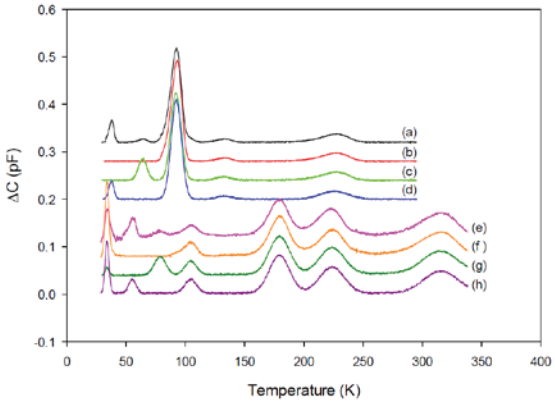

Fig. 2: DLTS spectra of post (a-d) and pre-irradiated (e-h) diodes fabricated on substrates with different impurity concentrations.

By careful experimentation using substrates with different impurity concentration (see Figure 2), we show that the defects in the pre- and post-irradiated samples are related. We present these results and discuss the possible origin of the defects.

3. References

[1] F. Hönnigera, E. Fretwursta, G. Lindström, G. Kramberger, I. Pintilie, R. Röderd, Nucl. Inst.Meth. A **583** (2007) 104–108

Comments on the refractive index of $Al_xGa_{1-x}As$

JAA Engelbrecht[1] and JAA Engelbrecht[2]

[1]Centre for HRTEM /Physics Department, Nelson Mandela University, Gqeberha, South Africa
[2]Department of Electrical and Electronic Engineering, Stellenbosch University, Stellenbosch, South Africa
Corresponding author e-mail address: Japie.Engelbrecht@mandela.ac.za

1. Introduction

$Al_xGa_{1-x}As$ is a ternary alloy semiconductor which is used in high-speed electronics and optoelectronic devices. Applications in optics and the design of optical devices require knowledge of the optical properties of the semiconducting material used, of which the refractive index is one of the important parameters. A range of articles are available reporting on the refractive index of $Al_xGa_{1-x}As$. Many investigations reported on formulas to calculate the refractive index as a function of the As molar fraction x and/or the energy/wavelength [1-8]. In most cases, the publications also contained theoretical and/or experimental results of the refractive index. A set of results for the refractive index of $Al_xGa_{1-x}As$ alloys from x = 0 to x = 0.804 were reported by Aspnes et al [9]. Experimental results for the refractive index n of $Al_xGa_{1-x}As$ were reported by a number of researchers [6,7, 9-12] (Fig.1). This investigation assessed the various formulae and experimental results to establish a simpler formula that best agreed with reported results of Aspnes et al [9].

2. Results

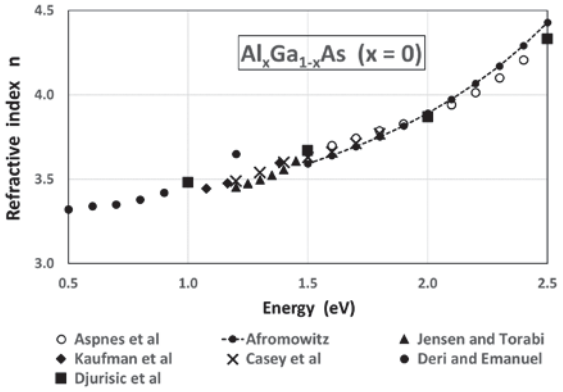

Fig. 1: Comparison of the values published by Aspnes et al [9] and experimental values measured by other researchers.

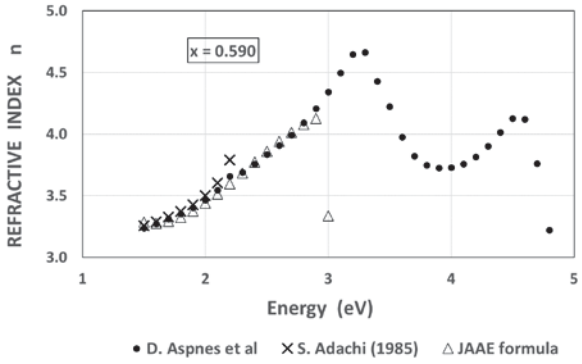

Fig. 2: Comparison of the proposed formula with the values of Aspnes et al [9], Adachi [2] and the proposed formula.

It is noted that the formula of Adachi [2], is limited to energy values less than 2.5 eV. A simple formula consisting of three polynomial equations was proposed to calculate the refractive index of $AlGa_{1-x}As_x$ as a function of both Al mole fraction x and the energy (or wavelength/wavenumber). The process contributing to the derivation of the three binomial equations will be explained. While the proposed formulae do not cover the entire range of the experimental values, it at least covers the range up to 3 eV (Fig. 2). Some challenges associated with the use of the three polynomial equations will also be presented.

3. References

[1] M.A. Afromowitz. *Solid State Comm.* **15** (1974) 59.
[2] S. Adachi. J. Appl. Phys. **58** (1985) R1.
[3] S. Adachi. J. Appl. Phys **35** (1987) 7454.
[4] S. Adachi. *Phys. Rev. B* **38** (1988) 12345.
[5] S. Adachi. *J. Appl. Phys.* **66** (1989) 6030.
[6] R.G. Kaufman, G.R. Hulse, D.J. Vezzetti, A.L. Moretti, K.A. Stair, G.P. Devane and T.E. Bird. *J. Appl. Phys.* **75** (1994) 8053.
[7] S.G. Hu, M.B.M Rizan, S.G. Matsik, A.G.U. Perera, G. Von Winckel, A. Stintz and S. Krishna, *J. Appl. Phys.* **97** (2005) 093529-1.
[8] P. Schygulla, P. Fuß-Kalluweit, O. Höhn and F. Dimroth. *J. Phys. D: Appl. Phys.* **53** (2020 495104.
[9] D.E. Aspnes, S.M. Kelso, R.A. Logan and R. Bhat. *J. Appl. Phys.* **60** (1986) 754.
[10] B. Jensen and A. Tobari, *IEEE J. Quantum. Electron.* **QE-19** (1983 877.
[11] R.J. Deri and M.A. Emanuel, *Integrated Photonics Research* **7** (Optical Society of America) (1995) paper IThG11.
[12] A.B. Djurišić, A.D. Rakić, P.C.K.Kwok, E.H. Li, M.A. Majewski and J. M. Elazar. *J. Appl. Phys.* **86** 445.

Development of 2D/3D stable tin-based halide perovskite solar cell

Mmantsae Diale[1], **Margdaline Ligavo, Alex Sembito, Sizwe Sibiya, Juvet N. Fru**

[1] *University of Pretoria, Department of Physics, Private Bag X20, Hatfield, 0208*
[2]*IUniversity of Nairobi, Department of Physics, P. O. Box 30197, Nairobi, 0010.*
Corresponding author e-mail address: Mmantsae.diale@up.ac.za

1. Introduction

Sn-based HaP were first introduced as conducting channels for this film field effect transistors some two decades ago. The successful use of Sn-based material as a light absorber in Schottky barrier solar cell with a PCE efficiency of 0.9%, encouraged researchers to pursue the material as a possible replacement of lead for stability of perovskites [1]. This led to the development of 2D/3D Sn-based perovskites as prospective future candidates for stable Ha-P solar cell, where the photo conversion efficiency (PCE) has steadily increased to 14.81% [2]. However, the fast and easy oxidation of $Sn^{2+}to$ Sn^{4+} in the system contributes to poor stability and low PCE of Sn-based perovskite solar cells. In this work, SnF_2 was gradually introduced in the $FASnI_3$ perovskite precursor solution alongside N-N'-diphenyl-P-phenylenediamine (DPP-DTT) antioxidant as a co- additive, and their effect on the performance and stability of the perovskite film studied. The results show improved stability from less than an hour with SnF_2 alone to more than 1300 hours with DPP-DTT. A 3D planar inverted FTO/PEDOT:PSS/FASnI3/PCBM:P3HT/Ag structure was fabricated, and the results shows that.

2. Results

The results show improved stability from less than an hour with SnF2 alone to more than 1300 hours with DPP-DTT. A 3D planar inverted FTO/PEDOT:PSS/$FASnI_3$/PCBM:P3HT/Au structure was fabricated, and the results shows that the photo-conversion efficiency improved with stability of the $FASnI_3$/SnF2/DPP-DDT.

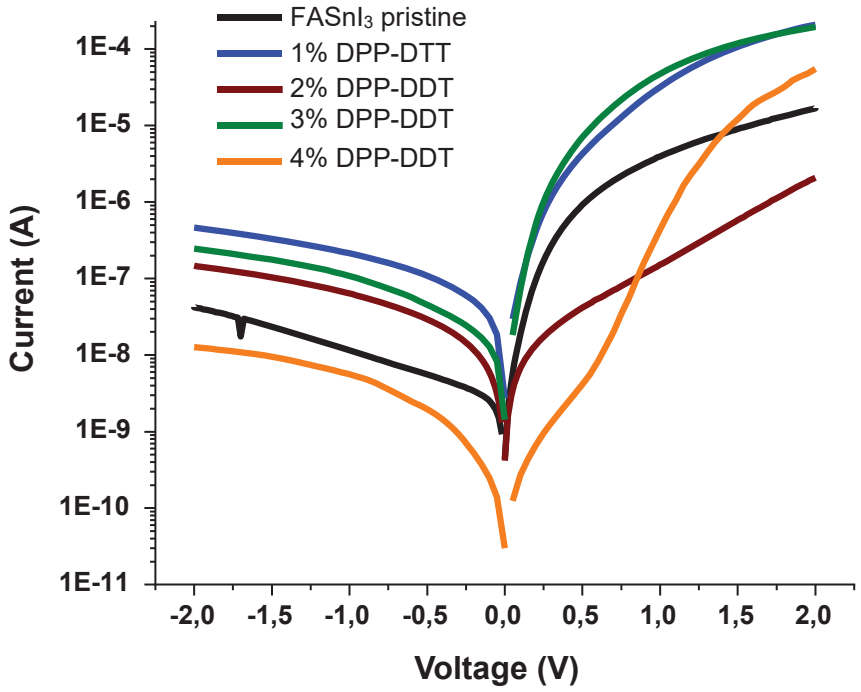

Fig. 1: I-V measurements of the dark current measurements of the solar cell.

3. References

[1] Jiupen Cao and Feng Yan, Review progress in tin-based solar cell, Energy Environ. Sci., 2021, 14, 1286.
[2] Yu, B.-B., Chen, Z., Zhu, Y., Wang, Y., Han, B., Chen, G., Zhang, X., Du, Z., & He, Z. (2021). Heterogeneous 2D/3D Tin-Halides Perovskite Solar Cells with Certified Conversion Efficiency Breaking 14%.

List of Posters

Reg No.	Poster No.	Presenter	Title
5	1	Sumedha Tamboli	Microwave-assisted hydrothermal synthesis of LaOF:Pr^{3+} for optical thermometry
7	2	E. Coetsee	Fluorescence properties of Tb^{4+} and Tb^{3+} inter-conversion states in CaF_2 phosphor material
9	3	Vhahangwele Makumbane	Pulsed laser deposition of Y_2O_3:Ho^{3+}, Yb^{3+}: structure and upconversion luminescence for different number of laser pulses
12	4	N.A.M. Saeed	Visible/infrared emission investigation of YOF:Ho^{3+} co-doped with Yb^{3+}
14	5	M.Y.A. Yagoub	Anomalous emission of Yb^{2+} in CaF_2:Tb^{3+}, Yb^{3+} up-conversion phosphor
15	6	Sarojini Jeeva Panchu	Encapsulation of Si QDs in Europium doped Zeolitic Imidazole Framework (Eu-ZIF-8) for photoluminescence tuning
16	7	Rethabile A. Phokojoe	Effect of Cr^{3+} on the SiO_2 nanoparticles prepared via sol-gel method
17	8	G.J. Odendaal	Reduction methods for Sm^{3+} to Sm^{2+} in strontium borates for solar energy applications
19	9	Umer Mushtaq	Structural and photoluminescence properties of Ho doped $BaAl_2O_4$ phosphors
21	10	Nisar Hussain	Color tunable nano-crystalline $Ba_2Nd_8(SiO_4)_6O_2$:Tb^{3+} phosphor for solid state lighting
22	11	Latief Mohi ud din	Effect of Tb^{3+} Doping on the Photoluminescence Properties of Zirconia Nanophosphors Synthesized via Sol-gel Route for LED Applications
23	12	Thandi Mazibuko	Structural properties of K_2NbF_7: Mn^{4+} red-emitting phosphors for application in warm white light emitting diodes
25	13	J. Divya	Structural and optical characteristics of Ho^{3+} doped α-Bi_2O_3 thin films deposited by pulsed laser deposition on glass substrates
26	14	Richard Harris	Producing ZnO nanostructures that exhibit NIR luminescence with a templated design procedure
28	15	Londiwe Khumalo	The influence of a binary phase ZnO-CuO on the poly-ε-caprolactone based nanocomposites
32	16	M.R. Mhlongo	The effect of Gd^{3+} co-doping on the morphology and optical properties of Sm^{3+} doped strontium oxide mixed phases prepared by sol-gel method
20	17	Abdulraoof Ali	Electrical characterization of α-particle irradiation-induced defects in GaN grown by electrodeposition
33	18	Zahlia Stacey	Alpha particle irradiation induced defects in ZnO thin film fabricated onto p-Si by thermal spray pyrolysis
42	19	F. Taghizadeh	High-resolution Laplace deep level transient spectroscopy of the palladium Schottky effect on alpha radiation-induced defects in germanium
79	20	Jackie Nel	Investigation of the structural and temperature dependent electrical properties of MZnO (M = Ce and Sm) Schottky diode devices fabricated using the sol-gel spin coating technique
50	21	Mustafa Ahmed	Effect of Bi doping on the structural, optical and electrical properties of ZnO nanorods grown by chemical bath deposition

Mathematica

Mathematica is the world's most powerful global computing environment. Features include automated symbolic and numeric computation, Machine Learning, neural networks, dynamic interactivity, and a complete programming language.

Wolfram System Modeler

Using drag-and-drop from the built-in and expandable libraries, you can build industrial strength, multidomain models of your complete system.

Expert Choice

Make better, faster, more justifiable decisions with Expert Choice. Application areas include Strategic Planning, Vendor Selection, HR, Risk, and Resource Allocation

Systat

New and improved: More Statistics, More Graphs, Less Effort! SYSTAT has a 20 year track record of bringing you industrial strength statistics at an affordable price.

LINDO

Speed and ease-of-use have made LINDO Systems a leading developer of software tools for building and solving optimization models

BLUESTALLION technologies

Scientific, Technical and Engineering SOFTWARE

We are the proud distributors of the following products in South Africa

SigmaPlot

The technical graphing standard used by over 100,000 researchers worldwide. Now also includes the functionality of SigmaStat

Origin

Origin is the complete solution for data analysis and technical graphing. Import data from Excel and then perform advanced analysis (including non-linear fits, FFT, ANOVA, etc)

Hugin Expert

Hugin is a tool which enables you to construct decision support systems using bayesian Networks and their extension influence diagrams.

MathType

MathType is a powerful interactive tool for Windows and Apple OS that lets you create mathematical notation for word processing, web pages and presentations

AnyLogic

Anylogic is a professional simulation tool for complex discrete, continuous, hybrid and agent based systems. Powerful and flexible, it is used to model, simulate, visualize and analyze a diverse range of problems

For a free evaluation or more information, please call (011) 447 9916 or email: info@bluestallion.co.za
PO Box 786246, Sandton, 2146, South Africa

Reg No.	Poster No.	Presenter	Title
77	22	C.R. Thaba	Characterization of radiation-induced defects in germanium using DLTS and LDLTS
38	23	Sefako J. Mofokeng	Structural and up-conversion mechanism of spinel $Zn_2TiO_4:Er^{3+},Yb^{3+}$ phosphor
40	24	M.M. Duvenhage	The effect of annealing temperature on the phase change of spin coated $Y_2SiO_5:Ce^{3+}$ on silicon (100) substrate
44	25	Thapelo Seimela	Incorporation of Copper Nanoparticles in PEDOT: PSS for Organic Solar Cells
46	26	Mduduzi Mbongo	Thermoluminescence studies of spinel structure of $ZnGa_2O_4$
51	27	Seithati Qotso	Synthesis and characterization of P3HT-ZnO: FWCNTs for possible application in organic solar cells
54	28	Thabang J. Theka	Fabrication of Metal Organic Frameworks Derived Co_3O_4 Semiconductor Metal Oxides Loaded on TiO_2: Influence of Fe Loading on the Optical and Chemiresistive Characteristics of Co_3O_4/TiO_2 Heterostructure
56	29	D.V. Mlotswa	Luminescence properties of a Cr^{3+} doped $MgTa_2O_6/Mg_4Ta_2O_9$ composite phosphor
58	30	Ngcali Tile	Effect of dot size on the photolumenescence emission of GaSb/GaAs QDs
63	31	A.U Yimamu	The effect of electrolytic pH on the properties of electrodeposited CdTe thin films for solar energy application
41	32	RE Mapasha	Alteration of Li states on a self-healed graphane
65	33	RE Mapasha	Electrically active defects levels induced by trivalent substitution-interstitial defect-complexes in Ge
45	34	Fortune Moruta	Density Functional Theory Investigation of the Properties of the E-Centre in P, As and Sb doped Si
59	35	Sentserere Kgalema	Enhancement of Li and graphane interaction through extended H vacancy pathways for Li-ion batteries: Ab initio study
92	36	Gabriela Herrero-Saboya	Functionalizing barium hexaferrite nanoplatelets through push-pull systems: an ab initio approach
93	37	Nicolas Salles	Refactoring of ARTn: a plugin for electronic structure calculation and molecular dynamics codes
94	38	Matic Poberžnik	Investigation of the surface stability of barium hexaferrite bulk terminations by means of ab initio thermodynamics
95	39	Abdulgaffar Abdurrazaq	First principles calculation of multi-vacancies and multi-interstitials defects in Ge by the DFT + alpha method
66	40	Murendeni Nemufulwi	Preparation of highly sensitive Cr doped $ZnFe_2O_4$ fiber-like sensors for selective acetone detection
67	41	Karabo B. Morebodi	The effects of Eu^{3+} concentration on the photoluminescence of $Na_4Ca(PO_3)_6$: Eu^{3+} phosphors prepared by a solid state reaction method
68	42	T.K.W Mohapi	Effect of deposition voltage on the properties of electrodeposited CdZrS thin films for solar cell application
69	43	Casey Mcleavy	Experimental determination of $InSb_xAs_{1-x}$ bandgap energy
70	44	Mosima Kgomo	Highly ethanol responsive nanosensor layer based on mesoporous nanostructured cube-like Indium Oxide: Effects of Co, Ni and Cu dopants
71	45	Tebogo Motsei	Nanotechnology-based supercapacitor energy storage with microcontroller monitoring for application in battery-less electronics

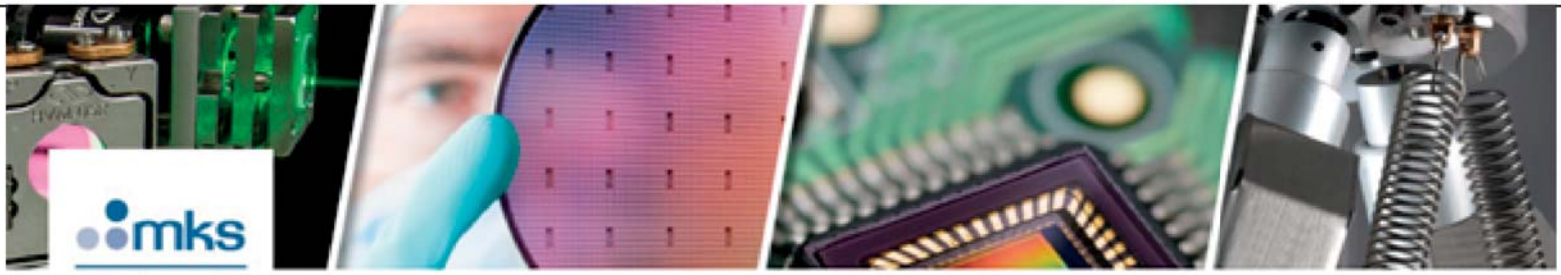

Wirsam Scientific is the proud sole agent of MKS Newport Solutions.

Newport's innovative solutions leverage core expertise in vibration isolation and sub-micron positioning systems, opto-mechanical and photonics subsystems, to enhance our customers' capabilities and productivity in the semiconductor, industrial technologies, life and health sciences, and research and defense markets.

The Newport product portfolio consists of a full range of solutions including:
• Montion control • Optical tables • Vibration isolations systems • Photonic instruments • Optics and opto-mechanical components • Light Analysis • Tables and Isolation Systems • MKS Vacuum and Gas Solutions.


Motion


Opto-mechanics


Optics


Lasers


Light Sources


Light Analysis


Tables & Isolation Systems


Laser Diode Control


MKS Vacuum & Gas Solutions


NEW! Products


Custom Products


Browse All Products

wirsam
SCIENTIFIC

For any enquires contact us: wirsamjb@wirsam.com
Tel: +27 (0)11 482-1060

Reg No.	Poster No.	Presenter	Title
74	46	Rethabile Makole	The study of the synergistic effects of Yb^{3+} rare-earth ions on the luminescence and gas sensing properties of Co_3O_4-In_2O_3 heterostructure
76	47	Assane Talla	Perpendicular orientation of microdomains of Poly (styrene-block-methylmethacrylate (PS-b-PMMA) thin films produced on Zinc oxide nanoparticle layer
78	48	T.M. Mohlala	Effect of radiation damage on the migration behaviour of Europium implanted into single crystalline 6H-SiC at RT and 350 ^oC
80	49	Zamaswazi Tshabalala	Influence of Pt-loading on the energy band gap and VOCs Sensing of metal titanate perovskite
81	50	Adiel Holtzhausen	Influence of coating techniques on the optical and structural properties of nanostructured hematite thin films
84	51	Jorma Hölsä	R^{3+} co-doping in persistent luminescence materials: pros and cons
86	52	Jorma Hölsä	Multifunctional Nano-TbO_2: Oxygen Retention, Nanopigment, Paramagnet
89	53	Andi Isni Pujirana	Characteristics of GaAs Thin Films Grown by MOVPE Using Triethygallium (TEGa) and Tertiarybutylarsine (tBAs)
90	54	Pebetsi Thokwane	Influence of Yb^{3+}-Nd^{3+} concentration on the upconversion luminescence and the defect structure of $NaGdF_4$ nanocrystals for possible application in perovskite solar cells
96	55	Eduard Madirov	New opportunities in plastics recycling through the use of luminescent upconversion phosphors
98	56	Boiketlo RJ. Thamaga	Structure, optical, and low-temperature detection of acetone induced by p-n NiO-CeO_2 decorated with Ag nanoparticles
99	57	Rapelang G. Motsoeneng	The Influence of Fe loading on the Optical and Gas Sensing Characteristics of ZnO/SnO_2 Heterostructures
30	58	Peter Viljoen	Effect of Stacking on Optical properties of GaSb/GaAs Quantum Rings

P1

Microwave-assisted hydrothermal synthesis of LaOF:Pr^{3+} for optical thermometry

Sumedha Tamboli[1], **Govind B. Nair**[1], **S. J. Dhoble**[2], **H. C. Swart**[1]

[1] *Department of Physics, University of the Free State, P. O. Box 339, Bloemfontein, 9300, South Africa*
[2] *Department of Physics, R.T.M. Nagpur University, Nagpur, 440033, India*
Corresponding author e-mail address: Tamboli.SJ@ufs.ac.za

1. Introduction

Lanthanide (Ln^{3+})-doped nanophosphors have demonstrated more promising traits than any other luminescent material for non-contact luminescence thermometry [1]. Ln^{3+}-doped nanophosphors offer chemically stable structures that exhibit repeatability, reproducibility, and photostability, which are important for luminescence thermometry. Luminescence thermometry is classified into six categories depending on the probed parameters: (1) band-shape, (2) spectral shift, (3) intensity, (4) bandwidth, (5) polarization, and (6) lifetime [2]. It is more convenient to monitor the variation in luminescence intensity with thermal changes; therefore, most of the studies have focused on exploring the dependence of luminescence intensity of the phosphor on temperature. Phosphors with single, dual, or multiple emitting centers have been investigated in recent years to develop highly efficient luminescence thermometers.

In this study, Pr^{3+}-doped LaOF nanophosphors were investigated for their temperature-dependent photoluminescence properties using blue laser (473 nm) excitation. Pr^{3+} acts as a single emitting center in the oxyfluoride host matrix, producing multiple emission bands in the visible and near-infrared regions. The fluorescence intensity ratios (FIRs) of the thermally-coupled and non-thermally coupled levels of Pr^{3+} were exploited to study their behaviour in the temperature ranging 303-573 K.

2. Results

LaOF:Pr^{3+} nanophosphors were synthesized using a microwave-assisted hydrothermal method. They crystallized in the trigonal phase with the space group $R\bar{3}m$. The optimum Pr^{3+} concentration in LaOF was 0.002. Under 473 nm blue laser excitation, the PL emission spectra in the visible and near-infrared (NIR) regions were recorded at different temperatures. The FIRs of the emission bands were calculated by using their integrated intensities. I_{994}/I_{1306} was found to be the best among all the FIRs of the LaOF:Pr^{3+} nanophosphor. The absolute and relative sensitivities of each FIRs are plotted in Fig. 1 and Fig. 2.

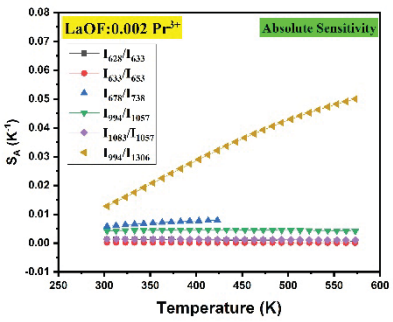

Fig. 1: Absolute sensitivity (S_A) for different FIRs of LaOF:0.002Pr^{3+} nanophosphor.

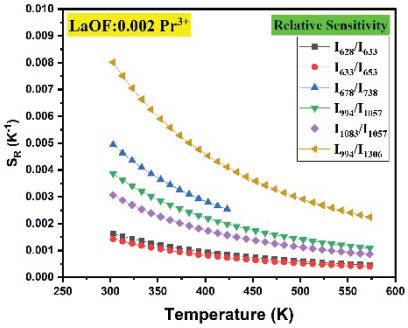

Fig. 2: Relative sensitivity (S_R) for different FIRs of LaOF:0.002Pr^{3+} nanophosphor.

3. References

[1] F. Jahanbazi and Y. Mao. *J. Mater. Chem. C.* **9** (2021) 16410-16439.
[2] D. jaque and F. Vetrone. *Nanoscale* **4** (2012) 4301.

Fluorescence properties of Tb^{4+} and Tb^{3+} inter-conversion states in CaF_2 phosphor material

E. Coetsee, M.Y.A. Yagoub, H.C. Swart

Department of Physics, University of the Free State, PO Box 339, Bloemfontein, ZA9300, South Africa
Corresponding author e-mail address: CoetseeE@ufs.ac.za

1. Introduction

Lanthanide ions-based luminescent materials has been prioritized at the forefront of research to improve the photovoltaic conversion efficiency of solar cells [1,2]. Down-conversion through trivalent lanthanide ion (Ln^{3+}) couples, Ln^{3+}-Yb^{3+}, has been demonstrated in various hosts. The use of the down-conversion layer is still far from practical applications due to the relatively weak 4f-4f absorption of the sensitizer (Ln^{3+}) ions [1]. In this article, we report the fluorescence properties of Tb^{4+} as a suitable sensitizer for Yb^{3+} ions for efficient near-infrared emission.

2. Results

The inter-conversion of Tb^{4+} and Tb^{3+} -doped CaF_2 nanoparticles was achieved by sintering the as-synthesized phosphor at 450 °C in an air atmosphere. Fig. 1 shows the variation in the reflectance spectra of the phosphors as a function of calcination time. The broad absorption peak that appeared with calcination time was associated with the Tb^{4+} absorption band. Fig. 2 presents a comparison of the Tb *3d* X-ray photoemission spectroscopy (XPS) fitted peaks between the as synthesized and calcined samples. The Vis and UV absorption and XPS results demonstrated that the ratio of Tb^{4+} ions in the phosphor material increased with the calcination time. These results; suggest that Tb^{4+} could be a suitable sensitizer for efficient NIR emissions.

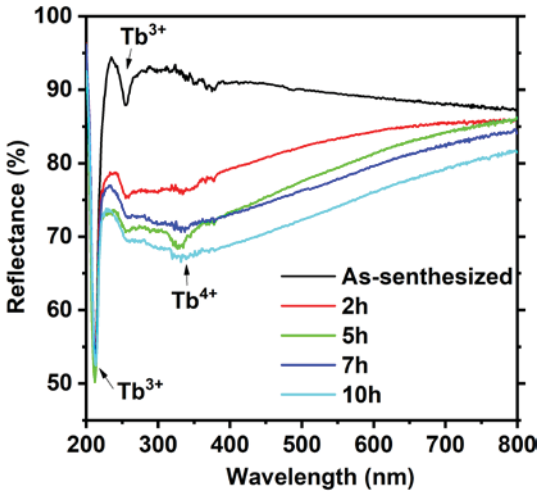

Fig. 1: Variation of the reflectance spectra as a function of annealing time of Tb doped CaF_2 calcinated at 450 °C.

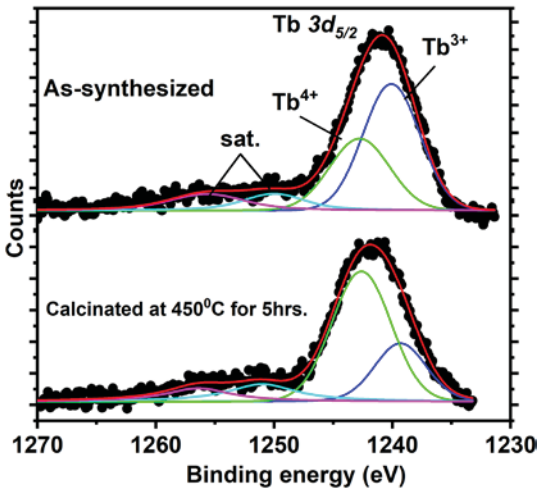

Fig. 2: XPS comparison of Tb *3d* for as synthesized and calcinated phosphor materials.

3. References

[1] B.M. Van der Ende, L. Aarts and A. Meijerink**,** *Phys. Chem. Chem. Phys.* **11** (2009) 11081-11095.
[2] M.Y.A. Yagoub, H.C. Swart and E. Coetsee, *J. Lumin.* **187** (2017) 96–101.

P3

Pulsed laser deposition of Y_2O_3:Ho^{3+}, Yb^{3+}: structure and upconversion luminescence for different number of laser pulses

Vhahangwele Makumbane, R.E. Kroon, M.Y.A. Yagoub and H.C. Swart

Department of Physics, University of the Free State, Bloemfontein, South Africa

Corresponding author email address: SwartHC@ufs.ac.za

1. Introduction

The poor absorption of low energy photons is one of the major factors influencing the low conversion efficiency of silicon (Si) solar cells [1, 2]. Upconversion (UC) phosphors, which utilize low energy photons that cannot be absorbed by the Si solar cell and convert them to high energy photons, have been explored to enhance the efficiency of Si solar cells [3]. For efficient energy enhancement of Si solar cells, the Ho^{3+}- Yb^{3+} couple has proven to be a highly efficient UC luminescence system [4]. Y_2O_3 is considered an ideal host for the Ho^{3+}-Yb^{3+} couple due to the similar ionic radii of Y^{3+} (0.900 Å), Ho^{3+} (0.901 Å) and Yb^{3+} (0.868 Å) [5]. Therefore, growth of Y_2O_3:Ho^{3+}, Yb^{3+} UC films of various thicknesses, using different number of laser pulses during pulsed laser deposition, may have a significant effect on the morphology, crystallinity, surface topography and particle size, which affect the performance of the Si solar cells. Therefore, it is important to investigate the influence of the number of pulses on the structural, morphological, optical and luminescence properties of UC Ho^{3+}, Yb^{3+} co-doped Y_2O_3 films.

2. Results

As shown in figure 1, the X-ray diffraction patterns of the prepared UC thin films are in good agreement with the standard diffraction peaks JCPDS 01-086-1107, indicating a single phase cubic structure with an $Ia\bar{3}$ space group. The UC emission spectra of the Y_2O_3:Ho^{3+}, Yb^{3+} phosphor excited at a wavelength of 980 nm are shown in figure 2. The UC emission exhibited intense green emission bands assigned to the $^5F_4 \rightarrow {}^5I_8$ and $^5S_2 \rightarrow {}^5I_8$ transitions as well as weaker red and infrared emissions corresponding to the $^5F_5 \rightarrow {}^5I_8$ and $^5S_2 \rightarrow {}^5I_7$ transitions of the Ho^{3+} ions, respectively. From figure 2, the upconversion emission was significantly influenced by the number of laser pulses.

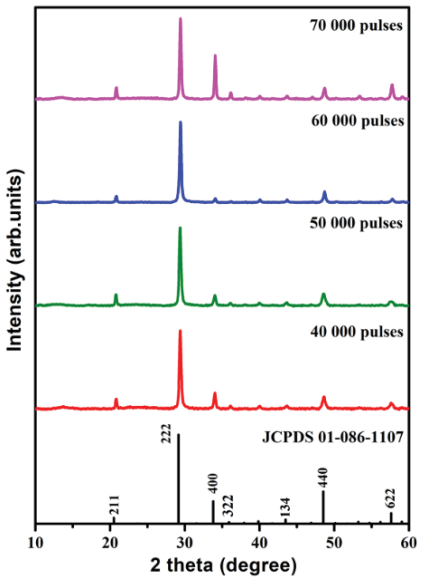

Fig. 1. XRD patterns for $Y_{2-x-y}O_3$:$Ho_{x=0.005}$,$Yb_{y=0.05}$ films with different number of pulses.

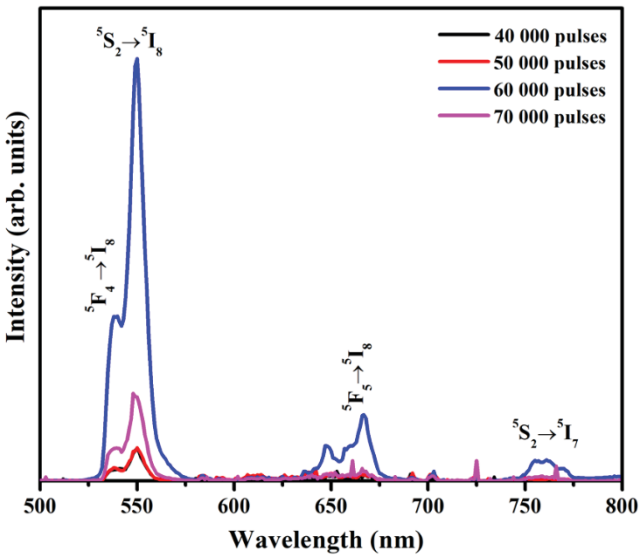

Fig. 2. UC emission for $Y_{2-x-y}O_3$:$Ho_{x=0.005}$,$Yb_{y=0.05}$ films with different number of pulses.

3. References

[1] Z. Zhang, J. Zhang, W. Zhou, M. Song, W. Li, Q. Hu, X. Zhao, Adv. Mater. Res. **66** (2009) 167.
[2] Y. Qu, X. Kong, Y. Sun, Q. Zeng, H. Zhang, J. Alloys Compd. **485** (2009) 493.
[3] G. Mialon, S. Turkcan, G. Dantelle, D. P. Collins, M. Hadjipanayi, R. A. Taylor, T. Gacoin, A. Alexandrou, J. P. Boilot, J. Phys. Chem. **C114** (2010) 22449.
[4] S.D. Jackson, Y. Li. Electron. Lett. **40** (2004) 1474.
[5] R.D. Shannon, Acta Cryst. **A32** (1976) 751.

Visible/infrared emission investigation of YOF:Ho^{3+} co-doped with Yb^{3+}

N.A.M. Saeed, E. Coetsee and H.C. Swart

Department of Physics, University of the Free State, PO Box 339, Bloemfontein, ZA9300, South Africa
Corresponding author e-mail address: Nadirazhari989@gmail.com

1. Introduction

Stoichiometric yttrium oxyfluoride (YOF) has been investigated for many years due to its intrinsic properties for different applications, such as for spectral converters for solar cells [1-3]. It combines properties of both oxides and fluorides, such as low phonon energy, transparency, ionicity, thermochemical properties, and mechanical stability [2,3]. The crystal structure of YOF is a rhombohedral structure (space group: $R\bar{3}m$ (166)) with one site available for occupation [1-3]. This allows lanthanide ions such as trivalent holmium to emit in a wide range from the visible to the infra-red regions due to the abundant meta-stable excited energy levels [1].

2. Results

Down-conversion and up-conversion emission for a set of co-doped YOF:Ho^{3+},Yb^{3+} samples are depicted in fig. 1 and 2, respectively. In fig. 1, the down-conversion process was performed under Ho^{3+} excitation at 449 nm, which shows infrared emission due to the energy transfer from Ho^{3+} to Yb^{3+} ions. Fig. 2 shows the up-conversion visible emission of different concentrations of Yb^{3+} ions with a pulsed laser excitation of 980 nm. The optimized concentration for both the down- and up-conversion emission is approximately 7 mol% of Yb^{3+}. The Yb^{3+} emission at 971 nm in the down-conversion process, however, has an optimum concentration at 3 mol% of Yb^{3+} due to the concentration-quenching of the Yb^{3+}-Yb^{3+} interaction. Therefore, this, material could be a promising candidate for application as a spectral converter in Si solar cells.

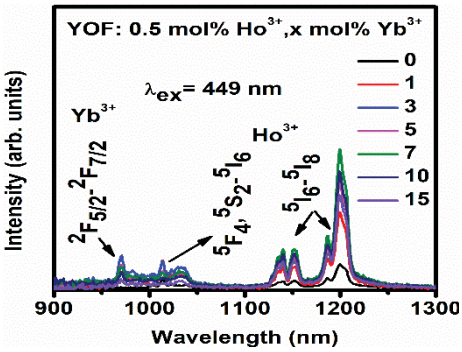

Fig. 1: Down-conversion emission of YOF:Ho^{3+},Yb^{3+}.

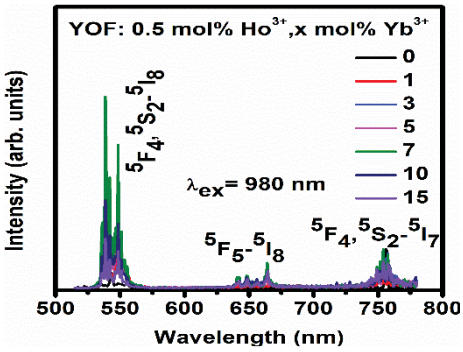

Fig. 2: Up-conversion emission of YOF:Yb^{3+},Ho^{3+}.

3. References

[1] N.A.M. Saeed, E. Coetsee and H.C. Swart, *Mater. Res. Bull.* 159 (2023) 112089 - 112099.
[2] Y. Zhang, D. Geng, X. Kang, M. Shang, Y. Wu, X. Li, H. Lian, Z. Cheng and J. Lin, *Inorg. Chem.* 52 (2013) 12986 - 12994.
[3] Y. Zhang, X. Li, D. Geng, M. Shang, H. Lian, Z. Cheng and J. Lin, *Cryst. Eng. Comm.* 16 (2014) 2196 - 2204.

P5

Anomalous emission of Yb^{2+} in CaF_2:Tb^{3+}, Yb^{3+} up-conversion phosphor

M.Y.A. Yagoub, H.C. Swart, E. Coetsee

Department of Physics, University of the Free State, PO Box 339, Bloemfontein, ZA9300, South Africa
Corresponding author e-mail address: yagoubM@ufs.ac.za

1. Introduction

Recently, lanthanide (Ln) doped nanophosphors have attracted considerable interest due to their appealing applications in photodynamic therapy, sensing materials and solar cell devices. Among Ln-based materials, fluorides have received attention due to their low phonon energies, low toxicity and excellent photochemical stability. In many fluoride compounds the broadband emission of Yb^{2+} is subject to a very large (0.6–1.2 eV) Stokes shift and it behaves peculiarly with temperature changes [1]. The anomalous emission of Yb^{2+} in Yb-doped materials is a prototypical case [1,2]. The interplay between the anomalous and 5*d*–4*f* emissions in Yb^{2+}- doped fluorite-type crystals results in complex electronic spectroscopy, which has been the focus of research for decades. The origin of such broadband emission remains under investigation. In this article, we report the anomalous emission of Yb^{2+} in CaF_2:Tb^{3+}, Yb^{3+} up-conversion phosphor.

2. Results

Fig.1 shows the up-conversion emission of Tb^{3+}-Yb^{3+} co-doped CaF_2. The up-conversion spectrum exhibits emission bands in the visible and near infrared (NIR) regions. The sharp emission peaks in the visible region are associated with Tb^{3+} ion 4f-4f transitions [3]. The broad NIR emission is related to the anomalous emission of Yb^{2+} ions [4]. The power dependence emission intensities of the 543 nm and NIR transitions are presented in fig. 2. The calculated values for the 543 nm and NIR transitions indicated that a two-photon process was involved. The NIR emission confirmed the existence of a theoretical intervalence emission between the Yb ions.

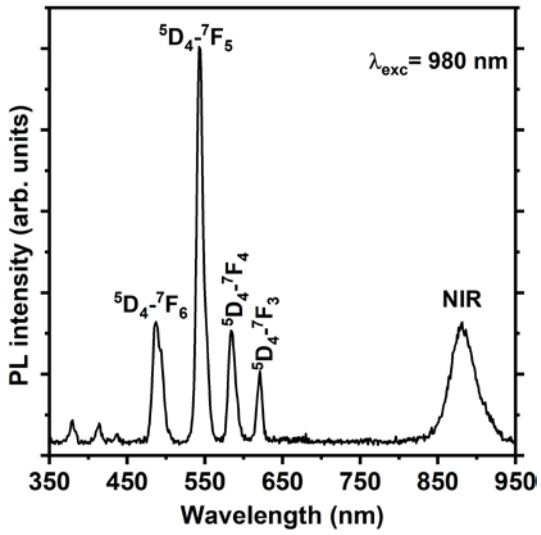

Fig. 1: Up-conversion luminescence spectra of CaF_2: 5 mol% Yb^{3+}, 5 mol% Tb^{3+} excited with 980 nm wavelength at room temperature.

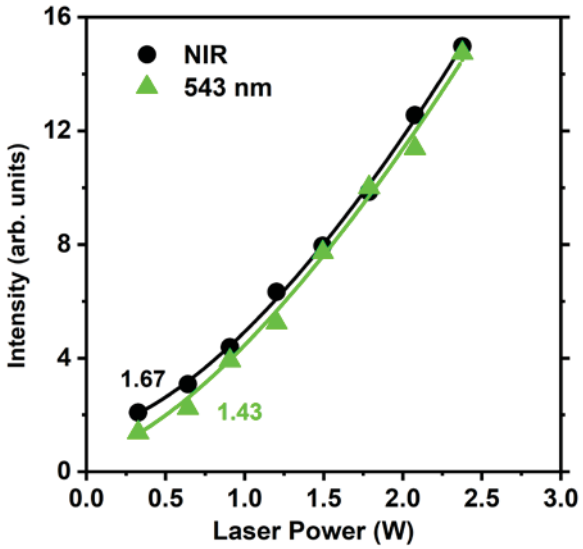

Fig .2: The dependence of up-conversion emission intensity as a function of laser pump power for the CaF_2:Yb^{3+}, Tb^{3+} phosphor.

3. References

[1] R.B. Hughes-Currie, K.V. Ivanovskikh, J.R. Wells, M.F. Reid, R.A. Gordon, L. Seijo, Z. Barandiara, *J. Phys. Chem. Lett.* **8** (2017) 1175−1178.
[2] Z. Barandiarán, L. Seijo, *J. Chem. Phys.* **141** (2014) 234704-234725.
[3] M.Y.A. Yagoub, H.C. Swart and E. Coetsee, *Mater. Res. Bull.* **156** (2022) 111986-111996.
[4] B. Moine, B. Courtois, C. Pedrini, *J. Phys. France,* **50** (1989) 2105-2119.

Encapsulation of Si QDs in Europium doped Zeolitic Imidazole Framework (Eu-ZIF-8) for photoluminescence tuning

Sarojini Jeeva Panchu[1], Sandeep Eswaran Panchu[2] and Hendrik C. Swart[1]

[1]*Department of Physics, University of the Free State, P.O. Box 339, Bloemfontein 9300, South Africa.*
[2]*Crystal Growth Centre, Anna University, Chennai, 600 025, Tamil Nadu, India.*
Email: SwartHC@ufs.ac.za

1. Abstract

Among the emerging optoelectronic devices, colloidal quantum dots (QDs) have significant potential for both absorption and emission of light. Solid state thin films are not widely used due to their unfavourable charge and energy transfer mechanisms. We have developed silicon quantum dots (Si QDs) encapsulated with various concentration of europium doped ZIF-8 (Eu-ZIF-8). The Eu-ZIF-8@Si QDs maintain the internal spacing of the Si-QDs in ZIF-8 network and also improving energy absorption. The Photoluminescence spectra indicates that the Si QDs emission was enhanced via Eu-ZIF-8 through inhibition of inter-QD energy transfer, which prevents large accumulation of Si-QDs. Thus, the control over the Si-QDs within ZIF-8 network pavs the way for multidimensional QD structures with tailored electronic couplings and dielectric matrices. The power conversion efficiency and photostability of any emerging photovoltaic technology are critical to its commercial success. It is well known that ions are easily lost in perovskite material during synthesis that increasing degradation rates and adversely affects perovskite solar cells (PSCs). Utilizing encapsulated multifunctional materials comprising of zeolitic imidazolate framework-8 (ZIF-8) as the interface between active and hole transport layer, a method was described for compensating the vacancies that results in increasing the light harvesting properties as well as reducing the degradation rate in PSCs.

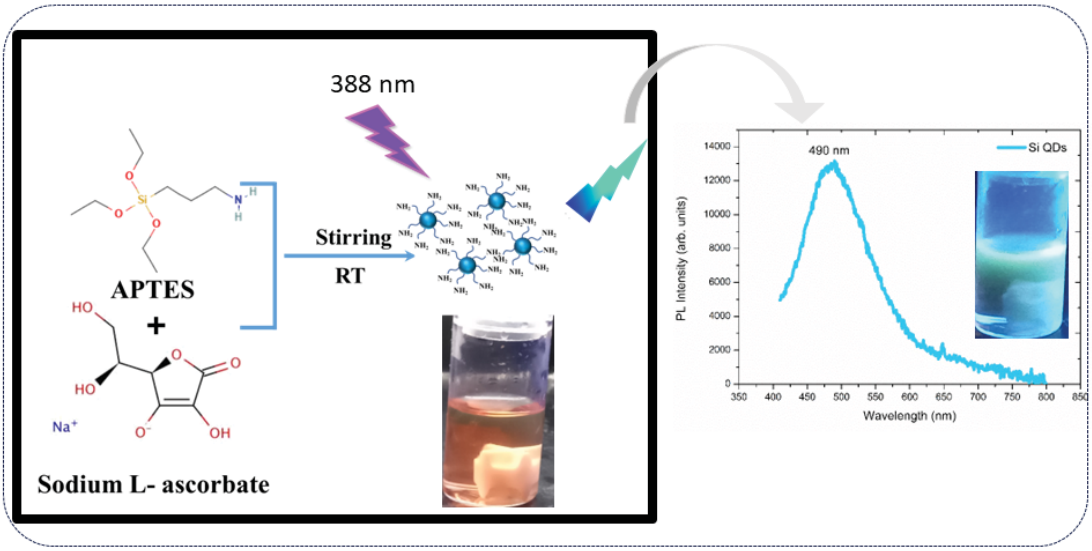

Fig.1: Schematic Diagram of Si QDs synthesis and its Photoluminescence spectrum.

3. References

[1] Z. Li, C. Xiao, Y. Yang, S. P. Harvey, D. H. Kim, J. A. Christians, M. Yang, P. Schulz, S. U. Nanayakkara, C.-S. Jiang, J. M. Luther, J. J. Berry, M. C. Beard, M. M. AlJassim and K. Zhu, Extrinsic ion migration in perovskite solar cells, Energy Environ. Sci., 2017, 10, 1234–1242.
[2] Wu, L. Y.; Mu, Y. F.; Guo, X. X.; Zhang, W.; Zhang, Z. M.; Zhang, M.; Lu, T. B. Encapsulating Perovskite Quantum Dots in Iron-Based Metal–Organic Frameworks (MOFs) for Efficient Photocatalytic CO2 Reduction. *Angew. Chem., Int. Ed.* **2019**, *58*, 9491– 9495.
[3] Konstantatos, G.; Huang, C. J.; Levina, L.; Lu, Z. H.; Sargent, E. H. Efficient infrared electroluminescent devices using solution-processed colloidal quantum dots. *Adv. Funct. Mater*. **2005**, *15*, 1865– 1869.

P7

Effect of Cr^{3+} on the SiO_2 nanoparticles prepared via sol-gel method

Rethabile A. Phokojoe[1], Rantooa G. Moji[1], Moipone A. Malimabe[1], Hendrik C. Swart[2], Lehlohonolo F. Koao[1],

[1]Department of Physics and Chemistry, University of the Free State (Qwaqwa campus), Private Bag X13, Phuthaditjhaba, 9866, South Africa
[2]Department of Physics, University of the Free State, P.O. Box 339, Bloemfontein, 9300 South Africa
Corresponding author e-mail address: koaolehlohonolo@gmail.com

1. Introduction

In the past decade, researchers have drawn attention to the development of doped nanomaterials. The studies of nanomaterials have attracted researchers because they exhibit improved physical and chemical properties [1]. Silicon dioxide (SiO_2) has been investigated as an alternative to crystalline hosts for X-ray scintillators because of its chemical stability, non-hygroscopic nature, and the possibility of incorporating larger concentrations of luminescent ions [2]. The Cr^{3+} doped SiO_2 nanoparticles were prepared using sol-gel method due to advantages such as simple equipment, cost effective, less hazardous and the low temperature reaction. Cr^{3+} doped nanomaterials show interesting luminescence properties that make them useful as night vision materials, lasers and bio imaging, etc. Their emissions are strongly influenced by the crystal field around Cr^{3+}. In the work described here, the influence of Cr^{3+} concentration on the structure, optical and luminescent properties of SiO_2 is investigated. The results provided some important indications, such that Cr^{3+} concentration has a great influence on the structure, optical and luminescent properties for extending optical and luminescent applications.

2. Results

The X-ray diffraction results showed that at low percentages of Cr^{3+} the structure consisted of amorphous SiO_2. However, at high concentration of Cr^{3+} there was structural transformation. The scanning electron microscopy micrographs show irregular agglomerated particles. The morphology was found to be independent on the concentration of the Cr^{3+}. The EDX measurements confirmed the presence and uniform distribution of Si, O and Cr. The UV–vis spectra analysis showed a red shift with an increase in the concentration of Cr^{3+}. From (Fig. 1) the photoluminescence results showed that the undoped SiO_2 reveal maximum luminescence band at around 412 nm with the two shoulders at around 380 nm and 490 nm. The emissions were attributed to the defects within the SiO_2 backbone of O–Si–O network. It is clear from Fig. 1 that with an increase in the amount of Cr^{3+} defects emission from dopant emerges at around 662 nm. The emission corresponds to the $^2E \rightarrow {}^4A_2$ transition of Cr^{3+}. From Fig. 2 it was noted that the luminescence intensity decreases with an increase in the amount of Cr^{3+}.The CIE colour chromaticity diagram showed that the emission colour could be tuned from bluish to reddish-orange. The main aim of this work is to contribute on the development of innovative alternative materials for practical application such as in light-emitting materials.

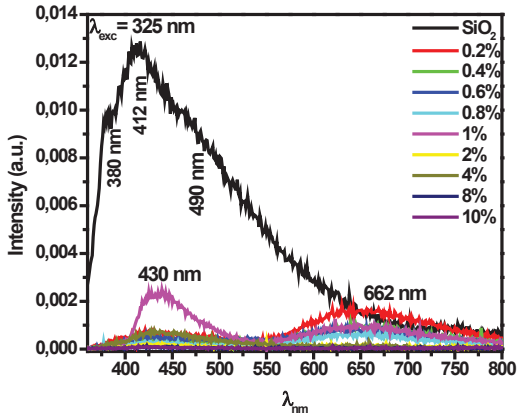

Fig. 1: PL emission spectra of SiO_2 nanoparticles prepared at various percentages of Cr^{3+}.

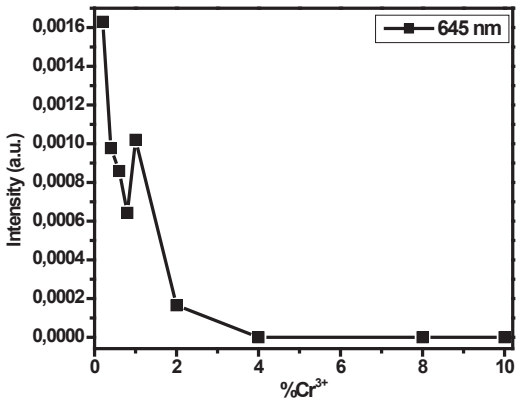

Fig. 2: Emission intensity as a function of different percentages of Cr^{3+}.

3. References

[2] W. Q. Peng, G. W. Cong, S. Q. Qu and Z. G. Wang, *Opt. Mat.* **29** (2006) 313-317.
[1] H.A.A. Seed Ahmed, O.M. Ntwaeaborwa, R.E. Kroon, *J. Lumin.* **135** (2013) 15–19.

Reduction methods for Sm^{3+} to Sm^{2+} in strontium borates for solar energy applications

G.J. Odendaal, L.J.B. Erasmus, R.E. Kroon, H.C. Swart

Department of Physics, University of the Free State, P. O. Box 339, Bloemfontein, 9300, South Africa
Corresponding author e-mail address: OdendaalGJ@ufs.ac.za

1. Introduction

The luminescent properties of Sm doped strontium borate phosphors have attracted considerable attention owing to the red luminescence of divalent Sm^{2+} and their potential application for down shifting solar radiation to increase the efficiency of solar cells. Trivalent Sm^{3+} ions should be eliminated because they reduce the luminescent intensity and alter the colour chromaticity of the material [1]. Previous studies have shown that co-doping with Eu is effective in reducing of Sm^{3+} and enhancing the intensity of the Sm^{2+} luminescence in the desired wavelength range [2]. Since Eu is expensive and its luminescence is not desired, the current objective was to investigate whether other co-dopants were effective for reducing Sm^{3+} to Sm^{2+} ions. In this study, SrB_6O_{10}:Sm, X, where X = Eu, Mg, Ca, Ba, Y or La, were prepared using a high temperature solid-state reaction method and their photoluminescence (PL) emission and excitation were studied to assess the effect of the co-dopant on the Sm ions.

2. Results

Scanning electron microscope images of a selection of the SrB_6O_{10} structures displayed a pebble-like structure enclosed by a web-like morphology. SrB_6O_{10}:Sm,Mg showed the most intense Sm^{2+} emission intensity compared to the other samples co-doped with Ca, Ba, Y or La at an excitation wavelength of 325 nm as illustrated in Fig 1. Fig. 2 compares the enhancement of samples co-doped with Mg or Eu showing that co-doping with Mg produced superior results (stronger Sm^{2+} emission) than doping with Eu.

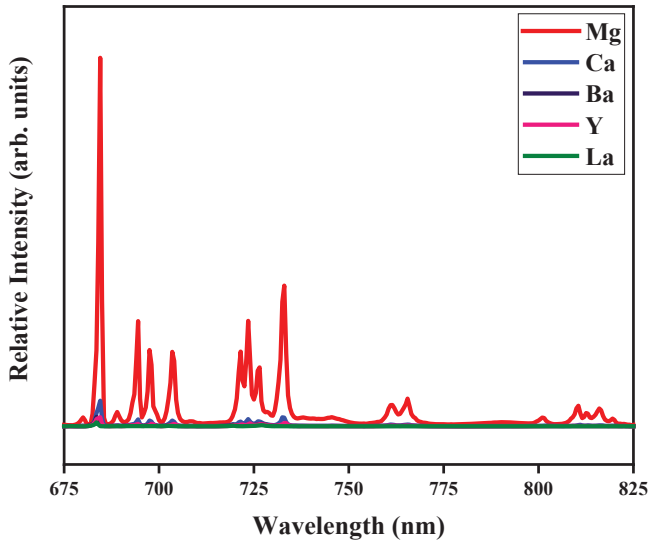

Figure 1: Emission spectra of $Sr_{0.9}B_6O_{10}$:$Sm_{0.05}$,$X_{0.05}$ materials, where X relates to different ions Mg, Ca, Ba, Y and La measured at an excitation wavelength of 325 nm.

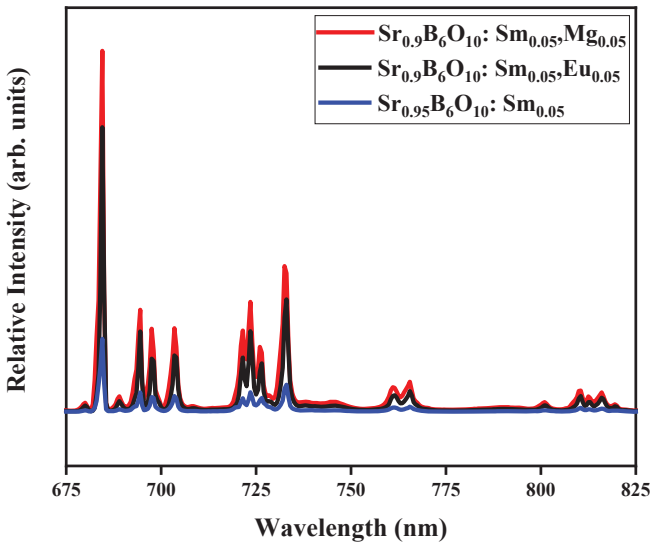

Figure 2: Emission spectra of $Sr_{0.95}B_6O_{10}$:$Sm_{0.05}$, $Sr_{0.9}B_6O_{10}$:$Sm_{0.05}$,$Mg_{0.05}$ and $Sr_{0.9}B_6O_{10}$:$Sm_{0.05}$,$Eu_{0.05}$ measured at an excitation wavelength of 325 nm.

3. References

[1] C. Kulshreshtha, S. H. Cho, Y. S. Jung, and K. Sohn. J. Electrochem. Soc. **154** (2007) 86–90.
[2] Q. Zeng, Z. Pei, S. Wang, and Q. Su. J. Alloys Compd. **277** (1998) 238–241.

P9

Structural and photoluminescence properties of Ho doped $BaAl_2O_4$ phosphors

Umer Mushtaq[1], Vijay Kumar[1,2], Hendrik C Swart[2]

[1]*Department of Physics, National Institute of Technology Srinagar, Jammu and Kashmir - 190006, India*

[2]*Department of Physics, University of the Free State, P.O. Box 339, Bloemfontein ZA9300, South Africa*

Corresponding author's e-mail address: umernitsgr@gmail.com (Umer Mushtaq)

1. Introduction

Rare earth-doped alkaline earth-based aluminates have drawn much interest as a topic of study because of their interesting characteristics, including high quantum efficiency [1], extended afterglow, and quick scintillation attributable to their tolerance to chemical and thermal changes. Until recently, the combination of yellow light emitting and blue light-emitting luminescent materials has been the preferred method for the generation of white light owing to its cost effectiveness and ease of production, and the demand for such phosphors has been on the rise [2]. Emergency signs, sensing, use in optoelectronics, high energy detectors, and in vivo imaging, are other applications for luminescent materials [3]. The fact that such luminescent materials can be reduced and retained in the divalent form without the use of a reducing environment simplifies their synthesis [4].

2. Results

Polycrystalline barium aluminate ($BaAl_{2-x}O_4$:xHo^{3+} (x=0 – 6 mol. %)) was synthesized using the urea-assisted combustion synthesis technique. The phase, purity, and crystallinity of the synthesized samples were validated by X-ray diffraction (XRD) analysis, figure 1 (a). Rietveld refinement of the observed XRD data of the undoped sample allowed us to further establish the structural parameters along with its crystal structure, which was found to be hexagonal with space group $P6_3$ as shown in figure 1(b). Rietveld refinement give the values of α, β and γ as 90°, 90° and 120° respectively; a, b and c as 5.2Å, 5.2Å and 8.7Å and unit cell volume as 205.9 $Å^3$. Morphological analysis was performed via field emission scanning electron microscopy, where the size of the crystals was observed to be on the nanometric scale. The elemental composition of all the synthesized samples was confirmed via EDS. Quantitative analysis about the absorbance of $BaAl_2O_4$:xHo^{3+} was performed with the help of UV-Vis spectroscopy, and its analysis was done by the use of the Kubelka-Munk function to check the effect of doping on the optical bandgap of this phosphor. The optical bandgap was found to be range from 5.1 eV – 5.4 eV with increasing doping concentration. To analyze the luminescence properties of the prepared nanophosphor, photoluminescence spectroscopic technique was used. After using an excitation wavelength of 330 nm, a broad emission profile was observed with two emission peaks centered at 495 and 510 nm that correspond to $^2D \rightarrow {}^8S_{7/2}$. The analysis of PL showed the tuning property of barium aluminate from blue emission to green.

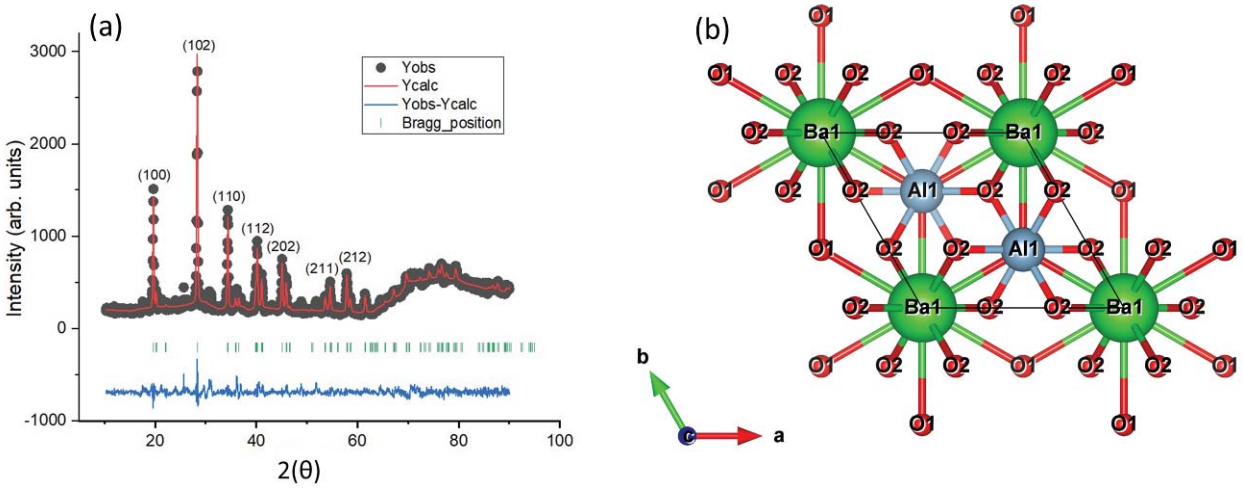

Figure 1: (a) Rietveld refined XRD plot for undoped $BaAl_2O_4$ along with the hkl values of the peaks. (b) the hexagonal structure of the unit cell of barium aluminate obtained after Rietveld refinement on the XRD data of an undoped sample.

3. References

[1] Rojas-Hernandez, Rocío Estefanía, et al. *Renewable and Sustainable Energy Review*, **81** (2018): 2759.
[2] Lee, Seonghoon, and Soo Yeon Seo. *Journal of the electrochemical society*,**149(11)** (2002): J85.
[3] Aitasalo, Tuomas, et al. *The Journal of Physical Chemistry B*,**110(10)** (2006): 4589.
[4] Stefani, Roberval, et al. *Optical Materials*, **31(12)** (2009): 1815.

Color tunable nano-crystalline $Ba_2Nd_8(SiO_4)_6O_2:Tb^{3+}$ phosphor for solid state lighting

Nisar Hussain[1], Umer Mushtaq[1], Vijay Kumar[1,2], H. C Swart[2]

[1,2]*Department of Physics, National Institute of Technology Srinagar, Jammu and Kashmir,19006 India*
[3]*Department of Physics, University of the Free State, Bloemfontein 9300, South Africa*
Corresponding author email address: hussainrana214@gmail.com (N. Hussain)

1. Introduction

In recent years, various rare-earth-doped phosphors such as phosphates, borates, aluminates, and silicates have been widely investigated [1–2]. Among these phosphors, the rare-earth-doped silicate phosphors have been applied in the design of the white-light-emitting diodes (wLEDs) because of their low energy consumption, long lifetime, and high structural, thermal, and chemical stabilities [3]. The optical properties of the phosphors were determined by photoluminescence (PL) spectroscopy, including the fluorescence decay curves and energy transfer efficiency. Trivalent terbium (Tb^{3+}) is known as an activator for green luminescent materials and has been widely used in fluorescent-lamp designs due to its ^7F_J, $^5D_3$, and $^5D_4$ states [4]. In this study, a series of single-doped phosphors, $Ba_2Nd_{8-x}(SiO_4)_6O_2:xTb^{3+}$ (BNSO) (x = 0.01, 0.03, 0.05, 0.07, and 0.09 mol%), were synthesized by using the solid-state method. Tb^{3+}-emission characteristics were demonstrated by UV-light excitation at 444 nm. As the Tb3+ concentration was changed, the emission and excitation spectra were recorded. According to the Commission International de l'Éclairage (CIE) chromaticity, the synthesized BNSO: Tb^{3+} phosphors show tuning from sky blue to green as the Tb^{3+} content increases. These results show that when the Tb^{3+} concentration is adjusted, synthesized phosphors can act as pure-green emitters for the UV-excited wLEDs.

2. Results

XRD measurements confirmed the phase purity of the synthesized solid-state Tb^{3+}-doped $Ba_2Nd_8(SiO_4)_6O_2$ phosphors. All the synthesized phosphors for which the doping concentration was varied, showed similar XRD patterns (Fig. 1). The diffraction peaks of the synthesized phosphors matched the $Ca_2La_8(SiO_4)_6O_2$ JCPDS Card No. 29-0337 standard data. The synthesized phosphors have an apatite-like structure with no other impurities and belong to space group $P6_{3/2}$ [1]. PL excitation (PLE) spectrum of the $Ba_2Nd_8(SiO_4)_6O_2:Tb^{3+}$ phosphors was monitored at 544 nm. The spectrum shows that the Tb^{3+} exhibits two types of emission: one is in the blue emission that is due to the $^5D_3$–^7F_J transition, and the other is in the green emission that is due to the $^5D_4$–^7F_J (J = 1–6) transition.

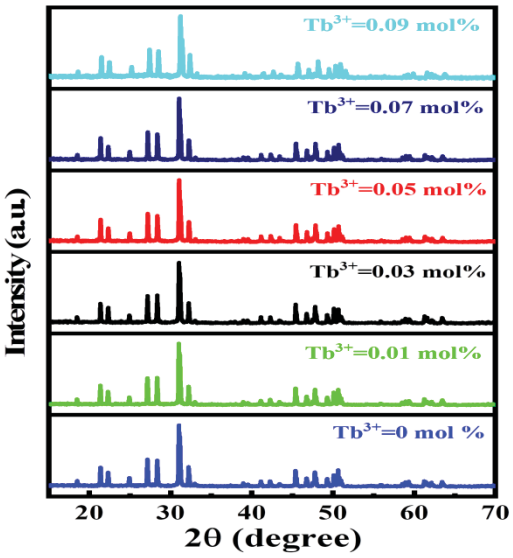

Fig. 1: XRD patterns of Tb^{3+}-activated $Ba_2Nd_8(SiO_4)_6O_2$ phosphors.

3. References

[1] Liu N, Mei L, Liao L, Fu J, Yang D. *Scientific reports.* **29;9(1)**,2019:1-9.
[2] Zhou R, Wang L, Xu M, Jia *D. Journal of Alloys and Compounds.* **25**; 2015:136-40.
[3] Han S, Wang Y, Zeng W, Chen W, Li G. *Journal of luminescence.***1**; 2014:66-9.
[4] Huang X, Li B, Guo H. *Journal of Alloys and Compounds.* **25**; 2017:2773-80.

P11

Effect of Tb^{3+} Doping on the Photoluminescence Properties of Zirconia Nanophosphors Synthesized via Sol-gel Route for LED Applications

Latief Mohi ud din[1], Irfan Ayoub[1], Vijay Kumar[1,2], Hendrik C Swart[2]

[1]Department of Physics, National Institute of Technology Srinagar, Jammu and Kashmir - 190006, India
[2]Department of Physics, University of the Free State, P.O. Box 339, Bloemfontein ZA9300, South Africa
Corresponding author's email address: latiefmohiuddin@gmail.com (Latief Mohi ud din)

1. Introduction

The need for robust, energy-efficient, and economical phosphor materials, particularly for lighting and display applications, has never been as demanding as it is now. Significant progress has already been made in the development of different phosphor materials, but the use of such materials in diverse fields requires that the components of the fabricated devices from the phosphors function under demanding, hostile environments, from space to varying challenging weather, temperature, and pressure conditions on Earth [1]. Recently, zirconia has attracted the attention of researchers as a viable and potent host phosphor material due to its unique chemical, thermal, and mechanical stability [2] and a suitable band gap, which makes it an excellent choice to be utilized in aggressive conditions [3].

2. Results

The sol-gel technique was used to create a trivalent lanthanide ion (Tb^{3+}) doped zirconia nanophosphor series with Terbium (III) nitrate pentahydrate as the dopant precursor (0, 1, 3, 5, and 7 mol%) and Zirconium (IV) propoxide as the zirconia precursor. The synthesized powders were annealed at a temperature of 600ºC. The photoluminescence properties of the powder samples were examined, and their potential as downconversion/downshifting phosphor materials was explored. The phase structure and crystallinity were validated by the X-ray diffraction and the Rietveld refinement using the fullprof software, and it was concluded that the host zirconia is primarily in the tetragonal phase [JCPDS; 00-081-1544, tetragonal, space group 137: $P4_2/nmc$]. Scanning electron microscopy was carried out to study the morphology, complemented by the EDS for the elemental composition of the samples. UV-VIS analysis and the corresponding Tauc plots revealed the impact of doping concentration on the optical band gap of the nanophosphors. PL emission spectra analysis at an excitation wavelength of 300 nm revealed an increase in the emission peak centered around 540 nm with increasing doping, which was attributed to the strong green emission from $^5D_4 \rightarrow {}^7F_5$ transition of Tb^{3+} ions. The results lend credence to the potential of the synthesized Tb doped zirconia as an efficient phosphor material for solid state lighting devices.

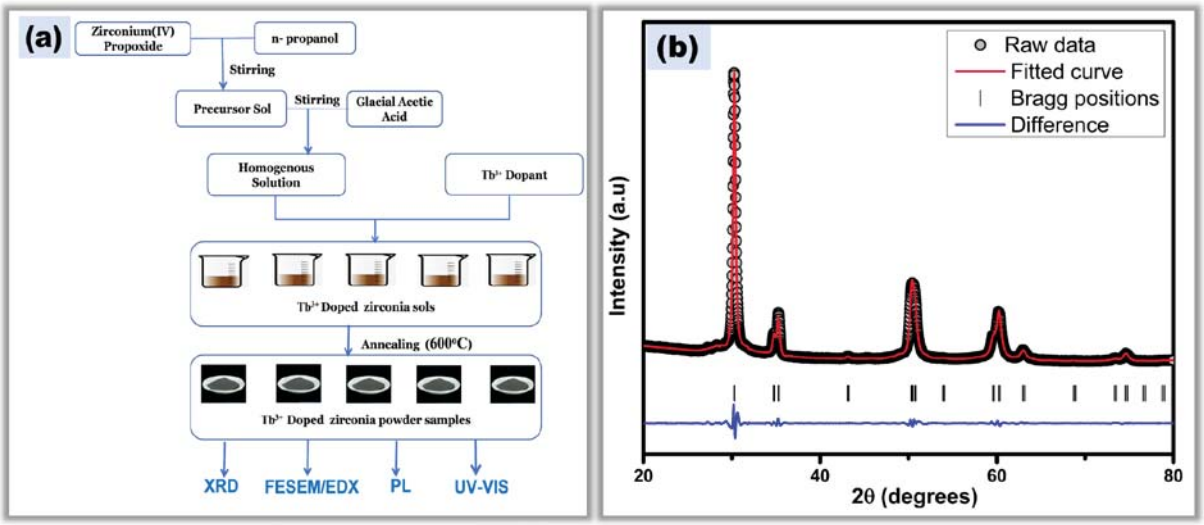

Figure 1: (a) Schematic representation of the synthesis of Tb^{3+}-doped zirconia nanophosphors, and (b) Rietveld refinement of undoped zirconia hosts validating the tetragonal phase.

3. References

[1] Y.H. Song, E.K. Ji, S.H. Bak, Y.N. Kim, D.B. Lee, M.K. Jung, B.W. Jeong, D.H. Yoon, Chem. Eng. J. 287 (2016) 511–515. https://doi.org/10.1016/j.cej.2015.11.093.
[2] A. Hirvonen, R. Nowak, Y. Yamamoto, T. Sekino, K. Niihara, J. Eur. Ceram. Soc. 26 (2006) 1497–1505. https://doi.org/10.1016/j.jeurceramsoc.2005.03.232.
[3] Y. Zhuo, A. Mansouri Tehrani, A.O. Oliynyk, A.C. Duke, J. Brgoch, , Nat. Commun. 9 (2018). https://doi.org/10.1038/s41467-018-06625-z.

Structural properties of K_2NbF_7: Mn^{4+} red-emitting phosphors for application in warm white light emitting diodes

Thandi Mazibuko, David E. Motaung, Hendrik C. Swart

Department of Physics, University of the Free State, 205 Nelson Mandela Dr, Bloemfontein, 9301
Corresponding author e-mail address: mazibukote@ufs.ac.za

1. Introduction

In comparison to current light sources like incandescent and fluorescent bulbs, white solid-state lighting devices have become more and more desirable light sources due to their energy efficiency, prolonged lives, environmental friendliness, and thermal stability [1-4]. Current white light emitting diodes (WLEDs) are created by fusing a blue LED (often with a GaN chip) with YAG: Ce^{3+}, a broad yellow emitting phosphor [1, 2, 5, 6]. However, WLEDs made in this manner have poor colour quality because they lack a red-emitting wavelength [1, 2, 4, 5]. This indicates that they have a poor colour rendering index (R_a <70) and a high colour-correlated temperature (CCT > 6000 K), limiting their use in backlit displays and WLEDs [1, 2, 5, 6].

It makes sense to add a blue excitable red-emitting phosphor to the mixture to address this disadvantage. These kinds of WLEDs' luminous characteristics can be enhanced by the inclusion of red phosphors, which will also encourage their widespread use [6]. Thus, there has been a lot of research interest in the study of red phosphors.
Mn^{4+} activated fluoroniobates are excellent candidates for use in WLED devices because they absorb in the blue area and emit in the red region [1, 2, 3, 5, 6]. K_2NbF_7:Mn^{4+}, in particular, displays two broad excitation bands at about 360 nm and 475 nm, as well as several narrow red emission peaks in the spectral range of 600 - 650 nm [1, 2, 5, 6]. The two excitation bands are associated with the spin-allowed and parity-forbidden transitions of Mn^{4+} from $^4A_{2g}$ to $^4T_{1g}$ and $^4T^{2g}$, respectively, according to the Tanabe-Sugano diagram [1, 2, 5, 6]. While the $^2E_g \rightarrow {}^4A_{2g}$ transition is responsible for the emission peaks.

2. Results

Fig. 1 shows the K_2NbF_7 crystal structure diagram. The Crystallography Open Database website was used to retrieve the CIF file, which was then read by VESTA software (version 3.5.8), to produce the crystal structure. Each Nb^{5+} (green sphere) in the host of K_2NbF_7 coordinates to $7F^-$(grey sphere) to form a $[NbF_7]^{2-}$ decahedron, and they are joined by K^+ (purple sphere), according to the crystal structure of K_2NbF_7. These $[NbF_7]^{2-}$decahedrons exhibit the point group C_{2v} symmetry [8, 9]. This contribution will outline the structural properties of K_2NbF_7: Mn^{4+} red-emitting phosphors synthesized without the use of HF.

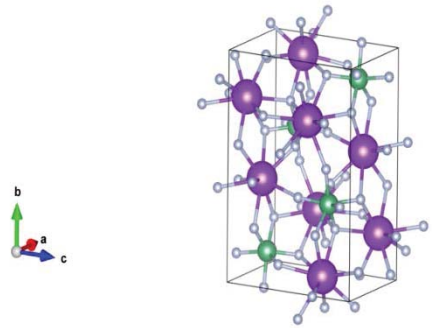

Fig.1: The crystal structure diagram of K_2NbF_7 retrieved from CIF file [7]

3. References

[1] H. Ming, J. Zhang, S. Liu, J. Peng, F. Du, J. Huang, L. Xia and X. Ye. *Opt. Mater*. 86 (2018) 352.
[2] G. Pang, F. Hong, X. Liu, Y. Zhang, C. Zhang, T. Dong, Z. Fu, G. Liu, J. Wang, D. Li and X. Dong. *Dalton. Trans*. 50 (2021) 171290.
[3] N. Kumada, S. Yanagida, T. Takei and B. Hong. *Mater. Res. Bull*. 115 (2019) 170.
[4] X. Dong, Y. Pan, D. Li, H. Lian and J. Li, *Cryst. Eng. Comm*. 20 (2018) 5641.
[5] T. Jansen, F. Baur and T. Justel. *J. Lumin*. 192 (2017) 644.
[6] J. Wu, Z. Li, L. Luo, Y. Xiong, L. Jiang, R. Guo and L. Meng. *J. Alloys. Compd*. 863 (2021) 158058.
[7] J. Hoard. *J. Am. Chem. Soc*. 61 (1939) 1252.
[8] C. Torardi, L. Brixner, and G. Blasse. *J. Solid. State. Chem*. 67 (1987) 21.
[9] G. Brown, and L. Walker. *Acta. Crystallogr*. 20 (1966) 220.

P13

Structural and optical characteristics of Ho^{3+} doped α-Bi_2O_3 thin films deposited by pulsed laser deposition on glass substrates

J. Divya, N.J. Shivaramu, H.C. Swart

[1]*Department of Physics, University of the Free State, Bloemfontein, ZA-9300, South Africa*
Corresponding author E-mail address: swarthc@ufs.ac.za (H.C. Swart)

1. Introduction

A wide bandgap semiconductor Bi_2O_3 has a characteristic polymorphism favoring asymmetric oxygen coordination around Bi, originating from the $6s^2$ lone pair electrons of Bi [1]. The physical properties of rare earth (RE) doped Bi_2O_3 polymorphic crystal structures, lead to broad potential applications such as optoelectronics, ionic conductors, photocatalysts [2], and gas sensors. Among the seven polymorphs ever reported [3], the most stable phase is α-Bi_2O_3 with a monoclinic structure (point group: $P2_1/c$) at lower temperatures. Among the RE ions, Ho^{3+} is one of the most attractive candidates for use as a dopant, because of its favorable energy level structure. The Ho^{3+} doped samples exhibited strong luminescence in the green and near-infrared regions. This study presents the structural, surface morphology, chemical, and optical properties of Ho^{3+}-activated Bi_2O_3 thin films grown by pulsed Nd–YAG laser deposition on glass substrates. The deposition process was performed at various substrate temperatures (T_s) from room temperature (RT) to 400 °C and oxygen partial pressures from 5–200 mT to investigate the properties of the films and their mutual influence.

2. Results

The X-ray diffraction (XRD) patterns indicated that the films deposited at 400 °C had an α-Bi_2O_3 phase. Furthermore, an improved film crystallinity with an α-Bi_2O_3 phase at oxygen partial pressure of 20 mT. The impacts of various substrate temperatures and an oxygen partial pressure on the morphology and the thickness of the films were analysed using a field emission scanning electron microscope (FESEM). The spherical shape with an average grain size increased from 41 to 53 nm with the impact of substrate temperature. The thin films deposited at low oxygen partial pressure of 5-20 mT with T_s = 400 °C exhibited nano-needles with an average size of 80 nm and length of ~750 nm (see Fig.1(a)). The optical band gap of the α-Bi_2O_3:Ho^{3+} thin films was calculated using the diffused reflectance spectra and was found to be ~ 2.8 eV. The photoluminescence (PL) excitation spectra of the α-Bi_2O_3:Ho^{3+} thin films showed a strong peak with a maximum of 450 nm and was attributed to the $^5I_8 \rightarrow {}^5G_6$, $^5F_1$ transition of Ho^{3+}. The PL spectra of α-Bi_2O_3:Ho^{3+} thin films under excitation at 450 nm showed a broad and highly intense green emission observed at 548 nm ascribed to the $^5F_4/{}^5S_2 \rightarrow {}^5I_8$ and the relatively weak red emission peaks at 654 and 753 nm were attributed to the $^5F_5 \rightarrow {}^5I_8$ and $^5S_2 \rightarrow {}^5I_7$ transitions of Ho^{3+} (see Fig.1(b)). The nano-needle grains of the α-Bi_2O_3:Ho^{3+} exhibited a maximum PL intensity at 20 mT oxygen partial pressure. This indicates that oxygen pressure and substrate temperature during deposition have important influences on the structural, surface morphology and optical properties of Bi_2O_3:Ho^{3+} thin films.

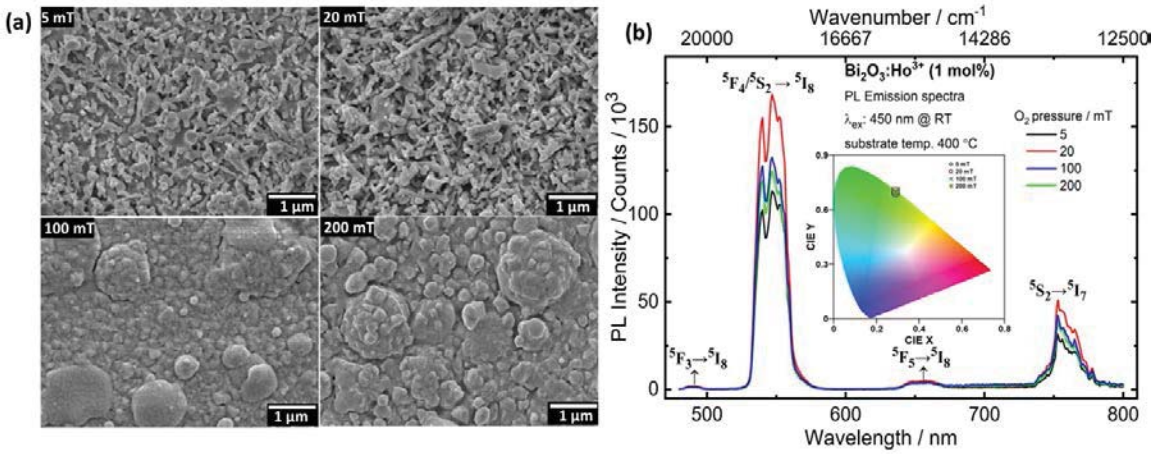

Fig. 1: (a) FESEM images and (b) PL spectra of Bi_2O_3:Ho^{3+} thin films deposited in the different oxygen partial pressures at T_s=400 °C.

3. References

[1] A. Walsh, D.J. Payne, R.G. Egdell and G.W. Watson, *Chem. Soc. Rev.* **40** (2011) 4455.
[2] K. Brezesinski, R. Ostermann, P. Hartmann, J. Perlich and T. Brezesinski, *Mats. Chem. Mater.* **22** (2010) 3079.
[3] M. Weber, M. Schlesinger and M. Mehring, *Cryst. Growth Des.* 16 (2016) 5678.
[4] J. Divya, N.J. Shivaramu, E. Coetsee, R.E. Kroon, W. Purcell and H.C. Swart, *J. Alloys Compd.* **842** (2020) 155641.

Producing ZnO nanostructures that exhibit NIR luminescence with a templated design procedure

O. Bashiar[1], R.E. Kroon[1], R.A. Harris[1]

[1]Physics, University of the Free State, Nelson Mandela Ave. Bloemfontein, 9301, South Africa
Corresponding author e-mail address: harrisra@ufs.ac.za

1. Introduction

ZnO is an important metal-oxide semiconductor [1]. When this material is used to synthesise nanoparticles (NPs) and nanostructures (NSs), numerous different types of optoelectronic technologies may be produced ranging from light emitting devices (like light emitting diodes - LEDs) to solar energy harvesting technologies [2,3]. ZnO NSs are known to have photonic effects (adsorption and luminescence) in the ultraviolet and visible part of the electromagnetic spectrum. However, to produce the same in the near-infrared band (NIR) of the spectrum is challenging. This is often achieved by doping with many different dopants or exploiting plasmon resonance effects in the NSs [4]. However, these complicated procedures are often costly and difficult to scale for commercial applications. Nonetheless this remains a popular and ongoing field of study.

In this study we investigate a route to a low-cost device fabrication scheme with important implications on optoelectronics technology to enhance the performance of photovoltaic and photoluminescent devices over a wide electromagnetic spectrum by including the NIR band. This is done by comparing two sets of ZnO NSs produced with pulsed laser deposition (PLD) as the main technique. Furthermore, a templated design scheme is used one of the sets to investigate the feasibility of controlling the growth orientation of the NSs and the resulting effect on the optical properties (including the NIR band of the spectrum) of the produced NSs.

2. Results

Figure 1 shows the photoluminescence (PL) spectra of two samples prepared with PLD (as is) in two different atmospheres; oxygen and argon, respectively. These samples were used as a control and their PL spectra only show second order peaks in the NIR band. Figure 2 shows the PL spectra of samples prepared with the templated design scheme. For these samples, at 725 nm, NIR luminescence is observed.

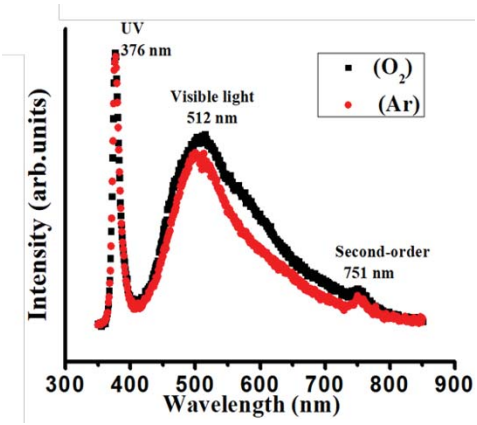

Fig. 1: PL spectra of two samples prepared with PLD as is showing only the 2nd order PL in the NIR band.

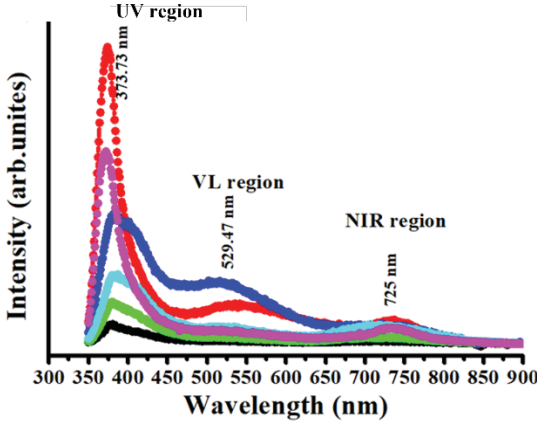

Fig. 2: PL spectra of samples prepared with the templated design scheme, showing the NIR luminescence.

3. References

[1] Xudong Wang,Xudong Wang,, Jinhui Song,, Christopher J. Summers, et al., The Journal of Physical Chemistry B, **110** (15), (2006), 7720-7724.
[2] Ü. Özgüra, Ya. I. Alivov, C. Liu, A. Tekeb et al., Journal of applied physics, **98** (4), (2005) 41301.
[3] E. M. Kaidashev, et al, Applied Physics Letters, **82** (22), (2003) 3901.
[4] Mohammed A. Ibrahem, Emanuele Verrelli, Fei Cheng, Ali M. Adawi, Jean-Sebastien G. Bouillard, and Mary O'Neill, Journal of Applied Physics 131, 103103 (2022);

P15

The influence of a binary phase ZnO-CuO on the poly-ε-caprolactone based nanocomposites

Londiwe Nikiwe Khumalo[1], Moipone A. Malimabe[1], Lehlohonolo F. Koao[2]

[1]Department of Chemistry, University of the Free State (Qwa Qwa campus), Private Bag X13, Phuthaditjhaba, 9866, South Africa

[2]Department of Physics, University of the Free State (Qwa Qwa campus), Private Bag X13, Phuthaditjhaba, 9866, South Africa

Corresponding author(s) e-mail address:mokoenama@ufs.ac.za

1. Introduction

Binary transition metal oxides have unique properties and in the areas of material science and technology have potential applications [1,2]. It is not known what effect the addition of binary phase metal oxide nanoparticles has on poly(ε-caprolactone) (PCL)-based nanocomposites in terms of structure, morphology, thermal and optical properties. The novelty of the project therefore relies on the possibility of influencing the structural, morphology, thermal behaviour as well as the optical properties of PCL/ZnO-CuO (ZC) nanocomposites. The aim is to come up with alternative properties of poly-ε-caprolactone (PCL) and to investigate the effects of metal oxides specifically, ZC on the poly-ε-caprolactone (PCL) matrix.

2. Results

The X-ray diffraction (XRD) confirmed the combined hexagonal wurtzite and cubic of ZnO and CuO respectively in the nanomaterials and orthorhombic for semi-crystalline PCL in the prepared nanocomposite films. The morphology changed from aggregated particles to smaller homogenous spherical-like structures. The differential scanning calorimetry (DSC) showed that the degree of crystallinity of nanocomposites films increased in the presence of the nanopowders. Nanocomposites displayed poor thermal stability compared to PCL. Optical properties revealed improvement in conductivity of nanocomposites with the addition of ZC to PCL.

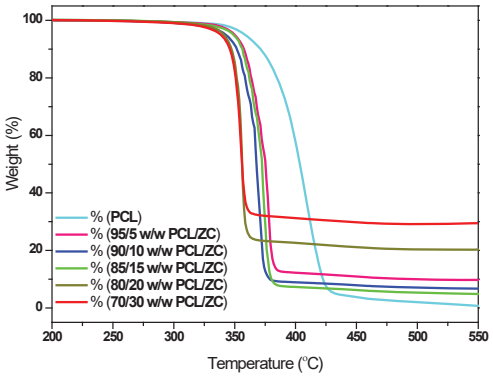

Figure 1

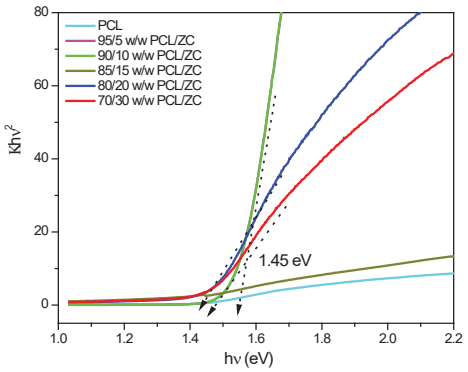

Figure 2

Keywords: Binary phase metal oxides, band gap, nanocomposites, degree of crystallinity.

References

[1] E. L. Foletto, D. Sallet, F. M. Stringhini, D. A. Bertuol, C. A. O. do Nascimento, and O. Chiavone-Filho, J. Alloys Compd. **588**, 305 (2013).
[2] N. Pathak, S. K. Gupta, K. Sanyal, M. Kumar, R. M. Kadam, and V. Natarajan, Dalt. Trans. **43**, 9313 (2014).

The effect of Gd^{3+} co-doping on the morphology and optical properties of Sm^{3+} doped strontium oxide mixed phases prepared by sol-gel method

M.R. Mhlongo[1], V. M. Maphiri[2], S.V. Motloung[1,3], L.F. Koao[4], T.E. Motaung[5,6], T.D. Malevu[1], R. E. Kroon[7]

[1]*Department of Physics, Sefako Makgatho Health Sciences University, P.O. Box 94, Medunsa, 0204, South Africa*

[2]*Department of Mathematics, Non-Destructive Testing and Physics, Vaal University of Technology, Vanderbijlpark, 1900, South Africa*

[3]*Department of Chemical and Physical Sciences, Walter Sisulu University, Mthatha, 3886, South Africa*

[4]*Department of Physics, University of the Free State (Qwaqwa Campus), Private Bag X 13, Phuthaditjhaba, 9866, South Africa*

[5]*Department of Chemistry, Sefako Makgatho Health Science University, P. O. Box 65, Medunsa, 0204, South Africa*

[6]*Department of Chemistry, University of South Africa, P.O. Box 392, UNISA 0003, South Africa*

[7]*Department of Physics, University of the Free State, P. O. Box 339, Bloemfontein, 9300, South Africa*

Corresponding authors: rebsmhlongo@gmail.com

1. Introduction

Rare earth activated nanophosphor materials have received special attention because of their exceptional luminescence properties that lead to a wide range of applications, such as in solid-state lasers, white light emitting diodes, fibre amplifiers, solar cells and medical diagnosis equipment [1]. Samarium (Sm^{3+}) ion is widely used as an activator of reddish orange emission from 560 to 645 nm due to its $^4G_{5/2} \rightarrow {}^6H_{5/2}$, $^4G_{5/2} \rightarrow {}^6H_{7/2}$ and $^4G_{5/2} \rightarrow {}^6H_{9/2}$ transitions [2]. Mixed phases of Strontium oxide (SO) nanophosphor doped with Sm^{3+} and co-doped with different Gd^{3+} concentrations were synthesized using sol-gel method. The crystal structure, phase quantification, morphology and luminescence properties of the prepared nanophosphor were analysed using x-ray diffraction (XRD), X'pert scores, scanning electron microscopy (SEM) and photoluminescence (PL), respectively.

2. Results

SO: Sm^{3+}, x% Gd^{3+} nanophosphors were successfully prepared using sol-gel technique. The XRD patterns showed that the prepared material is composed of the mixed phases of monoclinic ($SrAl_2O_4$ and $SrAl_4O_7$) and cubic ($Sr_3Al_2O_6$). SEM shows transformation from small irregular particles to big particle sizes and rod-like structures. Fig 1 shows the emission peak at 311nm attributed to $^6P_{7/2} \rightarrow {}^8S_{7/2}$ transitions of Gd^{3+}. Other peaks are from $Sm3^+$ transitions $^4G_{5/2} \rightarrow {}^6H_{5/2}$, $^4G_{5/2} \rightarrow {}^6H_{7/2}$, $^4G_{5/2} \rightarrow {}^6H_{9/2}$ and $^4G_{5/2} \rightarrow {}^6H_{11/2}$.

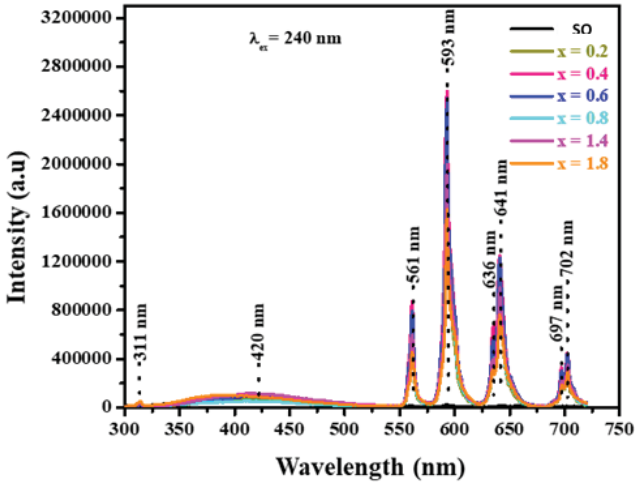

Fig. 1: Emission spectrum of SO: Sm^{3+}, x% Gd^{3+} nanophosphor

3. References

[1] A. K. Vischwakarma, M. Jayasimhadri, *J. Lumin.* 176 **(2016)** 112.
[2] H.R. Shih, Y.S. Chang, *Materials* 10 **(2017)** 779

P17

Electrical characterization of α-particle irradiation-induced defects in GaN grown by electrodeposition.

Abdulraoof Ali[1, 2], **Helga Danga**[1] **Jacqueline Nel**[1], **Walter Meyer**[1]

[1]*Physics Department, University of Pretoria, Pretoria 0002, South Africa*
[2]*Faculty of education, University of Elimam Elmahdi, Kosti White Nile, Sudan*
**Corresponding author e-mail address: abdalraof34@gmail.com,u18374710@tuks.co.za*

1. Introduction

There are several different semiconductor materials on the market, but GaN demonstrates a higher level of radiation hardness than Si, SiC, and GaAs [1], which is causing researchers to explore the development of GaN-based radiation sensors for use in particle physics, astronomy, or nuclear science, among other applications [1].
Radiation-induced defects in semiconductors may be detected and identified by having a solid understanding of the thermodynamics and electronic characteristics of these intentionally introduced defects [2]. In order to determine the impact of irradiation on the performance of electronic materials and the consequent deterioration of devices made from these materials, various factors must be taken into account, including the type and intensity of the radiation. Particle irradiation can create point and extended defects in a crystal lattice [2]. In this study, a new defect was introduced in the GaN thin film by exposing it to different influences of α-particle irradiation, which was characterized using deep-level transient spectroscopy to determine the signature of this defect.

2. Results

Current-voltage (IV) and capacitance-voltage (CV) characteristics were used to evaluate the Schottky barrier diodes as deposited and after irradiation. An ideality factor, saturation current, and Schottky barrier height were determined for the device. DLTS measurements were performed on Au/GaN/Al Schottky diodes as deposited and following α-irradiation to investigate the electrically active defects.

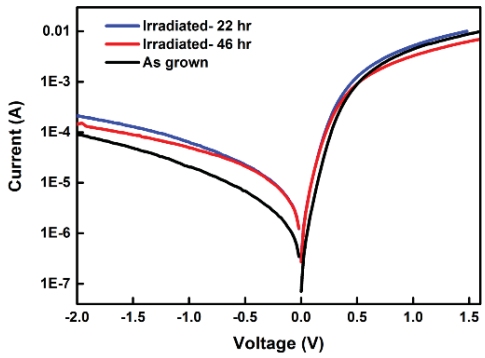

Fig.1: The *IV* characteristics of the Au/GaN/Al Schottky diodes as deposited and after irradiation by α-particles.

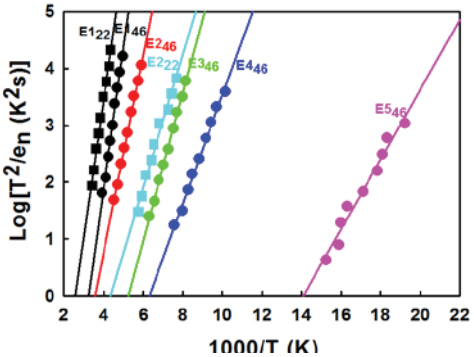

Fig. 2: Arrhenius plots of defects detected using DLTS of irradiated Au/GaN/Al.

3. References

[1] Goodman, S. A., Auret, F. D., & Myburg, G. (1994). Defect annealing of alpha-particle irradiated n-GaAs. *Applied Physics A, 59*(3), 305-310.
[2] Sandupatla, A., Arulkumaran, S., Ing, N. G., Nitta, S., Kennedy, J., & Amano, H. (2020). Vertical GaN-on-GaN Schottky Diodes as α-Particle Radiation Sensors. *Micromachines*, *11*(5), 519.

Alpha particle irradiation induced defects in ZnO thin film fabricated onto p-Si by thermal spray pyrolysis

Zahlia Stacey, Mmantsae Diale

Department of Physics, University of Pretoria
Lynwood Rd. Hatfield, Pretoria, 0002
zahlia@fastrak.co.za

1. Introduction

Defects induced by alpha particle irradiation in a Zinc Oxide (ZnO) thin film was investigated in this work.

ZnO is used in a large range of applications. Thin films can be fabricated using many different techniques. The spray pyrolysis technique was used in this work. It is a popular technique due to its low cost and simplicity. Defects in semiconductors can be either impurities or crystalline defects. For space applications, the device should be able to function in a highly radioactive environment.

This device was fabricated using the following method. P-type Silicon (Si) was cleaned using a three-step degreasing process [1]. A precursor solution was created using 120ml of Deionized water and 1.3283g of Zinc acetate di-hydrate ($C_4H_6O_2Zn{\cdot}2H_2O$). This precursor was then deposited on the clean Si using a thermal spray pyrolysis technique [2]. This device was then annealed in a furnace in air at 500°C for an hour. The device's surface properties were characterized using X-ray diffraction (XRD). A Palladium (Pd) ohmic contact was deposited using a thermal evaporative system, this contact was then annealed in a furnace in Argon (Ar) gas at 200°C for 20 minutes. Schottky contacts comprising of Aliminium (Al) and Gold (Au) were deposited using the same evaporative system. Current-voltage (*I-V*) and capacitance-voltage (*C-V*) measurements were performed on the device. Deep level transient spectroscopy was performed on the as deposited device. The device was then exposed to Alpha radiation for different time periods. DLTS was performed on the sample, after every 30 minutes of irradiation, to observe the change in defects induced by the irradiation.

2. Results

XRD proved that ZnO was successfully deposited onto p-type Si. *I-V* and *C-V* measurements showed that the device had good rectification. DLTS showed the defects in the device.

The as deposited device had 2 defects, 2 new defects were introduced after irradiation, this can be seen in figure 1 bellow. The intensity of these defects increases with an increase in the irradiation duration.

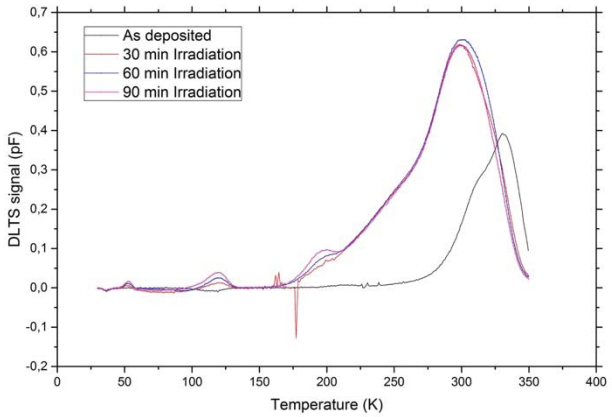

Fig. 11: DLTS spectrum of the device after different irradiation durations.

3. References

[1] F. D. Auret, S. M. M. Coelho, J. M. Nel, and W. E. Meyer, "Electrical characterization of defects introduced in n-Si during electron beam deposition of Pt," Physica Status Solidi (A) Applications and Materials Science, vol. 209, no. 10, pp. 1926–1933, 2012, doi: 10.1002/pssa.201200578.
[2] J. S. Nyarige, T. P. J. Krüger, and M. Diale, "Structural and optical properties of hematite and L-arginine/hematite nanostructures prepared by thermal spray pyrolysis," Surfaces and Interfaces, vol. 18, no. July 2019, p. 100394, 2020, doi: 10.1016/j.surfin.2019.100394.

P19

High-resolution Laplace deep level transient spectroscopy of the palladium Schottky effect on alpha radiation-induced defects in germanium

F. Taghizadeh, H. T. Danga, F. D. Auret, W. E. Meyer

Department of Physics, University of Pretoria, Private Bag X20, Hatfield 0028, Pretoria
Corresponding author e-mail address: F.Taghizadeh@tuks.co.za

1. Introduction

High resolution Laplace Deep Level Transient Spectroscopy (L-DLTS) was used to study the effects of palladium (Pd) Schottky contacts on electrical properties of Alpha radiated n-type germanium with $1x10^{15}$ cm^{-3} free carrier concentration. Normally, after alpha radiation, 5 peaks (E1, E2, E3, E4 and E5) are observed using conventional DLTS between 20 – 300 K temperature range. By making use of Laplace DLTS, we observed that E5 consists of 2 peaks (E and E'), it also reported previously by [1]. In our new study we investigated the effect of the Pd Schottky on our samples. In this study we observed a big change in the Capacitance-Voltage (*CV*) results due to the Pd effects, and the DLTS spectrum after *CV* measurements indicated that some of irradiated defects were removed and that there were new defects that had been introduced. The Arrhenius plot, depth profile and pulse width measurements were done for this study.

2. Results

Fig.1 demonstrates the Arrhenius plots of Pd Schottky contacts on radiated n-type Ge sample. Four peaks with activation energies of (E 0.12, E 0.19, E 0.23 and E 0.35) eV were observed.

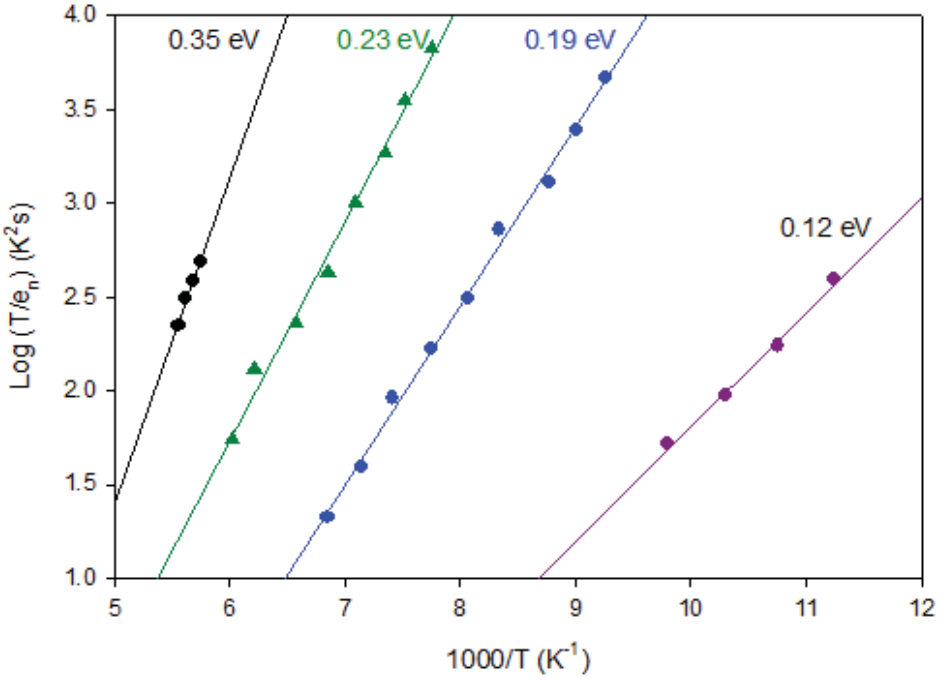

Fig.1: Arrhenius plot of Pd effects on alpha radiated Ge.

3. References

[1] A. W. Barnard, "Electrical characterization of alpha- particle irradiation-induced defects in germanium," no. August, 2017.

Investigation of the structural and temperature dependent electrical properties of MZnO (M = Ce and Sm) Schottky diode devices fabricated using the sol-gel spin coating technique

Mustafa Ahmed[1, 2], Walter Meyer[1] and Jackie Nel[1]

[1] *Departments of Physics, University of Khartoum, Faculty of Education, P O Box 320, Omdurman, Sudan*
[2] *Departments of Physics, University of Pretoria, Hatfield, Private bag X20, Hatfield, South Africa*
Corresponding author e-mail address: mustafa.sonbl@gmail.com

1. Introduction

Zinc oxide (ZnO) is one of the promising environmental friendly semiconductor materials having a direct wide band gap (3.37 eV) and large exciton energy (60 meV) at room temperature which makes it well suited for use in optoelectronic devices performing in the near ultraviolet (UV) part of the electromagnetic spectrum [1, 2]. ZnO nanostructures such as nanowires, nanoflowers, nanorods, ZnO thin films have been studied extensively in the recent years due to their wide range of applications in electronic devices such as light emitting diodes [3], solar cells [4] and Schottky diode devices [5]. ZnO has superior physical properties such as high breakdown electric field, radiation tolerance and high thermal conductivity, which are comparable to GaN and SiC, and are also better than those of GaAs and Si. Doping of ZnO is considered as one of the most effective methods to alter the properties of ZnO. Transition metals such as Al, Ag and Co have been extensively used as dopants [6, 7, 8]. Rare earth elements such as La, Ce and Sm have also been used as dopants for ZnO to improve its optical and electrical properties due to their availability of *4f* electrons and their fluorescence which results in good optical and electrical properties. In this study, the effect of Ce and Sm co-doping ZnO thin films on the structural, and temperature dependent electrical properties will be presented.

2. Results

Figure 1 shows the room temperature X-ray diffraction (XRD) pattern of Ce and Sm co-doped ZnO prepared using the sol-gel spin coating. The XRD pattern revealed that the Ce and Sm co-doped ZnO thins have the wurtzite crystal structure with a small CeO_2 peak detected at ~28°. Figure 2 depicts the *I-V* curves of the fabricated Ce and Sm co-doped ZnO thin film Schottky diode devices based on Pd Schottky contact with the structure Pd/CeSmZnO/n-Si/AuSb measured in the temperature range 320 – 160 K. The rectifying behaviour of the Schottky diodes improved with decreasing the temperature (see Fig. 2) with a rectification of 9 orders of magnitude at -2 V. This indicates that, there is strong temperature dependence of the fabricated Schottky diode devices. Moreover, analysis of the temperature dependent *I-V* will be studied in more detail using conventional thermionic emission theory. In addition to that, the *I-V* characteristics will also be studied using the Cheung-Cheung and Nord functions. Furthermore, the effect of using Pt as a Schottky contacts with the structure Pt/CeSmZnO/n-Si/Ti-Al on the electrical properties will also be studied in more details using the aforementioned methods.

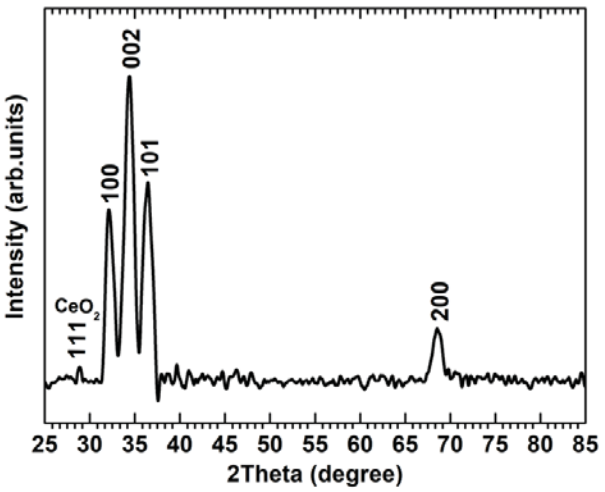

Fig. 1: XRD spectra of Ce and Sm co-doped ZnO thin films annealed at 500 ˚C in air.

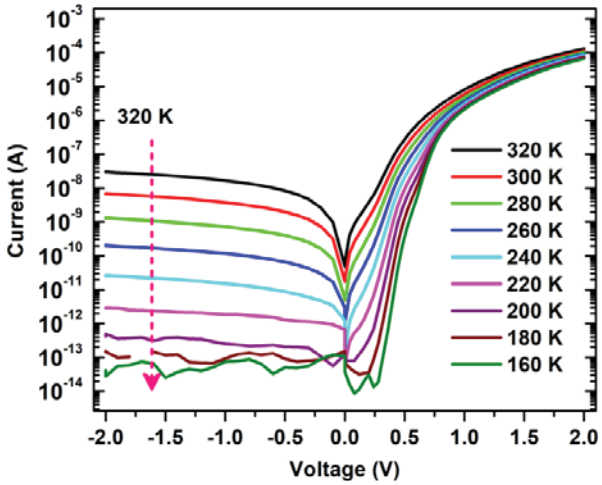

Fig. 2: *I-V* curves of the Ce and Sm co-doped ZnO thin films Schottky diode devices based on Pd/Ce, Sm:ZnO/n-Si/AuSb in the temperature range 320-160 K.

3. References

[1] R. Vispute, V. Talyansky, et al, Appl. Phys. Lett. **73** (3) (1998) 348–350.
[2] E. Hashem, M. Hamza, A. El-Shazly, M. Sanad, M. Hassan, S. Abdellatif, Nanotechnol. **32** (8) (2020) 085701
[3] D. Hwang, S. Kang, J. Lim, E. Yang, J. Oh, J. Yang, S. Park, Appl. Phys. Lett. **86** (22) (2005) 222101
[4] T. Ortiz, C. Conde, T. M. Khan, B. H, Appl. Phys. A **123** (4) (2017) 1–6.
[5] R. Vinodkumar, I. Navas, S. Chalana, K. Gopchandran, V. Ganesan, et al, Appl. Surf. Sci. 257 (3) (2010) 708–716
[6] K. Khojier, Mater. Sci. Semicond. Process. **121** (2021) 105283
[7] N. Ali, B. Singh, V. AR, S. Lal, C. Yadav, K. Tarafder, S. Ghosh, J. Phys. Chem. C **125** (14) (2021) 7734–7745
[8] P. Chithira, T. T. John, J. Magn. Magn. Mater. **496** (2020) 165928

P21

Effect of Bi doping on the structural, optical and electrical properties of ZnO nanorods grown by chemical bath deposition

Mustafa Ahmed[1, 2], Zelalem Urgessa[1], JR Botha[1] and Andre Venter[1]

[1] Department of Physics, University of Nelson Mandela, Summerstrand P O Box 77000, South Africa
[2] Departments of Physics, University of Khartoum, Faculty of Education, P O Box 321, Sudan
Corresponding author e-mail address: mustafa.sonbl@gmail.com

1. Introduction

One-dimensional (1D) semiconductor nanomaterials such as nanowires, nanorods, nanotubes and nanobelts have attracted the attention of the scientific community due to their unique properties and potential use in a wide range of devices, such as photodiodes [1], single electron transistors [2] and sensing applications [3 Notably, tailoring the physical properties of materials underpin materials and device engineering. Undoped (n-type) 1D ZnO structures have a wide band gap of 3.37 eV and a large room temperature exciton binding energy of 60 meV. These properties render ZnO ideal for optoelectronic devices operating in the UV range [4]. One of the most effective ways to alter the properties of ZnO is by doping with some cations. Specifically, the addition, group V elements such as As, Sb and Bi may produce p-type ZnO with improved optical and electrical properties [5]. As an example, Bi in various ionization states (Bi+3, Bi+2, Bi+1 and Bi0) form radiative deep-level centres that facilitate tuneable UV emission in several materials [6]. This makes Bi a good candidate as a dopant for use in optoelectronic devices. In this work, we report on the chemical bath deposition and characterization of ZnO nanorods. These nanorods were synthesised using different Bi concentrations in the solution (0 to 5 at. %) on aluminium doped ZnO (AZO) substrates. The structural, optical and electrical properties will be investigated in detail.

2. Results

X-ray diffraction (XRD) patterns of four ZnO samples (0, 1, 3 and 5 at.% Bi in the solution) are shown in Figure 1. Notably, the nanorods have a wurtzite crystal structure with a preferred orientation along the [002] direction. Additionally, a change in lattice parameter (due to the Bi incorporation) is evidenced by the shift in the peak as appearing in the XRD spectrum. Figure 2 displays room temperature photoluminescence (PL) properties of as-grown samples. The PL band-to-band emission line decreased significantly with an increase in Bi concentration, while the converse is observed for (what is believed to be) deep-level related emission. The effect of Bi on the PL properties will be discussed in further detail. Moreover, UV-visible spectroscopy (UV-vis), and X-ray photoelectron spectroscopy (XPS) results, as well as the electrical properties of the Schottky diode devices on these samples will be discussed in more detail.

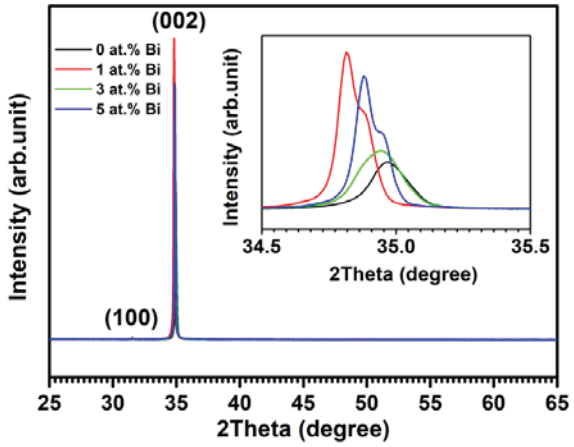

Fig. 1: XRD patterns of ZnO nanorods grown from solutions with different Bi concentrations. The inset shows the (002) diffraction peak.

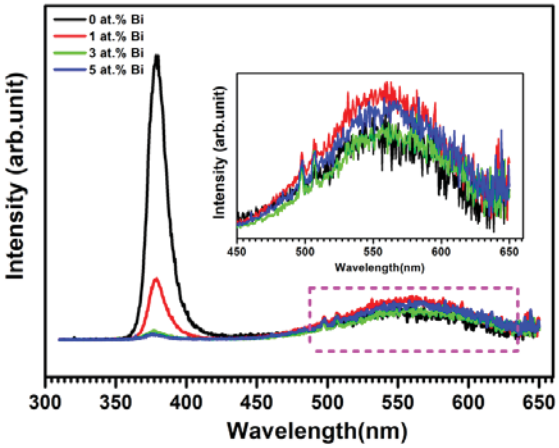

Fig. 2: Room temperature PL spectra of the four samples. The inset shows the deep-level emission only.

3. References

[1] L. Wang, R.X. Yan, Z.Y Hao, L. Wang, J.H Bao, X. Wang, Q. Peng and Y.D Li. Angew. Chem. Int. Ed. **44** (2005) 6054 – 6057.
[2] F. Vetrone, J.C. Boyer and J.A. Capobianco. Adv. Mater. **16** (2005) 23 – 14.
[3] L.F. Dong, Z.L. Cui and Z.K Zhang. Nano. Struct. Mater. **8** (1997) 815 – 823.
[4] G.C. Yi, C. Wang and W.I.I. Park. Semicond. Sci. Technol. **20** (2005) 22 – 34.
[5] Singh, B.K. and Tripathi, S, J. Lumin.**198** (2018) 427-432.
[6] Pathak, Trilok K and Swart, HC and Kroon, RE, Spectrochim. Acta A Mol. Biomol. Spectrosc. **190** (2018) 164-171.

Characterization of radiation-induced defects in germanium using DLTS and LDLTS

C.R. Thaba, F. Taghizadeh, F. D. Auret and M.M. Diale

Physics Department, University of Pretoria,
Private bag X20, Hatfield 0028, Pretoria, South Africa

ABSTRACT
The electrical properties of E and E' defects in germanium (Ge) introduced by alpha particle radiation were studied using high-resolution Laplace deep-level transient spectroscopy (L-DLTS). From the Arrhenius plot, it was observed that the E-centre consists of two components with similar DLTS signatures, but they have different properties, given that they have different activation energies of 0.375 eV and 0.370 eV. The electric field dependence of the E defect was measured at different temperatures to distinguish between Poole-Frenkel and phonon-assisted tunnelling. The defect depth profile measurements for the E-centre showed that as we probe deeper into the bulk of the semiconductor, the concentration of the E-centre defect decreases. The DLTS amplitude of both E and E' defects increased as the filling pulse width increased from a few microseconds to a millisecond. However, the DLTS amplitude of E was observed to be 4 times larger than the DLTS amplitude of E', and both defects are structurally different.

Keywords: Alpha radiation induced defects in Ge; Laplace Deep-Level Transient Spectroscopy; Electric field; Capture cross section.

P23

Structural and up-conversion mechanism of spinel $Zn_2TiO_4:Er^{3+}$, Yb^{3+} phosphor

Sefako J. Mofokeng and Luyanda L. Noto

Department of Physics, CSET, University of South Africa, Johannesburg, 1710, South Africa

Corresponding author e-mail address: Sefakojmofokeng@gmail.com

1. Introduction

Researchers are interested in phosphor nanomaterials-based up-conversion (infrared radiation into visible region) luminescence via rare earth elements (RE) for a variety of applications. This is because the up-converting mechanism can be integrated into a variety of developments such as lighting technologies, optical converters, biosensors, storage sensors, and many others [1 - 3]. This study investigated the structural and photoluminescence properties of spinel Zn_2TiO_4 phosphor co-activated with Er^{3+} and Yb^{3+} ions. The prepared phosphor material was investigated for possible applications in up-conversion.

2. Results

The XRD pattern confirmed the formation of the spinel $Zn_2TiO_4:Er^{3+},Yb^{3+}$ phosphor material. The photoluminescence spectrum of $Zn_2TiO_4:Er^{3+},Yb^{3+}$ phosphor showed green and red emission peaks associated with $^2H_{11/2} \rightarrow {}^4I_{15/2}$, $^4S_{3/2} \rightarrow {}^4I_{15/2}$ and $^4F_{9/2} \rightarrow {}^4I_{15/2}$ *f-f* transitions of Er^{3+} ions, as shown in Fig. 1(a). The CIE diagram suggests that the observed emission is greenish yellow, as shown in Fig. 1(b).

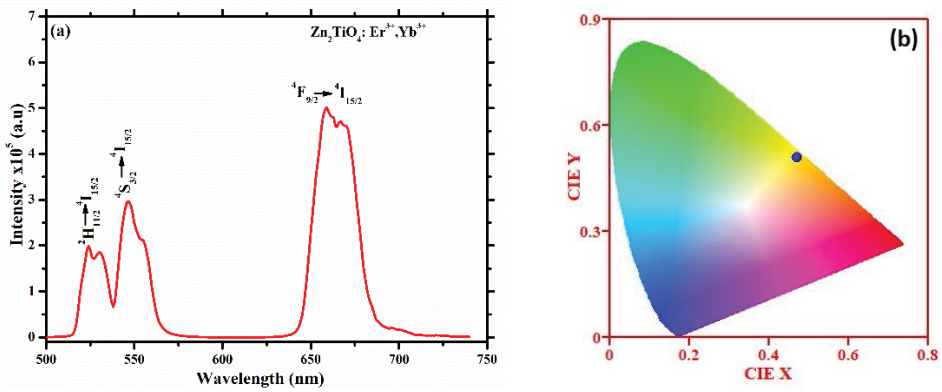

Fig. 1: (a) Up-conversion spectrum and (b) CIE coordinate plot of spinel $Zn_2TiO_4:Er^{3+},Yb^{3+}$ nanomaterial

3. References

[1] Z. He, X.Y. Sun, an dX. Gu, *Ceram. Int.* (2017) **43(9)** 7378–7382
[2] X. Li, Y. Yu and Z. Zheng, *Ceram. Int.* (2016) **42(1)** 490–494.
[3] S. Wang, Y. Guo, and C. Liu, *J. Non-Cryst. Solids* (2023) **(601)** 122076 –122083.

The effect of annealing temperature on the phase change of spin coated $Y_2SiO_5:Ce^{3+}$ on silicon (100) substrate

A.O. Mashalane, M.M. Duvenhage, H.C. Swart

Department of Physics, University of the Free State, P.O. Box 339, Bloemfontein, ZA 9300, South Africa.

Corresponding author email address: duvenhagem@ufs.ac.za

1. Introduction

$Y_2SiO_5:Ce^{3+}$ is a blue emitting phosphor that is used in field emission displays and scintillators [1-2]. Y_2SiO_5, with a band gap of 7.4 eV, is a good host due to its chemical and thermal stabilities. Y_2SiO_5 contains two crystal phases: X_1 and X_2, with the X_2 phase obtained by annealing at temperatures greater than 1190 °C [3]. In this study spin coating was used as fabrication technique of the thin films. It provides a cheaper alternative to pulsed laser deposition. Commercially available $Y_2SiO_5:Ce^{3+}$ was dissolved in isopropanol to make a 0.05 mol% solution, which was spin coated on Si (100) substrates at 1000 rpm. The samples were annealed at 1200 °C, 1250 °C and 1300 °C to investigate the phase change from X_1 to X_2.

2. Results

Figure 1 shows the X-ray diffraction patterns of the different annealed samples. The samples displayed a monoclinic structure. The as prepared and annealed films at 1200 °C displayed an X_1-phase, whereas those annealed at 1250 °C and 1300 °C displayed an X_2-phase. Figure 2 depicts the photoluminescence (PL) spectra. Two peaks at 395 and 430 nm was observed. This is due to the 5d to 4f transitions of Ce^{3+} ions and the 4f level splitting into $^2F_{5/2}$ and $^2F_{7/2}$ levels [1], [3]. The as prepared sample is showing the highest intensity. The second peak for the sample annealed at 1300 °C is blue shifted to 420 nm. The morphology of the samples was analysed by scanning electron microscopy and the films showed randomly orientated particles. Energy dispersive x-ray spectroscopy and X-ray photoelectron spectroscopy (XPS) provided chemical information about the samples and confirmed that all the elements were present. XPS also showed that both Ce^{3+} and Ce^{4+} were present in the samples.

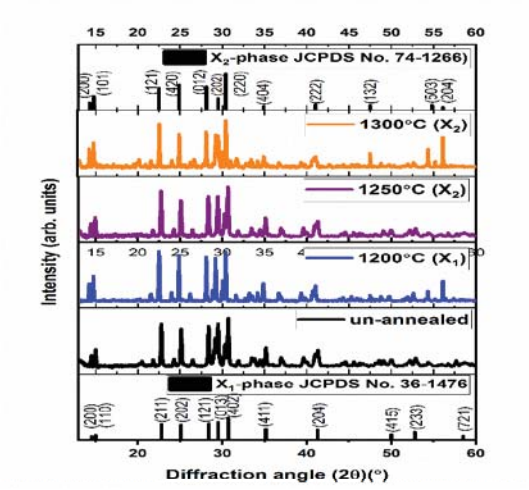

Figure 1. XRD spectra of spin coated films indicating the X_1 and X_2 phases.

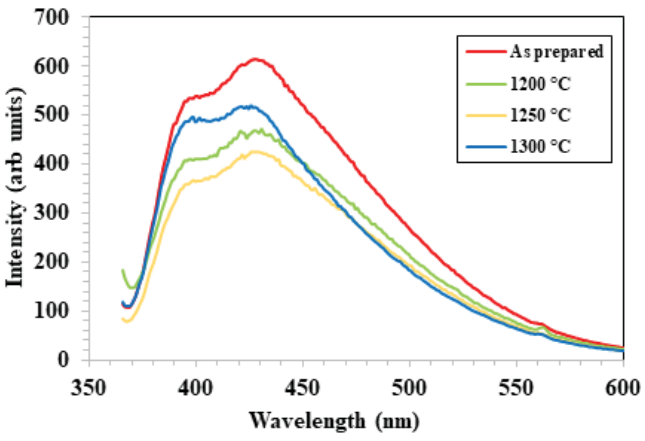

Figure 2. PL emission spectra of the films annealed at different temperatures.

3. References

[1] E. Coetsee, J.J. Terblans, O.M. Ntwaeborwa and H.C. Swart. Physica B **404** (2009) 4426-4430.
[2] W. Chewpralitkul, C. Wanarak, T. Szcyesniak, M. Moszynski, V. Jary, A. Beitterova and M. Nikl. Opt. Mater. **35** (2013) 1679-1684.
[3] T. Aitasaldo, J. Holsa, M. Lastusaari, J. Nittykoski, F. Pellé. Opt. Mater. **27** (2005) 1511-1515.

P25

Incorporation of Copper Nanoparticles in PEDOT: PSS for Organic Solar Cells

Thapelo Seimela[1], Justine Nyarige[1], Nolwazi Nombona[2] and Mmantsae Diale[1]

[1]Department of Physics, University of Pretoria, Pretoria,
[2]Department of Chemistry, University of Pretoria, Pretoria
Corresponding author e-mail address: mmantsae.diale@up.ac.za

1. Introduction

Metal-polymer nanocomposites, which are metallic nanoparticles (NPs) embedded in a conducting polymer matrix, have received a lot of attention in the past two decades due totheir tunable magnetic, mechanical, electrical, and optical properties. In this study, copper (Cu) NPs were synthesized by a chemical reduction usingdeionised (DI) water as the solvent. Copper sulphate ($CuSO_4$) was reduced by sodium borohydride ($NaBH_4$) with ascorbic acid (AA) as the antioxidant and Polyvinyl pyrrolidone (PVP) as the capping agent. Three different volumes (10, 20 and 30 µL) of Cu NPs were deposited in poly(3,4-ethylene dioxythiophene): poly(styrene sulfonate) (PEDOT: PSS) which is a conductive polymer with a good work function and the blend poly(3-hexylthiophene):phenyl-C61-butyric acid methyl ester (P3HT: PCBM) which is used as an active layer, respectively spin-coated on ITO substrates. Variation of annealing temperatures (120, 140, and 160 °C) was then performed on the device containing 20 µL of Cu NPs since it gave better results. The transmission electron microscopy (TEM) results showed spherical shapes of Cu NPs with an average grain size of 6.01 ± 2.89 nm. The scanning electron microscopy (SEM) results illustrated the coverage of both polymers containing Cu NPs. These micrographs showed the increase of the Cu NPs associated with increased volume. The UV-Vis spectroscopy revealed that the samples were absorbing in the visible range by showing the plasmonic resonance at approximately 562 nm for Cu NPs along with peaks of PEDOT: PSS, PCBM and P3HT at 533, 333 and 445 nm respectively. The inclusion of Cu NPs has resulted in merging peaks of PCBM and P3HT which became amorphous afterwards. The X-ray diffraction (XRD) patterns confirmed the FCC structure of Cu NPs with (111), (200), and (220) phases in which the (111) peak was the most intense. Raman spectroscopy also confirmed the existence of P3HT: PCBM, PEDOT: PSS and Cu NPs by showing the different vibration bonds of each structure. The intensities differ according to the different volumes of the Cu NPs. ITO/PEDOT: PSS: CuNPs/P3HT: PCBM/Ag device was fabricated with the above volumes in which electrical properties showed a maximum PCE of 5 % with 20 µL Cu NPs.

2. Results

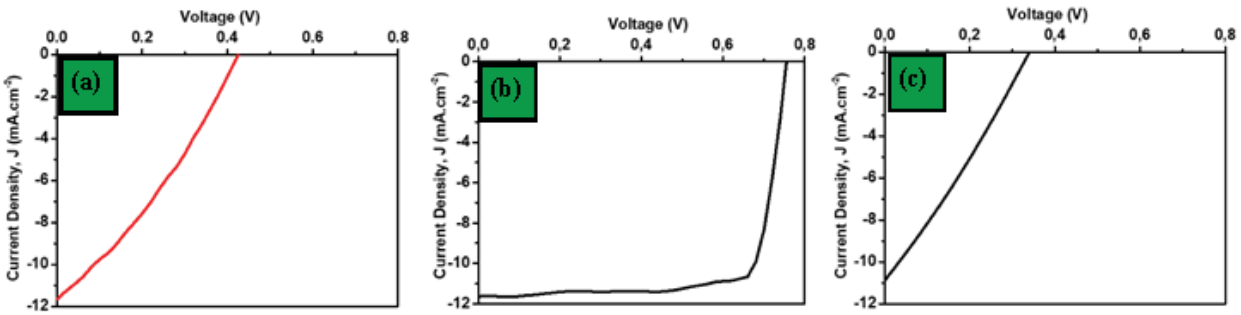

Figure 1: J–V characteristic curves under illumination that compared the performance of OSC at annealing temperatures of (a) 120 °C, (b) 140 °C and 160 °C.

3. References

[1] M. Girtan and M. Rusu, "Role of ITO and PEDOT: PSS in stability/degradation of polymer: fullerene bulk heterojunctions solar cells," *Solar Energy Materials and Solar Cells,* vol. 94, no. 3, pp. 446-450, 2010.
[2] F. Otieno *et al.*, "Improved efficiency of organic solar cells using Au NPs incorporated into PEDOT:PSS buffer layer," *AIP Advances,* vol. 7, p. 085302, 08/01 2017.

Thermoluminescence studies of spinel structure of $ZnGa_2O_4$

Mduduzi Mbongo, Sefako J. Mofokeng and Luyanda L. Noto

Department of Physics, CSET, University of South Africa, Johannesburg, 1710, South Africa

Corresponding author e-mail address: mbongomdu@gmail.com

1. Introduction

Zinc gallate is a ternary spinel oxide belonging to Fd3m cubic space group with a wide-band gap that is in the range of 4.4 – 5.0 eV and high transmittance under ultraviolet light. It has superior chemical and thermal stability under high electric field and high vacuum conditions, making it a good candidate for applications in vacuum fluorescent displays, field emission displays and electroluminescent devices. It is a self-activated phosphor with blue emission upon excitation that originates from the corner sharing GaO_6 [1, 2]. Thermally stimulated luminescence is a well-explored technique for studying electron trapping centers in solid materials. It involves stimulation of trapped electrons from electron trapping centers using thermal energy. The kinetics order involved when the electrons are trapped and de-trapped, the depth of the electron trapping centers and the population of the trapped electrons can be determined from data obtained. This information can be extracted using several methods, which include the dose response, initial rise, Chen's peak shape, isothermal and variable heating rate methods, just to mention a few [3]. In this work we present thermoluminescence studies of $ZnGa_2O_4$ prepared by solution combustion method using nitrates of zinc and gallium fueled by urea.

2. Results

XRD patterns depict the formation of the cubic spinel structure of $ZnGa_2O_4$ nanomaterial corresponding JCPDS card number 38-1240 with space group Fd3m, as shown in Fig. 1. Fig. 2 depict the thermoluminescence (TL) glow curve of $ZnGa_2O_4$ nanomaterial. The TL signal of the glow curve was enhanced by increasing the irradiation dose, and a slight peak shift to higher temperatures was observed, indicating that the kinetics followed by electrons during trapping and de-trapping by electron trapping centres were of general order kinetics [3].

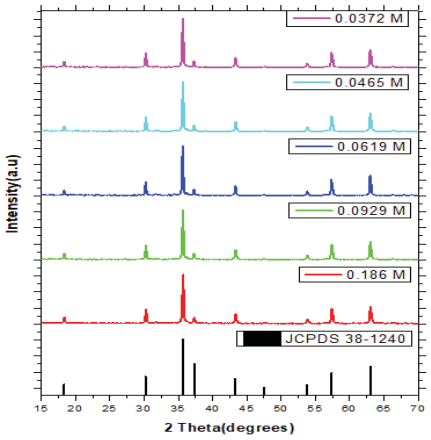

Fig. 1: XRD pattern of spinel structure of $ZnGa_2O_4$

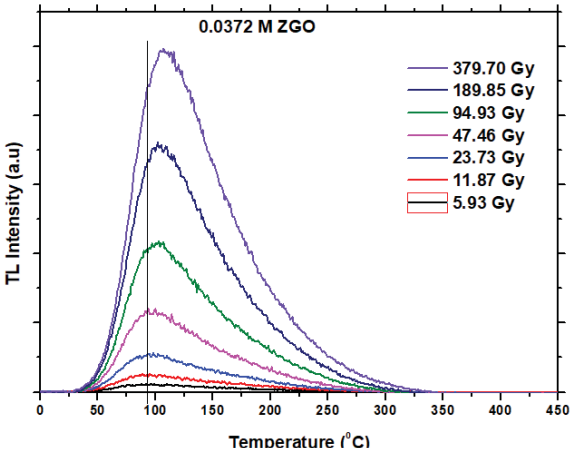

Fig. 2: The TL glow curves recorded when the samples were exposed to various doses of beta radiation

3. References

[1] *L.L. Noto, M. Mbongo. J. Phys. B (2019) 411768*
[2] *Y. Wang, H. Zhang. et al. J. App. Phys. 125 (2019) 095701*
[3] *C. Furetta, Handbook of Thermoluminescence, World Scientific publishing company, 2003.*

P27

Synthesis and characterization of P3HT-ZnO: FWCNTs for possible application in organic solar cells

Seithati Qotso[1,2], Pontsho Mbule[1], Bakang Mothudi[1]

[1]Department of Physics, CSET, University of South Africa, Johannesburg, 1710, South Africa.
[2] Department of Electrical Engineering, CSET, University of South Africa, Johannesburg, 1710, South Africa
Corresponding author e-mail address: qotsoas@gmail.com

1. Introduction

Organic solar cells (OSCs) have emerged as a new competitor to conventional solar cells and have gained a lot of attention in the industry and academia for the past decades, due to their advantages of being flexible solar panels [1], low cost [2], light weight [3], simple fabrication [4] and large-scale production for the PV industry [5]. OSCs consisting of zinc oxide (ZnO) nanorods and semiconducting polymer such as poly(3-hexylthiophene) (P3HT) in the active layer have been studied extensively over the past decade [6]. In this study, ZnO nanorods were synthesized by wet chemical sol-gel microwave assisted method and thioglycerol (TG) was used as a capping agent.

2. Results

We optimized ZnO:FWCNT by varying the concentration of FWCNT, and the photoluminescence (PL) results showed that ZnO: 3% FWCNT has the highest emission intensity as shown in Fig. 1(a). The focus is to incorporate ZnO: 3% FWCNT with P3HT to study the structure, morphology, optical and electrical conductivity properties. Furthermore, P3HT-ZnO:3% FWCNT at 1:1 ratio as shown in Fig. 1(b) significantly quenched the P3HT emission and this phenomenon is known to be beneficial for enhanced charge carrier mobility, lengthened free-carrier diffusion path and an increased phonon activity in organic solar cells. The purpose is to improve P3HT absorption and conductivity for applications in organic solar cells.

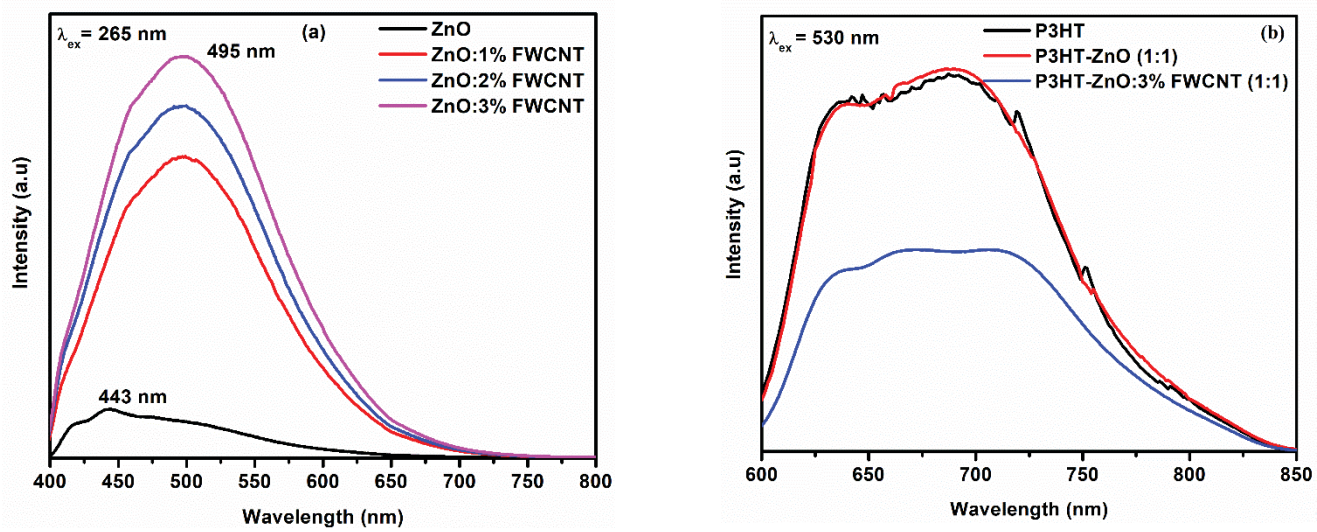

Fig. 1: Emission spectra of (a) ZnO, ZnO doped with 1, 2 and 3% of FWCNT excited at 265 nm (b) P3HT, P3HT-ZnO (1:1) and P3HT-ZnO:3% FWCNT (1:1) excited at 530 nm.

3. References

[1] K. Kalyanasundaram, M. Gratzel, *J. Mater. Chem.* **22** (2012) 24190 – 24194.
[2] J. Nozik, J. Miller, *Chem. Rev.* **110** (2010) 6443 – 6445.
[3] R. Luna-Rubio, M. Trejo-Peria, D. Vargas-Vázquez, G. Ríos-Moreno. *J, Sol. Energy,* **86** (2012) 1077 – 1088.
[4] G. Muller-Furstenberger, M. Wagner, *Ecol. Econ.* **62** (2007) 648 – 660.
[5] M. R. Simmons, In The Coming Saudi Oil Shock and the World Economy; John Wiley & Sons: Hoboken, NJ, USA, 2005.
[6] H. Qiu, J. H. Shim, J. Cho, J. M. Mativetsky, ASC Appl. Energy Mater. **1** (2018) 6172-6180.

Fabrication of Metal Organic Frameworks Derived Co_3O_4 Semiconductor Metal Oxides Loaded on TiO_2: Influence of Fe Loading on the Optical and Chemiresistive Characteristics of Co_3O_4/TiO_2 Heterostructure

Thabang J. Theka, Hendrik C. Swart, David E. Motaung

Department of Physics, University of the Free State, Bloemfontein, Park West, 9301

Corresponding author e-mail address: thekatj@ufs.ac.za

1. Introduction

Metal organic frameworks (MOFs) are solid crystal porous materials composed of metal cations linked by organic ligands. They are used in a variety of applications including, gas separation and storage, sensing, luminescence, and catalysis[1]. Furthermore, studies have reported that loading of metal elements is a very much effective approach for improving the optical properties and gas sensing performance of the MOF-derived SMOs. Studies have reported that loading can affect the crystallite sizes, catalytic activity, and luminescence properties associated with surface defects, such as oxygen vacancies[2]. Among the SMOs, the spinel structure of Iron (Fe) loaded on MOFs-derived Co_3O_4 contains excellent conductivity, and oxygen-rich surface vacancies. Additionally, for Fe-Co_3O_4, Fe^{3+} ions partly diffuse into the crystal lattice of Co_3O_4, establishing Lewis basic sites of O in the low coordination O^{2-} anion, OH^- group and Co^{2+}-O^{2-} pair, and Lewis acidic sites of unsaturated coordination Fe^{3+}.[3] Consequently, Fe-Co_3O_4 possess an excellent synergistic influence for improved optical properties, which could be useful for gas sensing characteristics. Thus, due to their exceptional heterointerfacial properties, Co_3O_4/TiO_2 and 0.5-2 wt.% Fe loaded on MOFs-derived Co_3O_4/TiO_2 heterostructure were synthesized using co-precipitation method. The tested samples showed improved selectivity towards benzene, toluene, ethylbenzene, and xylene (BTEX) compounds.

2. Results

Fig. 1 shows the photoluminescence (PL) characteristics of the Co_3O_4/TiO_2 and 0.5-2 wt.% Fe loaded on MOFs-derived Co_3O_4/TiO_2 heterostructures. It is observed from the figure that the PL emission increases with increasing the Fe loading, which justifies higher surface defects on the Fe/Co_3O_4/TiO_2 heterostructure. Higher surface defects associated with oxygen vacancies were observed for the 1wt.% Fe/Co_3O_4/TiO_2, leading to improved sensing performance towards BTEX compounds.

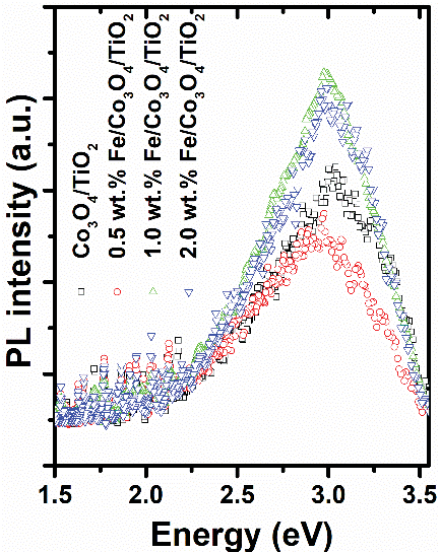

Fig. 1: PL spectra of Co_3O_4/TiO_2 and 0.5-2 wt.% Fe loaded on MOFs-derived Co_3O_4/TiO_2 heterostructures.

3. References

[1] U. Czaja, N. Trukhan and U. Müller, *Chem. Soc. Rev.*, vol. 38, pp. 1284-1293, 2009.
[2] P.F. Cheng, F. Dang, Y.L. Wang, J. Gao, L.P. Xu, C. Wang, L. Lv, X. Li, B. Zhang, B. J. Liu, Sens. Actuators B: Chem. 328 (2021), 129028.
[3] X. Zheng, Q. Zhu, H. Peng, Y. Quan, J. Wen, Chem. Phys. Lett. 779 (2021), 138846.

P29

Luminescence properties of a Cr^{3+} doped $MgTa_2O_6/Mg_4Ta_2O_9$ composite phosphor

D.V. Mlotswa[1], V.R. Orante-Barrón[2], D. Poelman[3], L.L. Noto[1]

[1]Department of Physics, University of the South Africa, P.O.Box 392, Republic of South Africa.
[2]Departamento de Investigación en Polímeros y Materiales, Universidad de Sonora, Apartado Postal 130, Hermosillo, Sonora 83000 México
[3]Ghent University, LumiLab, Department of Solid State Sciences, Ghent, Belgium

Corresponding author e-mail address: mlotsdv@unisa.ac.za

1. Introduction

Near-infrared (NIR) phosphors play a vital role in photonic, optoelectronic and biological applications. While the discovery of a broad-band NIR phosphor remains a challenge. In this respect, luminescent properties of a new Cr^{3+} doped composite $MgTa_2O_6/Mg_4Ta_2O_9$, Cathodoluluminescence (CL) mapping, Thermoluminescence (TL) and Decay curve measurements are recorded. A new persistent luminescent (PLUM) composite material $MgTa_2O_6/Mg_4Ta_2O_9:Cr^{3+}$, which displays CL intensity that is phase dependent, was synthesized by solid-state chemical reaction route at 1200 ^{0}C for 8 hours. X-ray diffraction (XRD), scanning electron microscopy (SEM) and energy dispersive spectroscopy (EDS) maps were used to confirm the multi-phase, multi-particle shapes and to assign each particle shape to a corresponding phase of the phosphor, respectively. CL maps were obtained simultaneously with the EDX maps and showed both the luminescence emerging from intrinsic and extrinsic defect center [2].

2. Results

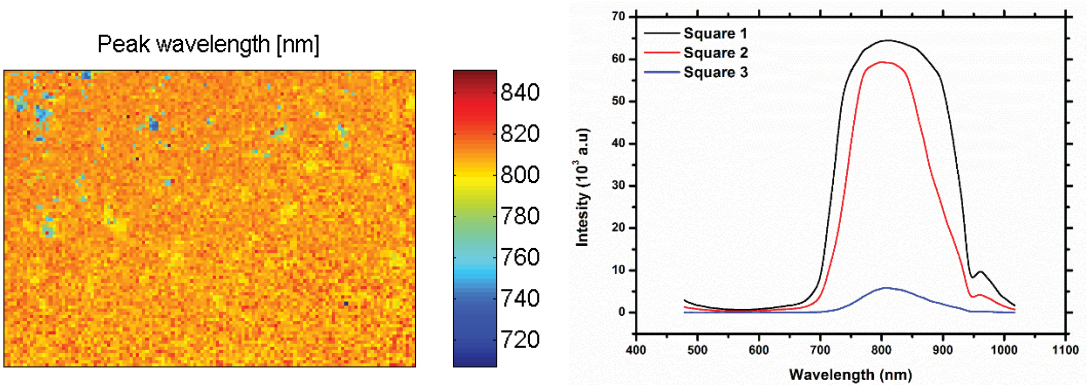

Fig. 1: CL maps of $MgTa_2O_6/Mg_4Ta_2O_9$ showing (a) barycentric wavelength and (b) total intensity in different parts on the scanned area.

3. References

[1] L.L. Noto, S.K.K.Shaat, D.Poelman, M.S.Dhlamini, B.M.Mothudi, H.C.Swart, Ceram. Int 42 (2016) 9784.
[2] L.L. Noto, S.K.K.Shaat, D.Poelman, P.F.Smet, L.Martin, M.Y.A.Yagoub, S.M. Dhlamini, O.M.Ntwaeaborwa, H.C.Swart, Ceram. Int 42 (2016) 5503.

Effect of dot size on the photolumenescence emission of GaSb/GaAs QDs

Ngcali Tile[1], Assane Talla[1], Johannes Reinhardt Botha[1]

[1] *Physics Department, Nelson Mandela University, Summerstrand, Gqeberha, South Africa*

Corresponding author e-mail address: Ngcali.tile@mandela.ac.za

1. Introduction

Quantum dots (QDs) formed through the creation of Gallium Antimonite (GaSb) nanostructures in a Gallium Arsenide (GaAs) matrix have some unique and appealing properties that are being continually exploited for various applications such as solar cells and infrared detectors [1,2]. This system has a type-II band alignment providing strong spatial confinement for holes, and only binding electrons via the Coulomb interactions. The optical properties of quantum dots depend on the physical properties such as alloying, size and shape. A Metal Organic Vapor Phase Epitaxy (MOVPE) system provides a set of deposition conditions that would allow one to tune the size and distribution of GaSb nanofeatures on GaAs to an extent.
In this work we study the effect of dot size on the photolumenescence emission of GaSb/GaAs QDs. Two samples of GaSb/GaAs QDs grown via MOVPE under similar conditions but with different dot sizes are being investigated. Uncapped GaSb nanostructures on GaAs grown under similar conditions as the QDs being investigated for PL were scanned by scanning probe microscopy (SPM) in order to determine their morphology (shape, size and density).

2. Results

Figure 1 shows SPM images of samples of uncapped GaSb QDs on GaAs substrates. Average height, area and diameter for sample 1 and 2 are 5 nm and 5 nm, 995 nm² and 619 nm², 35 nm and 27 nm respectively. It is clear that sample 1 has smaller dot size than sample 2.

Figure 2 shows PL spectra for samples A (corresponding to smaller dots) and B (corresponding to larger dots). There are two visible peaks from both spectra (A and B) at lower energies and at higher energies. The higher energy peaks are attributed to the wetting layer (WL), while the lower energy peaks are attributed to the QDs.
The WL emission energy for both samples is similar at around 1.32 eV. However, the QD emission energy is different with A peaking at a higher energy (1.67eV) than B (1.09). This suggests that the WL thickness is similar for both samples while the size of the embedded dots is different, with A being smaller than B as expected [3]. Peak intensities for A are generally higher than that of B, suggesting better optical quality for A. Also, The QD/WL ratio for A is higher than that of B meaning more recombinations in the QD for A than in B. The strain on GaAs matrix caused by larger GaSb dots could cause defects in the material which then act as recombination centres for carriers. These defects are expected to be more around the dots than around the WL.

Temperature dependent PL measurements will be performed to determine the thermal stability of the QD PL emissions and deduce on defects. Transmission Electron Microscopy will be used to determine the chemical composition of the dots and determine the extent of strain between GaSb and GaAs.

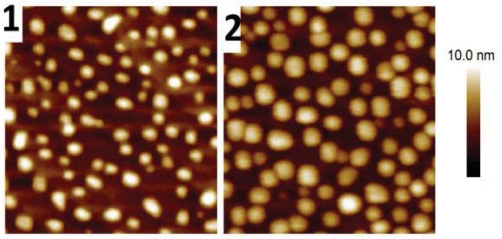

Fig. 1: 0.5 µm × 0.5 µm SPM images of samples of uncapped dots grown at the same conditions as the dots in samples A and B. Dots in 1 and 2 correspond to A and B respectively.

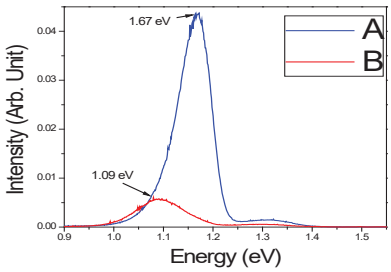

Fig. 2: 10 K PL spectra of QD samples A, B and C, excited with 80 mW. The high energy, low intensity peaks correspond to the WL while the low energy high intensity peaks correspond to QD emission.

3. References

[1] P.J. Carrington, A.S. Mahajumi, M.C. Wagener, J.R. Botha, Q. Zhuang, and A. Krier, Physica B 407, 1493 (2012).
[2] R.B. Laghumavarapu, A. Moscho, A. Khoshakhlagh, M. El-Emawy, L.F. Lester, and D.L. Huffaker, Appl. Phys. Lett. 90, 173125 (2007).
[3] E. O. Chukwuocha and M. C. Onyeaju, IJSTR 1, 7, 21 (2012).

P31

The effect of electrolytic pH on the properties of electrodeposited CdTe thin films for solar energy application

A.U Yimamu[1], B.F Dejene[2], O.K Echendu [3,4], J.J Terblans[1], H.C Swart[1] and S.J Motloung[1]

[1]Department of Physics, University of the Free State, Bloemfontein/QwaQwa Campus, South Africa
[2]Department of Chemical and Physical, Walter Sisulu University (Mthatha), Mthatha, South Africa
[3] Department of Physics, Federal University of Technology, P. M. B, 1526, Owerri, Nigeria
[4]Africa Center of Excellence in Future Energies and Electrochemical Systems (ACE-FUELS), Federal University of Technology, P, M, B, 1526, Owerri, Nigeria
Corresponding author's e-mail address: ahemed.dilla2010@gmail.com, tlousj@gmail.com

1. Introduction

The cadmium chalcogenide group is a promising candidate for further developments in solar energy applications. The absorber layer plays a significant role in thin film solar cell devices since photon absorption principally take place in it for the production of photo-generated charge carriers that give rise to the photocurrent. Owing to its unique properties, cadmium telluride (CdTe) is used as an absorber layer in thin-film solar cells. For the growth of CdTe thin film, hydrogen evolution, which can directly impact the development of the depositing layer, is one of the main issues during electrodeposition [1]. This can be managed by systematic adjustments of the pH of an electrolytic solution. In this study, CdTe thin films were prepared from a cadmium acetate-based solution using a two-electrode electrodeposition technique at different deposition pH values. The structure, optical properties, surface morphology, elemental composition, and surface roughness of the as-deposited CdTe thin films were investigated. The crystallite sizes of the CdTe thin films were calculated using Scherer's formula [2].

2. Results

Structural analysis revealed that the deposited CdTe thin films have polycrystalline cubic zinc blend structure at the pH values of 3.0 and 3.5. When the pH values were 1.8 and 2.5, hexagonal peaks were observed. The (111) preferential orientation peak intensity for the cubic phase varied with the pH. The crystallite size was estimated to be 16, 44, and 31 nm at the pH values of 2.5, 3.0, and 3.5, respectively. The optical analysis showed that absorbance varied with pH, and the energy band gap was recorded as 1.47, 1.46, and 1.5eV with pH values of 2.5, 3.0, and 3.5, respectively. Scanning electron microscopy (SEM) images showed that the glass substrate was uniformly covered by CdTe thin film while the surface morphology of the CdTe changed with pH. Elemental composition analysis using EDX confirmed the presence of both Cd and Te, and their atomic percentages varied with pH. Scanning probe microscopy (SPM) measurements showed that the average surface roughness was recorded as 50.08, 78.73, and 24.00 nm for pH values of 2.5, 3.0, and 3.5, respectively. The overall results show that the best CdTe film quality, for solar cell applications, was produced when the pH value was 3.0.

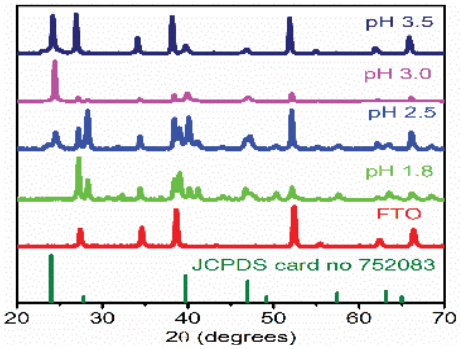

Fig. 1: XRD patterns of CdTe thin films grown at different pH values.

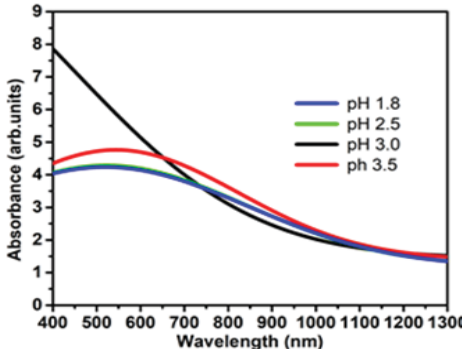

Fig. 2: Absorbance as a function of wavelength for CdTe films grown at different pH values.

3. References

[1] Agasti A, Mallick S, Bhargava P . J Mater Sci Mater Electron.(2018).**29**:4065
[2] Surabhi S, Anurag K, Kumar SR.Chalcogenide Lett(2022) **19**:143

Alteration of Li states on a self-healed graphane

RE Mapasha[1], SP Kgalema[1], and E Igumbor[2]

[1]Department of Physics, University of Pretoria, Pretoria 0002, South Africa.
[2]Department of Mechanical Engineering Science, University of Johannesburg, Johannesburg, South Africa

Corresponding author e-mail address: edwinmapasha@up.ac.za

1. Introduction

Recently, two dimensional (2D) materials have attracted an enormous interest due to their potential for future nanoelectronics applications, owing to their peculiar physical and electrical properties. These considerations apply particularly well to layered graphitic systems: graphene and its derivatives (graphane, florographene and chlorographene) [1]. Graphane is a wide band semiconductor with a density functional theory (DFT) value of 3.4 eV [1]. Experimentally, graphane samples have been achieved from hydrogen plasma, and are stable at room temperatures [2]. The setback with graphane for technological application is due to its inetness leading to its failure to interact with foreign atoms. Creation of vacancies and doping (through ion-implantation, electro-thermal reactions, etc.) is an effective method [3]. Creation of more vacancies can make graphane more reactive to accommodate more foreign atoms densities[4]. Li atom is a preferred candidate for Li-ion storage and can interact with vacancies through ionic bonding. In this work, we adsorb Li atom on the different CH pair divacancies in graphane to study the stability and electronic properties using first-principle methods.

2. Results

The energetic stability, structural and electronic properties of different Li configurations on self constructed topological 5-9-5 and 9-5-9 defects were examined. These lithiated configurations have high binding energies significantly more than that of Li on graphene and bulk metalic lithium, suggesting a plausible materials for experimental characterizations. All the lithiated configurations relaxes towards the vacancy with 5-9-5 defect having a 0.00 Å height (insertion). The Li atom introduces delocalised states within the band gap, exhibiting metallic character with considerable electronic states at the Fermi level, which can provide good electrical conductivity during the battery cycle. These results suggest that Li configurations on self constructed topological 5-9-5 and 9-5-9 defects can be utilized as a promising anode material for the application in Li-ion batteries with fast charge/discharge rates.

3. References

[1] J. O. Sofo, A. S. Chaudhari, and G. D. Barber, Phys. Rev. B 75, 153401 2007.
[2] D. C. Elias, R. R. Nair, T. M. G. Mohiuddin, S. V. Morozov, P. Blake, M. P. Halsall. A. C. Ferrari,
[3] D.W. Boukhvalov, M. I. Katsnelson, A. K. Geim, and K. S. Novoselov, Science 323, 610 (2009).
[3] J. J. Palacios, J. Fernandez-Rossier, and L. Brey, Phys. Rev. B 77, 195428 (2008).
[4] B.S. Pujari and D.G. Kanhere, J. Phys. Chem. C 113 210637 (2009).

P33

Electrically active defects levels induced by trivalent substitution-interstitial defect-complexes in Ge

E. Igumbor[1], O. Olaniyan[2] , G. M. Dongho-Nguimdo[3] and R. E. Mapasha[4]

[1]Department of Mechanical Engineering Science, University of Johannesburg, Johannesburg, South Africa
[2]Department of Chemistry University of Free-State, 9300 Bloemfontein, South Africa
[3]Department of Electrical and Electronic Engineering, College of Technology, University of Buea, P.O.Box 63, Buea, Cameroon.
[4]Department of Physics, University of Pretoria, Pretoria 0002, South Africa.
Corresponding author e-mail address: edwinmapasha@up.ac.za

1. Introduction

Point defects such as defect-complexes have significant impact on the physical, optical, and electrical properties of semiconductors [1,2]. Recent studies have shown that defect-complexes induced deep-levels could be applied in quantum information. In particular, the nitrogen-vacancy center in 4H-SiC and in diamond, has been courted for application in quantum information. Several defect-complexes formed by *n* and *p*-type impurities have been reported in silicon and germanium [3]. However, there is no report on the substitution and interstitial defect-complexes formed by trivalent impurities in germanium. Hence, their inherent electrically active defect levels in are not known. In this study, we used the hybrid density functional theory to predict the structural and electronic properties, formation and defect levels induced by the trivalent substitution-interstitial ($B_{Ge}B_i$, $Al_{Ge}Al_i$, $Ga_{Ge}Ga_i$ and $In_{Ge}In_i$) defect-complexes in Ge.

2. Results

The partial density of states (PDOS) was predicted. The $B_{Ge}B_i$, $Al_{Ge}Al_i$, $Ga_{Ge}Ga_i$ and $In_{Ge}In_i$ behave like *p*-type semiconductors as shown in Fig 1. The ground state of the host atoms was populated by the s-orbital of the impurity atoms. The $Ga_{Ge}Ga_i$, under equilibrium conditions is the most energetically favourable defect with formation energy of 3.95 eV. All the trivalent atoms bounded with substitution and interstitial atoms without dissociation. With respect to their ability to form as a cluster defect, the $In_{Ge}In_i$ is the most stable defect-complex with a binding energy of 2.91 eV. Except for the $Ga_{Ge}Ga_i$ which neutral charge dominates the Fermi level from the valence to conduction band, all other substitution-interstitial defect-complexes were electrically active. While the $B_{Ge}B_i$, and $Al_{Ge}Al_i$ induced single acceptor level, the $In_{Ge}In_i$ induced donor levels as shown in Fig 2. The acceptor defect level induced by the $B_{Ge}B_i$ is deep and that of the $Al_{Ge}Al_i$ is a shallow defect level close to the conduction band.

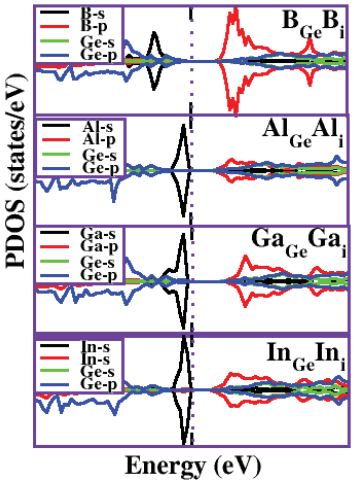

Fig. 1: Plot of partial density of states od defect-complexes in Ge

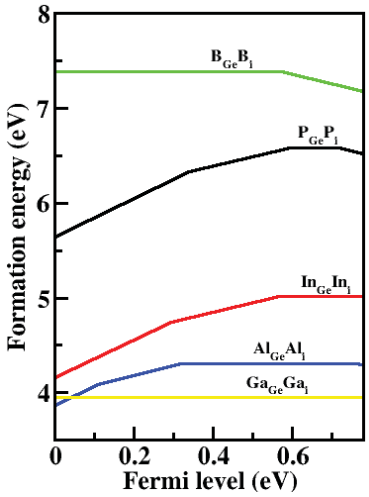

Fig. 2: Formation energy as a function of Fermi level position.

The results of this study are essential as they provide theoretical insights for the experimental characterisation of the substitution and interstitial defect-complexes formed by trivalent impurities in germanium. Also, the results of this study are intended to be significance for application in electronic devices.

3. References

[1] S. Assali, M. Elsayed, J. Nicolas , MO. Liedke, A. Wagner A, M. Butterling, R. Krause-Rehberg, O. Moutanabbir. Applied Physics Letters 114(25):251907.
[2] E. Igumbor, O. Olaniyan, GM. Dongho-Nguimdo, E. Mapasha, S. Ahmad, E. Omotoso, WE Meyer. Materials Science in Semiconductor Processing (150) 106906
[3] Bouzid, A. and Pasquarello, A., 2019. Defect Formation Energies of Interstitial C, Si, and Ge Impurities in β-Ga2O3. physica status solidi (RRL)–Rapid Research Letters, 13(8), p.1800633.

Density Functional Theory Investigation of the Properties of the E-Centre in P, As and Sb doped Si

Chantel Maré, Fortune Moruta, Walter Meyer

[1] *Department of Physics, University of Pretoria, Pretoria, South Africa*

Corresponding author e-mail address: walter.meyer@up.ac.za

1. Introduction

Radiation-induced defects cause performance loss and degradation over time in semiconductor devices. A thorough understanding of the properties of such defects is required for the sustainable development of modern electronics used in high radiation environments e.g. those used in satellite technology and medical devices. To this end, it is important to correlate experimental results with theoretical calculations.

Density functional theory (DFT) is the most commonly used method to model such defects. The results of the DFT calculation can then be correlated with that obtained by experimental techniques, specifically deep level transient spectroscopy (DLTS), which characterises the electrical properties of defects, to obtain a complete understanding of the defect.

The defect consisting of a vacancy-donor pair (E-centre) in Si has been studied by many techniques. Typical dopants in Si include P, As and Sb. Auret *et al.* [1] have shown that high-resolution Laplace-DLTS can distinguish between the E-centres formed by these three dopants. In this study we have used density functional theory with hybrid functionals to investigate the electronic properties of these defects and compare them with properties that may be determined by DLTS.

Calculations were performed using Quantum Espresso on a 216 atom (3×3×3 cubic unit cell) supercell using a 2×2×2 **k**-point mesh and a cut-off energy of 40 Ry for all calculations. The CoFFEE [3] routine was used to perform the Freyschold Neugebauer van der Walle (FNV) [4] corrections for charged supercells. Structures were relaxed using the PBE functional and SCF calcuations were done using the PBE0 functional.

2. Results

Using the procedure above, we found charge transition levels corresponding to a donor level at 0.098, 0.105 and 0.133 eV relative to the conduction band for V-P, V-As and V-Sb, respectively, relative to the valence band and an acceptor level 0.193, 0.193 and 0.186 eV for V-P, V-As and V-Sb, respectively, relative to the conduction band. This agrees reasonably well with experimental results by Larsen *et al.* [5], who experimentally found an acceptor level 0.45 eV below the conduction band and a donor level 0.27 eV above the valence band.

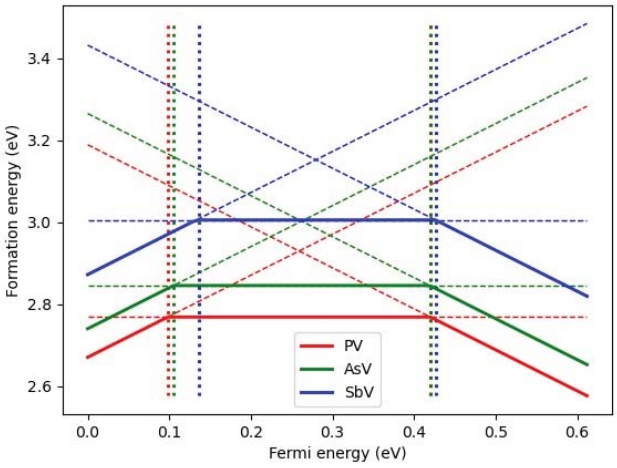

Fig. 1: Formation energy as a function of Fermi-level relative to the valence band for V-P, V-As and V-Sb defects in Si.

In addition, we compare our modelled results with experimental data from DLTS including capture cross-sections, field effect and annealing properties.

3. References

[1] G. Herrero-Saboya, L. Martin-Samos, A. Jay, A. Hemeryck and N. Richard. *J. Appl. Phys.* **127** 085703 (2020)
[2] F.D. Auret, A.R. Peaker, V.P. Markevich, L. Dobaczewski, R.M. Gwilliam, F.D. Auret, A.R. Peaker, R.M. Gwilliam, *Physica B* **376** 73-76 (2006)
[3] M.H. Naik and M. Jain, arXiv:1705.01491v4 [cond-mat.mtrl-sci], https://doi.org/10.48550/arXiv.1705.01491 (2017)
[4] C. Freysold, B. Grabowski, T. Hickel, J. Neugebauer, G. Kresse, A. Janotti, C.G. van de Walle, *Rev. Mod. Phys.* **86** 253 (2014)
[5] A.N. Larsen, A. Mesli, K.B. Nielsen, H.K. Nielsen, L. Dobaczewski, J. Adey, R. Jones, D.W. Palmer, P.R. Briddon and S. Öberg, *Phys. Rev. Lett.* **97** 106402 (2006)

P35

Enhancement of Li and graphane interaction through extended H vacancy pathways for Li-ion batteries: Ab initio study

Sentserere Kgalema[1], **Refilwe Mapasha**[1]

[1] [1]*Department of Physics, University of Pretoria, Pretoria 0002, South Africa.*

Corresponding author e-mail address: pskgalema@email.com

1. Introduction

The LIBs have been widely used as a power source for the operation of electronic devices for over two decades[1]. Recently, the LIBs faced great challenges to always meet the growing energy demand particularly with the electric vehicles on board. More research effort is needed to develop the next-generation Li-ion batteries with dramatic performance, such as peculiar high volumetric energy density, cyclability, charging rate, stability, and safety[2, 3]. The aforementioned properties can collectively be achieved from a special anode material; hence variety of anode materials are being extensively researched. In this work, we have given graphane an interest due to its high surface area, exceptional flexibility, wide band gap, excellent mechanical properties and simple manufacturing procedure using a variety of techniques[4]. First-principles density functional theory calculations were performed to study the energetic stability, electronic and electrochemical properties of Li atoms on the H vacancies ($\boldsymbol{V_H}$) following a Line pathway as well as the zigzag pathway on a graphane sheet for LIBs.

2. Results

The results of Li on a single H vacancy $\boldsymbol{V_{H1(L)}}$ revealed that it successfully induced interaction based on the improved binding energies, charge transfer and significantly shortened Li height, as compared to those of pristine graphane. An increase in H vacancies along the line pathway from one $\boldsymbol{V_{H1(L)}}$ to five $\boldsymbol{V_{H5(L)}}$ leaves behind localized electrons ready to interact with the Li atom resulting in high binding energies ranging from 1.82eV to 2.92eV. While creation of H vacancies along the zigzag pathway from one $\boldsymbol{V_{H1(Z)}}$ to five $\boldsymbol{V_{H5(Z)}}$ leaves behind electrons that pair and repel Li atom away yielding undesired low binding energies which become a setback for LIBs. For the increment of Li content following a line $\boldsymbol{V_H}$ pathway, the binding energies of Li on configurations $\boldsymbol{V_{H1(L)}}$ to $V_{H5(L)}$ tend to reduce in order, endearingly are still higher than the minimum Li standard bulk cohesive energy of 1.63 eV, suggesting a possible uniform dispersion of Li atoms with less clustering on the graphane sheet. A transition from insulator to metallic behaviour was observed with induced new Li states at the vicinity of the fermi level, which will enhance electron transmission in the graphane sheet. At five Li content adsorbed along the line configurations, a relatively high storage capacity of 207.49 mAh/g with its corresponding lithiation potential of 1.48 V are achieved and are comparable to the other previously studied 2-dimensional anode materials with high Li concentration.

3. References

[1] Blomgren, G.E., *The development and future of lithium ion batteries.* Journal of The Electrochemical Society, 2016. **164**(1): p. A5019.
[2] Deng, D., *Li-ion batteries: basics, progress, and challenges.* Energy Science & Engineering, 2015. **3**(5): p. 385-418.
[3] Simon, P., Y. Gogotsi, and B. Dunn, *Where do batteries end and supercapacitors begin?* Science, 2014. **343**(6176): p. 1210-1211.
[4] Brahma, S., A.C. Lee, and J.-L. Huang, *Graphene as an Anode Material in Lithium-Ion Battery*, in *Lithium-Ion Batteries and Solar Cells*. 2021, CRC Press. p. 149-166.

Functionalizing barium hexaferrite nanoplatelets through push-pull systems: an *ab initio* approach

Gabriela Herrero-Saboya[1], **Matic Poberznik**[1], **Layla Martin-Samos**[1]

[1] *CNR-IOM, via Bonomea 265 c/o SISSA, 34134 Trieste, Italy*
Corresponding author e-mail address: gherrero@sissa.it

1. Introduction

Barium hexaferrite (BHF) nanoplatelets are permanent magnets, whose magnetic easy axis is perpendicular to their basal directions [1] (Fig. 1). Aiming at increasing their functionality, polarised organic ligands could be bonded to their surface, constituting a magneto-electric (ME) particle. To date, small functional groups (e.g. phosphonates) have been successfully attached to their surfaces [2], proving that the nanoparticles can be functionalized.

2. Results

An atomistic scale description of the ME particles, capable of providing physicochemical insights and/or feedback for the synthesis of the novel systems is presented. Magnetic properties of the BHF platelets, the dipole moments of the organic ligands and the platelet-ligand interactions were investigated in the framework of the density functional theory (DFT). More concretely, an on-site Coulomb repulsion (i.e. the DFT+U method) is included, showing that the magnetic moment of the BHF platelets arises from the ferrimagnetic distribution of iron ions. The electric dipole moment of different push-pull molecules in vacuum was also calculated, together with the intramolecular charge transfer. As a first step in the characterisation of the ME particle, the relative cohesion energy of different monolayers of these molecules in vacuum was also determined. A critical intermolecular distance was identified, below which a significant decrease of the dipole moment occurs. Finally, preliminary results on the hybridised system are reported: the preservation of the magnetic moment of the platelets and a small charge reorganisation throughout the ligand once attached to the surface.

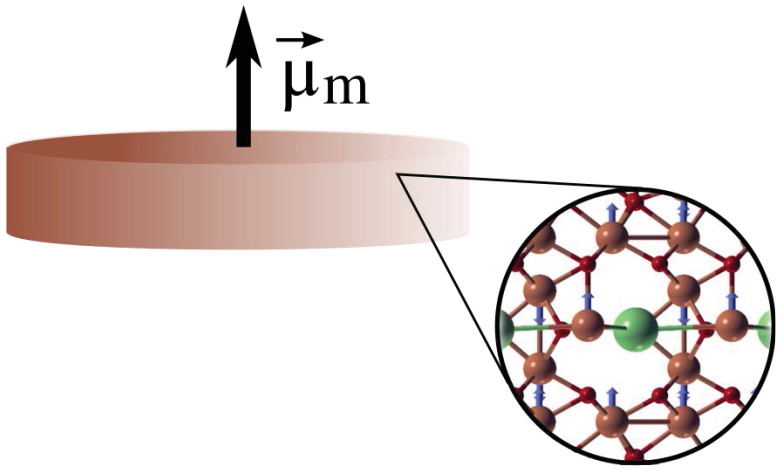

Fig. 1: Barium hexaferrite nanoplatelets as one of the basic constituents of the Magneto-Electric particles.

3. References

[1] D. Makovec et al., Nanoscale, **10** (2018) 14480.
[2] D. Lisjak, et al., ACS Omega, **504** (2020) 237.

P37

Refactoring of ARTn: a plugin for electronic structure calculation and molecular dynamics codes

Matic Poberžnik,[1] Miha Gunde,[1] Antoine Jay,[2] Anne Hemeryck,[2] Nicolas Richard,[3] Nicolas Salles,[1] Normand Mousseau,[4] and Layla Martin-Samos[1]

[1]*CNR-IOM Democritos c/o SISSA, via Bonomea 265, IT-34136, Trieste, Italy*
[2]*LAAS-CNRS, Université de Toulouse, CNRS, F-31555, Toulouse, France*
[3]*CEA, DAM, DIF, Bruyères-le-Châtel, F-91297, Arpajon, France*
[4]*Département de Physique, Université de Montréal, C.P. 6128, succursale Centre-ville H3C 3J7 Montréal Canada Montréal, Canada*
Corresponding author e-mail address: nsalles33@gmail.com

1. Introduction

The Activation Relaxation Technique nouveau (ARTn) [1], is an automatic algorithm for identification of saddle points on potential energy surfaces. Its current implementations rely on external software to calculate the energy/forces (E/F) of the current configuration, i.e., an E/F engine, and are based on a top-down approach, where ARTn generates the input for the engine and extracts the data from the output. However, such an approach has resulted in many different implementations of the algorithm, each tailored to a specific engine.

2. Results

In this contribution a refactoring of the ARTn algorithm is presented, so that the algorithm is called by the engine when an ARTn saddle point search is requested. To this end, the algorithm has been rewritten in the form of a library (pARTn) that biases a minimisation algorithm of the engine to perform an ARTn saddle point search instead. The coupling of the library to two engines will be presented: on the DFT code, quantum-ESPRESSO [2] and the molecular dynamics code LAMMPS [3].

3. References

[1] G. T. Barkema and N. Mousseau. Phys. Rev. Lett. **77** (1996).
[2] P. Giannozzi, O. Andreussi, T. Brumme, O. Bunau, M. B. Nardelli, M. Calandra, R. Car, C. Cavazzoni, D. Ceresoli, M. Cococcioni, N. Colonna, I. Carnimeo, A. D. Corso, S. de Gironcoli, P. Delugas, R. A. DiStasio, A. Ferretti, A. Floris, G. Fratesi, G. Fugallo, R. Gebauer, U. Gerstmann, F. Giustino, T. Gorni, J. Jia, M. Kawamura, H.-Y. Ko, A. Kokalj, E. Küçükbenli, M. Lazzeri, M. Marsili, N. Marzari, F. Mauri, N. L. Nguyen, H.-V. Nguyen, A. O. de-la Roza, L. Paulatto, S. Poncé, D. Rocca, R. Sabatini, B. Santra, M. Schlipf, A. P. Seitsonen, A. Smogunov, I. Timrov, T. Thonhauser, P. Umari, N. Vast, X. Wu, and S. Baroni. Journal of Physics: Condensed Matter **29** (2017) 465901.
[3] A. P. Thompson, H. M. Aktulga, R. Berger, D. S. Bolintineanu, W. M. Brown, P. S. Crozier, P. J. in 't Veld, A. Kohlmeyer, S. G. Moore, T. D. Nguyen, R. Shan, M. J. Stevens, J. Tranchida, C. Trott, S. J. Plimpton. Computer Physics Communications, Volume **271** (2022) 108171.

Investigation of the surface stability of barium hexaferrite bulk terminations by means of *ab initio* thermodynamics

Matic Poberžnik[1], **Gabriela Herrero-Saboya**[1], **Layla Martin-Samos**

[1] *CNR-IOM, via Bonomea 265 c/o SISSA, 34134 Trieste, Italy*
Corresponding author e-mail address: matic.poberznik@ijs.si

1. Introduction

Barium hexaferrite (BHF) is a ferrimagnetic material that has been the subject of numerous studies in the past decades. More recently, attention has been placed on the unique BHF nanoplatelets, since they present a well-defined magnetic axis perpendicular to their basal plane [1]. Depending on the conditions of preparation, two different terminations of the BHF nanoplatelets were observed from high-angle annular dark field scanning transmission electron microscopy (HAADF STEM) measurements [1]. This contribution presents a systematic study of the relative stability of different terminations of bulk BHF by means of Density Functional Theory (DFT) calculations in order to provide computational support for experimental observations. Specifically, the Hubbard corrected Perdew-Burke-Ernzerhof functional (PBE+U) was employed in combination with a plane-wave basis set, where the different bulk terminations are modelled as slabs subject to periodic boundary conditions. Their relative stability is evaluated by means of the well-established first principles thermodynamics approach [2].

2. Results

Results show that, in the absence of other species (water, air, etc.), the barium terminated 2b surface or the iron terminated $4f_2$ are the most stable (see Fig 1.). The 2b surface is the most stable in oxygen/iron poor conditions, whereas the $4f_2$ surface is the most stable in oxygen/iron rich conditions. These results are relatively in line with experimental observations, where the 2b surface was identified in Ba rich conditions, whereas in Ba poor conditions, the 12k-O oxygen terminated surface was observed. Note, however, that under experimental conditions the surfaces are likely hydroxylated. Taking this into account, it was found that hydroxylating the surfaces leads to a change in the relative stability of the surfaces. More concretely, the fully hydroxylated 12k-O surface is found to be the most stable over the hydroxylated $4f_2$ surface, allowing leading to the conclusion that the results of calculations in this work are in line with experimental observations.

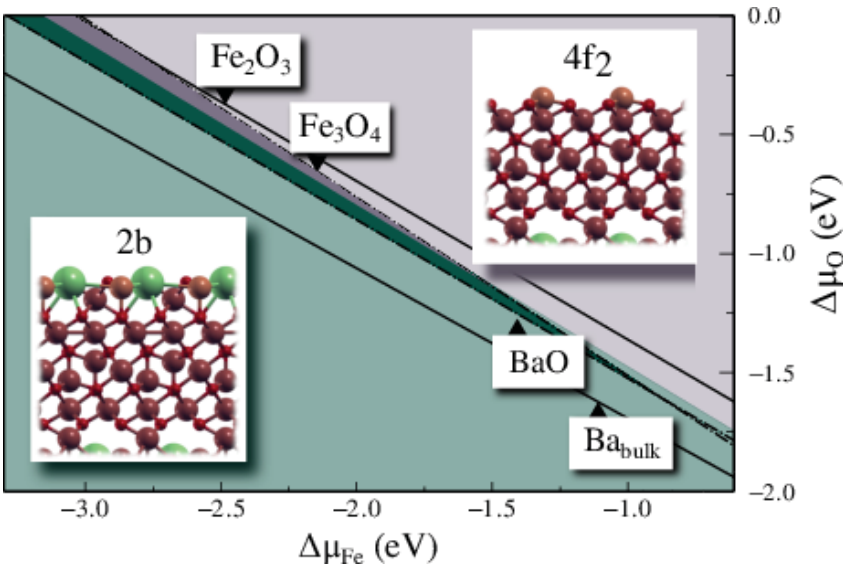

Fig. 1: The most stable surface terminations of BHF bulk in vacuum as a function of iron and oxygen chemical potentials

3. References

[1] D. Makovec et al. *Nanoscale* **10** (2018) 14480.
[2] K. Reuter and M. Sheffler. *Phys. Rev. Lett.* **90** (2003) 0461031.

P39

First principles calculation of multi-vacancies and multi-interstitials defects in Ge by the DFT + alpha method

Abdulgaffar Abdurrazaq[1], Ruggero Lot[1,2], Gabriela Herrero Saboya[2], Antoine Jay[1], Stefano De Gironcoli[2], Layla Martin Samos[1], Nicolas Richard[3], Anne Hemeryck[1]

[1] *Laboratoire d'analyse et d'architecture des systèmes, CNRS, 31031 Toulouse cédex 4, France*
[2] *CNR-IOM/Democritos National Simulation Center, Istituto Officina dei Materiali, c/o SISSA, via Bonomea 265, IT-34136 Trieste, Italy*
[3] *CEA, DAM, DIF, F-91297 Arpajon, France*

Corresponding author e-mail address: abdulgaffar.abdurrazaq@laas.fr

1. Introduction

The renewed interest in integrating germanium into nanoscaled microelectronic devices requires a fundamental understanding of the intrinsic defects that may exist in the material that could be the source of device malfunction or performance loss. The small electronic bandgap of Ge also makes it very difficult to identify defects by experimental techniques.

A method was developed and used to correct for the intrinsic error of DFT on the electronic band gap properties of germanium, and a thorough study of both multi-vacancies and multi-interstitial defect complexes is conducted. The formation energies of these clusters of defects are determined for several configurations and different charge states, allowing us to characterize their impact on the electronic properties compared to perfect crystalline germanium.

Preparation of highly sensitive Cr doped $ZnFe_2O_4$ fiber-like sensors for selective acetone detection

Murendeni Nemufulwi[1,2], **Hendrik Swart**[2], **Gugu Mhlongo**[1,2]

[1] *Centre for Nanostructures and Advanced Materials (CeNAM), DSI-CSIR Nanotechnology Innovation Centre, Council for Scientific and Industrial Research, Pretoria 0001, South Africa*
[2] *Department of Physics, University of the Free State, Bloemfontein ZA9300, South Africa*

1. Introduction

Semiconducting metal oxides are widely recognized as key sensing materials for gas detection in several fields. In particular, zinc ferrite has attracted increasing attention because of its sensitivity to volatile organic compounds, making it a potential sensing material for food spoilage detection and monitoring [1]. However, their high operating temperatures and poor selectivity hinder their practical application. This study aims to overcome these challenges by using a Cr dopant to reduce the operating temperature and enhance the response variance for accurate gas classification using principal component analysis. A combustion method was used to synthesize Cr-doped $ZnFe_2O_4$ (0.0, 0.5, 1.0, 1.5 and 2.0 Cr mol%) fiber-like products. X-ray diffraction and high-resolution transmission microscopy (HR-TEM) were used to analyze the microstructure and morphology of the products. HRTEM confirmed that the synthesized products possessed fiber-like structures. Photoluminescence (PL) and X-ray photoelectron spectroscopy were used to analyze the structural defects and surface composition analysis, respectively.

2. Results

PL emission spectra of the pure and Cr ZnFe2O4 ((0.0, 0.5, 1.0, 1.5 and 2.0 Cr mol%) are shown in figure 1. The gas sensing results showed that the sensor based on 1.0% Cr-doped $ZnFe_2O_4$ had an enhanced response of 283 to 90 ppm acetone at a low operating temperature of 90 °C, as shown in figure 2. Moreover, the sensor based on $ZnFe_2O_4$ doped with 1.0% Cr can be used as a single array sensor for gas classification. The improved sensing properties were attributed to the structural defects and proper gas diffusion.

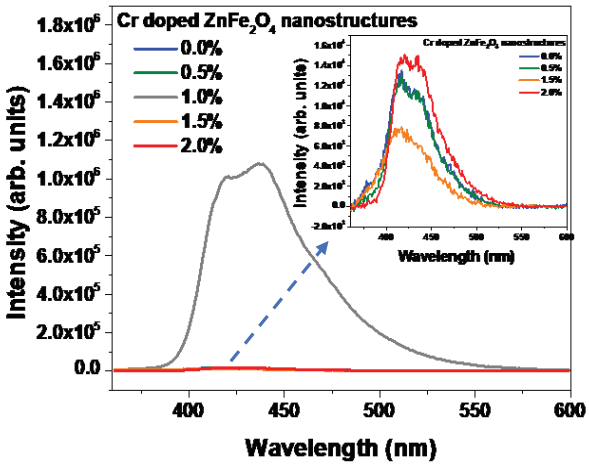

Fig. 1: PL emission spectra of the pure and Cr $ZnFe_2O_4$ ((0.0, 0.5, 1.0, 1.5 and 2.0 Cr mol%).

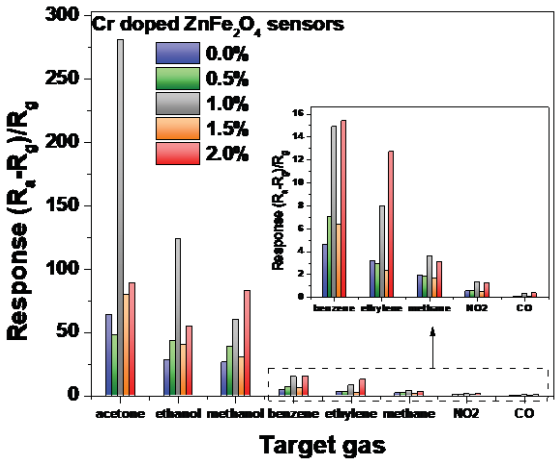

Fig. 2: Response comparison of the pure and Cr doped $ZnFe_2O_4$ sensors to different gases.

3. References

[1] M.I. Nemufulwi, H.C. Swart, K. Shingange, G.H. Mhlongo, Sensors and Actuators B: Chemical. **377** (2023) 133027.

P41

The effects of Eu^{3+} concentration on the photoluminescence of $Na_4Ca(PO_3)_6$: Eu^{3+} phosphors prepared by a solid state reaction method

Karabo B. Morebodi, S.N. Ogugua, H. C. Swart

Department of Physics, University of the Free State, P. O. Box 339, Bloemfontein, 9300, South Africa
Corresponding author:SwartHC@ufs.ac.za

1. Introduction

Rare earth materials that emit in the near infrared region play an essential role in the study of luminescence. In this work the focus was on the host $AB(PO_3)_6$, where A denotes the alkaline metals (Na^+) and B denotes the alkaline earth metal (Ca^{2+}) doped with europium (Eu^{3+}). $AB(PO_3)_6$ orthophosphates have excellent luminescence properties as hosts [1]. In addition, the incorporation of Eu^{3+} as a dopant is beneficial for the generation of white light, by producing a sharp emission in the red wavelength region. The invention of white light, by combining red, green, and blue (RGB) phosphors using near ultraviolet chips as excitation has been widely studied [2]. However, it is beneficial to investigate the effects of varying the concentration of the material at the same sintering temperature. $Na_4Ca(PO_3)_6$: Eu^{3+} nanophosphors were synthesized using the solid state reaction method annealing at 600 °C. The improvement in the optical properties using different doping concentrations of Eu^{3+} was studied through the emission of the photoluminescence (PL) spectrum.

2. Results

A series of $Na_4Ca(PO_3)_6$: *x*mol%Eu^{3+} (x=1.5,2.0,2.5 and 3.0) complexes were synthesized and characterized using various techniques. These phosphors exhibited a monoclinic, sharp and narrow crystal planes in the XRD, confirming the crystalline nature of the material. The optical bandgap of $Na_4Ca(PO_3)_6$: Eu^{3+} decreased when the concentration of Eu^{3+} was increased, probably due to the defects in the crystal lattice. The strong peak in Fig. 1 at 239 nm was assigned to the charge transfer band due to O^{2-} Eu^{3+}. The emission spectrum was excited at 240 nm and it was interesting to observe an increase in the intensity for the different Eu^{3+} concentrations in Fig. 2. The strong narrow bands emitting at 591 and 613 nm owing to the transition of $^5D_0 \rightarrow {}^7F_J$(j=1,2) and the CIE chromaticity coordinates found in the red region prove that these are promising candidates for white light emitting diode applications.

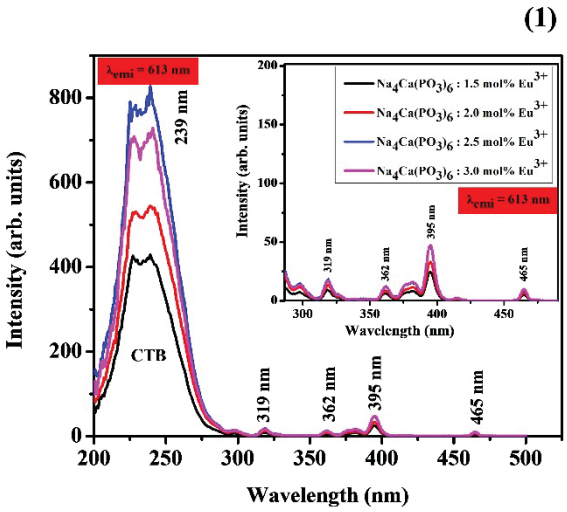

Fig. 1: PL excitation spectrum of the $Na_4Ca(PO_3)_6$:*x* mol% Eu^{3+} phosphor monitored at a 613 nm emission wavelength.

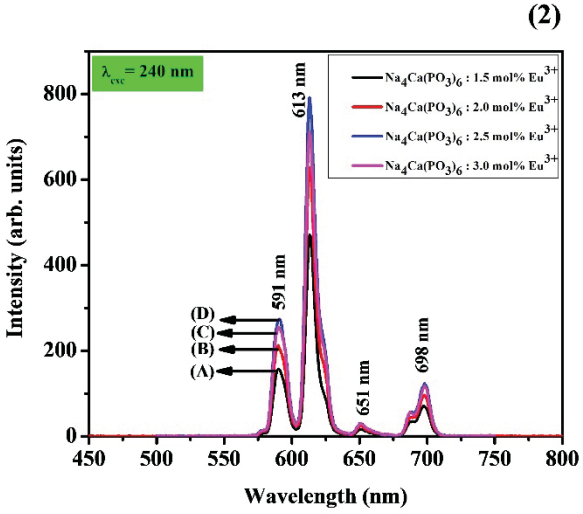

Fig. 2: PL emission spectrum of the $Na_4Ca(PO_3)_6$:*x* mol% Eu^{3+} phosphor at an excitation wavelength of 240 nm.

3. Reference

[1] Y.M. Pengs, Y.K. Su, R.Y. Yang, *Mater. Res. Bull*, **48(5)** (2013) 1946-1951
[2] S.R. Bargat, Y.R. Parauha, G.C. Mishra, S.J. Dhoble, *Molecular structure*, **1221** (2 020) 128838.

Effect of deposition voltage on the properties of electrodeposited CdZrS thin films for solar cell application

T.K.W Mohapi[1], A.U Yimamu[1], K.G Tshabalala[1] and S.J Motloung[1]

[1]Department of Physics, University of the Free State, Private bag X 01, Bloemfontein/QwaQwa campus, 9300, South Africa
Corresponding author email: 2014052167@ufs4life.ac.za, tlousj@gmail.com

1. Introduction

Wide energy band gap II-VI semiconductor chalcogenide thin films have recently received much attention due to their applicability in various applications and emissions in the blue and green spectral regions [1]. Cadmium Sulfide (CdS) is one of the families from this group and is employed as *n*-type window material in CdS/CdTe, CdS/CuInSe, and CdS/CuInGaSe solar cells [2]. It has a large energy band gap of 2.42 eV. For better performance, the energy band gap of this window material must increase to create a good band bending to reduce recombination in the CdS/CdTe interface and to reduce absorption loss. To achieve this, zirconium (Zr^{4+}) is added into CdS matrix. Zr is a transition metal ion with an ionic radius of 0.74 nm. On the other hand, Cd^{2+} is also a transition metal ion with ionic radius of 0.97 nm and is commonly used and is also widespread. The Zr ion in the current work is chosen because it can serve as a double donor. In this study, the effect of the deposition voltage on the properties of CdZrS was investigated.

2. Results

From XRD analysis, the CdZrS is a polycrystalline cubic zinc blend and hexagonal structure, as shown in figure 1. The peak intensity changed with the deposition voltage, and the (111) peak shift to higher 2 theta angles was observed after the addition of Zr. Figure 2 confirmed that the maximum absorbance was recorded for the host. Furthermore, the absorbance decreased when Zr was added and increased again with the deposition voltage. The energy band gap for the host (CdS) at 1450 mV was recorded as 2.46 eV. When Zr was incorporated into the host, the energy band gap increased from 2.75 to 3.25 eV as deposition voltage increased from 1450 to 1600 mV. SEM analysis confirmed that the glass substrate fluorine- doped tin oxide (FTO) was covered by the film. Elemental composition analysis confirmed the presence of all the elements forming the desired compound (CdZrS). The atomic percentage of Zr increases as the deposition voltage increases.

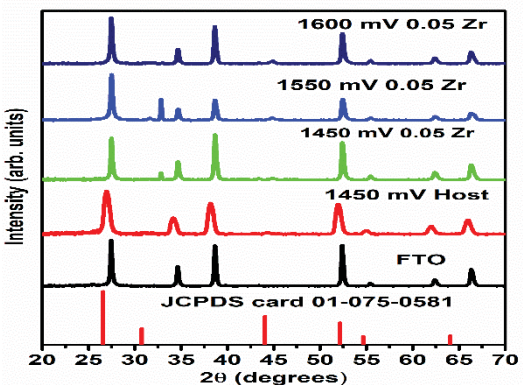

Fig. 1: XRD patterns of CdZrS thin films grown at a different voltages.

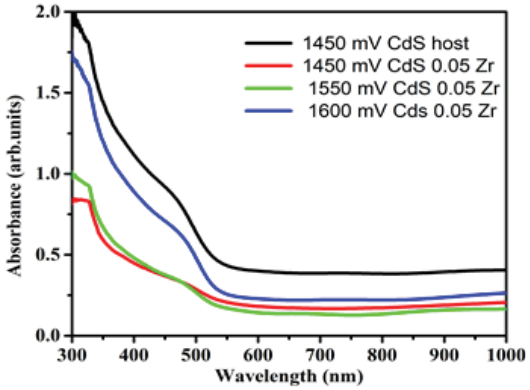

Fig. 2: Absorbance as a function of wavelength for CdZrS at different voltages.

References

[1] V. Narasimman, V. S. Nagarethinam, K. Usharani, and A. R. Balu, "Optik Optoelectronic, magnetic and antibacterial properties of Zr-doped CdS thin films," *Opt. - Int. J. Light Electron Opt.*, vol. 138, pp. 398–406, 2017.

[2] S. Z. Werta, O. K. Echendu, and F. B. Dejene, "Physica B : Physics of Condensed Matter Simplified two-electrode electrochemical growth and characterization of Cd 1 À x Zn x S thin films : Influence of electrolytic bath pH," *Phys. B Phys. Condens. Matter*, vol. 580, no. December 2019, p. 411939, 2020,

P43

Experimental determination of $InSb_xAs_{1-x}$ bandgap energy

Casey Mcleavy[1] and JAA Engelbrecht[2]

[1]Medical Physics Department, Division of Radiation Oncology, Groote Schuur Hospital, Cape Town, South Africa
[2]CHRTEM, Nelson Mandela University, Port Elizabeth, South Africa
Corresponding author e-mail address: casey.mcleavy@alumni.uct.ac.za

1. Introduction

$InSb_xAs_{1-x}$ is a ternary alloy semiconductor, which is an intermetallic compound that consists of three covalently bonded atoms. This semiconductor has emerged as an excellent material in the applications of mid-infrared optoelectronic devices, photodetectors, as well as light emitting diodes. The band gap energy of a semiconductor is an important characteristic as it is responsible for the material's electrical properties. This project aimed to experimentally determine the band gap energy for $InSb_xAs_{1-x}$ and determine whether the material is direct or indirect bandgap material. The reflectivity and transmission of three samples was measured using the Fourier Transform Infrared/Raman instrument at the Nelson Mandela University (NMU). The absorption coefficients of the samples were calculated from the transmittance measured and the thickness of each sample. Tauc plots were generated as a function of energy. The linear section of the curves was extrapolated to the x axis to obtain the experimental bandgap energy of each sample and after analysis of the Tauc plots, results showed that the samples were direct bandgap materials.

2. Results

The thicknesses of the samples were measured using the Focussed Ion Beam Scanning electron microscope and used to obtain the absorption coefficients for each sample. Fig. 1 shows the Tauc plot generated for one of the samples, namely E137.

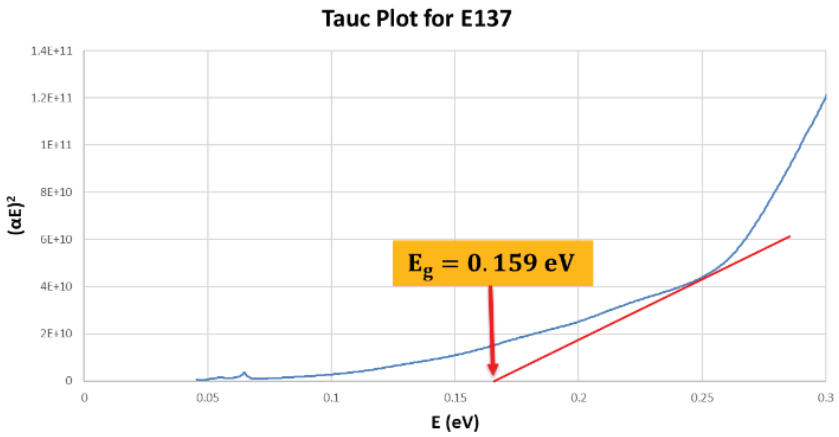

Fig. 1: Tauc Plot for sample E137.

The bandgap energies were determined from the Tauc plots for all three samples. The samples yielded very good results that agreed with theoretical values.

3. References

[1] Dhanaraj, Byrappa, Prasad, and Dudley. *Springer Handbook of Crystal Growth* (Springer-Verlag GmbH, 2010), Chap. 11.
[2] ASTM F-120 (1980), *American Society for Testing and Methods, USA.*

Highly ethanol responsive nanosensor layer based on mesoporous nano-structured cube-like Indium Oxide: Effects of Co, Ni and Cu dopants

Mosima Kgomo[1,2], **Hendrick Swart**[2], **Gugu Mhlongo**[1,2]

[1] *Centre for Nanostructures and Advanced Materials (CeNAM), DSI-CSIR Nanotechnology Innovation Centre, Council for Scientific and Industrial Research , Pretoria 0001, South Africa*
[2]*University of the Free State, Department of Physics, Bloemfontein ZA9300, South Africa, Address SwartHC@ufs.ac.za: GMhlongo@csir.co.za: mkgomo@csir.co.za*

1. Introduction

Energy saving and reliable gas sensor devices for the recognition of ethanol has been demonstrated to be of great necessity for the controlling of industrial discharges into the environment, identification of certain diseases in healthcare, food processing and modern agriculture [1,2]. In this study, pure, and Co, Ni, and Cu transition metal-doped In_2O_3 cube-like nanostructures were successfully synthesized via the hydrothermal approach, followed by annealing at 550 ℃. The effects of transition metal-doping on the ethanol gas sensing behavior of cube-like In_2O_3 nanostructures were investigated. Structural, surface area, and porosity analysis, as well as surface defect analysis, were conducted using transmission electron microscopy (TEM), BET, and photoluminescence (PL), respectively, to understand the improved ethanol gas sensing trend emerging from the incorporation of different dopant ions.

2. Results

The TEM images of the pure and Co-, Ni- and Cu-doped In_2O_3 nanostructures are shown in fig 1. Fig 2 demonstrates the response-recovery curves of the pure, 1 mol% Co, 1 mol% Ni, and 1 mol% Cu doped In_2O_3 nanosensor films from 10-50 ppm ethanol at 80 ℃. All the sensors demonstrated an increase in response after the introduction of the ethanol gas at different concentrations until reaching a maximum response value. A decline in response to the baseline was observed after the removal of the ethanol gas. The Cu-doped In_2O_3 based-sensor presented enhanced ethanol gas-sensing capabilities, with a response of 16 to 50 ppm of ethanol at 80 ℃. This enhanced ethanol gas sensing behavior can be attributed to the mesoporous nature of the cube-like Cu-doped In_2O_3 nanostructure comprising of a high surface area and a high content of surface defects, which allowed more channels for ethanol gas adsorption and desorption capacity.

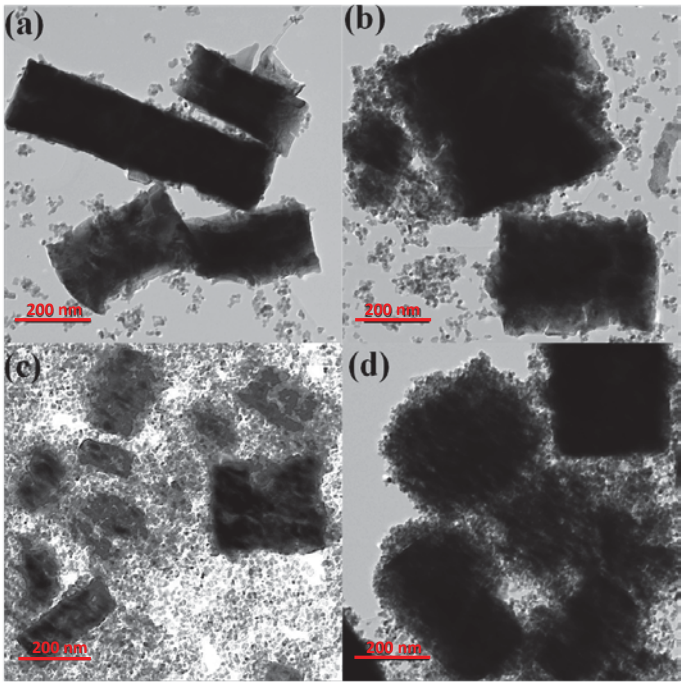

Fig. 1(a-d): TEM images of the pure, Co, Ni, and Cu doped In_2O_3 cube-like nanostructure.

3. References

[1] A. Loutfi, S. Coradeschi, G.K. Mani, P. Shankar, J.B.B. Rayappan, J. Food Eng. **144** (2015) 103-111.
[2] D. Smith, C. Turner, P. Španěl, J. Breath. Res. **1** (2007) 014004.

P45

Nanotechnology-based supercapacitor energy storage with microcontroller monitoring for application in battery-less electronics

Tebogo Motsei, Richard O. Ocaya

[1] *University of the Free State, Qwa-Qwa Campus, Phuthaditjhaba, South Africa*

Corresponding author e-mail address: dollymotsei@gmail.com

1. Introduction

The rapid growth of the population and the improving standard of living are some of the factors that are contributing to the increasing energy demand worldwide. Fossil fuels are the main source of energy for today's global population [1,2]. Supercapacitors are an emergent technology for clean energy storage besides batteries. They are less expensive, have smaller sizes, and are environmentally friendly. Supercapacitors are increasingly used for auxiliary energy storage in various fields, including the automotive industry, energy harvesting, portable electronic devices, and electrical grid stabilization systems. Their attributes such as power density, life cycle, temperature range, and charge/discharge period are beneficial. The study investigates supercapacitors based on local nanotechnology components. The goal is to create a robust electrical supply for portable devices and small-grid stabilization. The set-up involves the synthesis of nanocomponents and fabricating prototypes. Detailed analyses and characterizations use new and existing methods, i.e., scanning-electron microscopy, energy dispersive spectroscopy, x-ray diffraction, UV-Visible spectroscopy, photoluminescence, thermos-luminescence, thermos-gravimetric analysis, and others. The forms determine and optimize the performances of the devices for elemental composition, structure, and electrical/thermal properties. An electrical performance test platform will be built around a microcontroller to ensure that it obtains real-time data on the performance of the fabricated supercapacitors in typical usage conditions. The study also emphasizes sustainability and cost-effectiveness. A key research question focusses on the detrimental factors on energy density. It is also our interest to boost the long-term energy storage device. The goal is to surpass 90% efficiency with these supercapacitors by discussing the best new voltage and energy monitoring. The study also includes the analysis of electrodes, electrolytes, and their quiescent operating conditions for optimal electrochemical performance. The emphasis is on green, nanocomponent-based designs. The study also examines how to commercialize the devices under local and global challenges for reliable energy supply. Work on the project augment photovoltaic installations and low-power lighting systems.

2. Results

Supercapacitor is used to power an Arduino. It is charged through an external power supply. The supercapacitor works using a microcontroller. The microcontroller is connected directly to the battery so that the device can be powered when needed. The current from the microcontroller provides the energy needed to make this happen by turning off and on different sections of circuitry based on what you tell it to do. The first part is making sure that every section has enough power and is running at optimal speed because if one section does not work correctly or not fully tuned good results cannot be achieved.

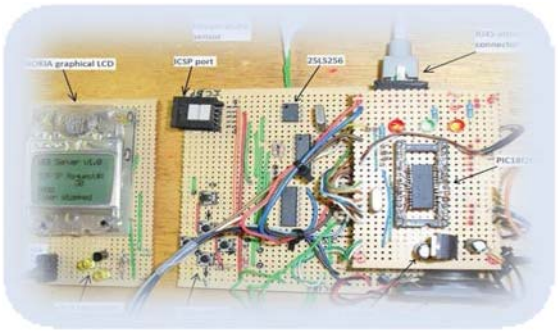

Fig. 1: Microcontroller test jig (PIC or Arduino).

3. References

[1] H. Tianfu, Q. Zehai, W. Dewu, and H. Zhibiao. Bamboo-based activated carbon@ MnO_2 nanocomposites for flexible high-performance supercapacitor electrode materials. Int. J. Electrochem. Sci, 10:6312–6323, 2015

[2] L. An-Ya, Lakshmanan S, T. Chuan-Ming, W. Fu-Kai, and H. Jhen-Ting. Effect of composition ratios on the performance of graphene/carbon nanotube/manganese oxide composites toward supercapacitor applications. ACS omega, 5(1):578–587, 2019.

The study of the synergistic effects of Yb^{3+} rare-earth ions on the luminescence and gas sensing properties of Co_3O_4-In_2O_3 heterostructure

Rethabile Makole, Hendrik C. Swart, David E. Motaung

Department of Physics, University of the Free State, Bloemfontein, Park West, 9301

Corresponding author e-mail address: Rethabilemakole09@gmail.com

1. Introduction

Enhanced luminescence in light emitting materials is greatly attributed to the presence of crystal defects and impurities introduced by doping. A number of studies have been conducted in which the incorporation of rare-earth ions in metal oxide-based hosts have shown to improve their optical, electrochemical and photocatalytic activity [1–3]. In a similar approach, this study was conducted to determine the possible effects of Yb^{3+} rare-earth ions on the optical and gas sensing properties of Co_3O_4-In_2O_3 (Co-In). A microwave-assisted hydrothermal method was adopted for the chemical synthesis of Yb^{3+}-doped Co-In nanostructure (Co-In:Yb). To effectively study the effects of Yb^{3+} rare-earth ion on the heterostructure, the dopant concentration was varied as 0.25, 0.5, 1 and 2 mol%. The synthesized nanostructures were tested towards benzene, toluene, ethylbenzene, xylene and acetone gases and correlated with the luminescence properties of Co-In:Yb nanostructure.

2. Results

Among the tested gases, Co-In:0.25Yb-based sensor displayed an unprecedented response of 50 and superior selectivity towards 100 ppm xylene in the presence of other interference gases at a lowered operating temperature of 100 ˚C (see Fig. 1(a) and (b)). The enhanced response in Co-In:Yb nanostructures as compared to Co-In was attributed to the crystal defects that manifested as oxygen vacancies in the Co-In crystal lattice as result of Yb^{3+} doping.

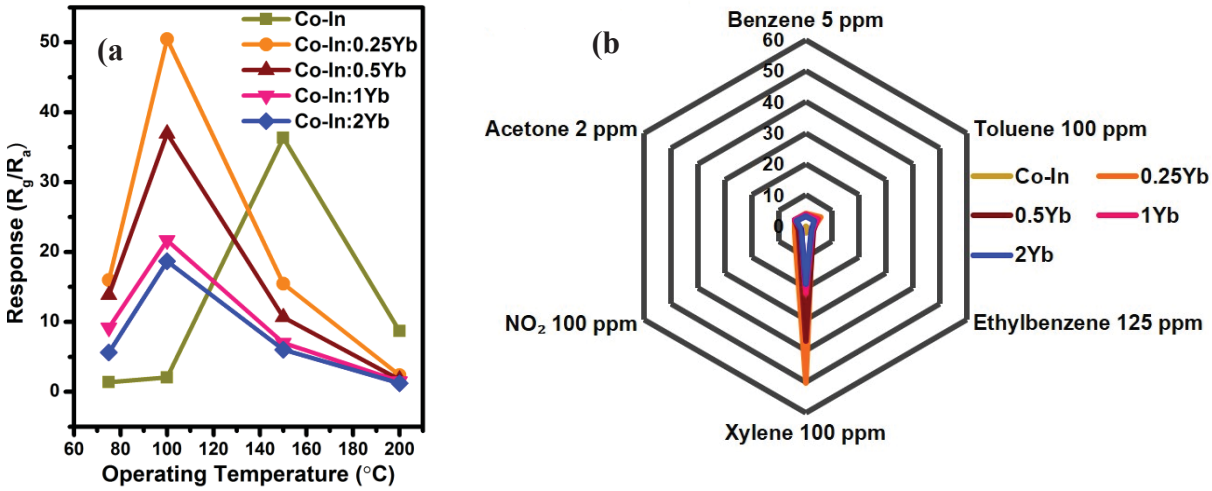

Fig. 1: (a) Gas response of Co-In and Co-In:Yb towards xylene as a function of temperature and (b) Radar selectivity plot of Co-In and Co-In:Yb.

3. References

[1] Geetha, V. T., Induja, S. & Puthilibai, G. *J. Supercond. Nov. Magn.* **33**, 1405–1411 (2020).
[2] Theerthagiri, J. *et al. Ionics (Kiel).* **26**, 2051–2061 (2020).
[3] Li, X. *et al. J. Alloys Compd.* **851**, (2021).

P47

Perpendicular orientation of microdomains of Poly (styrene-block-methylmethacrylate (PS-b-PMMA) thin films produced on Zinc oxide nanoparticle layer

Assane Talla[1], Zelalem Urgessa[1], Johannes Reinhardt Botha[1]

[1] *Department of Physics, P.O. Box 77000, Nelson Mandela University, Port Elizabeth 6031, South Africa.*
Corresponding author e-mail address: s217063969@mandela.ac.za

1. Introduction

The interest in the semiconductor industry in defining smaller feature sizes has drawn attention to block copolymers, particularly di-block copolymers. Block copolymer lithography based on microphase separation in thin films is a promising route for fabricating patterns with nanoscale features [1]. Among the possible configurations, the vertical cylindrical structure is most desirable because it can be used for templates or masks for feature development, mainly oriented wires or rods. A random copolymer is traditionally used to neutralize the substrate to induce perpendicular microdomain orientation [2]. However, removing the random copolymer is costly. It has been demonstrated that creating a rough surface on a substrate can promote perpendicular block copolymer orientation [3,4].

In this work, the perpendicular orientation of di-block copolymer components is produced when Poly (styrene-block-methylmethacrylate (PS-b-PMMA) is spun onto a disordered layer of zinc oxide (ZnO) nanoparticles followed by thermal annealing in a vacuum. It is shown that the ZnO nanoparticles create a corrugated surface on silicon, which induces perpendicular cylinders of PMMA within the PS matrix. This method is useful as the ZnO nanoparticles could also serve directly as a nucleation layer for the subsequent growth of ZnO nanorods or nanowires.

2. Results

Fig.1 shows the height image of a 1 μm by 1 μm ZnO NP layer on Si (100). Fig. 1a) presents the top view of the sample, and the 3D view is presented in (Fig. 1 b). The particles are well distributed on the surface but aggregated in some regions. The root mean square (Rq) variation across the 1 mm2 area is Rq = 1.4 nm, approximately seven times the value measured for the native silicon oxide (0.2 nm). The 3D image clearly illustrates variations in height across the micron surface, showing the degree of roughness higher than that of the silicon oxide. Fig. 2 shows a 1 μm^2 region of a PS-b-PMMA film prepared on a ZnO seed layer, in which mainly perpendicular cylinders were formed after annealing to thermodynamic equilibrium. In both the height and phase images, perpendicular PMMA domains can be observed. In a), the bright regions represent the PMMA domains. The PMMA is located within the PS matrix. The PMMA domains are hexagonally arranged, as illustrated by the green boxes in b), where the dark regions represent the PMMA domains.

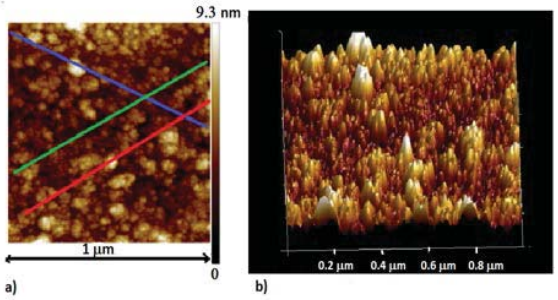

Fig. 1: Topography of 1μm^2 area of ZnO nanoparticles seed layer showing: a) the top view and b) the 3D view.

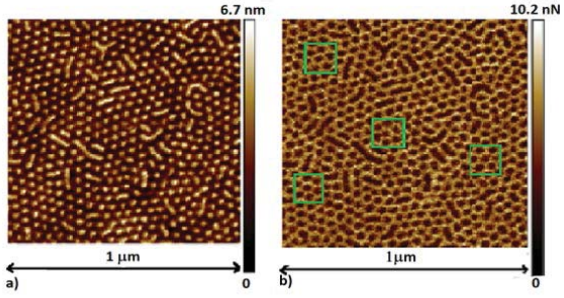

Fig. 2. SPM phase images of a PS-b-PMMA film on a ZnO nanoparticle layer showing: a) height and b) adhesion. The green boxes highlight the hexagonally arranged cylindrical PMMA domains.

3. References

[1] X. Gu, I. Gunkel and T. Russell. Transctions of Royal Society A, **371** (2013).
[2] S. Ji, C. Liu, J. G. Son, K. Gotrik, G. S. W. Craig, P. Gopalan, F. J. Himpsel, K. Char and P. F. Nealey. Macromolecule, **41** (2008) 9098.
[3] T. Kim, S. Wooh, S. G. Jeong and K. Char. Macromolecules, **46** (2013) 8144.
[4]Y. Zhu, K. Aissou, D. Andelman and X. Man. *Macromolecules*, **52** (2019) 1241.

Effect of radiation damage on the migration behaviour of Europium implanted into single crystalline 6H-SiC at RT and 350 ºC

T.M. Mohlala[1], J.B. Malherbe[1], M. Mlambo[2], T.T. Hlatshwayo[1]

[1]Department of Physics, University of Pretoria, Lynnwood Road, Pretoria 0002, South Africa
[2]Mintek, 200 Malibongwe Dr, Praegville, Randburg, 2194, South Africa
Corresponding author e-mail address: mohlalatshegofatso@yahoo.com

1. Introduction

The effect of radiation damage on the migration behaviour of europium (Eu) implanted into 6H-SiC was investigated. Eu ions of 270 keV were implanted separately into 6H-SiC wafers to a fluence of 1 x 10^{16} cm^{-2}at room temperature (RT) and 350 ºC. The as-implanted samples were then annealed at temperatures ranging from 1000 to 1400 ºC in steps of 100 ºC for 5 hours under vacuum. The migration behaviour of implanted Eu was monitored using Rutherford backscattering spectrometry (RBS), X-ray photoelectron spectroscopy was used to identify elements on the surface after annealing while Raman spectroscopy and scanning electron microscopy (SEM) were used to monitor the structural and surface morphological evolutions respectively. RT implantation amorphized SiC while implantation at 350 ºC retained crystallinity with defects. Annealing the as-implanted samples at 1000 ºC already resulted to some recrystallization. Full recrystallization was not achieved even after annealing at the highest annealing temperature of 1400 ºC. More Eu was lost through the surface in samples implanted at room temperature. A broadening of Eu depth profile was observed in the room temperature implanted samples annealed at 1000 up to 1200 ºC indicating diffusion taking place at these temperatures. Diffusion coefficients of 0.017, 0.024 and 0.31 nm^2/s were extracted at 1000 ˚C, 1100 ˚C and 1200 ˚C respectively. XPS results indicated that the Eu surface peak formed after annealing at 1000 ºC was associated with a europium oxalate compound. No diffusion of Eu was observed in a 350 ºC implanted samples. Hence radiation damage played a role in the migration of Eu implanted into 6H-SiC.

2. Results

Eu implantation into SiC was simulated using SRIM2013 [1]. The detailed full cascade calculation was used in the simulation with the displacement energies of 35 eV and 20 eV for silicon and carbon respectively [2].

Fig.1 shows the simulated results together with the experimental results of the 270 keV Eu ions implanted into 6H-SiC at RT and 350 ºC. The projected range of the experimental depth profiles of about 80 nm is in reasonable agreement with the simulated one of about 74 nm. About 19 dpa was retained on the surface with a maximum of 43 dpa retained at 50 nm below the surface. Both experimental depth profiles are broader than the simulated depth profile. The RT and 350 ºC implanted profiles compared very well. If 0.2 dpa is needed to amorphize SiC, about 140 nm of the RT implanted SiC will be amorphized [3]. The difference in height of the measured depth profiles might be due to slight difference in the fluence. The calculated fluences were 1.252 × 10^{16} and 1.140 × 10^{16} cm^{-2} for RT- and 350 ºC implanted samples respectively.

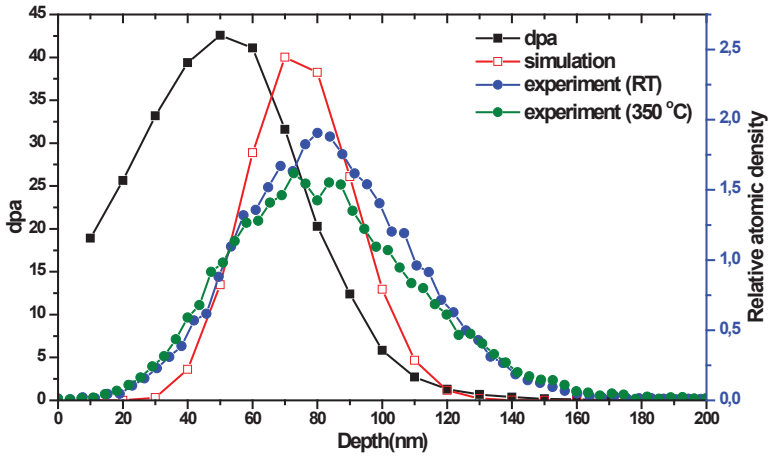

Fig.1: The Eu depth profiles from RBS of Eu implanted into SiC at RT and 350 ºC together with SRIM simulated Eu depth profile and displacement per atom (dpa).

3. References

[1] Ziegler, J. (2013). *SRIM Legal Disclaimer*. [online] Srim.org. Available at: http://www.srim.org/SRIM/SRIMLEGL.htm [Accessed 9 Mar. 2019].
[2] Devanathan, R., Weber, W. and Gao, F. (2001). Atomic scale simulation of defect production in irradiated 3C-SiC. *Journal of Applied Physics*, 90(5), pp.2303-2309.
[3] Snead, L., Zinkle, S., Hay, J. and Osborne, M., 1998. Amorphization of SiC under ion and neutron irradiation. *Nuclear Instruments and Methods in Physics Research Section B: Beam Interactions with Materials and Atoms*, 141(1-4), pp.123-132.

P49

Influence of Pt-loading on the energy band gap and VOCs Sensing of metal titanate perovskite

Zamaswazi Tshabalala, Hendrik Swart, David Motaung

Department of Physics, University of the Free State, P.O. Box 339, Bloemfontein ZA9300, South Africa

Corresponding author e-mail address: Tshabalala.zp@ufs.ac.za

1. Introduction

Air pollution poses a major threat in human health with more that 80% of the world's population breaths in air that contains toxic levels of pollutants, such as bioaerosols, volatile organic gases (VOCs) and nitrogen oxides (NOx) [1]. These contaminants bring forth ailments that affect respiratory system and in case of prolonged exposure may result to death. Various attempts have been made for detection of these pollutants, among which the use of nanostructured semiconductor metals oxides have been leading due to their unique physical and chemical properties giving rise to their catalytic behaviour. Therefore, herein, we investigate the gas sensing properties of nanostructures metal titanate ($ATiO_3$ where A= Ni, Zn) perovskite semiconductors achieved through a facile hydrothermal method following 1:1 mol ratio of precursors. Furthermore, the influence of surface sensitization using noble metals and phosphors on the surface defects, band structure and gas detection characteristics of the synthesized $ATiO_3$ nanostructures is also investigated.

2. Results

Powder X-Ray diffraction patterns confirmed the formation of highly crystalline metal titanate nanostructures in conjunction with JCPDS card number: 89-3743 and No. 39-0190 for $NiTiO_3$ and $ZnTiO_3$ respectively. The lattice parameters were obtained from the Reitveld refinement and deviations due to different ionic radii were observed. Diffuse reflectance UV-Visible spectra were used to estimate the energy gap of the nanostructures as shown in Figure 1. The $ZnTiO_3$ and Pt-$ZnTiO_3$ samples maintained a bright white colour and displayed high reflectance with a steep absorption edge lower than 400 nm. Whereas, three distinct adsorption bands were observed between 250 and 1200 nm for both $NiTiO_3$ and Pt- $NiTiO_3$ nanostructures and were attributed to the three spin allowed d–d transitions from the Ni^{2+} ions in octahedral environment. Additionally, the intense reflection peak at ~ 565 nm was associated with the green-yellowish colour of the samples. Using the Kubelka-Munk formula for indirect transition (n=1/2), the estimated energy band gaps were 3.30 eV, 3.34 eV for $ZnTiO_3$ and Pt-$ZnTiO_3$, while the band gaps at 2.91 eV, 3.15 eV were associated to $NiTiO_3$ and Pt- $NiTiO_3$, respectively. The ionization energy and the valence band maxima were then estimated by photoelectron yield spectroscopy (PYS) from which the existence of acceptor level within the forbidden band were confirmed (See Figure 2).The Photoluminescence emission spectra confirmed the presence of defects.

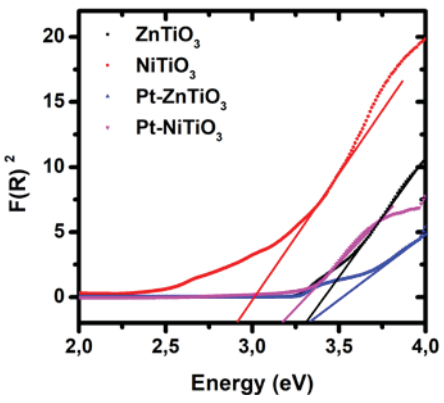

Fig. 1: Kubelka-Munk Function vs photon energy plot

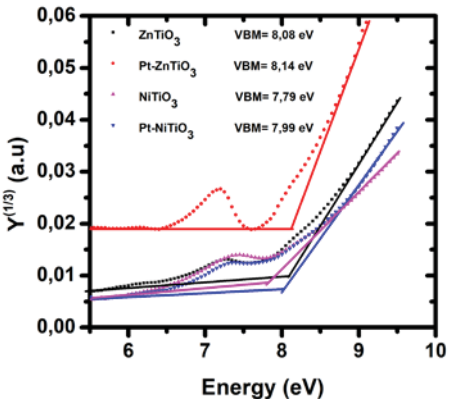

Fig. 2: PYS spectra with the estimated Ionization energy

3. References

[1] Z. Gao and X. Qu. Nanoscale Research Letters1 **15** (2020) 64-72.

Influence of coating techniques on the optical and structural properties of nanostructured hematite thin films

Adiel Holtzhausen[1], **Mmantsae Diale**[1]

[1] *University of Pretoria, Department of Physics, Private Bag X20, Hatfield, 0082, South Africa*
Corresponding author e-mail address: Mmantsae.diale@up.ac.za

1. Introduction

Hematite (α-Fe_2O_3) is an abundant n-type semiconductor material used for various applications such as pigments, gas sensors, photocatalysts and as photoanodes in photoelectrochemical water splitting [1]. Hematite is promising as a photoanode due to its favourable bandgap of 1.9 – 2.2 eV, thermal stability in aqueous mediums, high theoretical solar to hydrogen efficiencies of up to 15 % and low cost [2].

In this study, the influence of coating techniques on nanostructured hematite were studied. Hematite nanostructures were synthesized on fluorine-doped tin oxide glass substrates using chemical spray pyrolysis and colloidal dip coating. Iron(III)nitrate nonahydrate was used to prepare a precursor solution after which four thin film layers were synthesized using colloidal-based dip coating and spray pyrolysis techniques. Thereafter, the samples were annealed at 500 °C for one hour allowing for calcination from γ-Fe_2O_3 to α-Fe_2O_3. The optical and morphological properties of the α-Fe_2O_3 were studied using X-ray diffraction (XRD), Raman spectroscopy, field emission scanning microscopy (FE-SEM) and ultraviolet-visible spectroscopy (UV-vis).

2. Results

From XRD six peaks relating to hematite were found, namely the (012), (104), (110), (24), (122) and (124) peaks. The (104) and (110) peaks were indicative of the corundum structure and high purity of the hematite thin films. This was further confirmed by Raman spectroscopy. Seven vibrational modes of hematite were found in the first Brillouin zone namely two A_{1g} and five E_g modes. Furthermore, both the LO and 2LO modes were present confirming the ferromagnetic properties of hematite. FE-SEM revealed nanospheres for the dip coated film, whereas agglomerated nanorods and nanospheres were found for the spray pyrolysis film. Average grain intercept (AGI) was used to determine the grain sizing ranging from 45.82 nm for the spray-pyrolysis film to 50.00 nm for the dip coated film. Optical studies performed by UV-vis indicated good absorbance onset at 596.75 and 608.57 nm.

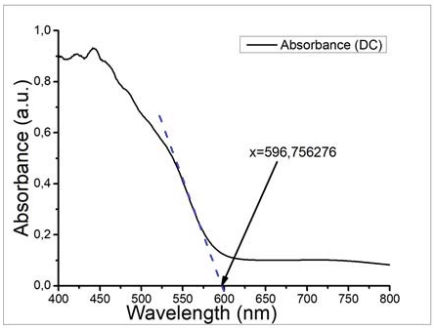

Fig. 1: Absorbance spectra of films prepared by dip coating. The inset shows the absorbance of the α-Fe_2O_3 sample.

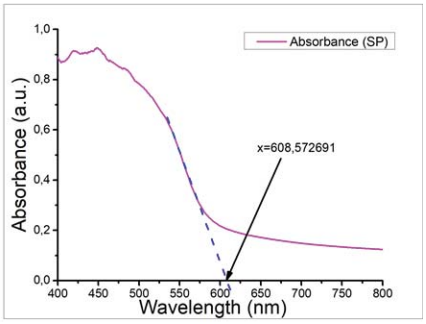

Fig. 2: Absorbance spectra of films prepared by spray pyrolysis. The inset shows the absorbance of the α-Fe2O3 sample.

From this work it was found that the optical, structural and morphological and structural properties of hematite could be influenced by the coating technique, which correlates to the photoelectrochemical performance of hematite anodes.

3. References

[1] P. I. Kyesmen., N. Nombona, and M. Diale. *Frontiers in Energy Research*. **9** (2021) 683293.
[2] J. S. Nyarige, T. P. J. Krüger, and M. Diale. *Materials Today Communications*. **25** (2020) 101459.

P51

R^{3+} co-doping in persistent luminescence materials: pros and cons

Mika Lastusaari[1], Hermi F. Brito[2], Lucas C.V. Rodrigues[2], Dariusz Hreniak[3], Hendrik C. Swart[4], Jorma Hölsä[1,2,3,4]

[1]University of Turku, Department of Chemistry, Turku, Finland
[2]Universidade de São Paulo, Instituto de Química, Departamento de Química Fundamental, São Paulo, Brazil
[3]Institute of Low Temperature and Structure Research, PAN, Wrocław, Poland
[4]University of the Free State, Department of Physics, Bloemfontein, South Africa

Corresponding author e-mail address: jholsa@utu.fi

1. Introduction

A number of persistent luminescence materials has been studied since the boom started in mid 1995 after the (re)discovery of Eu^{2+} doped and R^{3+} co-doped $SrAl_2O_4$ [1]. The persistent times extend from very short (blink of an eye) to several days. The short time emission does not really warrant the name "persistent luminescence" but "afterglow". Many of the materials are composed by the host - the most being alkaline earth aluminates or silicates with complex structures – despite the simple stoichiometries as $SrAl_2O_4$. The emitting centers are well-known from ordinary luminescent materials the strongest being Ce^{3+}, Pr^{3+}, Sm^{2+}, Eu^{2+}, Eu^{3+}, Tb^{3+} - excluding other than the rare earths. Safe and sound choices, though not really exciting. The common feature of the dopants is that they can be found in several (eg +2, +3, +4) oxidation states suggesting that, at least at some stage of the process, the oxidation states may change though the lifetimes of these transient species can be very short –below ns.

The exciting components of the persistent luminescence materials are the co-dopants the role of which is not very well defined or understood: some are necessary to balance the total neutrality of the compound, some may be sensitizers absorbing radiation the dopant (or host) cannot do, some seem to have no role at all – and those are the subject of this contribution. Finally, the dopants can act as co-dopants, as well.

2. Results

As a simple (sic!) example, in Pr^{3+} doped $CaTiO_3$ (perovskite), the host ingeniously adapts to the excess positive charge brought by the dopant by reducing a corresponding amount of Ti^{IV} to Ti^{3+} [2] (charge neutrality condition). Though the global charge balance is now satisfied, *two point defects now exist*, Pr^{3+} in the Ca^{2+} site with excess positive charge – *not* +3 since the inertia of the host structure mitigates the change from +2 to +3 almost completely – closer to 2.3 perhaps. But enough to *trap electrons*. The bond valence model (BVM) calculations give an educated guess for the excess charge (here +0.3). The $[Ti^{IV}O_6]$ octahedral unit has now excess negative charge and acts as a *hole trap*. Due to electrostatic attraction these two species are spatially correlated (a local system).

One has thus created a persistent luminescence material where the energy transfer between the two defects is enhanced – ideal for transferring the trapped and stored energy to yield persistent luminescence. And all this without much structural distortions since Ti^{3+} and Ti^{IV} are of the same size due to the Ligand Field Stabilization Energy (LFSE). To add insult to injury, instead of an optically inactive Ti^{IV} with $3d^0$ electron configuration one has an active Ti^{3+} $3d^1$ one which is very much capable to transfer the $t_{2g} \leftrightarrow e_g$ energy to other emittors than Pr^{3+}. If Ti^{3+} does not transfer the energy to other species, blue-green emission centered @ ca 500 nm and excitation @ 385 nm may be observed–though the latter is mostly masked by the Ti^{IV} absorption. Confusion would not be greater without the unfortunate *misbelief* [3] that Zr^{IV} and Hf^{IV} behave as Ti^{IV}; alas, Zr^{3+} (or Hf^{3+}) *do not exist* – but the Ti^{IV} impurities in ZrO_2 and HfO_2 do… Despite initial trouble, ZrO_2 doped with Ti^{IV}/Ti^{3+} yields efficient persistent luminescence [4]. Though even the existence of Ti^{3+} is fiercely opposed... Unfortunately, the of Pr^{3+} is weakish line emission with only limited practical importance.

Persistent luminescence mechanism and compositional requirements for Pr^{3+} doped $CaTiO_3$ are the most complicated examples of the R^{3+} co-doping since Pr^{3+} is also the dopant as well as co-dopant. Much less complicated materials on the list (in no order) below with the charge compensation scheme used or anticipated because of the compositional or structural analogies.

Abbreviated list of persistent luminescence materials: Y_2O_3 or Y_2O_2S:Eu^{3+},Mg^{2+},Ti^{IV}: $CaWO_4$:Eu^{3+},M^+; Y_2SiO_5:R^{3+} none; Sr_3SiO_5:Eu^{2+},R^{3+} interstitial O^{2-}: $MMgAl_2O_6$:Eu^{2+},R^{3+} interstitial O^{2-}; $M_3MgAl_2O_8$:Eu^{2+},R^{3+} interstitial O^{2-}: Lu_2O_3:Eu^{3+},M^{2+},Hf^{IV}; ZrO_2:Yb^{3+},Er^{3+} O^{2-}: vacancy; MAl_2O_4:R^{3+}(,R^{3+}) interstitial O^{2-}; $CdSiO_3$:R^{3+} & $CaSiO_3$:Dy^{3+} interstitial O^{2-}; $M_2ZnSi_2O_7$:Eu^{2+},Dy^{3+} interstitial O^{2-}; $CaZrO_3$:Pr^{3+},Li^+; MgO:Li^+,Ce^{3+}; *etc; etc*.

The idea of charge compensation is opposed by some since they assume that the sub/superscripts in compound formulae and reaction equations are just the invention of chemists to confuse serious scientists (instead of high-T ceramic superconducting materials as YBCO). But this is probably just a joke? Or is it?

3. References

[1] PF Smet, K Van den Eeckhout, OQ De Clercq, D Poelman, Persistent Phosphors, *Handbook Phys. Chem. Rare Earths* **48** (2015) 1-108. [2] NN Greenwood, A Earnshaw, *Chemistry of the Elements* (2nd ed, Butterworth-Heinemann, 1997) Chap. 21.
[3] C Gionco, MC Paganini, E Giamello, R Burgess, C Di Valentin, G Pacchioni, *Chem. Mater.* **25** (2013) 2243.
[4] JM Carvalho, LCV Rodrigues, J Hölsä, M Lastusaari, LAO Nunes, MCFC Felinto, OL Malta, HF Brito, *Opt. Mater. Expr.* **2** (2012) 331.

Multifunctional Nano-TbO_2: Oxygen Retention, Nanopigment, Paramagnet

Chris Joubert[1], Monica van der Walt[1], Edward Lee[2], Mart-Mari Duvenhage[2], Thomas Jüstel[3], Hendrik C. Swart[2], André M. Strydom[4], Dariusz Hreniak[5], Jorma Hölsä[2,5]

[1]University of the Free State, Department of Chemistry, Bloemfontein, South Africa
[2]University of the Free State, Department of Physics, Bloemfontein, South Africa
[3]University of Johannesburg, Physics Department, Johannesburg, South Africa
[4]Munster University of Applied Sciences, Department of Chemical Engineering, Steinfurt, Germany
[5]Institute of Low Temperature and Structure Research, PAN, Wrocław, Poland
Corresponding author e-mail address: jholsa@utu.fi

Dedicated to Prof Dr Paul CARO (1934 – 2016), Membre Correspondant de l'Académie des Sciences et Membre de l'Académie des Technologies, France. One of the pioneers to research the structure and properties of tetra- and trivalent terbium.

1. Introduction

Despite the common misbelief, rare earths (lanthanides) form materials with several oxidation states, eg +2 and +4 in addition to the common +3 [1]. That said, this applies only to a few rare earths (Ce^{IV}, Pr^{IV}, Sm^{II}, Eu^{II}, Tb^{IV} and Yb^{II}), or combination of states (3,2 or 3,4) and even the rare earth environment - eg Eu^{2+} is not observed in solutions. Other oxidation states, even in short lived transient species, should be dealt with suspicion if not rejected at once. Reason to states 2 or 4 is the high stability of the $4f^0$, $4f^7$ and $4f^{14}$ electron configurations. Simple, isn't it?

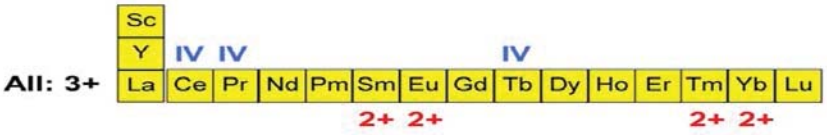

2. Results

Several interesting properties of the nanocrystalline tetravalent terbium dioxide (TbO_2) were studied for potential applications. Preparation of TbO_2 by heating the mixed valence ¨Tb_4O_7¨ in air/oxygen/ozone at high temperatures is futile but treating benignantly an aqueous ¨Tb_4O_7¨ slurry below 100 °C with acetic acid dissolves Tb^{3+} (increase in reaction time dissolves Tb^{IV}, alas). This reaction was known in 1960s and 1970s [eg 2] but later forgotten almost for good. The collapsed structure of the nanostructural ¨Tb_4O_7¨ produced even smaller particle sized TbO_2 as verified by high-res TEM. TbO_2 is stable at ambient conditions (temperature, pressure, humidity, light) even for year(s). In contrast, TbO_2 decomposes above ca 200 °C (Fig 1) hampering not only the oxygen retention but also the regeneration of the material by heating in air at elevated temperatures. Intermediate phases before the final Tb_2O3 (weight loss: ca 45 % at 975 °C) were observed but they are non-stoichiometric and useless for practical applications. Mitigation of the RO_2 structure from CeO_2 to PrO_2 to TbO_2 was probed by bond valence model [3]. The temperature evolution of paramagnetic susceptibility of TbO_2 showed no animalities from RT down to below 10 K. TbO_2 can thus be used as a magnetic probe in biological systems since the strong paramagnetism of TbO_2 did not suffer from the very small crystal size.

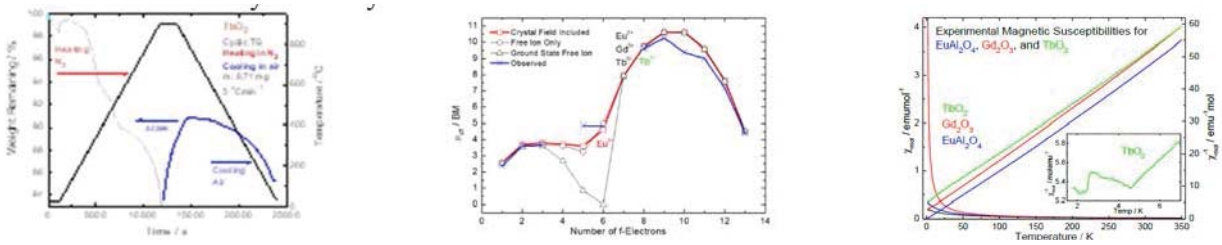

Fig. 1: Thermal Reduction/Oxidation behaviour of TbO_2 (left), paramagnetic moments of R^{3+} in ROBr at RT [3] (middle) and temperature evolution of paramagnetic susceptibilities for different Rn+ materials with the same $4f^7$ electron configuration of (right).

The bright red stable colour of TbO_2 (Fig. 2) enables the use as an optical probe in eg biological systems. A theoretical detail: the position of the $7F_6$ ($3H_4$) ground level of Tb^{3+} (Pr^{3+}) in the hosts' band gap shows that these two R^{3+} ions can produce persistent luminescence making the design of new materials feasible.

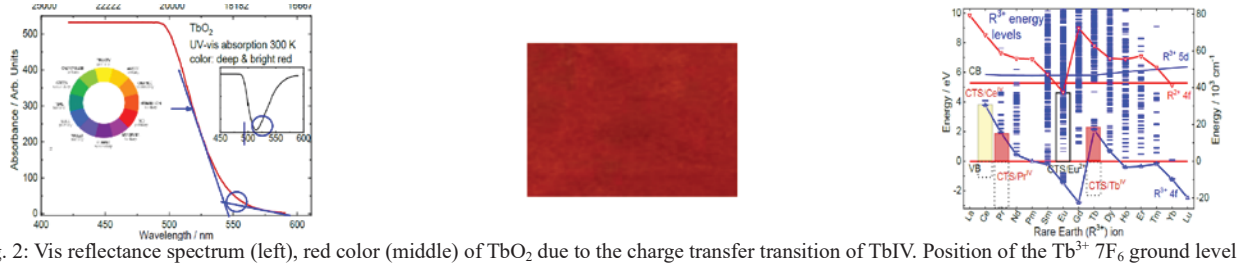

Fig. 2: Vis reflectance spectrum (left), red color (middle) of TbO_2 due to the charge transfer transition of TbIV. Position of the Tb^{3+} $7F_6$ ground level in the hosts' energy gap (right).

3. References

[1] NN Greenwood, A Earnshaw, Chemistry of the Elements (2 nd ed, Butterworth-Heinemann, 1997), Chaps. 20 & 30.
[2] G Brauer, B Pfeiffer, J. Less-Common Met. 5 (1963) 171.
[3] ID Brown, The Chemical Bond in Inorganic Chemistry: the Bond Valence Model, (2nd ed, Oxford University Press, 2016).
[4] J Hölsä, M Lastusaari, J Niittykoski, R Sáez Puche, Phys. Chem. Chem. Phys. 4 (2002) 3091.

P53

Characteristics of GaAs Thin Films Grown by MOVPE Using Triethygallium (TEGa) and Tertiarybutylarsine (tBAs)

Andi Isni Pujirana, N Tile, JR Botha, A Venter

Department of Physics, Nelson Mandela University, P.O. Box 77000, Gqeberha 6031, South Africa
Corresponding author's e-mail address: s226037592@mandela.ac.za

1. Introduction

Gallium arsenide (GaAs) is a well-studied semiconductor because of its unique electrical and optical properties and wide range of electronic applications [1]. It has a direct energy band gap of about 1.42 eV at room temperature. This property gives GaAs the highest energy conversion efficiency compared to other materials when making solar cell devices [1]. GaAs also has a high radiation resistance, resulting in solar cells made from this material being commonly used in space applications. Additionally, GaAs is suitably compatible with other semiconducting materials to produce a wide range of technologically relevant heterostructures, including high electron mobility transistors, and near-infrared detectors and emitters.

Successful homoepitaxial growth of high purity, unintentionally doped GaAs layers by MOVPE (metalorganic vapour phase epitaxy) has traditionally involved arsine (AsH_3) or tertiarybutyl arsenic (tBAs) as arsenic (As) precursor and trimethylgallium (TMGa) as gallium (Ga) precursor. Unfortunately, the high toxicity of AsH_3, caused by As-H bonds, its inefficient reaction with TMGa, and the incorporation of carbon impurities from the TMGa into the layers are inherent system weaknesses. However, triethylgallium (TEGa) can offer better thickness control when growing structures containing ultra-thin layers, such as superlattices and quantum dots, due to its lower vapour pressure than TMGa. TEGa was also reported to yield lower carbon contamination in MOVPE-GaAs [2] than TMGa. In this study, we report on combining tBAs and TEGa as precursors for homoepitaxial GaAs. This combination is relatively new and has previously been used to fabricate GaAs-based structures. However, there is no published systematic study of the MOVPE growth parameters for this combination of metalorganic resources.

2. Results

Figure 1 shows the temperature-dependent photoluminescence (PL) spectra of bulk homoepitaxial GaAs, grown at a V/III ratio, temperature and rate of 7.5, 650°C and 0.96 µm/h, respectively. Two sets of emission peaks are observed in the spectra. The peak at 1.514 eV is due to free excitons (FX), and the one at 1.515 eV is due to excitons bound to impurity atoms (BX). The second range of emission energy peaks at 1.489 eV represent a shallow donor-acceptor-related transition. Hall Effect measurements indicated that the grown layer was *n*-type, with a mobility (300 K) and corresponding carrier concentration of 4410 cm^2/Vs and ~4.2 x 10^{15} cm^{-3}, respectively. The effects of a variation in growth temperature and V/III ratio on the layer's morphology, and electrical and optical properties will be discussed in detail.

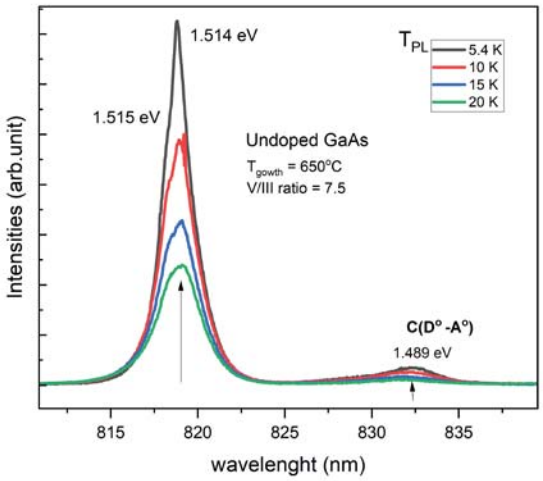

Figure 1. Temperature-dependent PL spectra of a 3.2 µm thick undoped GaAs epilayer.

3. References

[1] Meyer, M., & Metzger, R.A., "The Commercial Satelite Industry Convert to Compound Semiconductor Solar Cells", Compound Semiconductor, Nov/Dec. (1996).
[2] Ching-Che Lin, Szu-Hung Chen, Keng-Te Lin, Sih-Wei Chang, Wei-Yu Chen, Bo-Yi Chen, Ming-Chen Liu, Hsuen-Li Chen "Gallium Arsenide-Based Active Antennas for Optical Communication Photodetection with Robustness to Voltage and Temperature" May 2021.
[3] Oliver Maßmeyer* Johannes Haust Thilo Hepp Robin Günkel Johannes Glowatzki Carsten von Hänisch Wolfgang Stolz and Kerstin Volz "Revealing the Significance of Catalytic and Alkyl Exchange Reactions during GaAs and GaP Growth by Metal Organic Vapor Phase Epitaxy *ACS Omega* (2021)

Influence of Yb^{3+}-Nd^{3+} concentration on the upconversion luminescence and the defect structure of $NaGdF_4$ nanocrystals for possible application in perovskite solar cells

Pebetsi Thokwane, Luyanda Noto and Pontsho Mbule

Department of Physics, CSET, University of South Africa, Johannesburg, 1710, South Africa
Corresponding author's email: mbuleps1@unisa.ac.za/pebetsithokwane587@gmail.com

1. Introduction

Rare-earth doped up-conversion nanocrystals have become one of the most significant classes of nanoscale materials due to their potential applications in biological imaging, photonics, frequency up-converters, undersea optical communications, solar cells and temperature sensors [1]. These materials may combine two or more low-energy photons to create a detectable higher-energy photon, making them appropriate for applications in integrated optical devices, including perovskite solar cells (PSCs) [2]. In this study, we examine the properties of $NaGdF_4$ nanocrystals doped with the Yb^{3+}-Nd^{3+} pair at different relative concentrations to provide the greatest upconversion luminescence emission output for possible application in perovskite solar cells as spectral converters.

2. Results

Figure 1 illustrates the upconversion photoluminescence (UPL) emission spectra of the $NaGdF_4$ nanocrystals in their as-prepared state, doped with varying concentrations of Yb^{3+} (10–30 mol%) and Nd^{3+} (1–3 mol%) under the excitation wavelength of 980 nm. UPL bands centred at ~485, 542, 620, 660, 709 and 830 nm were observed, which correspond to the transitions of Nd^{3+} ions: $^4D_{3/2}\rightarrow{}^4I_{15/2}$, $^4G_{7/2}\rightarrow{}^4I_{9/2}$, $^4G_{7/2}\rightarrow{}^4I_{11/2}$, $^4G_{7/2}\rightarrow{}^4I_{15/2}$, $^2P_{3/2}\rightarrow{}^4F_{5/2}$ and $^4F_{3/2}\rightarrow{}^4I_{9/2}$, respectively. The UPL intensity of the nanocrystals decreased when Yb^{3+} was increased from 10% to 20% but increased at the concentration of 30%. This demonstrates the concentration quenching effect and may be due to the fact that surpassing the concentration threshold makes the sequential transfer of energy process less effective once the concentration threshold is exceeded [3]. The thermoluminescence glow curves were recorded (Figure 2) after exposing the sample to gamma rays with doses ranging from 0.74 to 47.46 Gy. Different measurements were done to determine the electron kinetics (Fig. 2), depth of the electron trapping centers and the thermoluminescence fading mechanism.

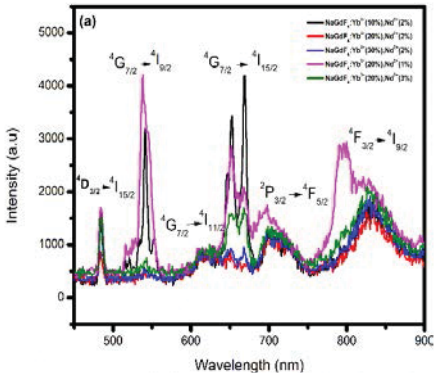

Fig 1. The Upconversion emission spectra of $NaGdF_4$:Yb^{3+},Nd^{3+}

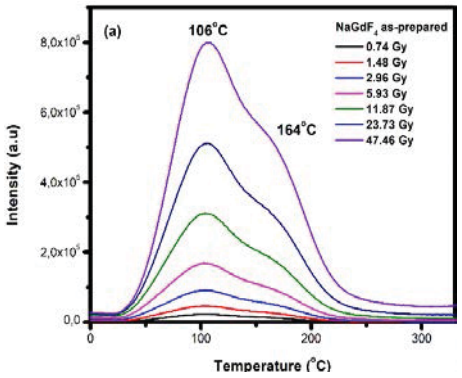

Fig 2. TL glow curves of $NaGdF_4$

3. References

[1] D. Hudry, A.M.M. Abeykoon, E. Dooryhee, D. Nykypanchuk, and J.H. Dickerson. *Chemistry of Materials*. **28**(2026) 8752.
[2] J. Chen and J.X Zhao. *Sensors*, ***12***(2012) 2414.
[3] M. Alkahtani, A.A. Almuqhim, H. Qasem, N. Alsofyani, A. Alfahd, S.M. Alenzi, A. Aljuwayr, Y.A. Alzahrani, A. Al-Badri, M.H. Alotaibi and A. Bagabas. *Nanomaterials.* **11**(2021) 2909.

P55

New opportunities in plastics recycling through the use of luminescent upconversion phosphors

Eduard Madirov[1], **Dmitry Busko**[1], **Ian A. Howard, Bryce S. Richards**[1,2], **Andrey Turshatov**[1]

[1] *Institute of Microstructure Technology, Karlsruhe Institute of Technology, Hermann-von-Helmholtz-Platz 1, 76344 Eggenstein-Leopoldshafen, Germany*
[2]*Light Technology Institute, Karlsruhe Institute of Technology, Engesserstrasse 13, 76131 Karlsruhe, Germany*
Corresponding author e-mail address: eduard.madirov@kit.edu

1. Introduction

In 2020, packaging will account for more than 60 percent of post-consumer plastic waste in Europe and more than 29 million tons of post-consumer plastic waste will be collected in the EU. Of this waste stream, only 35 percent is recycled, while 42 percent is reprocessed to produce energy and 33 percent ends up in landfills. At the same time, a major obstacle to a circular economy is that only 6 percent of Europe's total plastic demand, about 50 million tons, is met by recycled polymers because there are several dozen different packaging plastics, each with different compositions and properties. They all contain different chemical additives and cannot be recycled together, making it impossible to sort them into different types for recycling. Ideally, complete recycling will only be possible by differentiating by specification (e.g. polyethylene terephthalate (PET) food applications such as trays versus non-food applications such as personal care products) or even by manufacturer (brand). With the current state of the art (NIR sorter), packaging waste can only be sorted by base polymer, with only one plastic selected in one pass through the sorter. There are several new plastics recycling technologies that are still in development. One of them, tracer-based sorting (TBS) technology, can be implemented to improve the quality of plastics sorting. For such a technology, different luminescent sorting codes based on luminescent markers with specific excitation/emission and high quantum yield of luminescence need to be developed.

2. Results

There are many ways to make these markers. Inorganic materials doped with rare earth ions have several advantages over other options. These materials are chemically stable, offer a wide range of possible excitation and emission wavelengths, and have a relatively large Stokes shift, which reduces emission re-absorption. Rare earth doped crystals can exhibit both types of emission: Stokes, also known as downshifting (DS), and anti-Stokes, also known as upconversion (UC). While DS emission usually has higher efficiency, UC from the near infrared (NIR) to the visible range has other characteristics such as larger amount of usable emission bands, low level of autofluorescence and high signal-to-noise ratio that make this type of emission somewhat promising for sorting applications [1,2].

Fig. 1: Application of up-conversion based luminescent markers on labels (left bottle) and in the packaging material (right bottle) [2].

Co-doping with Er^{3+}/Yb^{3+}, Tm^{3+}/Yb^{3+} or Ho^{3+}/Yb^{3+} pairs of ions is a well-known method of obtaining UC emission under excitation in the range of Yb^{3+} absorption (940 – 1000 nm). Recently, it has been reported that hosts with MF2 (M=Ca, Sr, Ba, Pb) structure can achieve exceptionally high luminescence quantum yields up to 10 percent [3]. This work discusses the UC performance of the MF_2, Gd_2O_2S, and La_2O_3 crystals doped with Er^{3+}/Yb^{3+}, Tm^{3+}/Yb^{3+}, or Ho^{3+}/Yb^{3+} ions under 976 nm excitation and their possible application in TBS.

3. References

[1] G. Gao, et al., *Advanced Sustainable Systems*, **1**, (2017), 1600033.
[2] J. Woidasky, et al., *Resources, Conservation and Recycling*, vol. **161**, (2020), 104976.
[3] E. I. Madirov, et al., *J. of Mater. Chem. C*, **9**, (2021), 3493-3503.

Structure, optical, and low-temperature detection of acetone induced by p-n NiO-CeO_2 decorated with Ag nanoparticles

Boiketlo RJ. Thamaga, Rapelang G. Motsoeneng, Zamaswazi P. Tshabalala, Hendrik C. Swart, and David E. Motaung

University of the Free State PO Box / Posbus 339, Bloemfontein 9300, Republic of South Africa.
Corresponding author's e-mail address: boiketlothamaga@gmail.com

1. Introduction

The 21st epoch has seen significant growth in modernization and industrialization to provide a sophisticated life for humankind. With this advancement, incontrovertible complications have hindered ecology and public health owing to an increase in toxic, harmful gases, and e-waste. To get global businesses on track, devices, that can detect gases like acetone, which is produced from the breath of diabetic patients in the range of 2.5 ppm, which is higher than that of healthy individuals, i.e., 1.8 ppm.[1]. Currently, semiconductor metal oxide (SMO)-based sensors are more attractive, due to their high sensitivity, and selectivity towards volatile organic compounds (VOCs), particularly, acetone. Additionally, they provide a low-cost, non-invasive, and swift detection strategy. Within the SMOs family, CeO_2 has progressively turned out to be a capable material in the gas-sensing field, due to its unique features, such as a greater number of oxygen vacancies, which are useful to improve the response sensitivity. In addition, the redox chemistry between the two oxidation states, that is, Ce^{4+} and Ce^{3+} drives the material to be unique in gas-sensing.[2] Furthermore, NiO is a vital p-type SMO with an extensive energy band gap of 3.6–4 eV.[3] Its higher stability under moisture, and excellent sensitivity, makes it one of the best SMO materials for the detection of acetone. In addition, the fabrication of mixed SMO with both n and p-type conductivities with tunable features has attracted much attention. Therefore, herein we report the fabrication of Ag loaded on a p-n NiO-CeO_2 nanostructure using a hydrothermal synthesis method at a reaction temperature of 120 °C. The sensors tested for acetone, including other interference gases, such as benzene, ethanol, and carbon monoxide, showed higher sensitivity towards acetone at low operating temperatures of 75-100 °C.

2. Results

Fig 1. shows the optical bandgap and response of the sensors versus acetone concentrations (1.2-10 ppm), measured at 75 °C. The optical band gaps of Ag/NiO-CeO_2 in Fig. 1(a) decrease with an increase in the Ag loading. This bandgap reduction is in-line with the improved acetone sensitivity observed for the 1.0 wt.% Ag/ NiO-CeO_2-based sensor, see Fig. 1(b), pointing out that electrons are more inclined to transition and result in more production of photogenerated carriers, thus leading to improved performance. Moreover, as shown in Fig. 1(b), sensor 1.0 wt.% Ag/ NiO-CeO_2 sensor demonstrated a response of 13 at 1.2 ppm and 50 at 10 ppm acetone, signifying its higher sensitivity towards acetone. This behaviour is associated with the decoration of Ag on the surface of NiO-CeO_2 leading to a "spill-over" mechanism.

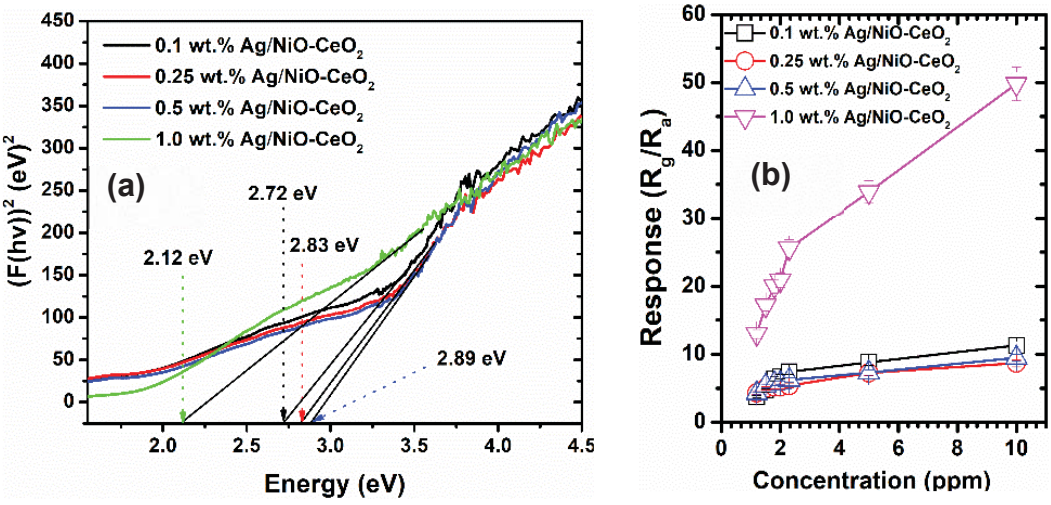

Fig. 1: (a) Band gap calculations using the Kubelka-Munk function and (b) response versus concentration for Ag/NiO-CeO_2 at different Ag concentrations.

3. References

[1] Q.A. Drmosh, I.O. Alade, M. Qamar, S. Akbar, Chem. Asian J. 16 (2021) 1519–1538.
[2] D.E. Motaung, Z.P. Tshabalala, et al., Alloys and Compounds, 906, (2022) 164317.
[3] C. Li, P.G. Choi, K. Kim, Y. Masuda, Sensors and Actuators: B. Chemical 367 (2022) 132143.

P57

The Influence of Fe loading on the Optical and Gas Sensing Characteristics of ZnO/SnO_2 Heterostructures

Rapelang G. Motsoeneng, Hendrik C. Swart, David E. Motaung

University of the Free State PO Box / Posbus 339, Bloemfontein 9300, Republic of South Africa / Republiek van Suid-Afrika.
Corresponding author's e-mail address: rapelangmotsoeneng11@gmail.com

1. Introduction

In the last few decades, pristine, doped, or composite materials based on zinc and or tin oxide have been broadly studied for a variety of practical applications, such as optical waveguides, phosphors, transparent conductive oxides, gas sensors and UV-light emitters [1, 2]. The wide bandgap (≈3.37 eV at room temperature [1]) of ZnO makes it a promising material for photonic applications in the UV or blue spectral range, while the high exciton-binding energy (60 meV) [1] allows efficient excitonic emission even at room temperature possesses excellent chemical stability. However, ZnO and SnO_2 are direct band gap semiconductors. Moreover, ZnO/SnO_2 exhibits improved optical properties owing to the presence of structural defects including oxygen vacancies (V_O), intrinsic Zn, and Sn defects. Moreover, the addition of transition metals on the surface of ZnO/SnO_2 heterostructures increases the defect state and enhances the catalytic behavior of the material, which is beneficial for achieving a high response in gas sensing applications [3]. Thus, in this study, ZnO/SnO_2 and transition-loaded ZnO/SnO_2 heterostructures were prepared using a hydrothermal approach. The gas-sensing performance of the nanostructures toward volatile organic compounds (VOCs) was tested. Their enhanced sensing performance was associated with the surface properties and the catalytic performance induced by the loading of Fe ions.

2. Results

Fig 1. shows the optical bandgap values of 2.53 and 2.15 eV for the ZnO/SnO_2 and $Fe/ZnO/SnO_2$, respectively extracted using a Tauc plot. As depicted in Fig. 1, the optical band gap decreases with the loading of Fe on the surface of ZnO/SnO_2. Usually, the reduced bandgap of $Fe/ZnO/SnO_2$ indicates that electrons are more prone to transition and can produce more photogenerated carriers, which will result in an improved change in sensor resistance and reduced operational temperature. This justifies the higher sensing performance of the $Fe/ZnO/SnO_2$ heterostructure-based sensor towards VOCs.

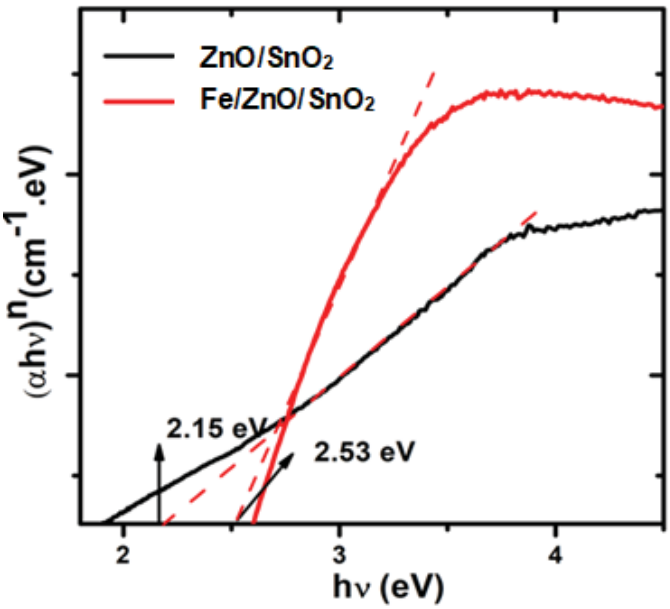

Fig. 1: Tauc plot of ZnO/SnO_2, $Fe/ZnO/SnO_2$.

3. References

[1] Y. Nakanishi, A. Miyake, H. Kominami, T. Aoki, Y. Hatanaka, G. Shimaoka, Appl. Surf. Sci. 142 (1999) 233.
[2] C.H. Lin, Bi-Shiou Chiou, C.H. Chang, J.D. Lin, Mater. Chem. Phys. 77 (2002) 647.
[3] K. Vanheusden, C.H. Seager, W.L. Warren, D.R. Tallant, J.A. Voigt, Appl. Phys. Lett. 68 (1996) 403.

Effect of Stacking on Optical properties of GaSb/GaAs Quantum Rings

Peter Joshua Viljoen[1], **Ngcali Tile**[1], **Peter James Carrington**[2], **Johannes Reinhardt Botha**[1]

[1] *Physics Department, Nelson Mandela University, Summerstrand, Gqeberha, South Africa*
[2]*Physics Department, Lancaster University, Lancaster LA1 4YB, UK*
Corresponding author e-mail address: s216813360@mandela.ac.za

1. Introduction

There have been numerous studies done on the photoluminescence (PL) of type-II GaSb/GaAs nanostructures, but these nanostructures are still actively being investigated as these systems could offer advantages in the application of solar cells [1, 2]. Quantum Rings (QRs) are nanostructures that are similar to quantum dots but have unique optoelectrical properties due to their topology [1]. GaSb/GaAs QRs are typically grown using Molecular Beam Epitaxy. The process involves depositing a thin GaAs buffer on a GaAs substrate, followed by deposition of a few monolayers of GaSb at lower temperatures. This is then followed by depositing a GaAs 'cold cap' at the same temperature as GaSb before a final GaAs spacer layer is deposited at higher optimum GaAs growth temperatures. Ring formation is expected to minimise the strain between the GaSb and GaAs layers and thus allow for the growth of multiple stacks. Multiple stacks should increase the optical response of QRs. In this study PL is used to investigate the effect of stacking on the optical properties of GaSb QRs embedded in a GaAs matrix.

Figure 1 shows schematics of the configurations of the samples being investigated. They include: (a) a sample containing a single layer of GaSb/GaAs QRs with the top layer uncapped, (b)10 layers of GaSb/GaAs QRs and (c) 50 layers of GaSb/QRs

2. Results

Figure 2 shows the normalised 5.5 K PL spectra of the GaSb/GaAs QR samples under investigation. The peaks occurring in the 1.380 to 1.480 eV region for all samples are attributed to GaAs matrix. The two prominent peaks around 0.91 eV and 1.34 eV are attributed to QR and WL respectively. The occurrence of these peaks at similar energies suggest that the average sizes of the embedded rings and wetting layer thicknesses is similar for all samples. However, the QR peak intensity with respect to the wetting layer for (b) is higher than that of (a). This can be expected because, first there are more available rings as recombination sites for a 10-stack compared to a single stack, and secondly, the process of forming multiple stacks involves more high temperature exposure for the rings which could anneal out some defects which could act as recombination centres. Interestingly, contrary to expectations, the QR peak intensity for the 50-stack sample is lower than that of 10-stack sample. This is possibly due to the defects on the sample which could be caused by dislocations caused by strain between GaAs and GaSb layers as the number of layers increased. Transmission Electron Microscopy (TEM) is required to verify this theory. Temperature dependent PL is being conducted in order further understand the optical behaviour of these structures. The origin of the 2 peaks appearing in the 1.060 to 1.080 eV is not yet known. It could be smaller GaSb clusters which formed during capping. TEM analysis will be conducted to provide clarity.

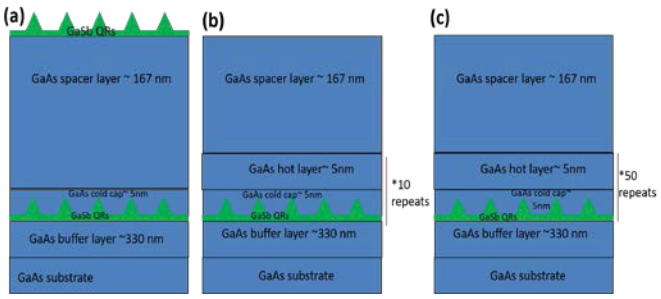

Fig. 1: Configurations of GaSb/GaAs QRs samples: (a) single layer of GaSb/GaAs QRs with top layer uncapped, (b) 10 layers of GaSb/GaAs QRs and (c) 50 layers of GaSb/GaAs QRs.

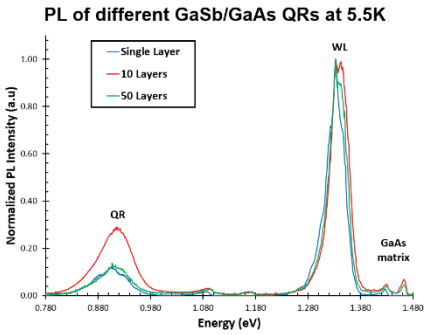

Fig. 2: Normalised PL spectra of the GaSb/GaAs QR samples.

3. References

[1] M. P. Young, C. S. Woodhead, J. Roberts, Y. J. Noori, M. T. Noble, A. Krier, E. P. Smakman, P. M. Koenraad, M. Hayne, and R. J. Young, "Photoluminescence studies of individual and few GaSb/GaAs quantum rings", AIP Advances 4, 117127 (2014)

[2] P. J. Carrington, D. Montesdeoca, H. Fujita, J. James, M. C. Wagener, J. R. Botha, A. R. J. Marshall, and A. Krier "Type II GaSb/GaAs quantum rings with extended photoresponse for efficient solar cells", Proc. SPIE 9937, Next Generation Technologies for Solar Energy Conversion VII, 993708 (23 September 2016)

NELSON MANDELA UNIVERSITY

Department of **Physics**

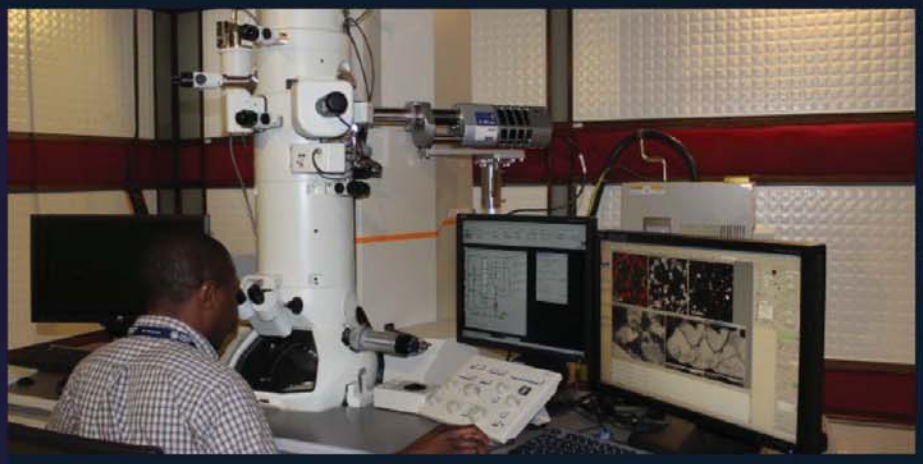

Electron Microscopy for Materials Research

The Centre for High Resolution Transmission Electron Microscopy (Centre for HRTEM) at Nelson Mandela University houses four state-of-the-art electron microscopes including the only aberration-corrected atomic resolution electron microscope in Africa. The wide range of research projects and MSc and PhD topics include:

- HRTEM and in situ HRTEM investigation of nanoparticle catalysts
- Irradiation damage and fission product transport in nuclear reactor materials
- Corrosion resistant nuclear reactor materials
- Refining of weldability limits of creep-aged power plant stainless steel
- Lifetime assessment of high value power plant components
- Characterisation of diamond, Pt, Ti and Al alloys, compound semiconductor structures and gold and platinum bearing ores

HRTEM
E hrtem@mandela.ac.za

Photovoltaics

Sustainable Energy for the Future

The Photovoltaics Research Group focusses on the characterisation of Photovoltaics (PV) materials, devices and systems. The facilities include:

- Photovoltaic Research Laboratory (PV Lab) for advance solar cell and PV module characterisation
- Outdoor Research Facility (ORF) for PV module and system monitoring and characterisation
- ISO17025 accredited Photovoltaic Test Laboratory (PVTL) – PVinsight (Pty) Ltd

The following Applied Physics skills are also acquired:

- Advance solar cell and PV module characterisation and evaluation
- Data acquisition an analysis, including curve fitting and parameter optimisation
- LabView programming and computer interfacing
- Data acquisition system design

For further information on student projects please contact the PVRG.

Prof Ernest van Dyk
E ernest.vandyk@mandela.ac.za

Semiconductor Materials Development

This research focuses on vapour phase and solution-based deposition of semiconductors for opto-electronic devices.

The Physics Department has unique equipment for the synthesis and characterization of semiconductor thin films and nano-structures, including a state-of-the-art reactor for compound semiconductor deposition.

We currently develop:

- Epitaxial InAsSb and related compounds for infrared detectors
- ZnO nanorods for high efficiency white LEDs and hybrid solar cells
- Nanostructured TiO2 for solar water splitting

Our active collaborations with several local and overseas universities over many years, including groups in Sweden, Germany and the UK, have forged excellent academic links.

For information on these exciting research topics contact:

Prof Reinhardt Botha
E reinhardt.botha@mandela.ac.za

Optical Fibre Telecommunication Research

Escalating bandwidth demands fuelled by smartphones, tablet computers, social media and cloud computing makes Telecommunications an extremely challenging and rewarding field.

Nelson Mandela University has one of the best equipped Optical Fibre Research laboratories in Africa.

We offer an exciting range of MSc and PhD projects featuring:

- Dispersion measurement, compensation and emulation
- Fibre-to-the-home (FTTH) technologies
- Square Kilometer Array related optical fibre topics
- Polarization effects, wavelength division multiplexing, non-linear effects
- Modelling and simulation, OTDR, fusion splicing, bit error rate testing

The Optical Fibre Research Unit is part of the Telkom-sponsored Centre of Excellence.

Scholarship opportunities are available for good, motivated students.

Prof Tim Gibbon
E tim.gibbon@mandela.ac.za

Notes

Notes

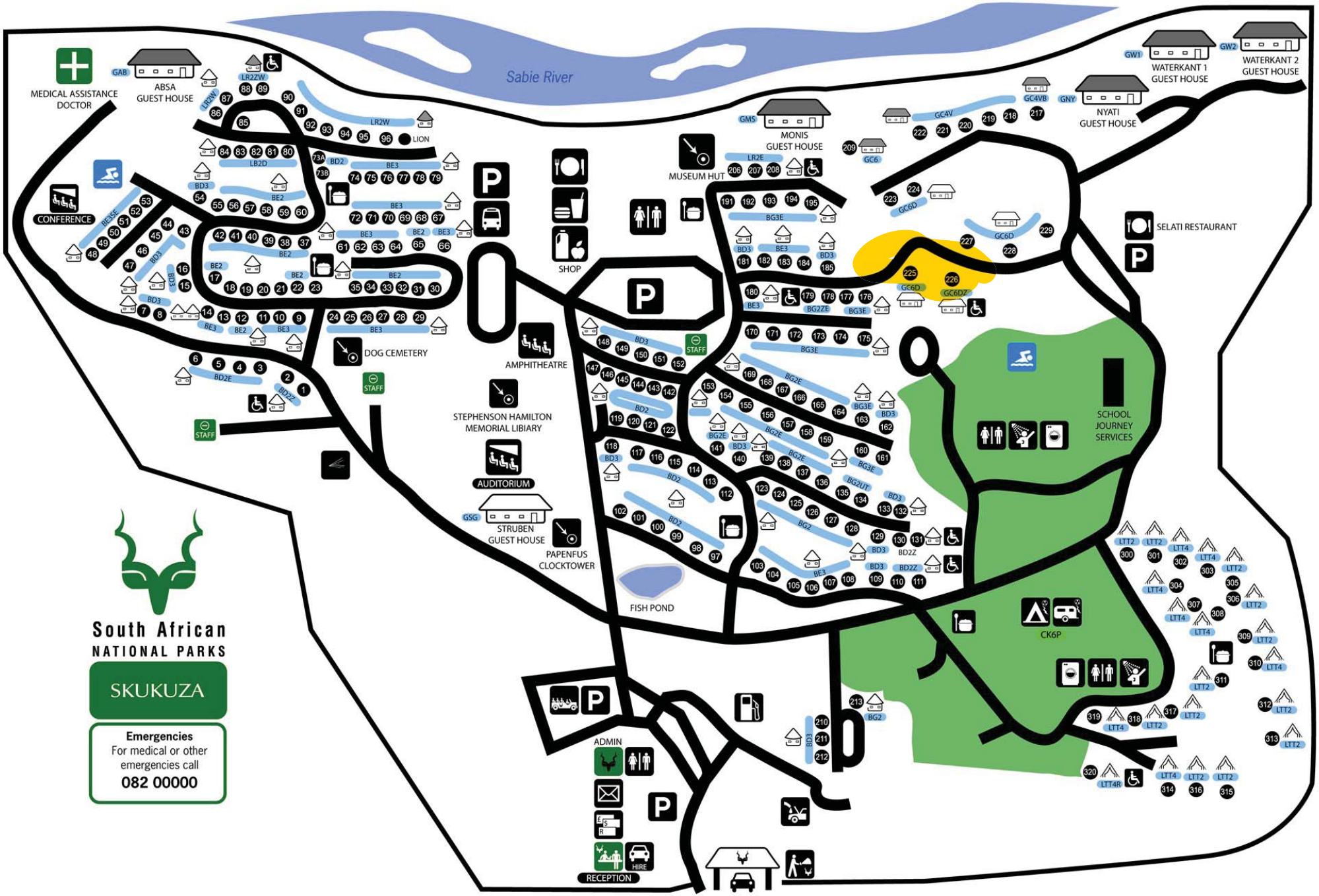

Please deposit keys in key box at gate before departure

EDINBURGH INSTRUMENTS

SCAN ME

MOLECULAR SPECTROSCOPY

Photoluminescence • UV-Vis • Raman
FTIR • Transient Absorption • Gas Lasers

WHAT'S NEW:

AGILE tunable white light source

Supercontinuum laser providing picosecond pulses with variable kHz to MHz repetition rates.

Nitrogen Sample Chamber

Gas tight sample compartment for both solutions and solids.

MANUFACTURED WITH PRIDE IN THE UNITED KINGDOM

edinst.com